INFORMATION TO USERS

This was produced from a copy of a document sent to us for microfilming. While the most advanced technological means to photograph and reproduce this document have been used, the quality is heavily dependent upon the quality of the material submitted.

The following explanation of techniques is provided to help you understand markings or notations which may appear on this reproduction.

1. The sign or "target" for pages apparently lacking from the document photographed is "Missing Page(s)". If it was possible to obtain the missing page(s) or section, they are spliced into the film along with adjacent pages. This may have necessitated cutting through an image and duplicating adjacent pages to assure you of complete continuity.

2. When an image on the film is obliterated with a round black mark it is an indication that the film inspector noticed either blurred copy because of movement during exposure, or duplicate copy. Unless we meant to delete copyrighted materials that should not have been filmed, you will find a good image of the page in the adjacent frame.

3. When a map, drawing or chart, etc., is part of the material being photographed the photographer has followed a definite method in "sectioning" the material. It is customary to begin filming at the upper left hand corner of a large sheet and to continue from left to right in equal sections with small overlaps. If necessary, sectioning is continued again—beginning below the first row and continuing on until complete.

4. For any illustrations that cannot be reproduced satisfactorily by xerography, photographic prints can be purchased at additional cost and tipped into your xerographic copy. Requests can be made to our Dissertations Customer Services Department.

5. Some pages in any document may have indistinct print. In all cases we have filmed the best available copy.

University
Microfilms
International

300 N. ZEEB ROAD, ANN ARBOR, MI 48106
18 BEDFORD ROW, LONDON WC1R 4EJ, ENGLAND

HAHN, WERNER ARTUR

POLLUTANT FORMATION IN FLAT LAMINAR OPPOSED JET DIFFUSION FLAMES

The University of Arizona PH.D. 1979

PLEASE NOTE:

In all cases this material has been filmed in the best possible way from the available copy. Problems encountered with this document have been identified here with a check mark ✓.

1. Glossy photographs ✓
2. Colored illustrations ✓
3. Photographs with dark background ✓
4. Illustrations are poor copy _____
5. Print shows through as there is text on both sides of page _____
6. Indistinct, broken or small print on several pages _____ throughout _____
7. Tightly bound copy with print lost in spine _____
8. Computer printout pages with indistinct print _____
9. Page(s) _____ lacking when material received, and not available from school or author _____
10. Page(s) _____ seem to be missing in numbering only as text follows _____
11. Poor carbon copy _____
12. Not original copy, several pages with blurred type _____
13. Appendix pages are poor copy _____
14. Original copy with light type _____
15. Curling and wrinkled pages _____
16. Other _____

University Microfilms International

300 N. ZEEB RD., ANN ARBOR, MI 48106 (313) 761-4700

POLLUTANT FORMATION IN FLAT LAMINAR OPPOSED JET DIFFUSION FLAMES

by

Werner Artur Hahn

A Dissertation Submitted to the Faculty of the

DEPARTMENT OF CHEMICAL ENGINEERING

In Partial Fulfillment of the Requirements
For the Degree of

DOCTOR OF PHILOSOPHY

In the Graduate College

THE UNIVERSITY OF ARIZONA

1 9 7 9

THE UNIVERSITY OF ARIZONA
GRADUATE COLLEGE

I hereby recommend that this dissertation prepared under my direction by Werner Artur Hahn

entitled Pollutant Formation in Flat Laminar Opposed Jet Diffusion Flames

be accepted as fulfilling the dissertation requirement for the Degree of Doctor of Philosophy.

Dissertation Director — Date: Oct 5, 1979

As members of the Final Examination Committee, we certify that we have read this dissertation and agree that it may be presented for final defense.

	01-OCT-79 Date
Thomas Pelton	19-oct-79 Date
W. M. McElfresh	22 Oct 1979 Date
W. R. Sears	8 Nov. 1979 Date
	Date

Final approval and acceptance of this dissertation is contingent on the candidate's adequate performance and defense thereof at the final oral examination.

11/78

STATEMENT BY AUTHOR

This dissertation has been submitted in partial fulfillment of requirements for an advanced degree at The University of Arizona and is deposited in the University Library to be made available to borrowers under rules of the Library.

Brief quotations from this dissertation are allowable without special permission, provided that accurate acknowledgment of source is made. Requests for permission for extended quotation from or reproduction of this manuscript in whole or in part may be granted by the head of the major department or the Dean of the Graduate College when in his judgment the proposed use of the material is in the interests of scholarship. In all other instances, however, permission must be obtained from the author.

SIGNED: 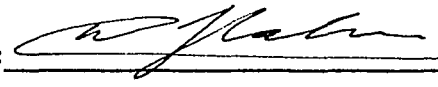

Dedicated to

Zlàtica, Elisabeth, and Herbert

for all they gave me

ACKNOWLEDGMENTS

The author wishes to express his sincere gratitude to his project director, Dr. Jost O. L. Wendt, for his guidance, his assistance, and his encouragement throughout the duration of the project. Dr. Wendt's deep knowledge and insight into transport phenomena were key contributions to the correct formulation and solution of the problem.

The author is deeply grateful to his wife, Ms. Zlàtica I. Kraljevich, for her support and patience, especially towards the end of the project.

The advice and constructive criticism of Dr. Thomas J. Tyson, Dr. C. J. Kau, and Mr. Timothy L. Corley from Energy and Environmental Research Corporation are gratefully acknowledged. In addition, the assistance of Mr. Eric C. Wootan in using the gas chromatograph is fully appreciated. The author also wishes to thank the faculty of the Department of Chemical Engineering, and Dr. William R. Sears, Dr. Donald M. McEligot, and Dr. Moran Coxon of the Aerospace and Mechanical Engineering Department.

The assistance of Mr. Richard W. van Reeth is gratefully acknowledged. Without his assistance in constructing spare parts at a moment's notice this work could not have been finished on the specified date.

The author is indebted to Ms. Candice R. Corley for her patience in figuring out his handwriting and for typing both the draft and final versions of this work.

The author is grateful to the U.S. Environmental Protection Agency for supporting this work under grant number R803715 and in part through a subcontract from the Energy and Environmental Research Corporation as part of the program on fundamental combustion research applied to pollution control.

TABLE OF CONTENTS

		Page
	LIST OF ILLUSTRATIONS	viii
	LIST OF TABLES	xii
	ABSTRACT	xiii
1.	INTRODUCTION	1
2.	THE LAMINAR OPPOSED JET DIFFUSION FLAME	8
3.	THEORY	14
	Governing Equations	17
	Analytical Simplifications	19
	Physical and Chemical Data	26
	Reaction Mechanisms	26
	Transport Properties	31
	Numerical Solution	33
4.	EXPERIMENTAL	45
	Combustor	45
	Analysis	48
	Procedure	51
5.	THE CARBON MONOXIDE OPPOSED JET DIFFUSION FLAME	53
	Introduction	53
	Numerical Solution	54
	Model Validation	56
	Nitric Oxide Formation	64
	Ammonia in the Fuel	64
	Ammonia in the Oxidizer	68
	Additional Predictions	71
6.	THE METHANE/OXYGEN/NITROGEN OPPOSED JET DIFFUSION FLAME	77
	Introduction	77
	Numerical Solution	77

TABLE OF CONTENTS--Continued

Page

Combustion of Dilute Methane 80
High Stretching Rate 80
Low Stretching Rate 89
Nitric Oxide Formation 97
High Stretching Rate 97
Effect of Stretching Rate 100
Additional Predictions 104
Dilute Fuel 104
Pure Fuel 116

7. CONCLUSIONS 121

8. RECOMMENDATIONS FOR FUTURE WORK 124

NOMENCLATURE 126

APPENDIX: COMPUTER PROGRAM 130

REFERENCES 187

LIST OF ILLUSTRATIONS

Figure		Page
1.	Opposed Jet Diffusion Flame	9
2.	Schematic of the Opposed Jet Diffusion Flame	15
3.	Collapsing Grid	35
4.	Opposed Jet Burners	46
5.	Combustor and Feed Lines	47
6.	Uncooled Probe	49
7.	Analysis Train	50
8.	$CO/N_2/O_2$ Flame: $\varepsilon = 7.24\ sec^{-1}$, H_2O and CO_2 Profiles	55
9.	$CO/N_2/O_2$ Flame: $\varepsilon = 7.24\ sec^{-1}$, CO and O_2 Profiles (Experimental Values Not Shifted)	57
10.	$CO/N_2/O_2$ Flame: $\varepsilon = 7.24\ sec^{-1}$, Temperature Profile (Experimental Values Not Shifted)	58
11.	$CO/N_2/O_2$ Flame: $\varepsilon = 7.24\ sec^{-1}$, Temperature Profile (Two Experiments, Experimental Values Shifted)	59
12.	$CO/N_2/O_2$ Flame: $\varepsilon = 7.24\ sec^{-1}$, CO and O_2 Profiles (Two Experiments, Experimental Values Shifted)	61
13.	$CO/N_2/O_2$ Flame: $\varepsilon = 7.24\ sec^{-1}$, Velocity Profile	62
14.	Velocity Profile Measured by Pandya and Weinberg (1964)	63
15.	$CO/N_2/O_2$ Flame: $\varepsilon = 7.24\ sec^{-1}$, NO Profile (One Experiment, NH_3 Injected from Fuel Side)	65
16.	$CO/N_2/O_2$ Flame: $\varepsilon = 7.24\ sec^{-1}$, Effect of NH_3 Concentration in Fuel on Peak NO (Two Experiments, NH_3 Injected from Fuel Side)	67

LIST OF ILLUSTRATIONS--Continued

Figure		Page
17.	$CO/N_2/O_2$ Flame: $\varepsilon = 7.24\ sec^{-1}$, NO Profile (One Experiment, NH_3 Injected from Oxidizer Side, Experimental Values Not Shifted)	69
18.	$CO/N_2/O_2$ Flame: $\varepsilon = 7.24\ sec^{-1}$, NO Profile (One Experiment, NH_3 Injected from Oxidizer Side, Experimental Values Shifted)	70
19.	$CO/N_2/O_2$ Flame: $\varepsilon = 7.24\ sec^{-1}$; NH_3, H_2, H, O, OH Profiles	72
20.	$CO/N_2/O_2$ Flame: $\varepsilon = 7.24\ sec^{-1}$, Profiles of Species Involving Nitrogen (NH_3 Injected from Fuel Side) . . .	73
21.	$CO/N_2/O_2$ Flame: $\varepsilon = 7.24$ and $18.1\ sec^{-1}$, Effect of Stretching Rate on Heat Release Profile	74
22.	$CO/N_2/O_2$ Flame: $\varepsilon = 7.24$ and $18.1\ sec^{-1}$, Effect of Stretching Rate on Rate of Formation of NO (NH_3 Injected from Fuel Side)	76
23.	$CH_4/N_2/O_2$ Flame: $\varepsilon = 7.24\ sec^{-1}$, Temperature Profile (One Experiment, Experimental Values Not Shifted)	82
24.	$CH_4/N_2/O_2$ Flame: $\varepsilon = 7.24\ sec^{-1}$, Temperature Profile (One Experiment, Experimental Values Shifted)	83
25.	$CH_4/N_2/O_2$ Flame: $\varepsilon = 7.24\ sec^{-1}$, CH_4 and O_2 Profiles (Two Experiments, Experimental Values Shifted)	85
26.	$CH_4/N_2/O_2$ Flame: $\varepsilon = 7.24\ sec^{-1}$, CO Profile (Two Experiments, Experimental Values Shifted)	86
27.	$CH_4/N_2/O_2$ Flame: $\varepsilon = 7.24\ sec^{-1}$, CO_2 Profile (Two Experiments, Experimental Values Shifted)	87
28.	$CH_4/N_2/O_2$ Flame: $\varepsilon = 7.24\ sec^{-1}$, H_2O Profile (One Experiment, Experimental Values Shifted)	88
29.	$CH_4/N_2/O_2$ Flame: $\varepsilon = 7.24\ sec^{-1}$, CH_4 and O_2 Profiles (Two Experiments, Experimental Values Not Shifted)	90
30.	$CH_4/N_2/O_2$ Flame: $\varepsilon = 7.24\ sec^{-1}$, CO Profile (Two Experiments, Experimental Values Not Shifted)	91

LIST OF ILLUSTRATIONS--Continued

Figure		Page
31.	$CH_4/N_2/O_2$ Flame: ε = 7.24 sec^{-1}, CO_2 Profile (Two Experiments, Experimental Values Not Shifted)	92
32.	$CH_4/N_2/O_2$ Flame: ε = 7.24 sec^{-1}, H_2O Profile (One Experiment, Experimental Values Not Shifted)	93
33.	$CH_4/N_2/O_2$ Flame: ε = 3.76 sec^{-1}, CH_4 and O_2 Profiles (One Experiment, Experimental Values Not Shifted)	94
34.	$CH_4/N_2/O_2$ Flame: ε = 3.76 sec^{-1}, CO and CO_2 Profiles (One Experiment, Experimental Values Not Shifted)	95
35.	$CH_4/N_2/O_2$ Flame: ε = 3.76 sec^{-1}, Temperature Profile (One Experiment, Experimental Values Not Shifted)	96
36.	$CH_4/N_2/O_2$ Flame: ε = 7.24 sec^{-1}, NO Profile (Two Experiments, Experimental Values Shifted, NH_3 Injected with Fuel)	98
37.	$CH_4/N_2/O_2$ Flame: ε = 7.24 sec^{-1}, NO Profile (One Experiment, Experimental Values Shifted, NH_3 Injected with Oxidizer)	99
38.	$CH_4/N_2/O_2$ Flame: ε = 7.24 sec^{-1}, NO Profile (Two Experiments, Experimental Values Not Shifted, NH_3 Injected with Fuel)	101
39.	$CH_4/N_2/O_2$ Flame: ε = 7.24 sec^{-1}, NO Profile (One Experiment, Experimental Values Not Shifted, NH_3 Injected with Oxidizer)	102
40.	$CH_4/N_2/O_2$ Flame: ε = 7.24 and 3.76 sec^{-1}, Effect of Stretching Rate on NO Profile (NH_3 Injected with Fuel)	103
41.	$CH_4/N_2/O_2$ Flame: ε = 7.24 sec^{-1}; CH_3, CH_2, CH_2O, and NH_3 Profiles (NH_3 Injected with Fuel)	105
42.	$CH_4/N_2/O_2$ Flame: ε = 7.24 sec^{-1}; H_2, OH, O, and H Profiles	106
43.	$CH_4/N_2/O_2$ Flame: ε = 7.24 sec^{-1}; CH, HO_2, and CHO Profiles	108
44.	$CH_4/N_2/O_2$ Flame: ε = 7.24 sec^{-1}; HCN, NH_3, and NO_2 Profiles (NH_3 Injected with Fuel)	109

LIST OF ILLUSTRATIONS--Continued

Figure		Page
45.	$CH_4/N_2/O_2$ Flame: ε = 7.24 sec^{-1}; N, CN, NH Profiles (NH_3 Injected with Fuel)	110
46.	$CH_4/N_2/O_2$ Flame: ε = 7.24 sec^{-1}; N_2O, HNO, and NCO Profiles (NH_3 Injected with Fuel)	111
47.	$CH_4/N_2/O_2$ Flame: ε = 7.24 sec^{-1}, Axial Velocity Profile	112
48.	$CH_4/N_2/O_2$ Flame: ε = 7.24 sec^{-1}, Effect of Stretching Rate on Heat Release Profile	114
49.	$CH_4/N_2/O_2$ Flame: ε = 7.24 and 3.76 sec^{-1}, Effect of Stretching Rate on Rate of Formation of NO (NH_3 Injected with Fuel)	115
50.	$CH_4/N_2/O_2$ Flame: ε = 48.9 sec^{-1}, Axial Velocity Profile (Pure CH_4, Air Flame)	117
51.	$CH_4/N_2/O_2$ Flame: ε = 48.9 sec^{-1}, CO and CO_2 Profiles (Pure CH_4, Air Flame)	119
52.	$CH_4/N_2/O_2$ Flame: ε = 48.9 sec^{-1}; CH , H O, and O Profiles (Pure CH_4, Air Flame)	120

LIST OF TABLES

Table		Page
1.	Methane Reaction Set	27
2.	Carbon Monoxide Reaction Set	29
3.	Conditions of $CH_4/O_2/N_2$ Flames	78
4.	Variation of Relaxation Factor in Solution of the Pure Fuel Flame	81

ABSTRACT

The laminar opposed jet diffusion flame is of interest because it is one of the few flames in which fuel pyrolysis reactions occur in the absence of oxygen and of burner surfaces. It is also of interest because it may be thought to simulate the strained reaction zones that dominate pollutant formation in turbulent diffusion flames. In this work, it is shown that the opposed jet diffusion flame has one additional useful attribute that distinguishes it from all other diffusion flames. This feature is the one-dimensionality of the flame with respect to temperature, concentration, and axial (but, clearly, not radial) velocity profiles. This is shown by first applying a similarity transform on the radial velocity, converting the partial differential equations to ordinary differential equations and then numerically solving the momentum, energy, and species balance equations in a fully coupled manner. The numerical, variable mesh algorithm required for the solution of the resulting large set of very stiff, boundary valued, ordinary differential equations is presented. The model then allows determination of the correct velocity boundary conditions such that the flame is (mathematically) flat and one-dimensional.

A moist carbon monoxide flame was realized in the laboratory, and the detailed species and temperature profiles in the reaction zone gave excellent agreement with the model, with no adjustable parameters. Furthermore, the predicted non-linear velocity profile was in

qualitative agreement with experimental data obtained elsewhere. The exact location of the reaction zone, however, was displaced by a small distance from that predicted.

The formation of nitric oxide in a carbon monoxide flame was investigated by doping either the fuel or the oxidizer with anhydrous ammonia. When the ammonia was injected with the fuel, agreement with theory was only qualitative, due, in part, to inaccuracies in the ammonia pyrolysis reaction mechanism used. On the other hand, when ammonia was injected with the oxidizer, very good agreement between theoretical predictions and experimental results was observed.

Theoretical estimations of the influence of the stretching rate on the flame zone structure indicate that an increase in the rate of stretching results in a decrease in the width of the reaction zone, and in an increase in the rates of the reactions taking place within. Of particular interest is the great influence the rate of stretching has on the rate of formation of nitric oxide since this provides an indirect link between turbulent intensity and pollutant formation in turbulent diffusion flames.

Two dilute methane flames, of different stretching rates, were realized in the laboratory and detailed temperature and species profiles were obtained. Experimental data, in particular those describing the effect of the rate of stretching on the flame zone structure, were in very good agreement with theoretical predictions.

The formation of nitric oxide in methane diffusion flames was studied by injecting ammonia into the fuel or the oxidizer. Very close

agreement between theory and experiment was achieved when ammonia was injected into the fuel. Agreement was less satisfactory when ammonia was injected into the oxidizer. The discrepancy might be due to a small error prediction of the location of the flame zone and/or inaccuracies in the reaction set used. The predicted effect of stretching rate on the nitric oxide profile was reproduced very well in the laboratory experiments.

CHAPTER 1

INTRODUCTION

The 1970 Clean Air Act Amendments designated NO_x as one of the pollutants requiring regulatory control to prevent potential widespread adverse health and welfare effects. In addition, the increasing demand for and decreasing supply of clean fuels (natural gas and treated oils) has initiated a shift towards combustion of so-called dirty fuels (coal and oils obtained from coal and shale). These fuels contain significant amounts of chemically bound fuel nitrogen, a significant fraction of which is oxidized to form oxides of nitrogen (NO_x) during the combustion process (Pershing and Wendt, 1976).

The kinetic mechanisms which form NO_x from fuel nitrogen are still not well understood. Specifically, there is some doubt about the validity of some fuel pyrolysis reactions involved in the reaction sets presently in use to simulate formation kinetics of fuel NO_x. These reactions are of great importance in determining the fractions of fuel nitrogen yielding NO and N_2. Their quantification has proved difficult because the vast majority of experimental information is obtained from well-stirred reactors or premixed flames where flammability limits do not allow combustion at the extremely fuel-rich mixtures in which these pyrolysis reactions are dominant. There is a need, therefore, to devise experimental and analytical tools that overcome these deficiencies, and

that focus on kinetic mechanisms that occur under pyrolysis conditions, prior to significant mixing with oxygen.

Of all the NO_x emitted by stationary sources, burning coal, oil, and/or natural gas, 80% is produced in some kind of turbulent diffusion flame (Mason and Waterland, 1977), or in environments strongly influenced by diffusion. However, description of complex kinetic phenomena controlling fuel species formation in unmixed, turbulent reactive flows is a difficult and controversial undertaking (Andrews, Bradley, and Lwakabamba, 1975). Some simplified approaches have proved useful in providing insight.

Unmixed, diffusion processes are important in both coal and oil flames. Wendt (1979) indicates that coal combustion in an industrial furnace proceeds in three different regimes. At first, volatile matter contained in the coal is driven out of the very rapidly heating particle so fast that it burns in a detached, premixed flame. Later on, as the rate of devolatilization decreases, a balance is established between the rate at which the volatiles appear and the rate at which the oxygen consumes them in an attached laminar diffusion flame. It is thought that this second regime of coal combustion is a salient feature insofar as fuel nitrogen conversion is concerned. Finally, after most of the volatiles have been driven off, oxygen reacts heterogeneously with the coal particle in a third regime of combustion, namely the char burnout.

Combustion of liquid fuels in turbulent flames can be seen, following Bracco (1973), as the combustion of many droplets which are surrounded by a stagnant gas. These droplets evaporate, decreasing in diameter, and the vapor maintains a laminar diffusion flame surrounding

the droplet. It is in this diffusion flame where fuel nitrogen is converted to NO_x. Other approaches (Styles and Chigier, 1976) claim that the entire droplet cloud is surrounded by a diffusion flame, enveloping a region in which primarily vaporization and pyrolysis occur. In both the coal and oil cases, fuel nitrogen may react under pyrolysis rather than oxidative conditions, prior to meeting oxygen in the flame zone.

Although the problem of turbulence has been studied for many years, it still presents formidable mathematical problems to the analyst. The most widely used approach to predict the behavior of a turbulent flow field consists of modelling the time average of the variables of interest. This type of approach was used by von Kàrmàn (1952), Hawthorne (1954), Snyder (1962), Williams (1970), and others to model turbulent gas flames. In these models, the importance of chemical kinetics has been reduced to a minimum through the assumption of infinitely rapid reactions that may be either reversible or irreversible. The results obtained with these models agree well with experimental evidence in predicting the length and shape of turbulent flames (Andrews et al., 1975). The approach is not suitable for prediction of formation of NO_x and other trace species in turbulent flames since this involves the use of large sets of finite rate, simultaneous and competitive chemical reactions.

Gibson and Libby (1972) present experimental data of the instantaneous concentrations of the reactants in the bulk of a turbulent reacting flow. These concentrations not only fluctuate, but are intermittent, suggesting that there are surfaces which separate regions with fuel present and oxidizer absent from regions with oxidizer present and

fuel absent. Chemical reaction between fuel and oxidizer takes place in narrow regions which can be envisioned as little laminar flamelets.

Williams (1974) suggests that the physical variable that links these flamelets to the turbulent flow field is the mean strain rate which imposes a stretching motion onto the laminar flame in its own plane. Marble and Broadwell (1977) present a formal theory, in which a conservation equation for the flame density (flame area per unit volume) is established. In their model, the equations representing the turbulent motion and those representing the flame density appear uncoupled and can be solved independently.

The evidence presented above indicates that a strained laminar diffusion flame(let) can be used as a prototype model to simulate the appropriate kinetic environment for some turbulent combustion processes. Formation of NO_x and other trace species, which depends on finite rate chemical kinetics rather than chemical equilibrium, can be studied in this prototype model. The necessary large sets of chemical reactions can be included in the model, and this gives considerable insight into the formation of trace species for a host of much more complex (turbulent) situations which are extremely difficult, if not impossible, to model in their entirety.

A first model of a laminar diffusion flame was proposed by Burke and Schuman (1928). They considered the flame formed at the interface of two concentric jets, one being fuel only and the other being air. In this configuration, fuel and air mix only by diffusion and if infinitely fast chemical reactions are assumed the flame is located at the locus of points where the fluxes of fuel and oxidant are in stoichiometric

proportion. The Burke-Schuman laminar flame, however, is generally not strained in its own plane. Although the model agreed very well with laboratory data in predicting the length and shape of these types of diffusion flames, it is not applicable to the study of blowout or the formation of trace species, since these phenomena are controlled, in part, by the kinetics of very complex reaction mechanisms involving many intermediate species rather than by chemical equilibrium considerations.

Bracco (1973) presented a model for the formation of NO_x from the combustion of fuel droplets in air. He assumed that a diffusion flame surrounded a shrinking drop and represented the combustion process, following Williams (1968), with a second-order overall reaction, thus obtaining the profiles of major combustion species and temperature as a function of distance from the surface of the drop. The formation of NO_x was then determined using the mechanism proposed by Zeldovich (1946). In addition, it was assumed that O radicals were in equilibrium with O_2 and that the pseudo-steady-state hypothesis could be applied to N radicals. This very simplified mechanism, however, does not consider the existence of kinetically controlled superequilibrium concentrations of O radicals or the alternative paths of fixation of molecular nitrogen first proposed by Fenimore (1971). Furthermore, it does not permit the study of formation of NO_x from fuel nitrogen, since, in this case, there exists a very strong interaction between the NO_x formation mechanisms and a host of fuel fragment and other radicals resulting from the fuel combustion reactions themselves.

Sternling and Wendt (1974) considered diffusion through a stagnant gas film and a reaction zone of finite thickness. If the rates of

the chemical reactions are assumed to be zero outside this reaction zone and if the species and temperature profiles are assumed to be parabolic, then the rate of reaction is constant in value throughout. The conservation equations arising from this model are then identical to those describing a well-stirred reactor, the volume of which is controlled by the rates of diffusion of oxygen into the reaction zone. The volume of the reactor can be related to local combustion intensity. Formation of NO in a hydrogen flame was simulated with a set of 17 chemical reactions. The obtained results showed the correct qualitative behavior when compared to experimental data but not quantitative agreement could be obtained.

Mitchell and Sarofim (1975) combined the approach used by Burke and Schuman (1928) and by Bracco (1973) to model the formation of thermal NO in laminar diffusion flames. In their work, the Burke-Schuman concept was employed to find the location of the flame front and the concentration profiles of the major species. The flame front was then considered to be a heat source and the energy equation was solved to obtain a temperature profile. The theoretical velocity and temperature profiles were combined with experimental values of the concentration of stable species to estimate the concentration of O atoms in the post-flame region, where the CO, CO_2, H_2O, H_2, O_2 system can be considered partially equilibrated. This O atom profile was then used to predict the formation of NO in the post-flame region using Zeldovich (1946) kinetics. Although good agreement with experiment was achieved, the need for experimental data describing some concentration profiles does not allow the use of this model as a purely predictive tool.

None of the above-mentioned models, although attractive in their simplicity, can be used as prototype models of more complex problems which involve convective flux of reactants into the reaction zone, the straining of the reaction zone, and/or the formation of NO_x from fuel-bound nitrogen.

The laminar flame chosen for this work is the Flat Opposed Jet Diffusion Flame. This prototype contains both convective and diffusive transfer of reactants to the flame front which is strained in its own plane. Furthermore, Williams (1974) shows how the strength of the two opposed jets can be related to the rate of stretching of the flame. The latter characteristic makes it an excellent prototype model in Marble's approach to single-phase, turbulent flames. A further advantage of this type of flame is that it burns without being in physical contact with a flameholder, which simplifies modelling considerably because no catalytic or significant heat sink effect of the holder has to be considered. Also, the flame can be realized on a laboratory scale and the experimental data necessary to verify the theory can be obtained.

The present work focuses on developing the mathematical model of a strained, laminar opposed jet diffusion flame. Convection and diffusion of reactants to the flame surface and a detailed reaction mechanism for the combustion of the fuel and formation of NO_x from atmospheric and fuel-bound nitrogen are considered. Furthermore, the scheme for the numerical solution of the stiff differential equations arising from the model is shown. Finally, the model is solved for moist carbon monoxide and methane flames and the predicted profiles of major and minor species and temperature are compared with experimental data.

CHAPTER 2

THE LAMINAR OPPOSED JET DIFFUSION FLAME

Whenever two opposed, coaxial gas jets, one a combustive gas and the other an oxidizer, impinge on one another under conditions such that combustion occurs, a surface of flame, an Opposed Jet Diffusion Flame, appears near the stagnation point of the jets. Under certain conditions, the luminous flame zone appears to be flat, in the neighborhood of the stagnation point. A photograph of a $CO/N_2/O_2$ Opposed Jet Diffusion Flame is shown at Figure 1.

In an early work, the Opposed Jet Diffusion Flame was employed by Potter and Butler (1959) and Potter, Heimel, and Butler (1960) to obtain information on burning rates of a wide variety of fuels. The method was used for fuels (such as rocket fuels) which were too reactive to be burned in a premixed mode and which ignited spontaneously in the presence of an oxidizer. The experiment consisted of first stabilizing an Opposed Jet Diffusion Flame and then increasing the flow rates of the two jets until extinction occurred in the center and an annual flame remained. The flow rate at which this phenomenon occurred was denoted as "Apparent Flame Strength." Spalding (1961) proposed a model to link Apparent Flame Strength to reaction rates obtained from premixed experiments. In this model, he assumed infinitely fast reactions to find the location of the flame front, the fluxes of reactants to it, and the rate

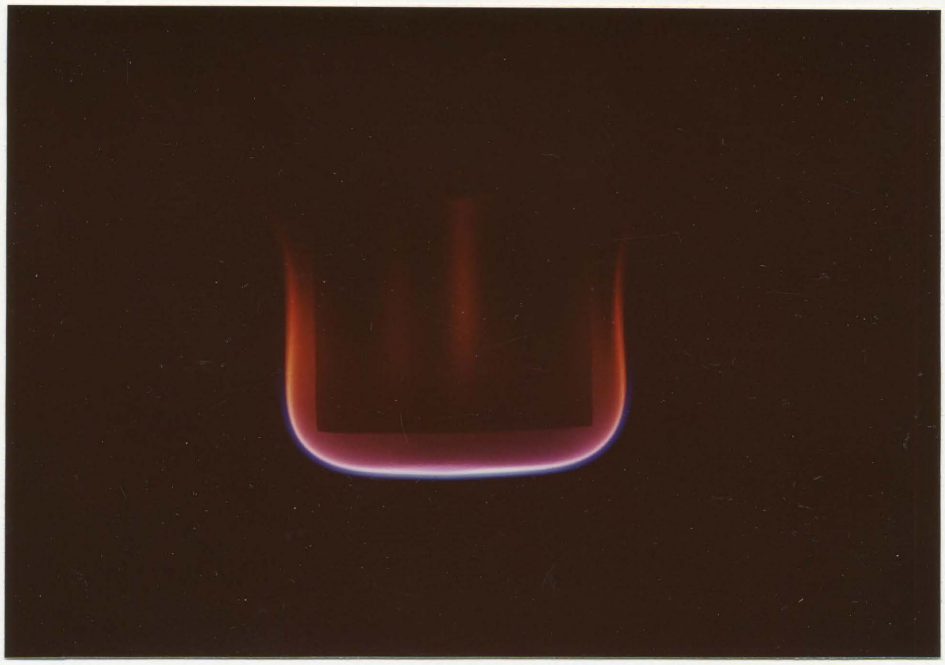

Figure 1. Opposed Jet Diffusion Flame.

at which these reactants are consumed. Subsequently, this rate of consumption was compared to the burning velocity of a premixed flame which was fed by the fluxes calculated previously. Extinction was defined as the condition in which the rate of consumption of products was equal to the burning velocity. Qualitative agreement between theory and the experimental results of Potter and Butler (1959) for a propane-air flame at atmospheric pressure was obtained. Further experimental studies on Apparent Flame Strength concerning the effect of pressure and burner diameter on it were presented by Anagnostou and Potter (1962). The results were compared to Spalding's theory and again agreed qualitatively in that the flame strength varies directly with burner diameter.

Pandya and Weinberg (1962) adapt the methods of optical interferometry and deflection mapping to measure the temperature field of an Opposed Jet Diffusion Flame. The radial temperature profile presented in this paper suggests that, in their flame, the temperature is a function of radial distance. This indicates that the temperature field of their flame is, in fact, not flat but two-dimensional. This may be a consequence of an improper velocity boundary condition. In 1964, the same authors extended this work and deduced the velocity field from their measurements. The results showed that the radial velocity component is linear with radial distance. The slopes of these lines depend on the axial coordinate, suggesting that the solution of nonreactive inviscid flows does not represent the flow field of their flame. The reported values of the axial velocity profile do not follow a straight line. This fact was attributed to scatter in the results by the author and a straight line was drawn through the points. It will be shown later in

the present work that the axial velocity profile is, indeed, not linear and that the measured values can be correct.

Fendell (1965) considered a model for extinction of the Opposed Jet Diffusion Flame. By assuming that all physical properties of the gases were constant and that the Lewis number was unity, he solved the conservation equations for the case of infinitely fast reaction. He also considered the case of one irreversible reaction of finite rate and very high activation energy. The latter assumption made it possible to employ asymptotic expansions. He further assumed in his model that the flow field is well represented by the solution of two inviscid incompressible jets impinging on a wall, i.e., the gradient of the vertical velocity component was considered to be constant.

The effect of an electric field on an Opposed Jet Diffusion Flame was studied theoretically by Jones, Becker, and Meinsohn (1972). Detailed kinetics were included in the model and the equations of conservation of species and energy were decoupled from momentum and continuity by assuming that the flame had no influence on the flow field.

Otsuka and Niioka (1972, 1973) realized that the very steep temperature gradients across an Opposed Jet Diffusion Flame have a great influence on the velocity profile. They presented a model in which the vertical velocity is not linear in the vertical distance. The velocity gradient was presented by a polynomial in temperature and through an heuristic argument a square-root dependence was chosen. Although this approach is an improvement over previous assumptions of a linear velocity profile, it is not the complete solution which can be obtained by

coupling the continuity and momentum equations to the equations representing conservation of species and energy.

More recently, Dayal and Pandya (1979) presented experimental evidence that a Flat Opposed Jet Diffusion Flame is obtained when using jets with different flow rates, where the latter were calculated using the method of Otsuka and Niioka (1973) described above.

All but one of the above-mentioned models include the assumption that the rates of reaction are either infinitely fast or have very high activation energies. Clearly, this does not allow their use to predict the formation of NO_x or other trace species since these phenomena are governed by large sets of chemical reactions, some of which are quite slow and/or have very small activation energies. Furthermore, it will be shown below that, when a flat (one-dimensional) flame is desired, the axial velocity component is different from that resulting from the impingement of an inviscid, incompressible jet in that it is not linear with vertical distance. Also, the ratio of the velocities of the two jets is different from unity and can only be determined after the complete model has been solved. A one-dimensional flame is a very desirable feature since it allows sampling at points different from the centerline of the jets, where the radial velocity component is greater and, thus, sampling can be accomplished under more isokinetic conditions.

In summary, the unresolved problems are:

1. Coupling of the continuity equations with those representing the conservation of energy and species.

2. Determination of the correct ratio of velocities of the opposing jets, in order to provide a flat flame.
3. Inclusion of finite rate combustion chemistry.

In the present work, the equations of continuity and momentum are coupled with the conservation of species and energy. The equations are then rendered one-dimensional through the use of a similarity transformation. Finally, the equations are solved numerically with the use of a fully implicit iterative scheme and a finite-difference formulation. The combustion process and the formation of NO_x from atmospheric and fuel-bound nitrogen is simulated with the use of a set of 86 reactions involving 28 different chemical species (Levy et al., 1979). The predicted profiles of major species and temperature are compared to experimental data.

The present application of the detailed reaction mechanism is a very severe test to its validity, since no experimental data to test the pyrolysis reactions in it were available in the past. These reactions are very important in the fuel-rich region of a diffusion flame.

CHAPTER 3

THEORY

Consider the problem of a reaction zone stabilized near the stagnation point of two infinitely wide, counterflow concentric coaxial jets. The flow is laminar everywhere, shown schematically on Figure 2. In the absence of a flame, the solution to this problem is given by the solution of two inviscid incompressible jets impinging on one another. Then, if the integral momenta at infinite axial distances are equal, the stagnation plane is a flat plane of symmetry (Milne and Thompson, 1961). The problem has some similarity with Hiementz flow (Schlichting, 1962) in that the outer solution to the equations of motion is the same. An important difference is that no inner solution is necessary since there is no wall present and no boundary layer at the interface of the two (unreacting) jets.

The fuel contained in one jet will diffuse into the other jet and the oxidizer will do likewise in the opposite direction, thus establishing a narrow zone in which fuel and oxidizer coexist. If the mixture is ignited, a thin surface of flame, a Laminar Opposed Jet Diffusion Flame, will be established. The temperature of the gases will rise sharply on one side of the flame and decrease sharply on the other side. This narrow temperature peak will affect the density of the gases and the velocity profile will now be different from that of the nonreacting flow. The form of said velocity profile cannot be established <u>a priori</u>

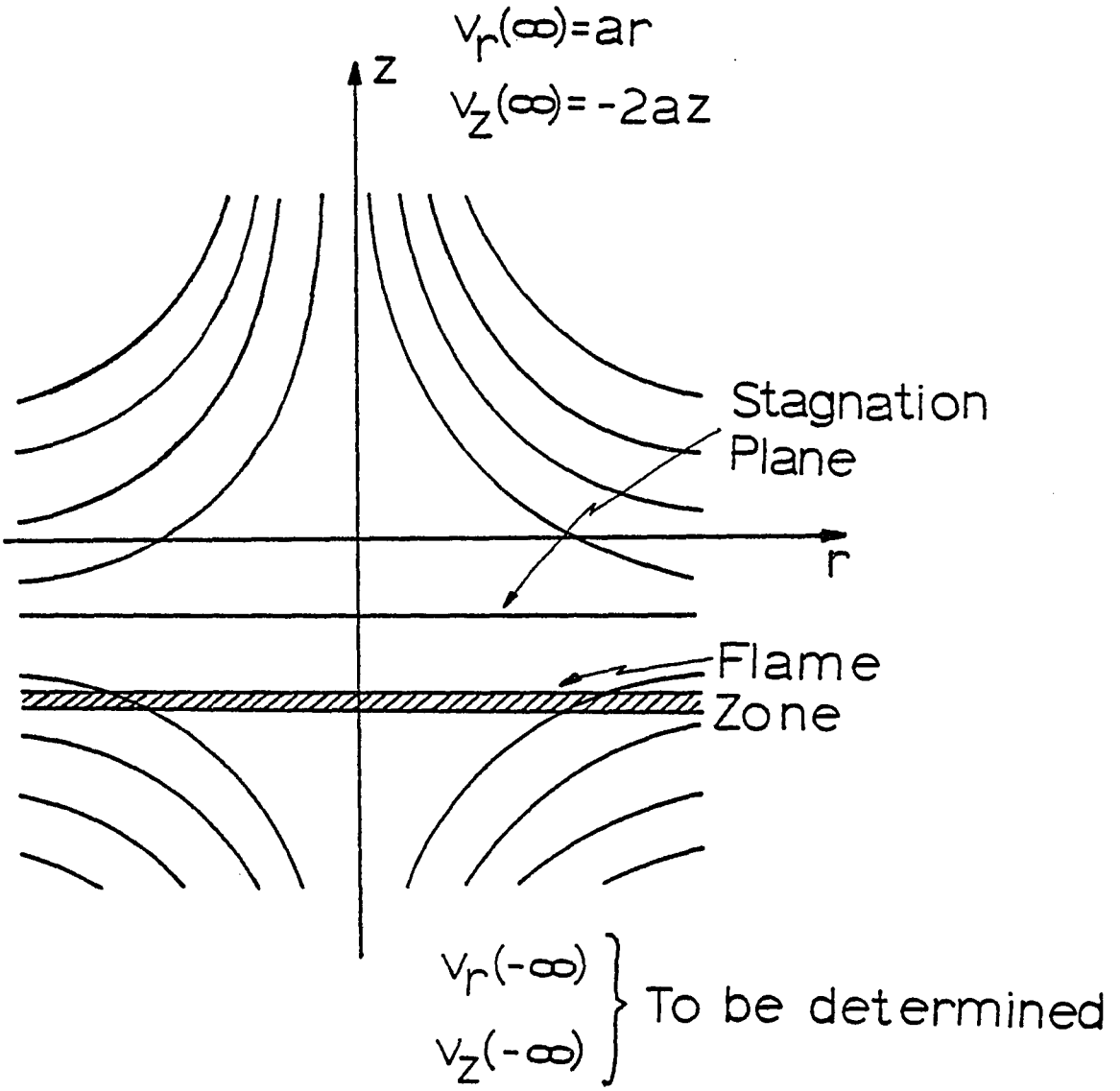

Figure 2. Schematic of the Opposed Jet Diffusion Flame.

and must be determined from the solution of the equations of motion coupled with the equations of conservation of species and energy.

Because the effect of the flame on the flow field is restricted to a very narrow region in space, the problem can be envisioned as being similar to a Boundary Layer in which case the viscous effects are restricted to a region which is small when compared to the overall dimensions of the problem. This analogy, together with the fact that the jets are infinitely wide, suggests that the equations representing the Opposed Jet Diffusion Flame may be solved with the use of a similarity transformation. However, no specific Prandtl boundary layer approximations are necessary, as will be shown below.

The theory presented below applies to two infinitely wide jets. This situation cannot be reproduced on a laboratory scale and finite jets, in width and spacing, have to be used. This does not affect the solution in the axial direction, since for a given stretching rate the flame will be unaffected by the physical spacing of the jets, provided this spacing is sufficiently large. The rate of stretching is maintained constant by making the incoming velocity proportional to the distance between the jets. Thus, the outer flow field is not affected and the flame does not "see" the change of spacing. The distance between the jets only becomes important when it is comparable to the region where the temperature changes are important. The finite width of the jets does affect the profiles in the radial direction and the theory of infinite jets is only applicable close to the centerline axis where edge effects are unimportant. It will be shown below that the point where

the assumption loses its validity can be determined experimentally by probing the flame at various radial locations and checking the radial independence of the temperature and concentration profiles.

In this section, the governing equations will be presented and it will be shown how, through the use of a similarity transformation, the ensuing set of partial differential equations can be transformed into a set of ordinary differential equations. These ordinary differential equations (ODE's) are, with one exception, stiff Boundary Value Problems. The stiffness arises through the greatly varying time constants of the reaction rates involved in the simulation of a flame. The numerical solution of these ODE's is discussed below.

Governing Equations

A complete description of the system shown on Figure 2 involves the simultaneous solution of the following equations:

1. Continuity:

$$\nabla\cdot(\rho\underline{v}) = 0 \qquad [1]$$

2. Momentum:

$$\rho\underline{v}\cdot\nabla\underline{v} = -\nabla P - \nabla\cdot\underline{\underline{\tau}} + \rho\underline{g} \qquad [2]$$

3. Energy:

$$-\nabla\cdot(cC_p T\underline{v}) - \nabla\cdot\underline{q} + \underline{v}\cdot\nabla P - \underline{\underline{\tau}}:\ \nabla\underline{v} + \left(\frac{\partial \ln V}{\partial \ln T}\right)_P \underline{v}\cdot\nabla P$$

$$+ \rho T\underline{v}\cdot\nabla C_p + \sum_{j=1}^{nr} r_j \Delta h_j = 0 \qquad [3]$$

4. Species:

$$\nabla \cdot \underline{N}_A = R_A \qquad [4]$$

where, following Field et al. (1967), heat loss to the ambient and thermal diffusion have been neglected.

The gaseous mixture is taken to be a compressible, ideal, Newtonian fluid. If it is also considered that Fourier's and Fick's laws apply, the set of constitutive equations is:

1. Ideal Gas Law:

$$PV = RT \qquad [5]$$

2. Newtonian Fluid:

$$\underline{\underline{\tau}} = - \mu \underline{\underline{E}} + \frac{2}{3} (\nabla \cdot \underline{v}) \underline{\underline{\delta}} \qquad [6]$$

with

$$\underline{\underline{E}} = \frac{1}{2} (\nabla \underline{v} + (\nabla \underline{v})^T) \qquad [7]$$

3. Fourier's Law:

$$\underline{q} = - k \nabla T \qquad [8]$$

4. Fick's Law:

$$\underline{N}_A - x_A c \underline{v} = - c D_A \nabla x_A \qquad [9]$$

This last constitutive equation implies the use of pseudo-binary diffusion and its use is only correct when the diffusing gases are dilute. However, if the proper pseudo-binary diffusion coefficient is defined it is a close approximation even for concentrated mixtures (Fairbanks and Wilke, 1950).

The boundary conditions to equations [1] through [9] are:

$$\underline{v} = U_\infty \hat{z} \qquad z = -\infty \text{ for all r's}$$

$$P = P_\infty \qquad z = \pm \infty \text{ for all r's}$$

$$T = T_\infty \qquad z = \pm \infty \text{ for all r's}$$

$$x_A = x_{A1} \qquad z = +\infty \text{ for all r's}$$

$$x_A = x_{A2} \qquad z = -\infty \text{ for all r's}$$

Analytical Simplifications

If it is recognized that the Mach number of the laminar flow field is small and it is further assumed that gravitational effects are negligible, due to the low density of the fluid, the reversible and irreversible work terms can be neglected in the energy equation. Equations [1] through [9] can now be combined and written in cylindrical coordinates as:

1. Continuity:

$$\frac{1}{r} \frac{\partial}{\partial r} (\rho r v_r) + \frac{\partial}{\partial z} (\rho v_z) = 0 \qquad [10]$$

2. r momentum:

$$\rho v_r \frac{\partial v_r}{\partial r} + \rho v_z \frac{\partial v_r}{\partial z'} = - \frac{\partial P}{\partial r} - \left[\frac{1}{r} \frac{\partial}{\partial r} (r\tau_{rr}) - \frac{\tau_{\theta\theta}}{r} + \frac{\partial \tau_{rz}}{\partial z'} \right] \quad [11]$$

3. z momentum:

$$\rho v_r \frac{\partial v_z}{\partial r} + \rho v_z \frac{\partial v_z}{\partial z'} = - \frac{\partial P}{\partial z'} - \left[\frac{1}{r} \frac{\partial}{\partial r} (r\tau_{rz}) + \frac{\partial \tau_{zz}}{\partial z'} \right] \quad [12]$$

with

$$\tau_{rr} = - \mu (2 \frac{\partial v_r}{\partial r} - \frac{2}{3} \nabla \cdot \underline{v}) \quad [13]$$

$$\tau_{\theta\theta} = - \mu (2 \frac{v_r}{r} - \frac{2}{3} \nabla \cdot \underline{v}) \quad [14]$$

$$\tau_{zz} = - \mu (2 \frac{\partial v_z}{\partial z'} - \frac{2}{3} \nabla \cdot \underline{v}) \quad [15]$$

$$\nabla \cdot \underline{v} = \frac{1}{r} \frac{\partial}{\partial r} (r v_r) + \frac{\partial v_z}{\partial z'} \quad [16]$$

$$\tau_{rz} = - \mu (\frac{\partial v_z}{\partial r} + \frac{\partial v_r}{\partial z'}) \quad [17]$$

4. Energy:

$$-\frac{1}{r}\frac{\partial}{\partial r}(rcC_pTv_r) - \frac{\partial}{\partial z'}(cC_pTv_z) + \frac{1}{r}\frac{\partial}{\partial r}(rk\frac{\partial T}{\partial r})$$

$$+\frac{\partial}{\partial z'}(k\frac{\partial T}{\partial z'}) = -\sum_{j=1}^{nr} r_j \Delta h_j \qquad [18]$$

5. Species:

$$\frac{1}{r}\frac{\partial}{\partial r}(rcD_A\frac{\partial x_A}{\partial r}) + \frac{\partial}{\partial z'}(cD_A\frac{\partial x_A}{\partial z'}) - \frac{1}{r}\frac{\partial}{\partial r}(crx_Av_r)$$

$$-\frac{\partial}{\partial z'}(cx_Av_z) = -R_A \qquad [19]$$

It can be shown that equations [10] through [19] can be reduced to a system of ordinary differential equations by the use of a similarity transformation. Assume the following forms of the solution:

$$v_r = \varepsilon r\psi(z') \; ; \quad v_z = v(z') \qquad [20]$$

$$\frac{\partial P}{\partial r} = f(r) \; ; \quad \frac{\partial P}{\partial z'} = g(z') \qquad [21]$$

$$\rho = \rho(z') \; ; \quad T = T(z') \; ; \quad x_A = x_A(z') \qquad [22]$$

The next step is to confirm that the above similarity hypothesis is consistent with the equations and the boundary conditions. Substituting [20] through [22] into the momentum, species and energy equations yields:

$$\frac{d}{dz'}(\rho v) + 2\varepsilon\rho\psi = 0 \qquad [23]$$

$$\varepsilon^2\psi^2 + \varepsilon v \frac{d\psi}{dz'} = - \frac{f(r)}{\rho r} + \frac{\varepsilon}{\rho} \frac{d}{dz'} \left(\mu \frac{d\psi}{dz'}\right) \qquad [24]$$

$$\rho v \frac{dv}{dz'} = - g(z') + 2\varepsilon\mu \frac{d\psi}{dz'} - \frac{4}{3} \varepsilon \frac{d}{dz'} (\mu\psi) + \frac{4}{3} \frac{d}{dz'} \left(\mu \frac{dv}{dz'}\right) \qquad [25]$$

$$-2\varepsilon c C_p T\psi - \frac{d}{dz'} (cC_pTv) + \frac{d}{dz'} \left(k \frac{dT}{dz'}\right) = - \sum_{j=1}^{nr} r_j \Delta h_j \qquad [26]$$

$$-2\varepsilon c x_A \psi - \frac{d}{dz'} (cx_A v) + \frac{d}{dz'} \left(cD_A \frac{dx_A}{dz'}\right) = - R_A \qquad [27]$$

The presumed similarity is true if the first term in the right-hand side of equation [24] is also independent of r, i.e., if $\partial P/\partial r$ is proportional to the radius.

For a distance from the flame front which is large compared to the thickness of this front, the velocity profiles are given by the solution of the potential flow of two jets impinging on a wall perpendicular to its axis. The velocity field is then given by (Bird, Stewart, and Lightfoot, 1960):

$$v_r = \varepsilon r \psi_\infty \; ; \quad v_z = - 2\varepsilon z \qquad [28]$$

and the pressure distribution can be formed applying Bernoulli's Theorem, since the inviscid flow is also irrotational:

$$P_\infty = P + \frac{1}{2} \varepsilon^2 \rho_\infty r^2 \psi_\infty^2 + 2\varepsilon^2 \rho_\infty z^2 \qquad [29]$$

$\frac{\partial P}{\partial r} = f(r)$ can now be calculated, far from the flame front, by differentiating equation [29]:

$$\frac{\partial P}{\partial r} = f(r) = - \varepsilon^2 \rho_\infty r \psi_\infty^2 \qquad [30]$$

Furthermore, the similarity hypothesis, equation [21], defines $\partial P/\partial r$ as being independent of axial position. Therefore, equation [30] can be substituted into equation [24] and it is apparent that all terms in this equation are independent of r. Likewise, all terms in each of equations [23] through [27] are functions of z' only. The similarity hypothesis, therefore, satisfies all the equations, and the boundary conditions, and is proved to be valid.

At this point, it is convenient to define a dimensionless temperature as $\theta = \frac{T-298}{298}$ and a dimensionless axial position as $z = z'/\ell$, where ℓ is the actual spacing between the burners in the laboratory experiment. The final set of ordinary differential equations can be written as:

$$\frac{d}{dz}(\rho v) = - 2\varepsilon\rho\psi\ell \qquad [31]$$

$$\frac{d^2\psi}{dz^2} + \left(\frac{1}{\mu}\frac{d\mu}{dz} - \frac{\rho v \ell}{\mu} \right) \frac{d\psi}{dz} - \frac{\varepsilon \ell^2 \rho}{\mu} \psi^2 = - \frac{\varepsilon \rho_\infty \psi_\infty^2 \ell^2}{\mu} \qquad [32]$$

$$g(z) = \frac{2\varepsilon\mu}{\ell}\frac{d\psi}{dz} - \rho \frac{v}{\ell}\frac{dv}{dz} + \frac{4}{3}\frac{1}{\ell^2}\frac{d}{dz}\left(\mu \frac{dv}{dz}\right) - \frac{4}{3}\frac{\varepsilon}{\ell}\frac{d}{dz}(\mu\psi) \qquad [33]$$

$$\frac{d^2\theta}{dz^2} + \left(\frac{1}{k}\frac{dk}{dz} - \frac{\ell c C_p v}{k} \right) \frac{d\theta}{dz} - \left(\frac{\ell}{k}\frac{d}{dz}(cC_p v) + \frac{2\varepsilon c C_p \psi \ell^2}{k} \right) \theta$$

$$= \frac{2\varepsilon c C_p \psi \ell^2}{k} + \frac{\ell}{k}\frac{d}{dz}(cC_p v) - \frac{\ell^2}{298k} \sum_{j=1}^{nr} r_j \Delta h_j \qquad [34]$$

$$\frac{d^2 x_A}{dz^2} + \left(\frac{1}{cD_A}\frac{dcD_A}{dz} - \frac{v\ell}{D_A} \right) \frac{dx_A}{dz} - \left(\frac{\ell}{cD_A}\frac{dcv}{dz} + \frac{2\varepsilon\psi}{D_A} \right) x_A$$

$$= - \frac{\ell^2}{cD_A} R_A \qquad [35]$$

The boundary conditions corresponding to equations [32], [34], and [35] are the known values of ψ, T, and x_A, respectively, at infinity or the position of the two burners for computational purposes. Care has to be taken in that the spacing of the burners has to be large compared to the flame thickness, otherwise no stable convergent solution can be obtained:

$$\left.\begin{array}{l} \theta = \theta_1 \\ x_A = x_{A1} \\ \psi = \psi_1 \end{array}\right\} \text{ at } \begin{array}{c} z = -\infty \\ \text{or} \\ z = -\ell/2 \end{array} \quad \text{and} \quad \left.\begin{array}{l} \theta = \theta_2 \\ x_A = x_{A2} \\ \psi = \psi_2 \end{array}\right\} \text{ at } \begin{array}{c} z = +\infty \\ \text{or} \\ z = +\ell/2 \end{array}$$

The momentum equation [31] requires only one boundary conditions, which is the exit velocity of the gaseous mixture from either one of the two jets:

$$v = v_1 \text{ at } x = -\frac{\ell}{2} \quad \text{or} \quad v = v_2 \text{ at } x = +\frac{\ell}{2}$$

The other velocity boundary condition is not known a priori and can only be found after the entire problem has been solved. The z momentum equation plays no role other than to calculate dp/dz as a function of z, i.e., g(z).

For infinitely wide jets, or for a region not too far from the centerline axis, the developments above lead to the following conclusions:

1. Temperature and concentration profiles are independent of radius regardless of complexity of reaction.
2. Momentum and energy balances are strongly coupled because of density changes in the flame zones.
3. The flame will affect the outer flow field.
4. Neither the condition of balanced flows nor of balanced momenta is correct for establishment of a flat flame. Rather, once the velocity of one jet is fixed, that of the other must be calculated by solving the complete set of ordinary differential equations [31] through [35]. Therefore, the problem must be solved theoretically before the proper experiment can be realized.
5. No Prandtl boundary layer assumption is necessary in order to solve the equations completely.

6. The problem is completely specified by:
   a. The stretching rate, ε, where this is calculated from the upstream velocity of one jet and the burner spacing.
   b. The inlet concentrations and temperatures of fuel and oxidant in each jet.

Further implications of the analysis above are discussed later in the context of theoretical predictions obtained.

Physical and Chemical Data

Reaction Mechanisms

The kinetic reaction mechanisms for formation of NO_x in methane flames was provided by Levy et al. (1979) and the reactions involved are listed in Table 1. When a wet CO flame was simulated, an appropriate subset of this mechanism was used; this subset is shown in Table 2.

The kinetic set includes pyrolysis reaction such as:

$$CH_4 + H = CH_3 + H_2$$

$$CH_4 + OH = CH_3 + H_2O$$

$$CH_4 + O = CH_3 + OH$$

which are necessary for the consumption of methane. Other reactions considered are chain branching reactions which are necessary in order to provide the free radicals for the chain propagation reactions. Finally,

Table 1. Methane Reaction Set.

CH_2O	+	M		=	CO	+	H_2	+ M
CHO	+	M		=	CO	+	H	+ M
CO_2	+	M		=	CO	+	O	+ M
CH_4	+	CH_2		=	CH_3	+	CH_3	
CH_4	+	H		=	CH_3	+	H_2	
CH_4	+	OH		=	CH_3	+	H_2O	
CH_4	+	O		=	CH_3	+	OH	
CH_3	+	OH		=	CH_2	+	H_2O	
CH_3	+	O		=	CH_2O	+	H	
CH_2	+	H		=	CH	+	H_2	
CH_2	+	OH		=	CH	+	H_2O	
CH_2	+	OH		=	CH_3	+	O	
CH_2	+	OH		=	CH_2O	+	H	
CH_2	+	H_2		=	CH_3	+	H	
CH_2	+	O		=	CHO	+	H	
CH_2	+	O_2		=	CH_2O	+	O	
CH	+	CO_2		=	CHO	+	CO	
CH	+	OH		=	CHO	+	H	
CH	+	O		=	CO	+	H	
CH	+	O_2		=	CHO	+	O	
CH_2O	+	H		=	CHO	+	H_2	
CH_2O	+	OH		=	CHO	+	H_2O	
CH_2O	+	O		=	CHO	+	OH	
CHO	+	HO_2		=	CH_2O	+	O_2	
CHO	+	O		=	CO	+	OH	
CO	+	OH		=	CO_2	+	H	
CO	+	O_2		=	CO_2	+	O	
H_2	+	M		=	H	+	H	+ M
OH	+	O	+ M	=	HO_2	+	M	
H	+	O_2	+ M	=	HO_2	+	M	
H_2O	+	M		=	OH	+	H	+ M
H	+	OH		=	H_2	+	O	
H	+	HO_2		=	OH	+	OH	
OH	+	H_2		=	H	+	H_2O	
OH	+	OH		=	H_2O	+	O	
OH	+	O		=	H	+	O_2	
HO_2	+	H		=	O_2	+	H_2	
HO_2	+	OH		=	H_2O	+	O_2	
HO_2	+	O		=	OH	+	O_2	
CH_4	+	CN		=	HCN	+	CH_3	
CH_3	+	HNO		=	CH_4	+	NO	
CH_2	+	N_2		=	HCN	+	NH	
CH_2	+	NO		=	CH_2O	+	N	
CHO	+	N		=	HCN	+	O	
HCN	+	OH		=	CN	+	H_2O	

Table 1, Continued.

HCN	+	N			=	CH	+	N2	
HCN	+	O			=	CH	+	NO	
CHO	+	N			=	CH	+	NO	
CN	+	CO2			=	NCO	+	CO	
CN	+	OH			=	NCO	+	H	
CN	+	H2			=	HCN	+	H	
CN	+	O			=	CO	+	N	
NCO	+	H	+			NH	+	CO	
CO	+	HNO			=	CO2	+	NH	
H	+	NO	+	M	=	HNO	+	M	
NO	+	O	+	M	=	NO2	+	M	
N2O	+	M			=	N2	+	O	+ M
H	+	HNO			=	H2	+	NO	
H	+	N2O			=	OH	+	N2	
H	+	N2O			=	NH	+	NO	
H	+	NO2			=	OH	+	NO	
HNO	+	OH			=	H2O	+	NO	
HNO	+	O			=	OH	+	NO	
HNO	+	O			=	NH	+	O2	
OH	+	N2O			=	HO2	+	N2	
N	+	OH			=	NO	+	H	
N	+	NO			=	N2	+	O	
N	+	O2			=	NO	+	O	
NH	+	H			=	N	+	H2	
NH	+	OH			=	H2O	+	N	
NH	+	OH			=	NO	+	H2	
NH	+	O			=	NO	+	H	
NH2	+	H			=	NH	+	H2	
NH2	+	OH			=	NH	+	H2O	
NH2	+	O			=	NH	+	OH	
NH2	+	O2			=	NH	+	HO2	
NH2	+	NH2			=	NH3	+	NH	
NH3	+	OH			=	NH2	+	H2O	
NH3	+	H			=	NH2	+	H2	
NH2	+	NO			=	N2	+	H2O	
NH3	+	O			=	NH2	+	OH	
NH3	+	O2			=	NH2	+	HO2	
NO	+	HO2			=	NO2	+	OH	

Table 2. Carbon Monoxide Reaction Set.

CO	+	OH		=	CO_2	+	H	
H_2O	+	M		=	OH	+	H	+ M
H	+	OH		=	H_2	+	O	
OH	+	H_2		=	H	+	H_2O	
OH	+	OH		=	H_2O	+	O	
OH	+	O		=	H	+	O_2	
H	+	O	+ M	=	OH	+	M	
N	+	OH		=	NO	+	H	
N	+	NO		=	N_2	+	O	
N	+	O_2		=	NO	+	O	
NH	+	H		=	N	+	H_2	
NH	+	OH		=	H_2O	+	N	
NH	+	OH		=	NO	+	H_2	
NH	+	O		=	NO	+	H	
NH_2	+	H		=	NH	+	H_2	
NH_2	+	OH		=	NH	+	H_2O	
NH_2	+	O		=	NH	+	OH	
NH_2	+	NH_2		=	NH_3	+	NH	
NH_3	+	OH		=	NH_2	+	H_2O	
NH_3	+	H		=	NH_2	+	H_2	
NH_2	+	NO		=	N_2	+	H_2O	
NH_3	+	O		=	NH_2	+	OH	

the reactions are terminated by the so-called chain termination reactions. The most important chain branching reactions are:

$$O + H_2 = H + OH$$

$$O + H_2O = OH + OH$$

$$H + O_2 = O + OH$$

the last reaction being the one responsible for the consumption of the oxygen. The chain termination reactions are typically recombination reactions of free radicals such as:

$$OH + HO_2 = H_2O + O_2$$

$$H + HO_2 = H_2 + O_2$$

$$H + OH + M = H_2O + M$$

$$H + H + M = H_2 + M$$

The time scales involved in combustion reactions are very different in that the chain branching reactions are typically very rapid in both directions and the chain termination and pyrolysis reactions are much slower. These differences in time scale cause the differential equations used to describe flames to be very stiff (Chan, Birnbaum, and Lapidus, 1978).

Transport Properties

The transport properties which are necessary in the solution of the model were estimated using correlations proposed by Reid and Sherwood (1958).

Diffusivities. The binary diffusion coefficient of species i diffusing in pure species j can be evaluated using the Chapman-Enskog relation, which gives:

$$D_{ij} = \frac{0.001858\ T^{3/2} \left[\frac{1}{M_i} + \frac{1}{M_j}\right]^{1/2}}{P\sigma_{ij}^{2}\Omega_D} \qquad [36]$$

where Ω_D is the collision integral for diffusion and is tabulated as a function of KT/ε_{ij}. The values of σ_{ij} and ε_{ij} can be evaluated as:

$$\sigma_{ij} = \frac{1}{2}(\sigma_i + \sigma_j) \quad \text{and} \quad \varepsilon_{ij} = \sqrt{\varepsilon_i \varepsilon_j} \qquad [37]$$

and σ_i and ε_i are parameters in the 6-12 Lennard-Jones potential function for species i.

For a mixture of more than two gaseous species, it is possible to evaluate a pseudo-binary diffusivity of species i in the rest of the mixture. The expression for this pseudo-binary diffusivity is:

$$D_A = D_{i,1,2,\ldots,n} = \frac{1 - y_i}{\sum_{\substack{j=1 \\ j\neq i}}^{n} \frac{y_j}{D_{ij}}} \qquad [38]$$

It has been shown (Fairbanks and Wilke, 1950) that this relation is valid at least for some mixtures.

Viscosities. The Chapman-Enskog expression for this property is:

$$\mu_i = 2.6693 \times 10^{-5} \frac{\sqrt{M_i T}}{\sigma_i^2 \Omega_\mu} \qquad [39]$$

where Ω_μ is the collision integral for viscosity and for thermal conductivity and is tabulated as a function of KT/ε_i. An approximate value of the viscosity of a mixture of gases can be obtained by the use of the following empirical formula:

$$\mu = \sum_{i=1}^{n} \frac{\mu_i}{1 + \sum_{\substack{j=1 \\ j \neq i}}^{n} \left(\frac{y_j}{y_i}\right) \phi_{ij}} \qquad [40]$$

with

$$\phi_{ij} = \frac{\left[1 + \left(\frac{\mu_i}{\mu_j}\right)^{1/2} \left(\frac{M_j}{M_i}\right)^{1/4}\right]^2}{2\sqrt{2}\left[1 + \frac{M_i}{M_j}\right]^{1/2}} \qquad [41]$$

Thermal Conductivities. The thermal conductivity of a pure gas can be evaluated from:

$$k_i = 1.9891 \times 10^{-4} \frac{(T/M_i)^{1/2}}{\sigma_i^2 \Omega_\mu} \qquad [42]$$

and the expression that allows the approximation for a mixture is:

$$k = \sum_{i=1}^{n} \frac{k_i}{1 + \sum_{\substack{j=1 \\ j \neq 1}}^{n} \frac{y_j}{y_i} G_{ij}} \qquad [43]$$

where

$$G_{ij} = 1.065 \frac{\left[1 + \left(\frac{k_i}{k_j} \right)^{1/2} \left(\frac{M_i}{M_j} \right)^{1/4} \right]^2}{2\sqrt{2} \left[1 + \frac{M_i}{M_j} \right]^{1/2}} \qquad [44]$$

Estimates of the parameters of the 6-12 Lennard-Jones potential function for each species were facilitated by the Energy and Environmental Research Corporation Staff (1979).

Numerical Solution

Equations [31] through [35] represent a system of simultaneous, stiff, non-linear, ordinary, second-order differential equations with mixed boundary conditions. Due to the non-linearity of the system, an analytical solution cannot be found and the use of a numerical iterative solution is necessary.

The approach chosen in the present work is to decouple the equations of continuity and momentum from the conservation of energy and species. The latter equations are solved iteratively in a fully implicit

manner. In each iteration step, the equation of momentum is solved implicitly and the equation of continuity is integrated using Simpson's rule, thus updating the values of the velocity profile.

Since it can be established a priori that the concentration and temperature gradients are not uniform, a collapsing grid (Figure 3) is used. The grid spacing is chosen to be coarse close to the burners, where the gradients are flat, and fine towards the center, where the flame front is expected to be located and the gradients are much steeper. The point around which the grid spacing is the finest is chosen to be the point where the temperature profile reaches its peak. The collapsing factor depends on the problem, but it should never exceed 10% because the unsymmetrical truncation error accumulates rapidly and makes the integration unstable if the grid is collapsed too rapidly (Kau, 1979).

After all the values corresponding to the unknown functions have been estimated on each one of the grid points, equations [34] and [35] are solved. Both equations can be written in a more general form as:

$$\frac{d^2C_i}{dz^2} + A_i(z)\frac{dC_i}{dz} + B_i(z)C_i = -R_i(z) \qquad [45]$$

with boundary conditions:

$$z = -1 \; ; \quad C_i = C_i^1$$

$$i = 1,2,\ldots,nsp+1 \qquad [46]$$

$$z = +1 \; ; \quad C_i = C_i^2$$

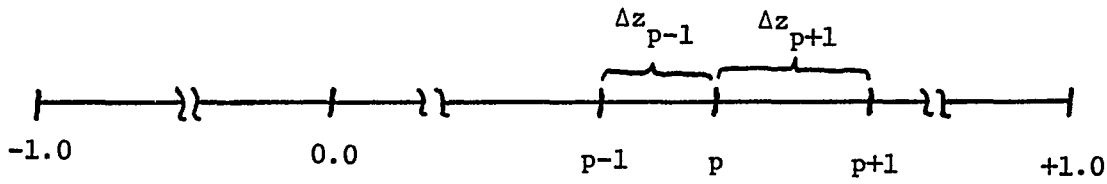

Figure 3. Collapsing Grid.

An explicit approach to solve equations [45] and [46] is to evaluate A_i, B_i, and R_i using values of a previous iteration and solve for C_i, thus decoupling the system of equations. This was tried but failed. Previous experience with a similar problem (Wendt and Schulze, 1976) also suggested that the shooting technique for solving boundary value problems would not work.

Tyson (1964) developed a technique for the solution of systems of stiff initial value problems in which the term $R_i(z)$ is expanded about the backward time step. This idea was later used by Wendt et al. (1979) to solve systems of stiff boundary value problems. They expand the term $R_i(z)$ in a Taylor Series about the backward iteration, giving:

$$R_i^{k+1}(z) = R_i^{k}(z) + \sum_{j=1}^{N} \left.\frac{R_i}{C_j}\right|^{k} (C_j^{k+1} - C_j^{k}) \qquad [47]$$

with N = nsp+1.

In addition to this expansion, the differentials can be expressed in central difference form. The formulas for the first and second derivatives in a collapsing grid are:

$$\frac{dC_i}{dz} = \frac{\Delta z_{p-1}}{\Delta z_{p+1}(\Delta z_{p+1} + \Delta z_{p-1})} C_{i,p+1} - \frac{\Delta z_{p-1} - \Delta z_{p+1}}{\Delta z_{p-1}\,\Delta z_{p+1}} C_{i,p}$$

$$- \frac{\Delta z_{p+1}}{\Delta z_{p-1}(\Delta z_{p+1} + \Delta z_{p-1})} C_{i,p-1} \qquad [48]$$

and

$$\frac{d^2C_i}{dz^2} = \frac{2}{\Delta z_{p+1} + \Delta z_{p-1}} \left[\frac{C_{i,p+1} - C_{i,p}}{\Delta z_{p+1}} - \frac{C_{i,p} - C_{i,p-1}}{\Delta z_{p-1}} \right] \qquad [49]$$

Substituting equations [47], [48], and [49] in equation [45], the following difference formula can be derived:

$$\alpha_{i,p} C_{i,p-1}^{k+1} + \beta_{i,p} C_{i,p}^{k+1} + \gamma_{i,p} C_{i,p+1}^{k+1} = - R_{i,p}^{k} - \sum_{j=1}^{N} \left. \frac{\partial R_i}{\partial C_j} \right|_p^k (C_{j,p}^{k+1} - C_{j,p}^{k}) \qquad [50]$$

with

$$\alpha_{i,p} = \frac{1}{\Delta z_{p-1}(\Delta z_{p+1} + \Delta z_{p-1})} [2 - \Delta z_{p+1} A_{i,p}] \qquad [51]$$

$$\beta_{i,p} = - \left[\frac{2}{\Delta z_{p+1} + \Delta z_{p-1}} \left(\frac{1}{\Delta z_{p+1}} + \frac{1}{\Delta z_{p-1}} \right) + \frac{(\Delta z_{p-1} - \Delta z_{p+1}) A_{i,p}}{\Delta z_{p+1} \Delta z_{p-1}} - B_{i,p} \right] \qquad [52]$$

and

$$\gamma_{i,p} = \frac{1}{\Delta z_{p+1}(\Delta z_{p+1} + \Delta z_{p-1})} [2 + \Delta z_{p-1} A_{i,p}] \qquad [53]$$

If the correction to the profiles is defined as:

$$\Delta C_{j,p} = C_{j,p}^{k+1} - C_{j,p}^{k} \qquad [54]$$

equation [50] becomes

$$\alpha_{i,p}\Delta C_{i,p-1} + \beta_{i,p}\Delta C_{i,p} + \gamma_{i,p}\Delta C_{i,p+1} = - R_{i,p}^{k}$$

$$- \sum_{j=1}^{N} \left.\frac{\partial R_i}{\partial C_j}\right|_p^k \Delta C_j - \alpha_{i,p} C_{i,p-1}^{k} - \beta_{i,p} C_{i,p}^{k}$$

$$- \gamma_{i,p} C_{i,p+1}^{k} \qquad (i = 1,2,\ldots,N)$$

$$(p = 1,2,\ldots,m) \qquad [55]$$

Equation [55] represents a set of N·m simultaneous algebraic equations for the values of the corrections $\Delta C_{i,p}$. The system can be rearranged, using matrix notation, as follows (Wendt et al., 1979):

$$(\alpha_{i,p};\ \beta_{i,p};\ \gamma_{i,p}) \begin{pmatrix} \Delta C_{i,p-1} \\ \Delta C_{i,p} \\ \Delta C_{i,p+1} \end{pmatrix} + \left[\frac{\partial R_i}{\partial C_j}\right]_p^k \begin{pmatrix} \Delta C_{1,p} \\ \Delta C_{2,p} \\ \vdots \\ \Delta C_{N,p} \end{pmatrix} = - F_{i,p} \qquad [56]$$

Equation [56] can be further rewritten as:

$$\left\{\begin{bmatrix} \alpha_1 & 0 & \cdots & 0 & \beta_1 & 0 & \cdots & 0 & \gamma_1 & 0 & \cdots & 0 \\ 0 & \alpha_2 & \cdots & 0 & 0 & \beta_2 & \cdots & 0 & 0 & \gamma_2 & \cdots & 0 \\ \vdots & \vdots & \ddots & \vdots & \vdots & \vdots & \ddots & \vdots & \vdots & \vdots & \ddots & \vdots \\ 0 & 0 & \cdots & \alpha_N & 0 & 0 & \cdots & \beta_N & 0 & 0 & \cdots & \gamma_N \end{bmatrix}_p^k\right.$$

$$\left. + \begin{bmatrix} \frac{\partial R_1}{\partial C_1} & \frac{\partial R_1}{\partial C_2} & \cdots & \frac{\partial R_1}{\partial C_N} \\ \frac{\partial R_2}{\partial C_1} & \frac{\partial R_2}{\partial C_2} & \cdots & \frac{\partial R_2}{\partial C_N} \\ \vdots & \vdots & \ddots & \vdots \\ \frac{\partial R_N}{\partial C_1} & \frac{\partial R_N}{\partial C_2} & \cdots & \frac{\partial R_N}{\partial C_N} \end{bmatrix}_p^k \right\} \begin{pmatrix} \Delta C_{1,p-1} \\ \Delta C_{2,p-1} \\ \vdots \\ \Delta C_{N,p-1} \\ \Delta C_{1,p} \\ \Delta C_{2,p} \\ \vdots \\ \Delta C_{N,p} \\ \Delta C_{1,p+1} \\ \Delta C_{2,p+1} \\ \vdots \\ \Delta C_{N,p+1} \end{pmatrix} = - \begin{pmatrix} F_{1,p} \\ F_{2,p} \\ \vdots \\ F_{N,p} \end{pmatrix} \qquad [57]$$

In order to simplify the notation, it is convenient to define the following matrices and vectors:

$$\underline{\underline{T}}_p = \begin{bmatrix} \alpha_1 & 0 & \cdots & 0 \\ 0 & \alpha_2 & \cdots & 0 \\ \vdots & \vdots & \ddots & \vdots \\ 0 & 0 & & \alpha_N \end{bmatrix}_p^k \quad ; \quad \underline{\underline{U}}_p = \begin{bmatrix} \gamma_1 & 0 & \cdots & 0 \\ 0 & \gamma_2 & \cdots & 0 \\ \vdots & \vdots & \ddots & \vdots \\ 0 & 0 & & \gamma_N \end{bmatrix} \qquad [58]$$

$$\underline{\underline{S}}_p = \begin{bmatrix} \beta_1 + \frac{\partial R_1}{\partial C_1} & \frac{\partial R_1}{\partial C_2} & \cdots & \frac{\partial R_1}{\partial C_N} \\ \frac{\partial R_2}{\partial C_1} & \beta_2 + \frac{\partial R_2}{\partial C_2} & \cdots & \frac{\partial R_2}{\partial C_N} \\ \vdots & \vdots & \ddots & \\ \frac{\partial R_N}{\partial C_1} & \frac{\partial R_N}{\partial C_2} & \cdots & \beta_N + \frac{\partial R_N}{\partial C_N} \end{bmatrix} \qquad [59]$$

$$\underline{\Delta C}_p = \begin{pmatrix} \Delta C_1 \\ \Delta C_2 \\ \vdots \\ \Delta C_N \end{pmatrix}_p \qquad \underline{F}_p = \begin{pmatrix} F_1 \\ F_2 \\ \vdots \\ F_N \end{pmatrix}_p \qquad [60]$$

Replacing equations [58], [59], and [60] in equation [57], we can write:

$$(\underline{\underline{T}}_p, \underline{\underline{S}}_p, \underline{\underline{U}}_p) \begin{pmatrix} \underline{\Delta C}_{p-1} \\ \underline{\Delta C}_p \\ \underline{\Delta C}_{p+1} \end{pmatrix} = - \underline{F}_p \qquad p = 1,2,\ldots,m \qquad [61]$$

The values of the vectors $\underline{\Delta C}_o$ and $\underline{\Delta C}_{N+1}$ which appear in this equation are the corrections to the boundary conditions and therefore they are identically zero.

Equation [61] represents a system of equations that can be arranged in a tridiagonal form of matrices as:

$$\begin{bmatrix} \underline{\underline{S}}_1 & \underline{\underline{U}}_1 & \underline{\underline{0}} & \cdots & \underline{\underline{0}} & \underline{\underline{0}} & \underline{\underline{0}} \\ \underline{\underline{T}}_2 & \underline{\underline{S}}_2 & \underline{\underline{U}}_2 & \cdots & \underline{\underline{0}} & \underline{\underline{0}} & \underline{\underline{0}} \\ \underline{\underline{0}} & \underline{\underline{T}}_3 & \underline{\underline{S}}_3 & \cdots & \underline{\underline{0}} & \underline{\underline{0}} & \underline{\underline{0}} \\ \vdots & \vdots & \vdots & \ddots & \vdots & \vdots & \vdots \\ \underline{\underline{0}} & \underline{\underline{0}} & \underline{\underline{0}} & \cdots & \underline{\underline{S}}_{m-2} & \underline{\underline{U}}_{m-2} & \underline{\underline{0}} \\ \underline{\underline{0}} & \underline{\underline{0}} & \underline{\underline{0}} & \cdots & \underline{\underline{T}}_{m-1} & \underline{\underline{S}}_{m-1} & \underline{\underline{U}}_{m-1} \\ \underline{\underline{0}} & \underline{\underline{0}} & \underline{\underline{0}} & \cdots & \underline{\underline{0}} & \underline{\underline{T}}_m & \underline{\underline{S}}_m \end{bmatrix} \begin{bmatrix} \underline{\Delta C}_1 \\ \underline{\Delta C}_2 \\ \underline{\Delta C}_3 \\ \vdots \\ \underline{\Delta C}_{m-2} \\ \underline{\Delta C}_{m-1} \\ \underline{\Delta C}_m \end{bmatrix} = - \begin{bmatrix} \underline{F}_1 \\ \underline{F}_2 \\ \underline{F}_3 \\ \vdots \\ \underline{F}_{m-2} \\ \underline{F}_{m-1} \\ \underline{F}_m \end{bmatrix} \qquad [62]$$

which can be expressed as:

$$\underline{\underline{A}}\ \underline{\Delta C}^* = - \underline{F}^* \qquad [63]$$

The block tridiagonal matrix $\underline{\underline{A}}$ is also a band matrix and, therefore, the solution to [63] can be obtained employing an LU decomposition, which is a very efficient method for this type of problem (Peaceman, 1977).

This method of solving a set of linear algebraic equations is based on the factorization of the matrix $\underline{\underline{A}}$ into a lower and an upper triangular band matrix such that:

$$\underline{\underline{A}} = \underline{\underline{L}}\ \underline{\underline{U}} \qquad [64]$$

Introducing this definition into equation [63], it can be rewritten as:

$$\underline{\underline{L}}\ \underline{\underline{U}}\ \underline{\Delta C}^* = - \underline{F}^* \qquad [65]$$

If $\underline{G}$ is defined as:

$$\underline{\underline{U}}\ \underline{\Delta C}^* = \underline{G} \qquad [66]$$

then

$$\underline{\underline{L}}\ \underline{G} = -\ \underline{F}^* \qquad [67]$$

and

$$\underline{\underline{U}}\ \underline{\Delta C}^* = \underline{G} \qquad [68]$$

Since $\underline{\underline{L}}$ and $\underline{\underline{U}}$ are triangular, the solution of equations [67] and [68] is straightforward. Equation [67] is referred to as the forward solution and equation [68] is the backward solution.

Once $\underline{\Delta C}^*$ is found from equation [63], the new values of the concentration and temperature profiles are obtained by adding these corrections to the previous values. The stiff and nonlinear nature of the problem forced the use of successive under-relaxation, i.e., $\Delta C = \lambda \Delta C^*$. The factor λ used started with a value of 1/8 and was increased by a factor of 2 every 5 iterations, but was not allowed to exceed unity, when the initial guess was a previously converged solution.

If the initial guess was an arbitrary initial profile, the factor λ started with a value of 0.001 and after every 20 iterations the intermediate profiles were examined and the value of λ reset according to the relative magnitude of the corrections in the last iteration. Future work in this area will allow incorporation of an automatic reset of λ in the program itself.

After corrected values for x_A and θ are obtained from the solution of equations [34] and [35], the r momentum equation [32] can be

solved to get a better estimate of the values of ψ. Since its third term is non-linear, the equation is linearized in the form:

$$\frac{d^2\psi^{n+1}}{dz^2} + \left(\frac{1}{\mu}\frac{d\mu}{dz} - \frac{\rho v \ell}{\mu}\right)\frac{d\psi^{n+1}}{dz} - \frac{a\ell^2\rho\psi^n}{\mu}\psi^{n+1} = -\frac{a\rho_\infty\psi_\infty{}^2\ell^2}{\mu} \qquad [69]$$

and the solution is found iteratively. If equation [69] is symbolically written as:

$$\frac{d^2\psi^{n+1}}{dz^2} + A(z)\frac{d\psi^{n+1}}{dz} + B(z)\psi^{n+1} = -C(z) \qquad [70]$$

it has the same form as equation [45] and, therefore, after expressing the differentials in central differences, it yields:

$$\alpha_p\psi_{p-1}{}^{n+1} + \beta_p\psi_p{}^{n+1} + \gamma_p\psi_{p+1}{}^{n+1} = -C_p \qquad [71]$$

with α, β, and γ being defined by equations [51], [52], and [53], respectively. Equation [71] is solved using the tridiagonal matrix algorithm until the values of ψ^{n+1} converge. The corrected values of θ and ψ can then be used to integrate the continuity equation [31] applying Simpson's rule. The formula for this integration rule, in a collapsing grid, is derived by replacing the derivative in equation [31] by its expansion in central differences and then calculating $(\rho v)_{p+1}$ from it as:

$$(\rho v)_{p+1} = \frac{\Delta z_{p+1}(\Delta z_{p+1} + \Delta z_{p-1})}{\Delta z_{p-1}} \left[- C_p + \frac{\Delta z_{p-1} - \Delta z_{p+1}}{\Delta z_{p-1}\, \Delta z_{p+1}} (\rho v)_p \right.$$

$$\left. + \frac{\Delta z_{p+1}}{\Delta z_{p-1}(\Delta z_{p+1} + \Delta z_{p-1})} (\rho v)_{p-1} \right] \qquad [72]$$

Equation [72] requires two previous points of the function (ρv) to be known in order to calculate a third one. The second point for the first step is found by applying Euler's method, which gives:

$$(\rho v)_1 = (\rho v)_o - \Delta z_1 2 \varepsilon \rho_\infty \psi_\infty \ell \qquad [73]$$

The error introduced by estimating $(\rho v)_1$ with this method is negligible, since far away from the flame front the function (ρv) is indeed linear with z.

CHAPTER 4

EXPERIMENTAL

A laboratory-scale, opposed jet burner, shown in Figure 4, was designed and constructed. It was then used to obtain the data necessary in the calibration and verification of the theoretical model of the Opposed Jet Diffusion Flame. Some experiments were also devoted to demonstrating the effect that the rate of stretching has on the rate of formation of NO.

Combustor

A schematic of the combustor and its feed lines is shown in Figure 5. Metered amounts of fuel (CH_4 or CO; Matheson, C.P. grade), oxygen and nitrogen are mixed and fed to the two opposing burners through Teflon tubing. The flow rate of these gases is measured with critical flow orifices of size ranging from 0.003 to 0.025 inches.

Nitrogen contained in the fuel is simulated in these experiments by the addition of anhydrous ammonia to the fuel stream. The flow rate of this additive is too low to allow the use of a critical orifice and it was measured with a restriction and an inclined differential manometer. The fluid used in the manometer was a light oil, which did not absorb ammonia to a measurable extent.

The combustion chamber is a 2x2x2-ft, sealed aluminum box which contains the two vertically mounted opposed burners, an uncooled quartz probe, I.D. = 0.06 cm, a platinum ignition wire, and a Pt, Pt/10% Rh

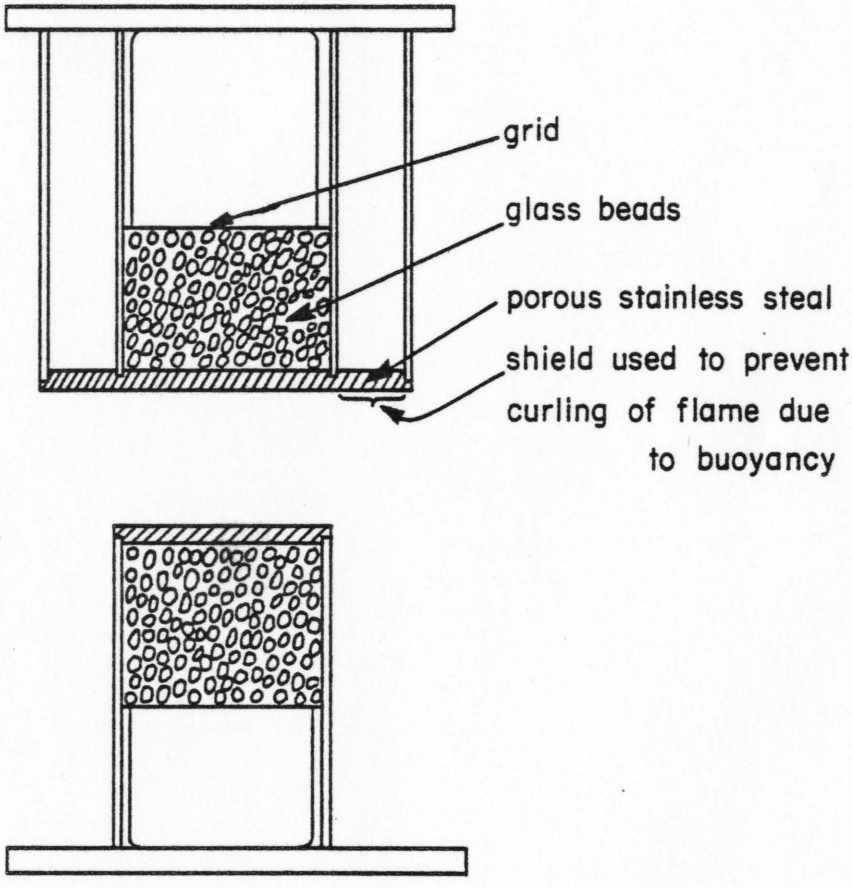

Figure 4. Opposed Jet Burners.

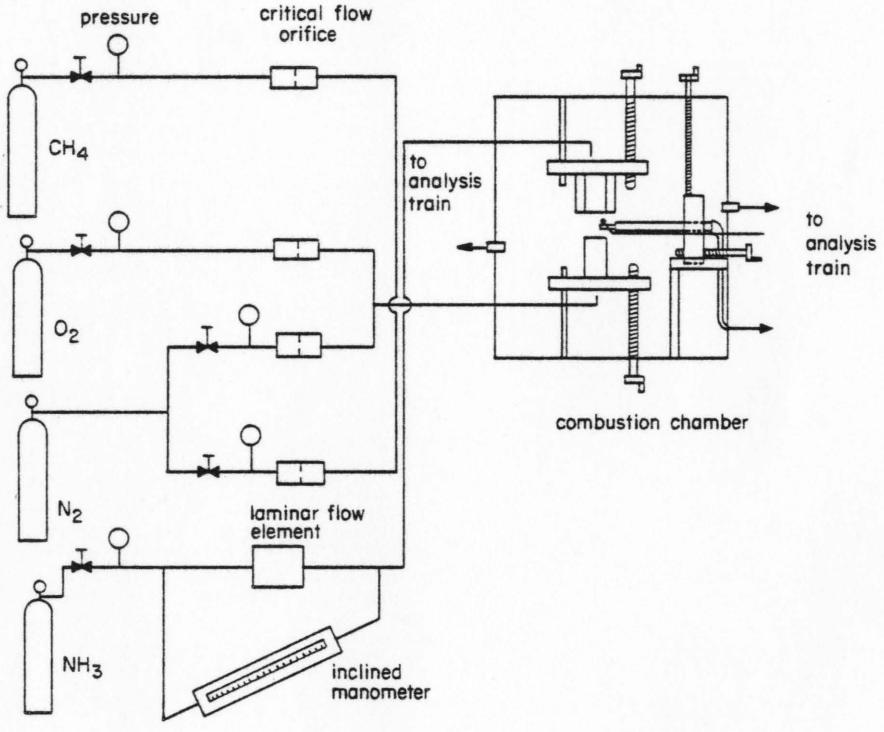

Figure 5. Combustor and Feed Lines.

thermocouple, which is mounted on the probe. The head of this thermocouple is approximately 0.006 inches in diameter and is uncoated. The two burners, shown in Figure 4, are made of 2.5-inch diameter stainless steel tubes which are filled with glass beads and sealed at the ends with a stainless steel porous disk. The function of the glass beads is to randomize the flow pattern of the gases, avoiding the formation of a velocity profile in the burners. The burners are mounted on independent screws so that their separation and positioning with respect to the sample probe can be easily altered, while two gliding bars on each burner keep them aligned within 0.25 cm.

The quartz probe, shown on Figure 6, is mounted together with the thermocouple on a two-dimensional traversing mechanism, making it possible to obtain vertical and radial concentration and temperature profiles.

Analysis

A schematic of the analysis train is shown in Figure 7. The sample is drawn with a vacuum pump at a rate at which no visual disturbance, due to sampling, is observed in the flame (approximately 0.13 l/min), which represents a residence time of 7 msec in the tip of the probe, before the sample is quenched. Although it would be desirable to have a shorter residence time, it is thought that the present probe is a reasonable compromise between probe effects and disturbances the probe could cause on the flame. The sample lines are kept warm and water contained in the sample is condensed in a flask immersed in an ice bath only after passing through the gas chromatograph sampling loop. The

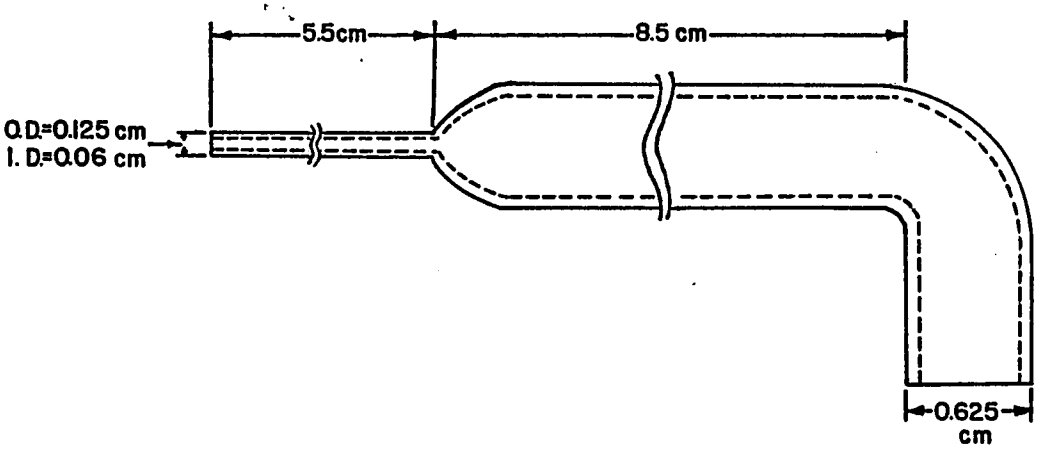

Figure 6. Uncooled Probe.

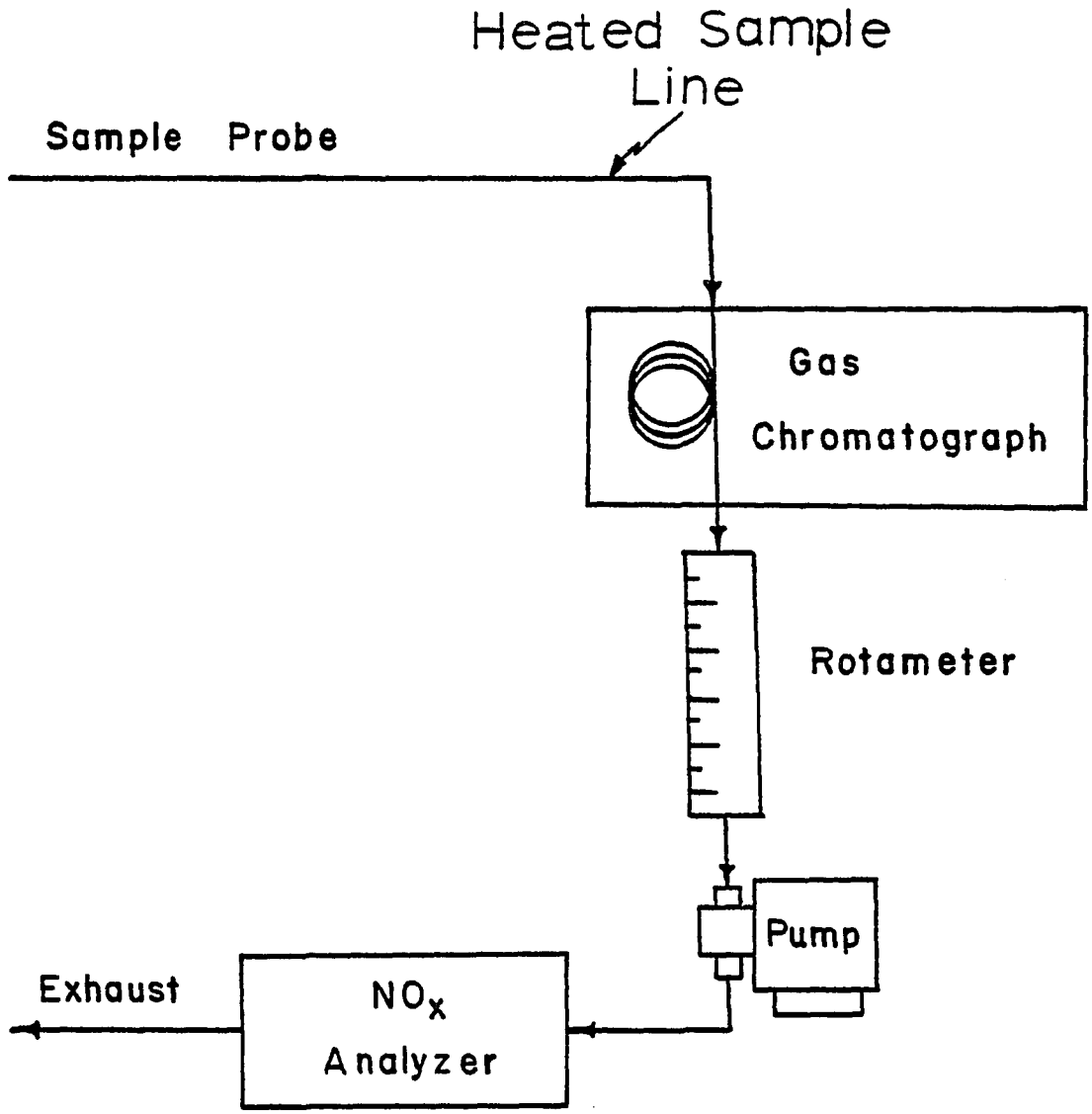

Figure 7. Analysis Train.

sample loop is filled at the same time that the sample flows through the Termo Electron Model 10-A, self-contained, Chemiluminescent NO/NO_x analyzer with stainless steel and molybdenum converters. It is assumed that when the NO reading reaches equilibrium the sample loop is filled and the gas contained in it can be pressurized to a standard pressure, in this case 15 psig, and then injected into a Perkin Elmer, Sigma II Gas Chromatograph, where it is analyzed for CO, CO_2, O_2, H_2, H_2O, and HCN, using a 10-ft mole sieve and a 6-ft Porpak T column. The oven temperature was set at 110°C and the carrier gas was 0.999999 helium at a flow rate of 10 ml/min. The sensors used were a hot wire detector and a nitrogen-phosphorus detector. Details of the gas chromatographic procedure can be found elsewhere (Wootan, In prep.).

Procedure

Care has to be taken during the ignition of the Opposed Jet Diffusion Flame so that the aluminum box does not contain an explosive mixture of gases left over from a previous experiment. In addition, if any O_2 is present in the box before igniting the flame, it causes the flame to destablize and flicker. To avoid both situations, the box is initially filled with nitrogen, and oxygen readings are taken. When the oxygen content of the box is less than 1%, the platinum ignition wire is placed between the burners and an electric current is applied to it. The temperature of the wire must be greater than 1500°K. Next, the flows of fuel and oxygen are turned on and when the flame is stabilized, the ignition wire is removed and turned off.

Samples of exhaust gas are drawn through ports mounted in the walls of the aluminum box at intervals of 10 minutes. It is assumed that when the concentrations of the exhaust gas reach an asymptotic value the flame is in steady state. Once this is achieved, the probe is placed on one side of the flame at a radial position different from the centerline. It is desirable to place the probe at the greatest possible radial distance from the centerline, to sample as isokinetically as possible, without placing it in that region where the edge effects of the finite jets become important. After placing the probe in the flame, the readings on the NO meter are observed and it is assumed that the entire sample line is filled with a homogeneous mixture when the readings on the NO meter reach an asymptotic value. At this moment, the sample is injected into the gas chromatograph and while it elutes the probe is moved 1 mm in the vertical direction and the sample line is filled with gases drawn from the new probe position. Simultaneously, a temperature reading is taken with the thermocouple.

After a complete profile of the flame is obtained, the flame is shut down by turning the gases off and the box is drained of combustion products and unburned reactants by purging it with nitrogen.

CHAPTER 5

THE CARBON MONOXIDE OPPOSED JET DIFFUSION FLAME

Introduction

In this chapter, the solution of the model for a wet CO flame is presented and compared with experimental data to validate the model. Also, special details of the numerical procedure required for solution of this specific problem are outlined.

The formation of NO is studied by injecting anhydrous ammonia into the flame with the fuel or the oxidizer stream. The predicted profiles of NO are compared to experimental results.

Finally, further theoretical predictions, such as profile of some stable species and free radicals, which were not measured in the experiments, and the effect of the rate of stretching on the heat release profile and the rate of formation of NO are presented and discussed.

The set of chemical reactions used is shown in Table 2. It consists of 22 reactions among 13 different chemical species. The mole fractions of fuel (from upper burner, $z' = -1.5$ cm) and oxygen (from lower burner, $z' = +1.5$ cm) were $x_{CO} = 0.362$ and $x_{O_2} = 0.191$, respectively; the fuel stream was saturated with water ($x_{H_2O} = 0.03$); and the balance in both flows was nitrogen.

For the data presented here, the burners were separated by a distance of 3 cm and the flow rate at the top burner was set at 20 l/min (10.9 cm/sec), which corresponds to a stretching rate of

7.24 sec^{-1}. The flow rate at the bottom burner was set at that predicted from the computer simulation and was 9.4 1/min, i.e., 5.10 cm/sec.

Numerical Solution

The initial guess employed for the solution of the differential equations was the solution of the equivalent Burke-Schuman flame, i.e., infinitely fast reactions were assumed. This approach provided the profiles of CO, O_2, CO_2, and temperature. At the center of the grid, the mole fractions of products and free radicals were arbitrarily set at $x_{H_2O} = 0.003$, $x_H = 0.23 \times 10^{-4}$, $x_O = 0.23 \times 10^{-4}$, and $x_{OH} = 0.23 \times 10^{-3}$.

During 400 iterations, the approach suggested by Wendt et al. (1979) was followed in that all but the diagonal elements of the Jacobian in the Taylor series expansion, given by equation [47], were neglected. In this manner, the differential equations were decoupled and could be solved using the tridiagonal algorithm (Carnahan, Luther, and Wilkes, 1969). An under-relaxation factor of 0.5 was used during these first iterations. Subsequently, the full Jacobian was considered and the solution converged with 25 additional iterations. The under-relaxation factor was initially 0.5 and was set equal to 1.0 after 10 iterations, i.e., no under-relaxation was necessary during the last 15 iterations. The 35-point grid used in this calculation is shown in the lower section of Figure 8.

It is of interest to note that the presence of ammonia in the flame does not affect the profiles of the major species and temperature. Only the concentration of some free radicals are affected slightly.

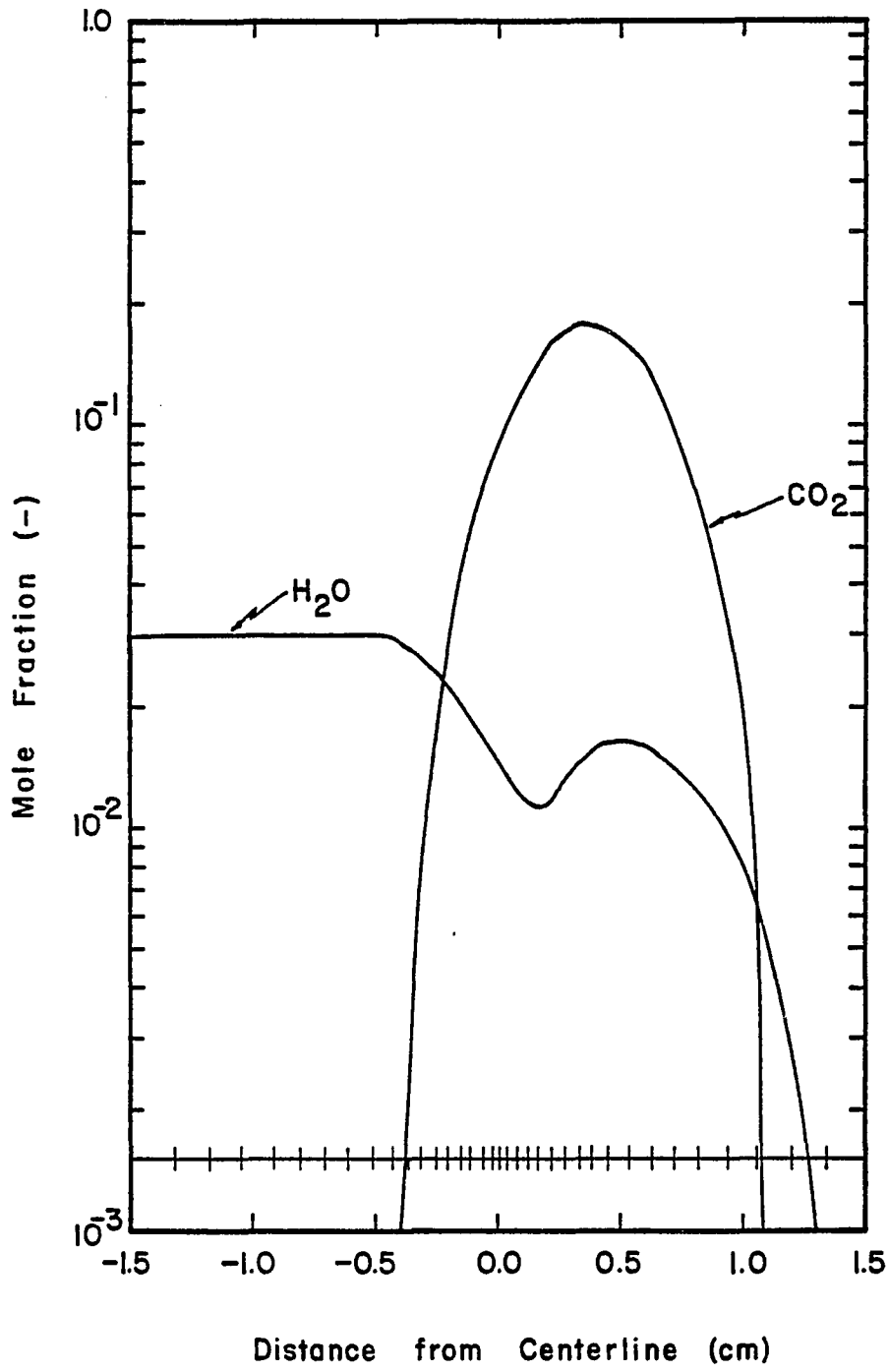

Figure 8. $CO/N_2/O_2$ Flame: $\varepsilon = 7.24\ sec^{-1}$, H_2O and CO_2 Profiles.

This suggests that if the flame is first simulated without considering nitrogen species and a much reduced reaction set, and the profiles so produced are used as initial guess for the solution of the entire set of reactions, then a considerable amount of computer time can be saved.

Model Validation

Figure 9 shows the predicted and measured profiles of CO and O_2. The experimental flame appears to be shifted approximately 2.5 mm towards the fuel-lean side. This same phenomenon can be observed on Figure 10, where the predicted and measured temperature profiles are shown. The temperature, measured with a thermocouple, was corrected for radiation heat losses using the following expression (Fristrom and Westenberg, 1965):

$$T_g = T_c + \frac{5.67 \times 10^{-5} \, d(T_c^4 - 298^4)}{2 \times 10^4} \qquad [74]$$

The diameter of the thermocouple head was estimated to be 0.015 cm.

The shift of the experimental results with respect to the theoretical predictions can be attributed to a variety of factors, some of which are: errors in the estimation of the diffusion coefficients of some free radicals, errors in the kinetic information of some of the key reactions in the mechanisms, and the assumption of an adiabatic flame.

The abscissa of Figure 10 is expanded in Figure 11 and the experimental values are plotted 2.5 mm to the left of the location where they were measured. The values shown in this figure correspond to

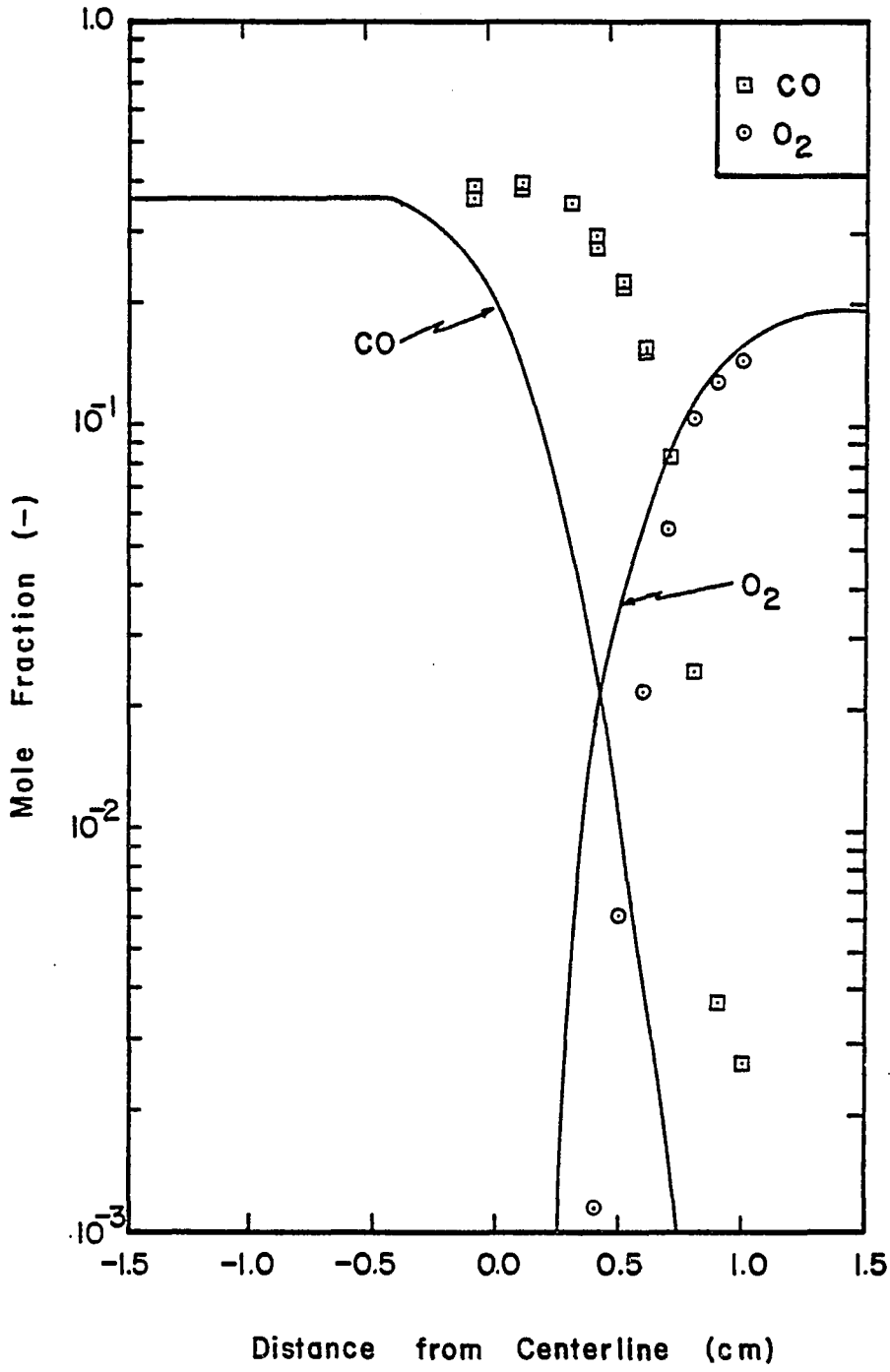

Figure 9. $CO/N_2/O_2$ Flame: $\varepsilon = 7.24\ sec^{-1}$, CO and O_2 Profiles (Experimental Values Not Shifted).

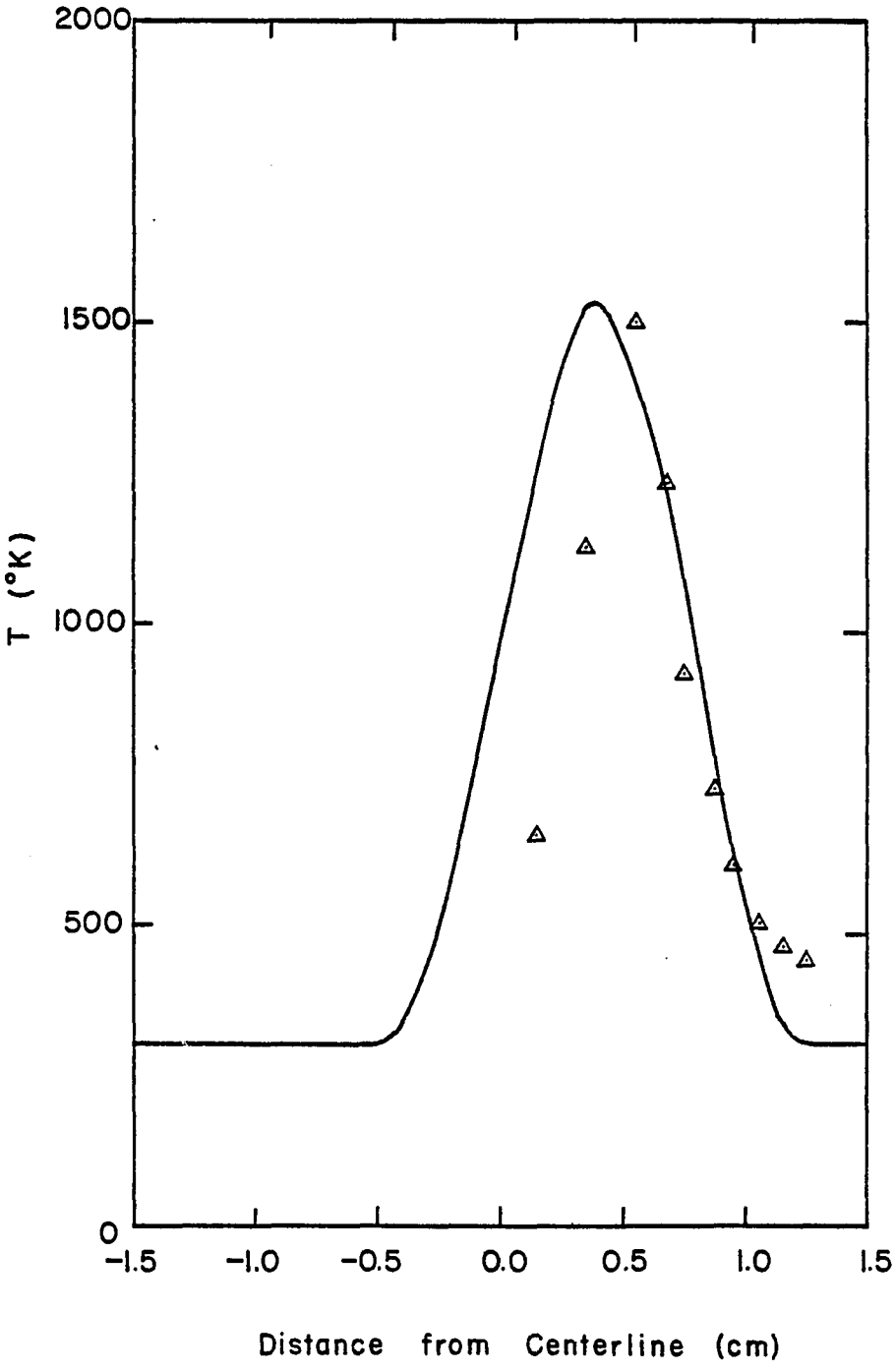

Figure 10. $CO/N_2/O_2$ Flame: $\varepsilon = 7.24\ sec^{-1}$, Temperature Profile (Experimental Values Not Shifted).

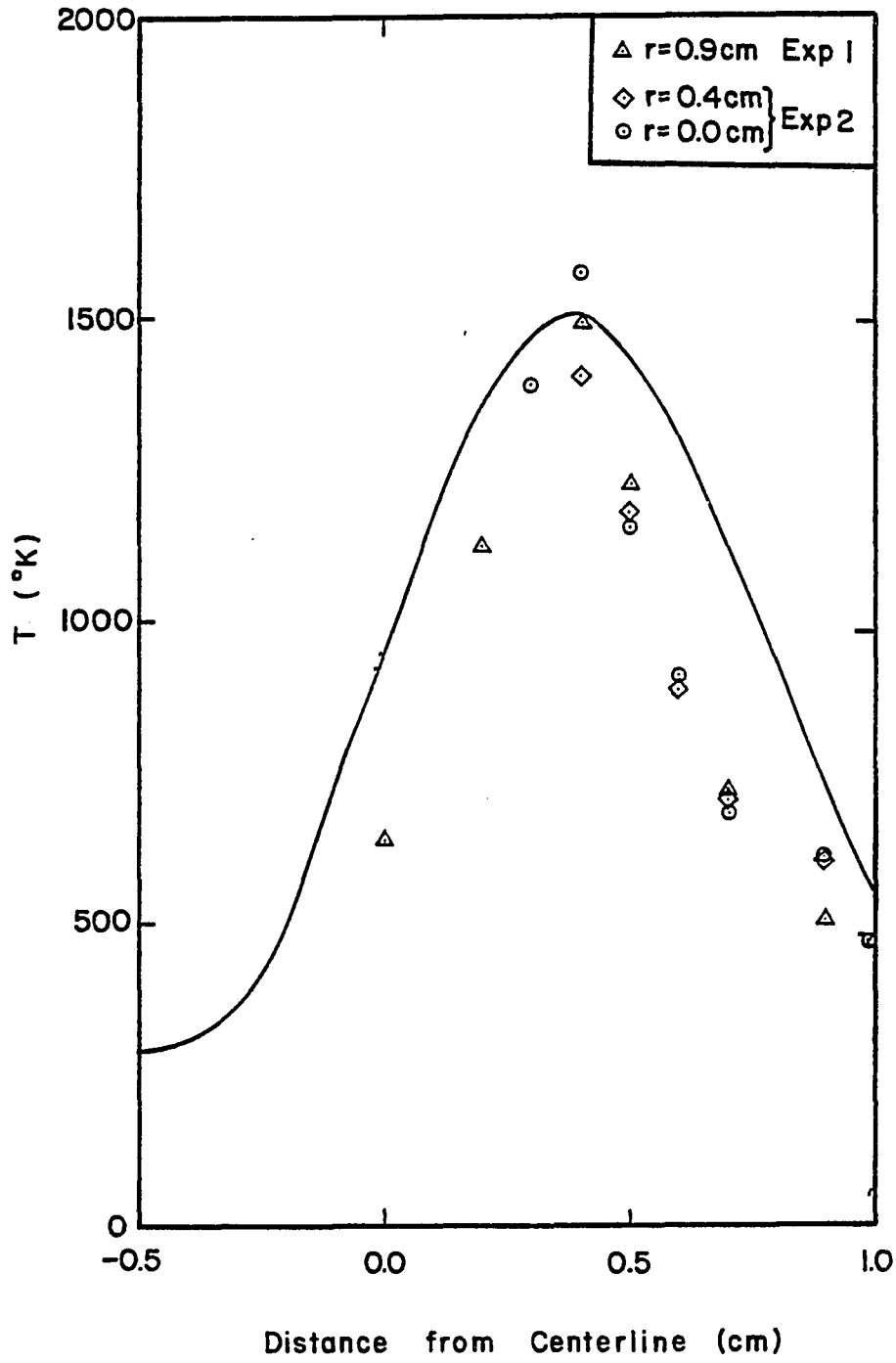

Figure 11. $CO/N_2/O_2$ Flame: $\varepsilon = 7.24\ sec^{-1}$, Temperature Profile (Two Experiments, Experimental Values Shifted).

temperatures obtained in two independent experiments and at three different radial positions. In Experiment 1, temperature and species profiles were obtained at a distance of 9 mm from the centerline. In Experiment 2, the same profiles were obtained at a distance of 4 mm from the centerline and temperatures were measured at the centerline. Species profiles were not measured at the centerline, since isokinetic sampling there is not possible (the radial velocity vanishes at the centerline). Figure 12 shows the CO and O_2 profiles corresponding to experiments 1 and 2.

The experimental data presented above demonstrate the reproducibility of the experiment and the one-dimensional nature of the flame. Although the agreement between experiment and theory is not perfect, the thickness of the reaction zone, which is a key parameter in the rate of formation of NO_x and other trace species, is very closely matched.

The predicted axial velocity profile is drawn on Figure 13 and it can be observed that it is linear near the burners and non-linear in the flame zone, where temperature effects become important. The velocity at $z' = -1.5$ cm was the specified boundary condition while the velocity at $z' = +1.5$ cm was a result of the computer simulation. Velocity measurements were not made in this work. Rather, recourse is made to qualitative comparison with literature data. Figure 14 represents the velocity profile measured by Pandya and Weinberg (1964) and it also shows that if a solid line is drawn through the experimental data instead of their dashed line, their profile agrees qualitatively with that shown on

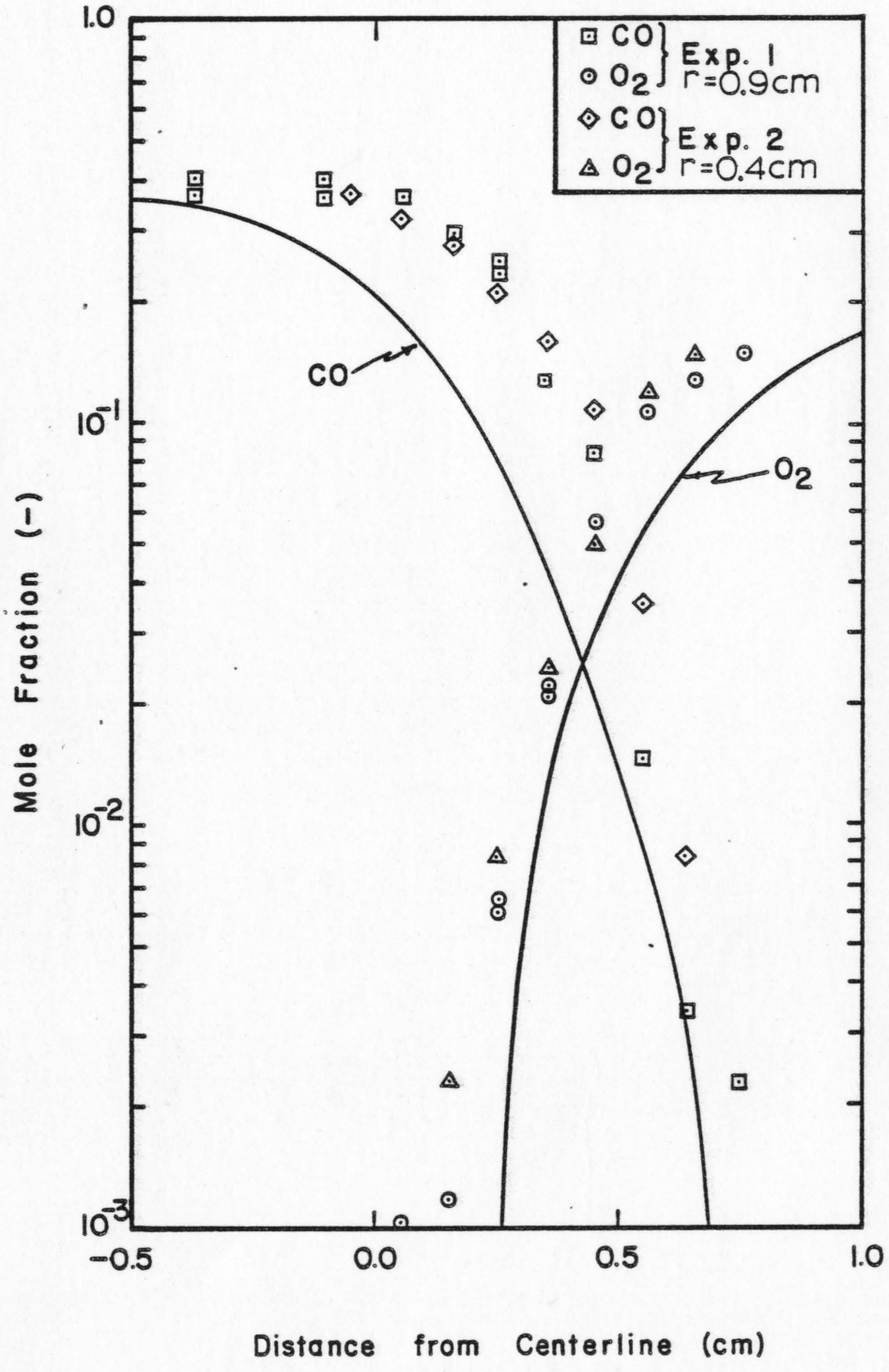

Figure 12. $CO/N_2/O_2$ Flame: $\varepsilon = 7.24\ sec^{-1}$, CO and O_2 Profiles (Two Experiments, Experimental Values Shifted).

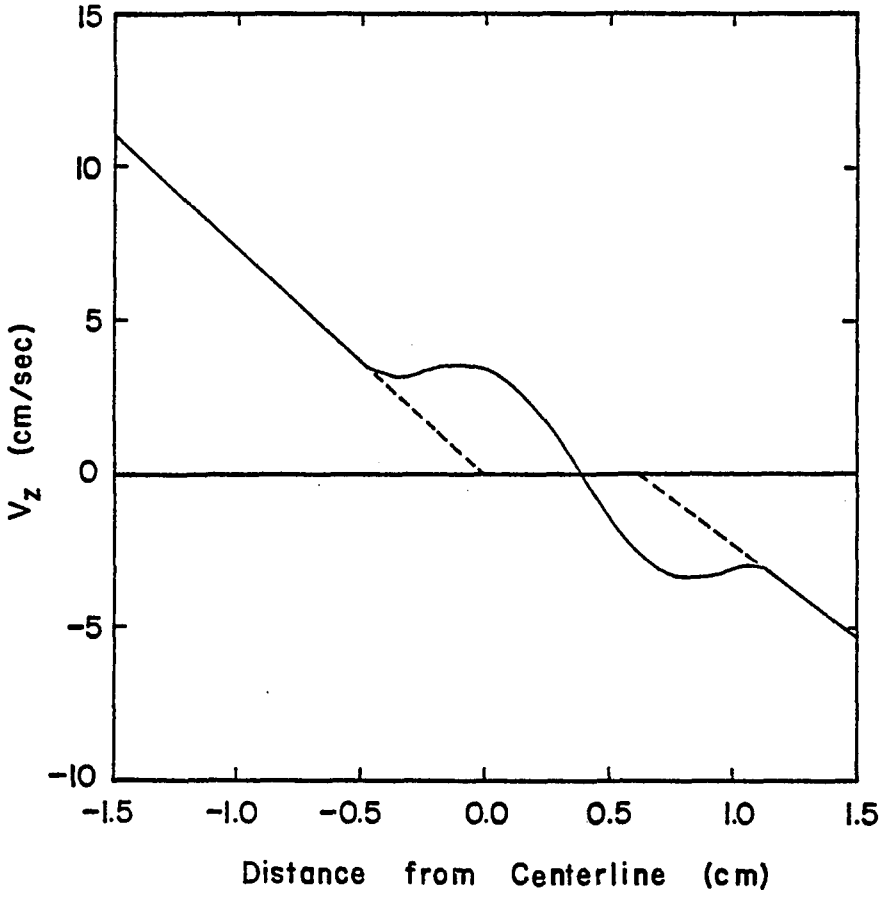

Figure 13. $CO/N_2/O_2$ Flame: $\varepsilon = 7.24\ sec^{-1}$, Velocity Profile.

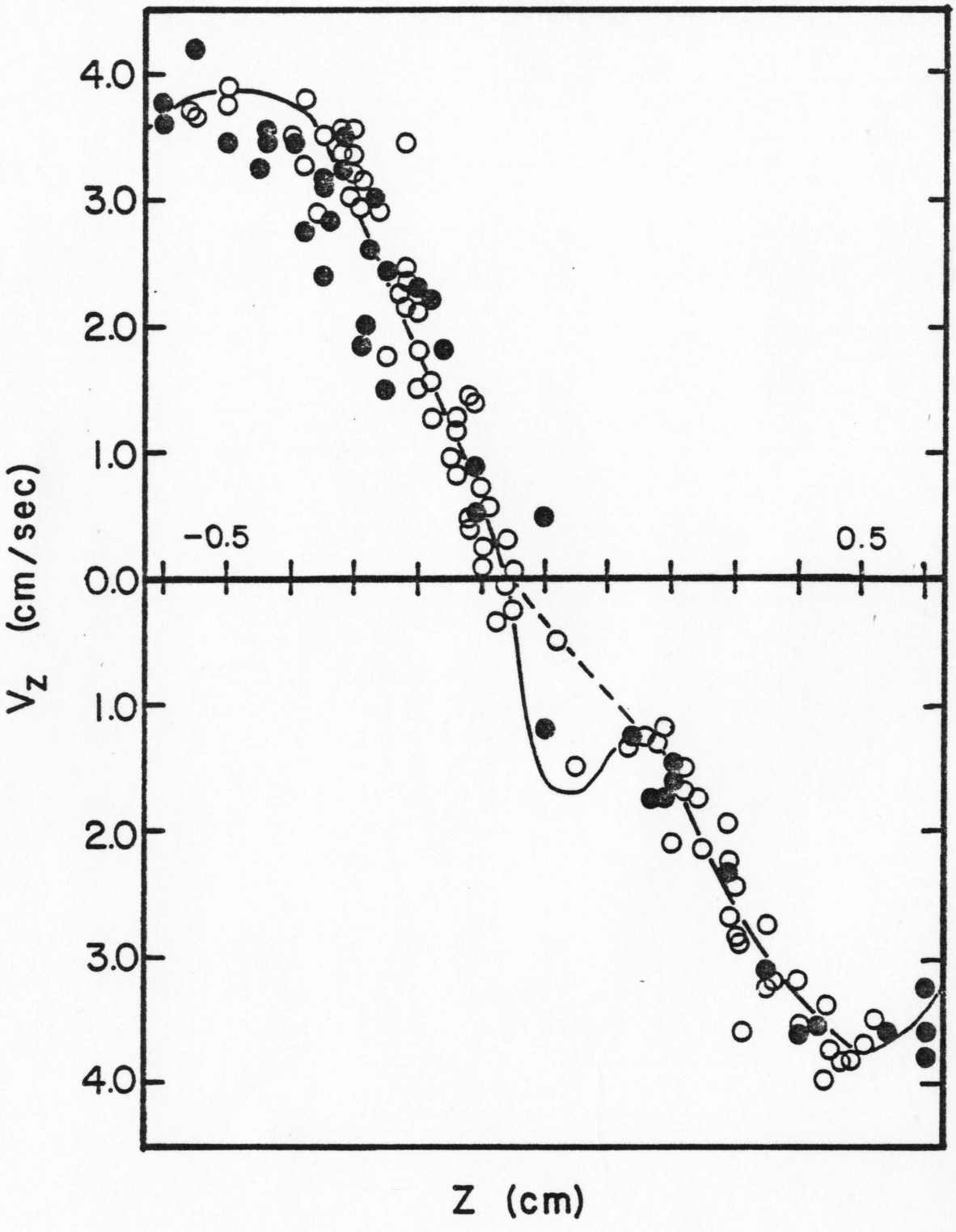

Figure 14. Velocity Profile Measured by Pandya and Weinberg (1964).

Figure 13. This indicates that the points which Pandya and Weinberg interpreted as scatter in the experimental results might have been correct measurements, and that the velocity profiles predicted in this work have qualitatively the correct shape.

From the evidence presented above, the following conclusions can be drawn:

1. It is possible experimentally to create a laminar opposed jet diffusion flame that is (mathematically) flat and that can be modeled using the theory developed in Chapter 3.
2. The experimental data obtained are reproducible.
3. As predicted by theory, the Laminar Opposed Jet Diffusion Flame is one-dimensional, with respect to species concentrations and temperature in the neighborhood (3/4 diameter of burner axis of symmetry).
4. The thickness of the reaction zone is well-modeled.
5. Temperature peak is very well predicted.
6. The predicted velocity profile agrees qualitatively with that measured by Pandya and Weinberg (1964).

Nitric Oxide Formation

Ammonia in the Fuel

Figure 15 represents the profile of NO when a mole fraction of 0.00362 (1% of the fuel) of anhydrous ammonia is injected with the fuel stream. Again, the experimental results are shifted 2.5 mm towards the fuel-rich side of the flame on the plot. Theory and experiment agree in

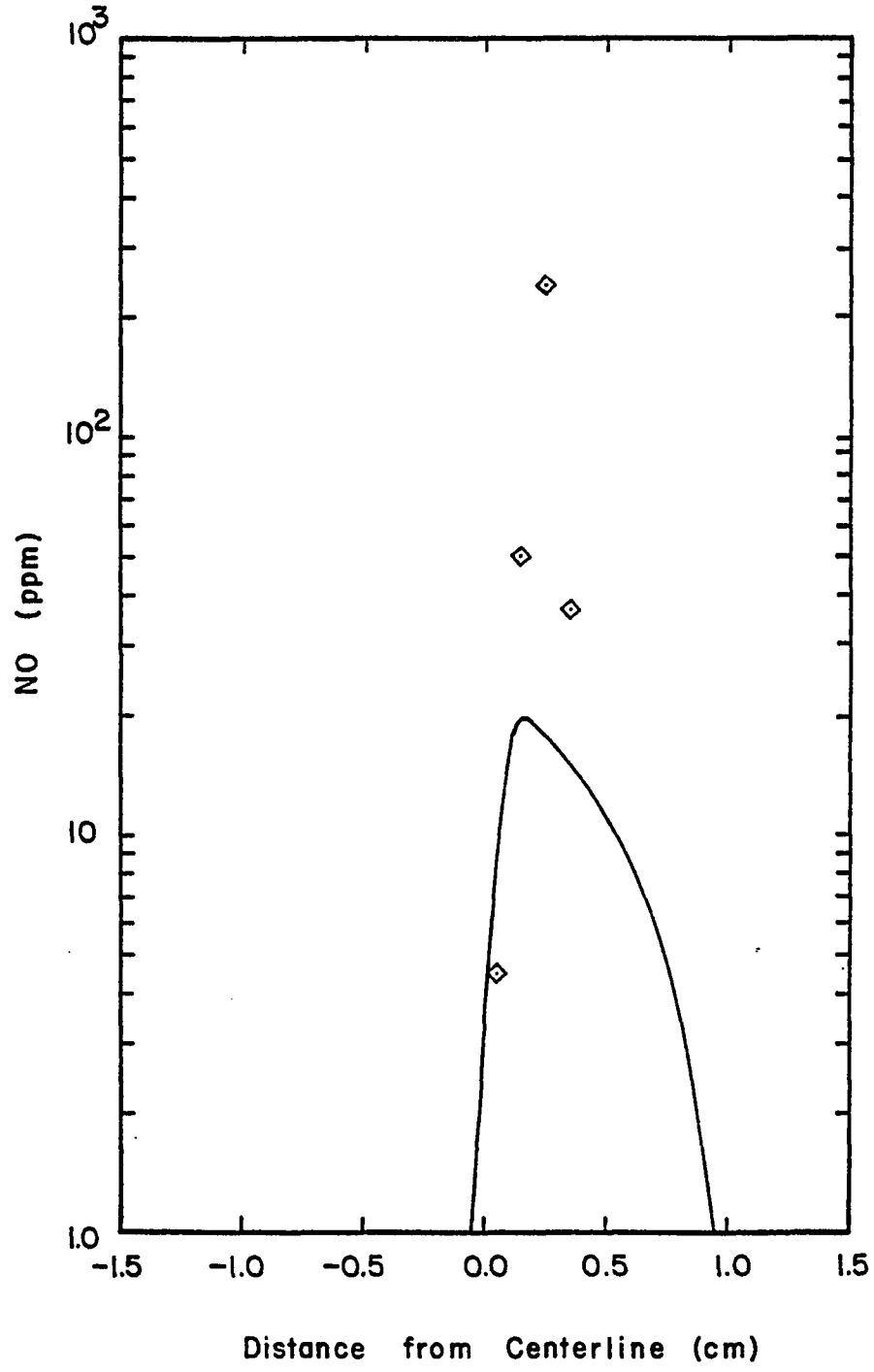

Figure 15. $CO/N_2/O_2$ Flame: $\varepsilon = 7.24\ sec^{-1}$, NO Profile (One Experiment, NH_3 Injected from Fuel Side).

the location at which NO appears on the fuel-rich side, but do not agree in the peak height or in the thickness of the region where NO exists. Theory predicts the peak to be much lower and broader than the peak measured in the laboratory. This disagreement may be caused by an error in predicting the location of the flame zone and a subsequent error in the prediction of the velocity profile. In this work, the velocity is predicted positive between -1.5 and +0.4 mm and the NO peak is located +0.15 mm. The positive value of the velocity causes the NO to convect into the fuel-lean side of the flame, giving rise to the slow decay of the NO concentration on that side of the peak. If the peak of the NO concentration is located at +0.5 mm, as was measured in the laboratory, it would be located near the stagnation point and the profile would decay much sharper. Another possible explanation of the disagreement is that the reaction mechanisms used to simulate the oxidation of fuel nitrogen in environments containing high concentrations of CO is not very well known, and some of the kinetic information may be erroneous.

Figure 16 shows the peak concentration of NO as a function of the concentration of ammonia in the fuel. Agreement between theory and experiment is only qualitative, the sharp discontinuity of the NO curve observed in the laboratory is only represented by a much less pronounced change of slope in the theoretical curve. This "break through" phenomenon can be explained by the shift that occurs in the actual flame, which moves the reaction zone towards the fuel-lean side of the flame; thus, the NH_i species come in contact with much higher

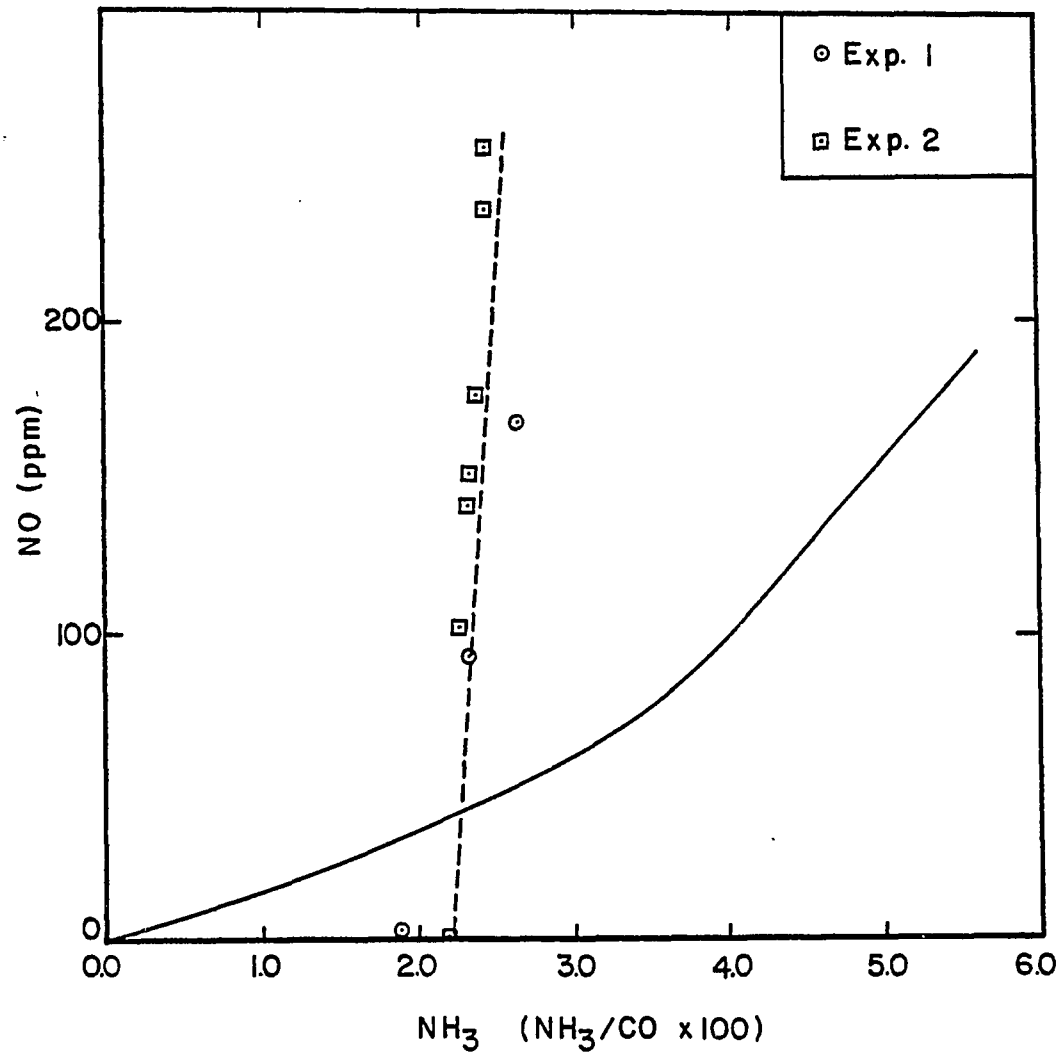

Figure 16. $CO/N_2/O_2$ Flame: $\varepsilon = 7.24\ sec^{-1}$, Effect of NH_3 Concentration in Fuel on Peak NO (Two Experiments, NH_3 injected from Fuel Side).

concentrations of oxygen containing radicals than is predicted by the theoretical model.

Ammonia in the Oxidizer

Figures 17 and 18 represent the NO profiles when a mole fraction of 0.00191 of ammonia is injected into the flame with the oxidizer. Figure 17 shows the experimental values as measured while Figure 18 shows them shifted 2.5 mm towards the fuel-rich side of the flame. In the last figure, the abscissa has been expanded. In both figures, it can be observed that the experimental values representing the peak height and its width are in excellent agreement with the computer simulation. This indicates that if some kinetic information in the reaction set representing the formation of NO is erroneous it is in the reactions that become important under fuel-rich conditions, namely the pyrolysis reactions.

The following conclusions can be drawn from the results presented above:

1. Theory and experiment do not agree when the ammonia is injected with the fuel. This can be explained through the shifting of the flame or erroneous information in the reactions representing the pyrolysis of ammonia or a combination of both.
2. Theory is unable to predict the "break through" phenomenon observed in the experiment when the amount of ammonia added to the fuel is varied.
3. Very good agreement between theory and experiment exists when the ammonia is added with the oxidizer.

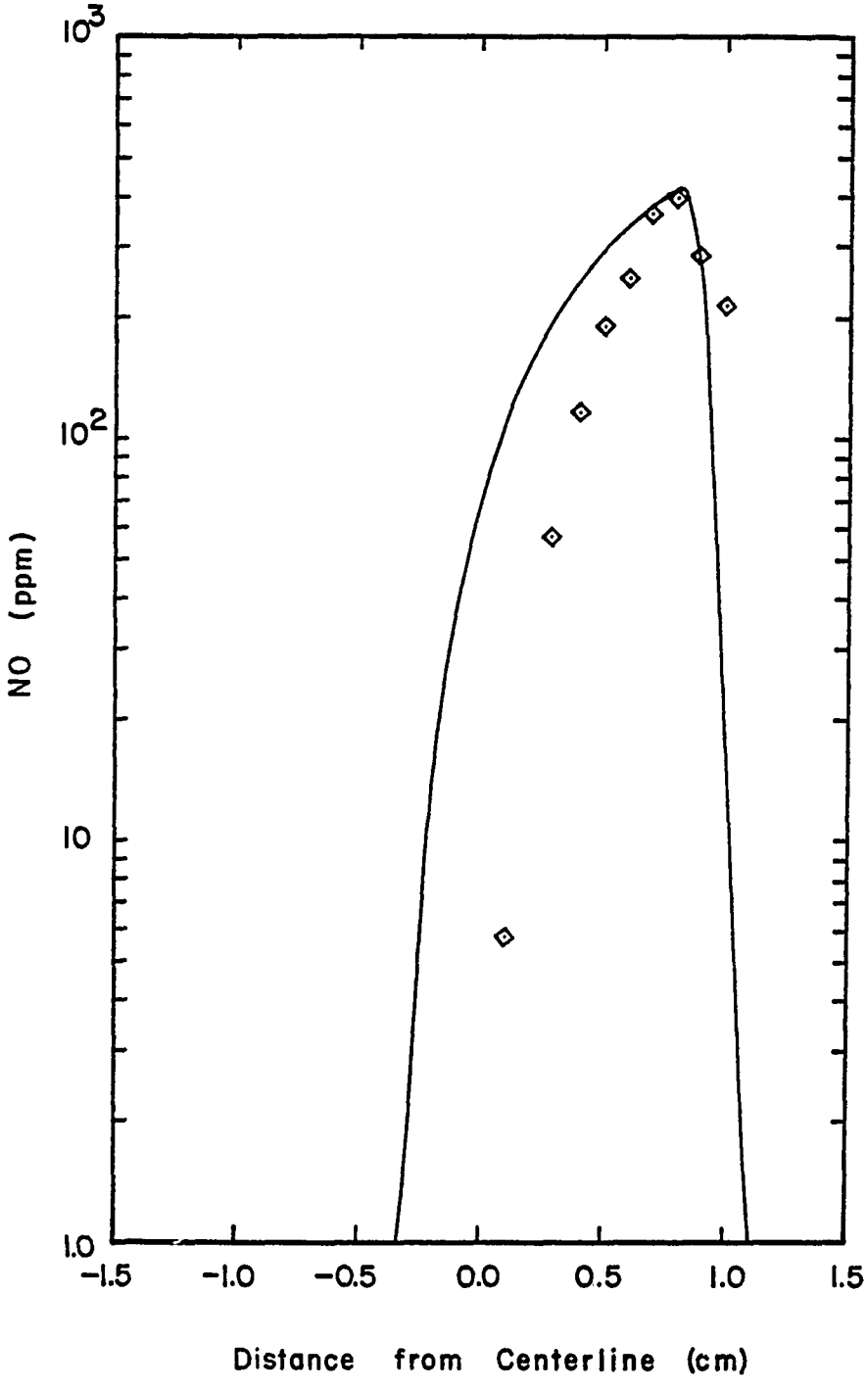

Figure 17. $CO/N_2/O_2$ Flame: $\varepsilon = 7.24\ sec^{-1}$, NO Profile (One Experiment, NH_3 Injected from Oxidizer Side, Experimental Values Not Shifted).

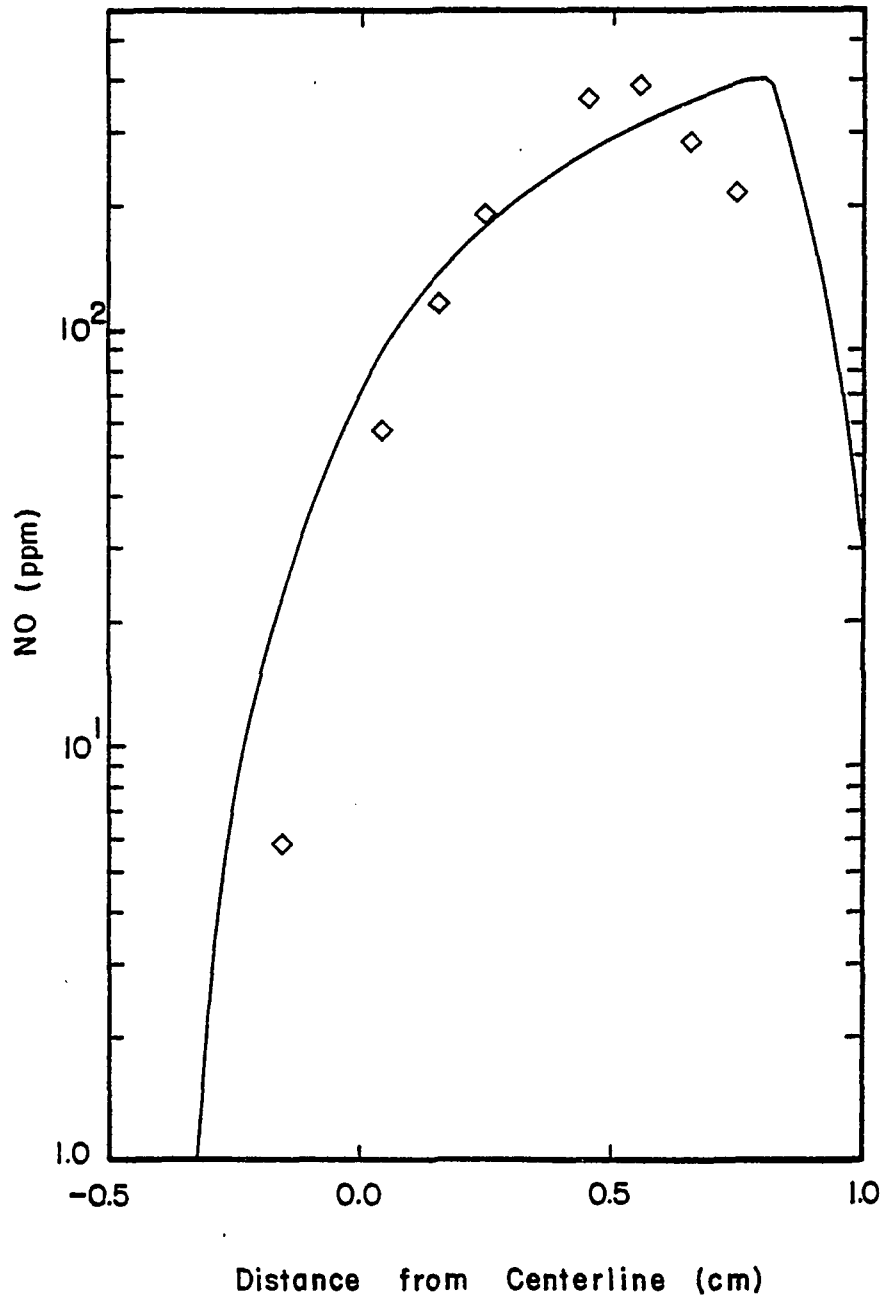

Figure 18. $CO/N_2/O_2$ Flame: $\varepsilon = 7.24\ sec^{-1}$, NO Profile (One Experiment, NH_3 Injected from Oxidizer Side, Experimental Values Shifted).

Additional Predictions

Figure 8 shows the calculated profiles of CO_2 and H_2O. It is interesting to note that water decomposes in the fuel-rich region, and the so formed free radicals and H_2 diffuse into the fuel-lean side of the flame where, in a very narrow zone, water is formed again.

Figure 19 represents the profiles of NH_3, H_2, and the free radicals involved in the combustion of wet CO. The peak values of the free radicals vary between 1000 and 3000 parts per million and their profiles show very sharp gradients, as was expected a priori. The H_2 peak has a maximum value of 6800 ppm and is much broader because of the much higher diffusion coefficient of this molecule. The concentration of NH_3 shows a very sharp decay well in the fuel-rich zone of the flame.

Figure 20 shows the species and radicals involving nitrogen in the case when NH_3 is injected with the fuel. It can be observed that the predicted peak values of N and NH are higher than the peak of NH_2 by a factor of 5.5. This is in contradiction to the prevailing view that N and NH are highly unstable and should not be present in such high concentrations in the flame. The high ratio of N and NH to NH_2 can be explained through uncertainty not only in the pyrolysis reactions of NH_3, but also in the thermochemistry involved, particularly in the heat of formation of NH and NH_2 (Corley, 1979).

The overall heat release, which is the true means of determining the reaction zone thickness is shown on Figure 21 for two different rates of stretching, namely $\varepsilon = 7.24\ sec^{-1}$ and $\varepsilon = 18.1\ sec^{-1}$. It can be observed that an increase in stretching rate causes a decrease in the

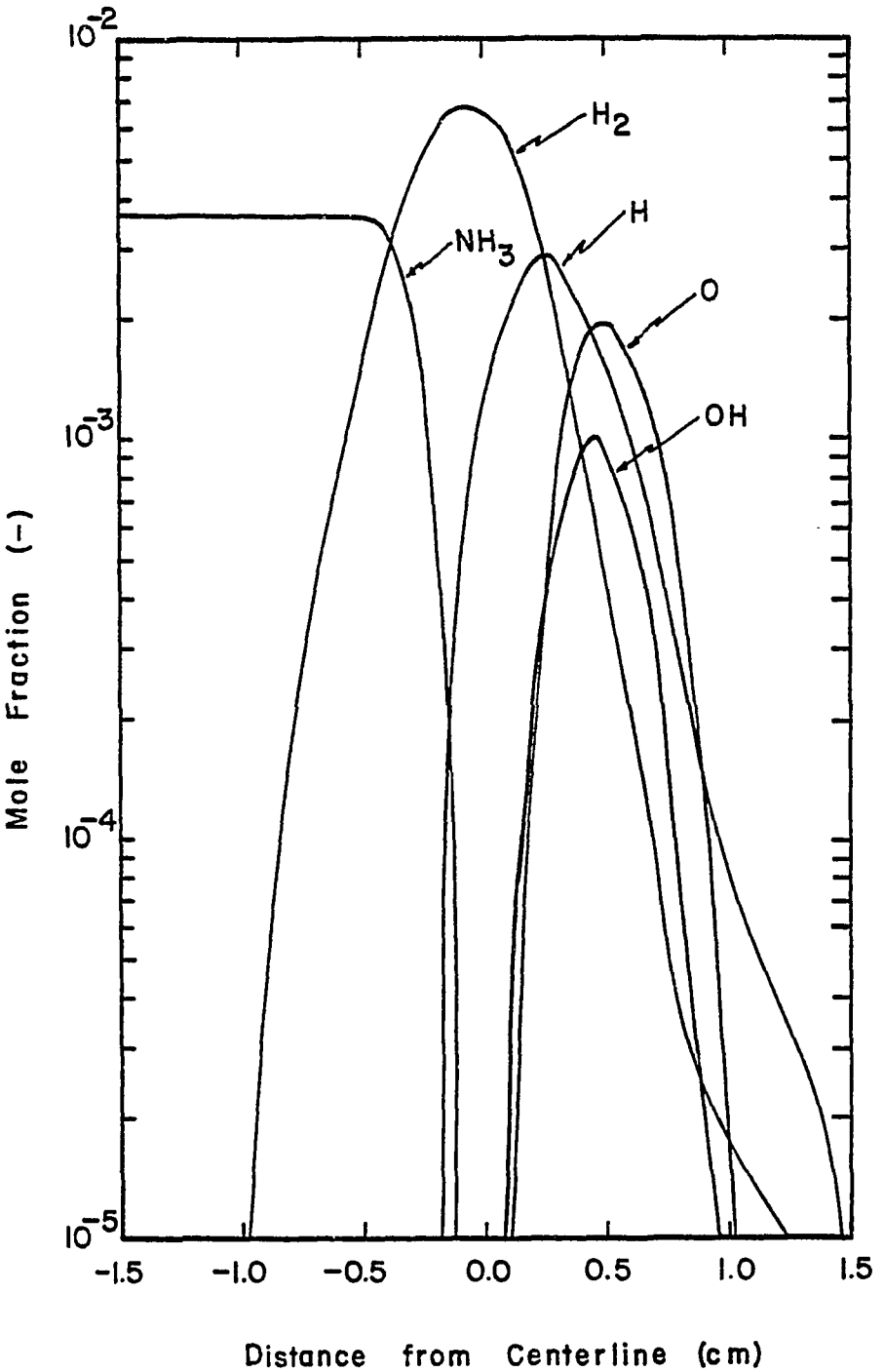

Figure 19. $CO/N_2/O_2$ Flame: $\varepsilon = 7.24\ sec^{-1}$; NH_3, H_2, H, O, OH Profiles.

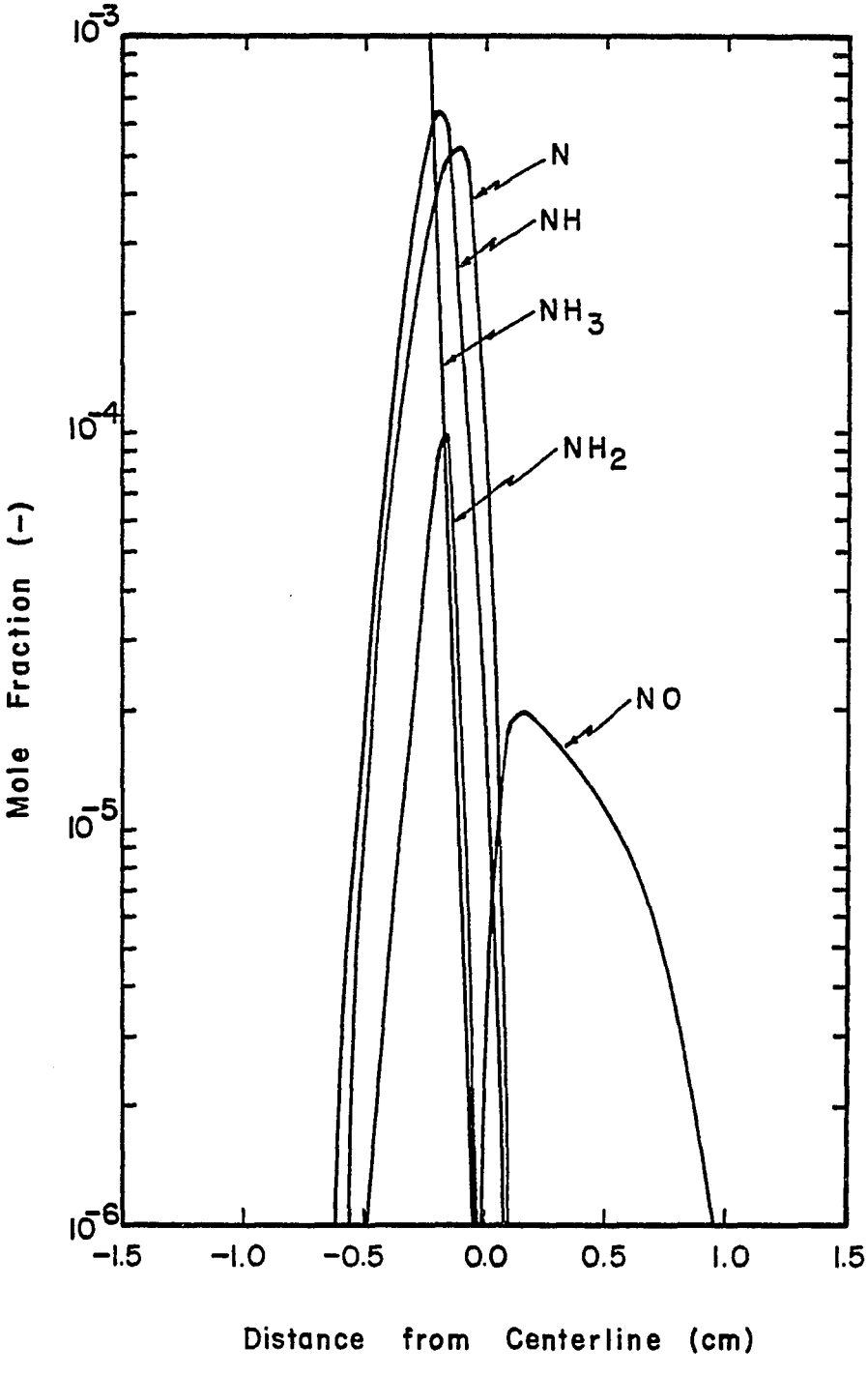

Figure 20. $CO/N_2/O_2$ Flame: $\varepsilon = 7.24\ sec^{-1}$, Profiles of Species Involving Nitrogen (NH_3 Injected from Fuel Side).

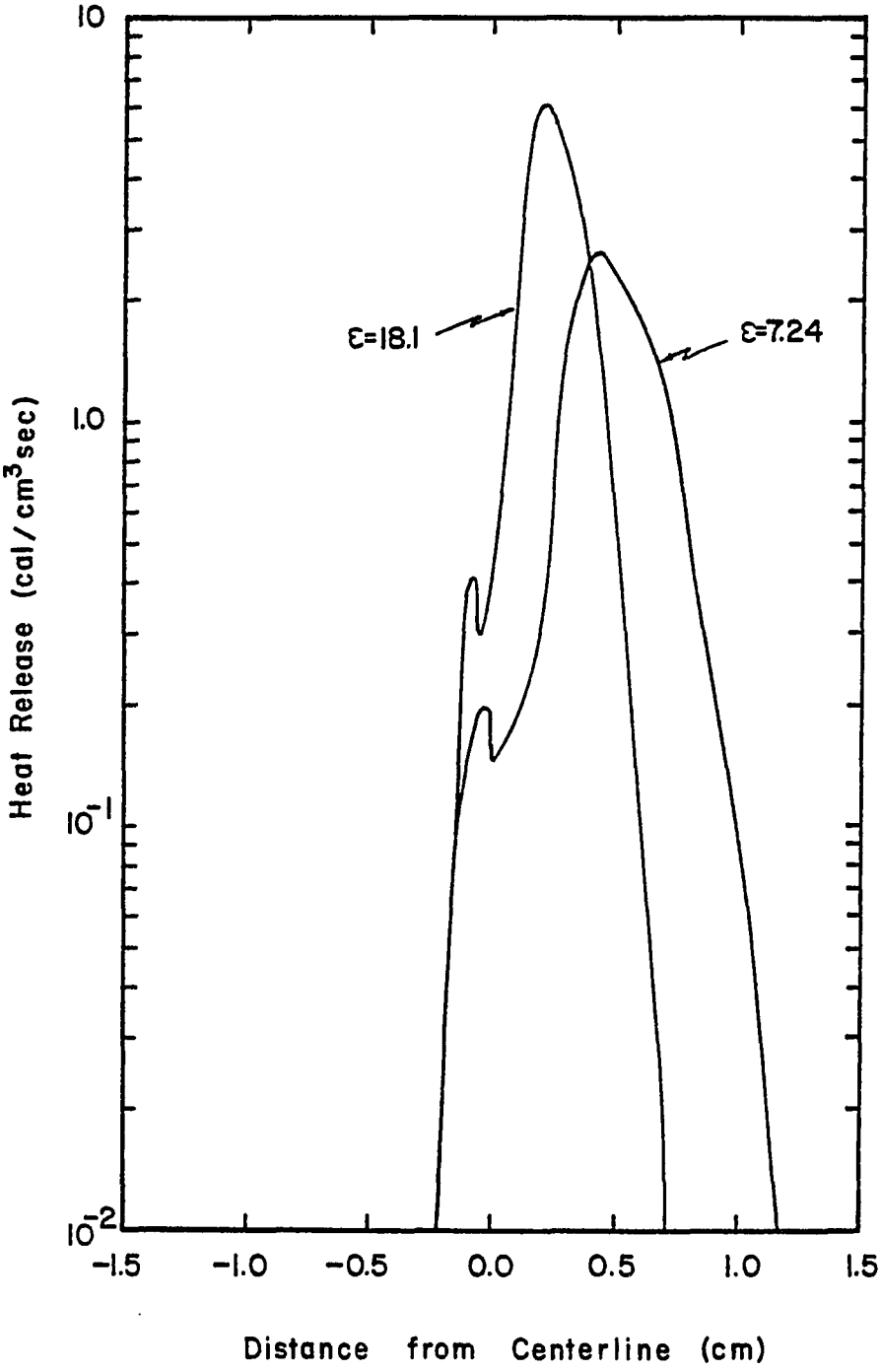

Figure 21. $CO/N_2/O_2$ Flame: ε = 7.24 and 18.1 sec^{-1}, Effect of Stretching Rate on Heat Release Profile.

width of the flame zone and also a higher peak of the heat release rate. This is to be expected, since increasing stretching rate should lead to increased local combustion intensity. The flame zone thickness is 1.37 cm for $\varepsilon = 7.24\ sec^{-1}$ and 0.95 cm for $\varepsilon = 18.1\ sec^{-1}$, and the corresponding peak heights are 2.5 cal $cm^{-3}sec^{-1}$ and 5.8 cal $cm^{-3}sec^{-1}$, respectively.

On Figure 22 the predicted effect of the rate of stretching on the rate of formation of NO is shown. It is observed that the reactions forming NO on the fuel-lean side of the flame and those destroying it on the fuel-rich side are equally important. Furthermore, the rate of formation of NO increased by an order of magnitude with an increase of a factor of 2.5 in the stretching rate, although if the profiles are integrated over all values of z, the difference is only a factor of 2. This result is consistent with the fact that increased stretching rate corresponds to increased local combustion intensity and that fuel NO is favored in regions of high combustion intensity in a typical turbulent diffusion flame.

The conclusions that can be drawn from the theoretical predictions are:

1. NH_3 is pyrolysized rapidly when it is injected with the fuel.
2. NH and N concentrations are predicted to be much higher than the concentration of NH_2.
3. The rate of stretching decreases the width of the reaction zone.
4. The peak height of the heat release profile increases with stretching rate.
5. The rate of formation of NO increases with stretching.

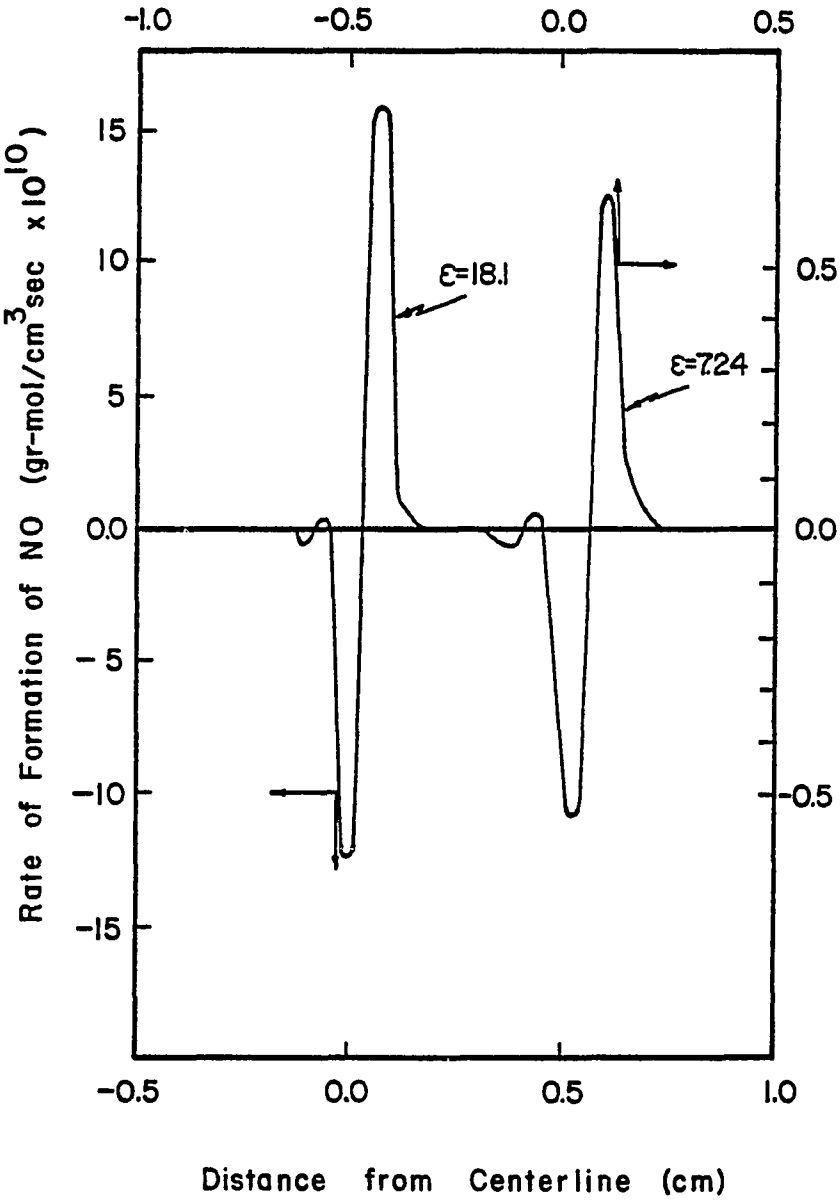

Figure 22. $CO/N_2/O_2$ Flame: ε = 7.24 and 18.1 sec^{-1}, Effect of Stretching Rate on Rate of Formation of NO (NH_3 Injected from Fuel Side).

CHAPTER 6

THE METHANE/OXYGEN/NITROGEN OPPOSED JET DIFFUSION FLAME

Introduction

This chapter reports results from both the model, solved for the case when the fuel is CH_4, and from the appropriate experiments. Predictions are compared with experimental results. Two stretching rates were investigated in this work. Details of the numerical procedure required to solve this specific problem are presented.

The formation of NO is studied by injecting NH_3 into both the fuel and the oxidizer. This provides insight into the validity of the kinetic information pertaining to different reactions of the complex reaction set.

Additional theoretical predictions are shown and the effect of the stretching rate on the heat release and on the rate of formation of NO is considered.

Six different cases are presented in this section, two dilute methane flames, at different stretching rates, and a concentrated methane flame. Experimental results are available for only the dilute flames. The conditions of these six flames are shown on Table 3.

Numerical Solution

The first simulated flame corresponds to Case 1. The initial guess, which is necessary to start the iterative solution technique, is the solution of the wet CO flame at the same stretching rate of

Table 3. Conditions of $CH_4/O_2/N_2$ Flames.

Case No.	Mole Fraction of CH_4	Mole Fraction of O_2	Mole Fraction of NH_3	Separation of Burners (cm)	Flow Rate of Fuel (l/min)	Flow Rate of Oxidizer (l/min)	Stretching Rate (sec^{-1})	NH_3 From	Theory	Experiment
1	0.10	0.52	0.0	3.0	20.0	9.22	7.24	--	yes	yes
1A	0.10	0.52	0.001	3.0	20.0	9.22	7.24	fuel	yes	yes
1B	0.10	0.52	0.0022	3.0	20.0	9.22	7.24	oxidizer	yes	yes
2	0.10	0.52	0.0	3.0	10.4	2.61	3.76	--	yes	yes
2A	0.10	0.52	0.001	3.0	10.4	2.61	3.76	fuel	yes	yes
3	0.98	0.20	0.0	2.0	104.0	55.0	48.9	--	yes	no

7.24 sec^{-1}. Species which are not present when simulating the combustion of CO are set equal to zero. Since this initial guess is close to the final solution, the full Jacobian of the Taylor series expansion of equation [47] can be used throughout the solution. The relaxation factor is set initially to 0.125 and doubled every 5 iterations, not allowing it to exceed unity. The converged solution was obtained after 50 iterations.

Next, case 2 is simulated using the solution of case 1 as the initial guess. The initial value of the under-relaxation factor is 0.25 and again it is doubled every 5 iterations until it reaches unity, where it is held constant. Convergence is achieved after 30 iterations.

The initial guess used in the solution of case 3 corresponds to the solution of a similar problem in cartesian coordinates obtained elsewhere (Kau, 1979). Although the initial guess employed is very close to the final answer, the relaxation factor could never be incremented above 0.5 without rendering the iterative scheme unstable. The very high stretching rate used in this case was necessary because the steep gradients of some of the reaction products causes them to diffuse very fast, making the net flux of these species to be directed towards the burner. The numerical scheme becomes unstable in this situation and diverges. Two solutions to this problem are available; one consists in increasing the stretching rate and convecting the species away from the burner. The other solution consists in separating the burners until the net flux of all species towards the burner is equal or less than zero.

The solution of the pure fuel case was achieved only with difficulty after 80 iterations, and then only after the initial guess was set close to the anticipated solution (Kau, 1979). Table 4 shows how the relaxation factor was varied.

Combustion of Dilute Methane

High Stretching Rate

Figure 23 shows the predicted and measured temperature profiles. The peak value of the experiment appears shifted 2.5 mm towards the fuel-lean side of the flame. In this experiment, an uncoated thermocouple of 0.002 in. Pt/Pt-10% Rh wire was used. No correction for radiative heat loss was performed on the measured values. The upper limit for the correction, calculated with equation [74], is 170°K at the peak. In Figure 24, the experimental points are shifted 2.5 mm to the left, so that the peaks of the theoretical and experimental profiles coincide. The same shift is performed on all the experimental species profiles corresponding to the high stretching rate flame. It is thought that the disagreement in the location of the flame front may be caused by uncertainties in the kinetic information involved in the used reaction set, the assumption that the flame is adiabatic, and the neglected thermal diffusion. On Figure 24, it can be observed that both the width and height of the temperature profile are very well predicted.

The adiabatic temperature of a stoichiometric mixture of the fuel and oxidizer here considered is 1912°K. The predicted peak temperature of the Opposed Jet Diffusion Flame is 170°K higher. This can be

Table 4. Variation of Relaxation Factor in Solution of the Pure Fuel Flame.

Iteration	Relaxation Factor
1-10	0.01
11-15	0.02
16-20	0.05
21-25	0.1
26-30	0.2
31-35	0.3
36-40	0.4
41-60	0.25
61-80	0.50

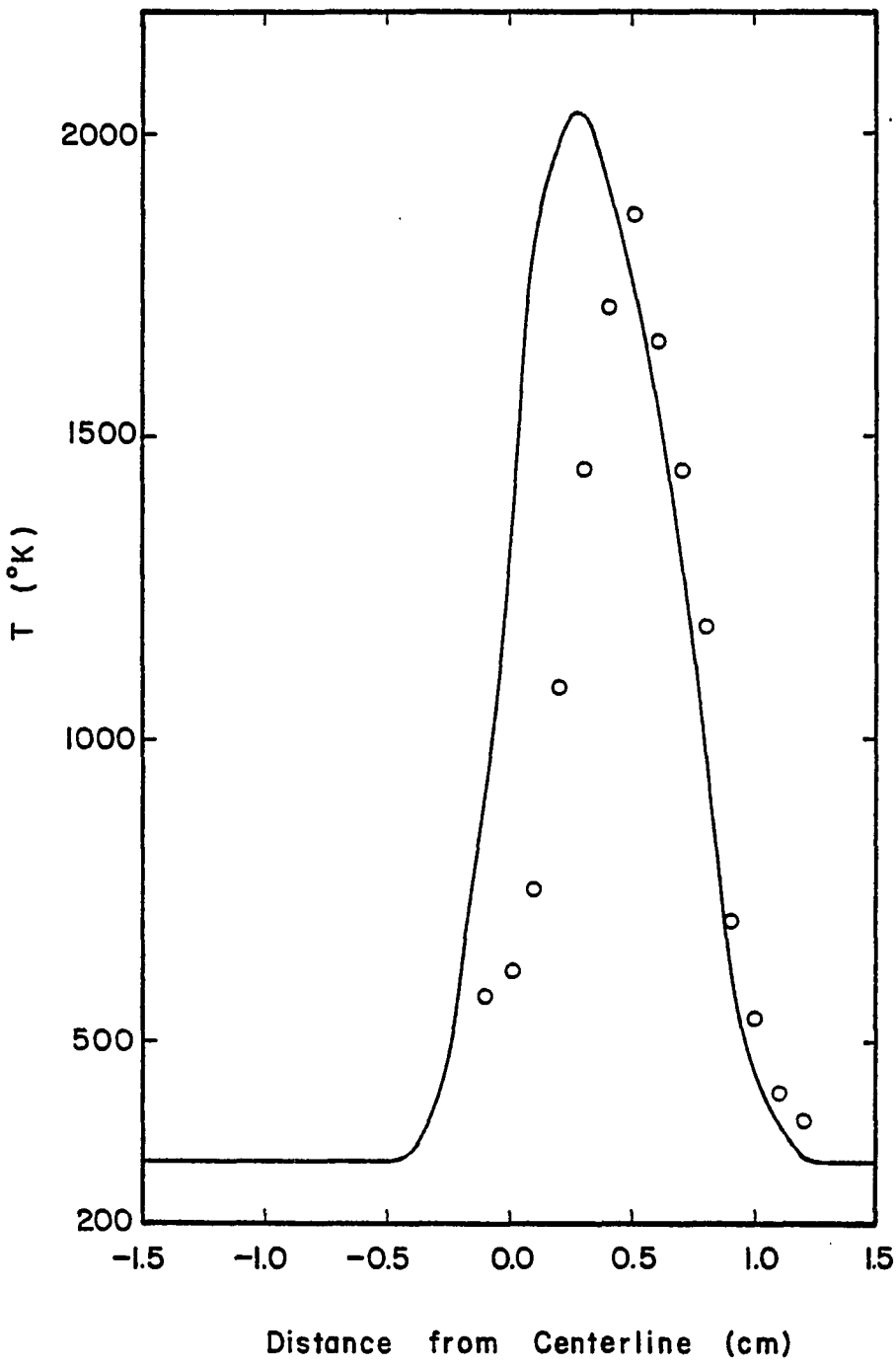

Figure 23. $CH_4/N_2/O_2$ Flame: $\varepsilon = 7.24\ sec^{-1}$, Temperature Profile (One Experiment, Experimental Values Not Shifted).

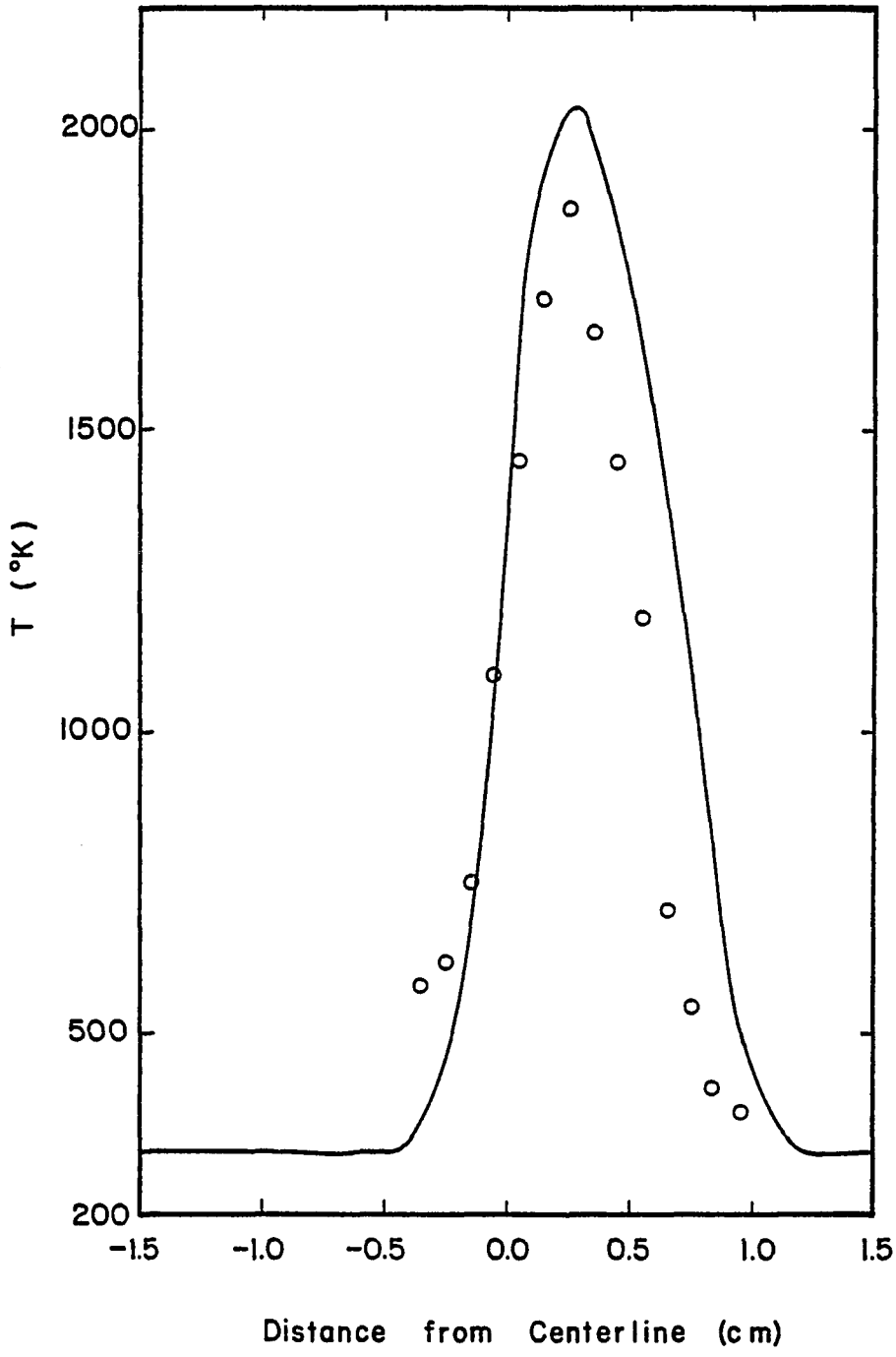

Figure 24. $CH_4/N_2/O_2$ Flame: $\varepsilon = 7.24\ sec^{-1}$, Temperature Profile (One Experiment, Experimental Values Shifted).

explained through the different diffusion coefficients of CH_4 and O_2 in nitrogen. CH_4 diffuses faster and the fluxes of reactants reaching the plane where the temperature peaks are slightly more concentrated than the inlet conditions, giving rise to a higher adiabatic flame temperature.

Figure 25 shows the theoretical and measured profiles of reactants corresponding to case 1. The experimental data correspond to two independent experiments with the probe positioned at a radial distance measured from the axis of symmetry of 0.4 cm in experiment 1 and 0.9 cm in experiment 2. These data support both the reproducibility of the experiment and the one-dimensional nature of the flame. Again, the latter point is consistent with theory. Although agreement between theory and experiment is not perfect, the reaction zone thickness is very well modeled.

Figures 26 through 28 represent the profiles of the combustion products, namely CO, O_2, and H_2O. The experimental values on Figures 27 and 28 correspond to the same experiments 1 and 2 discussed above. On all three figures, the measured profiles seem to be narrower than the theoretical predictions. This can be attributed to two possible causes: uncertainties in the kinetic information contained in the reaction set, or the shifting of the flame. The agreement between experimental and theoretical peak height is very good in all three cases, which is an indication that the model represents the Opposed Jet Diffusion Flame very well.

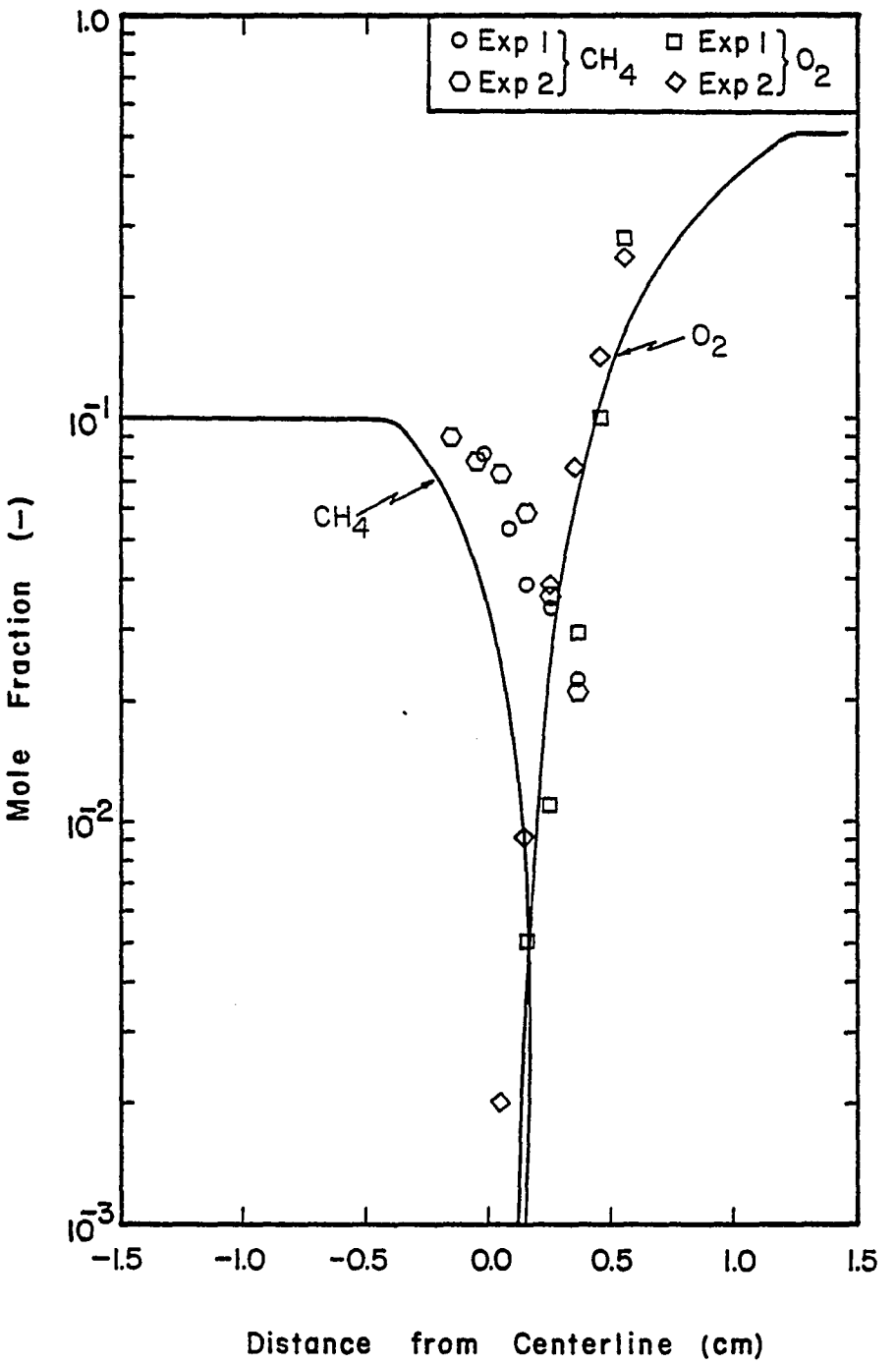

Figure 25. $CH_4/N_2/O_2$ Flame: $\varepsilon = 7.24\ sec^{-1}$, CH_4 and O_2 Profiles (Two Experiments, Experimental Values Shifted).

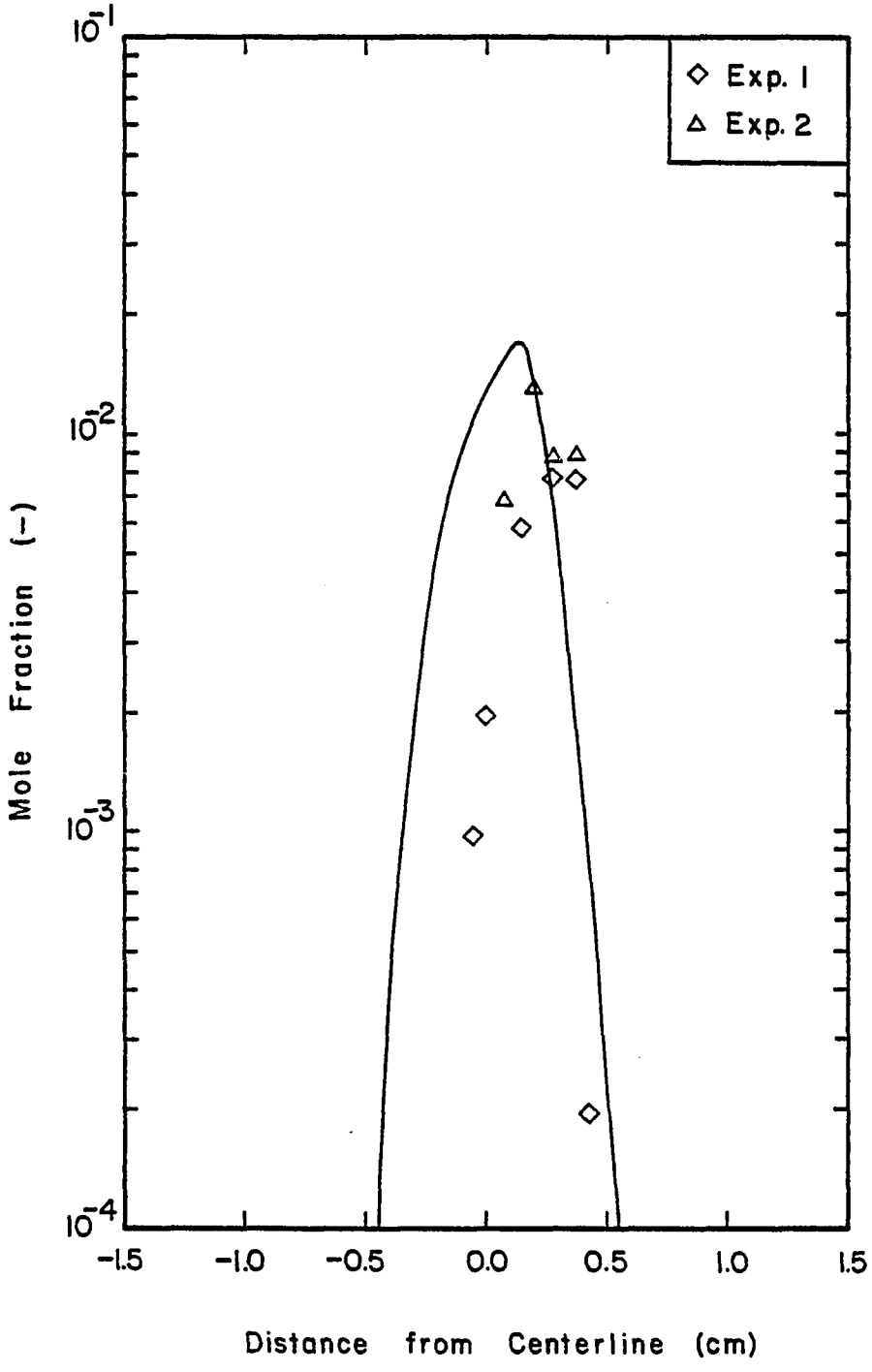

Figure 26. $CH_4/N_2/O_2$ Flame: $\varepsilon = 7.24\ sec^{-1}$, CO Profile (Two Experiments, Experimental Values Shifted).

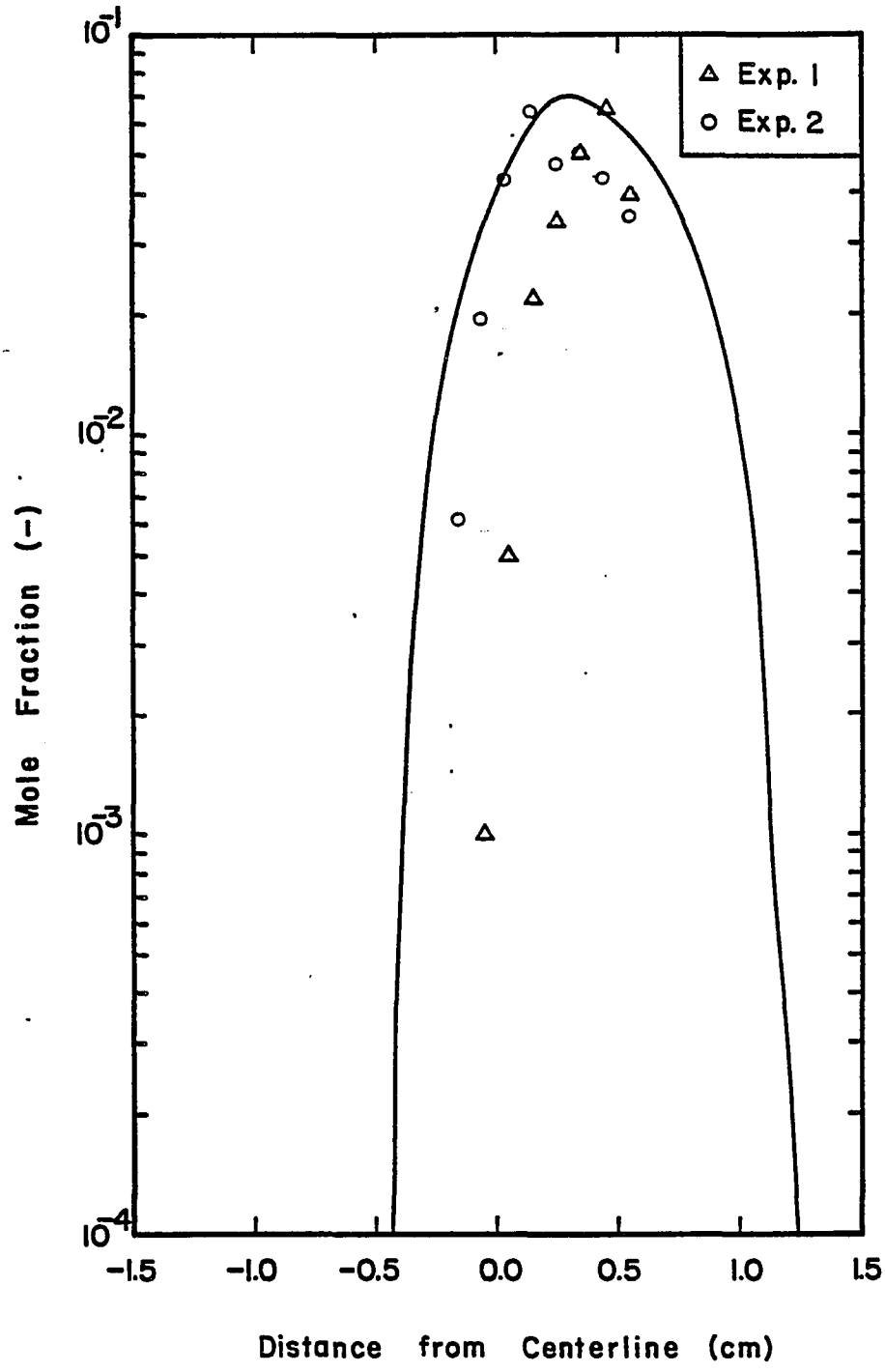

Figure 27. $CH_4/N_2/O_2$ Flame: $\varepsilon = 7.24$ sec^{-1}, CO_2 Profile (Two Experiments, Experimental Values Shifted).

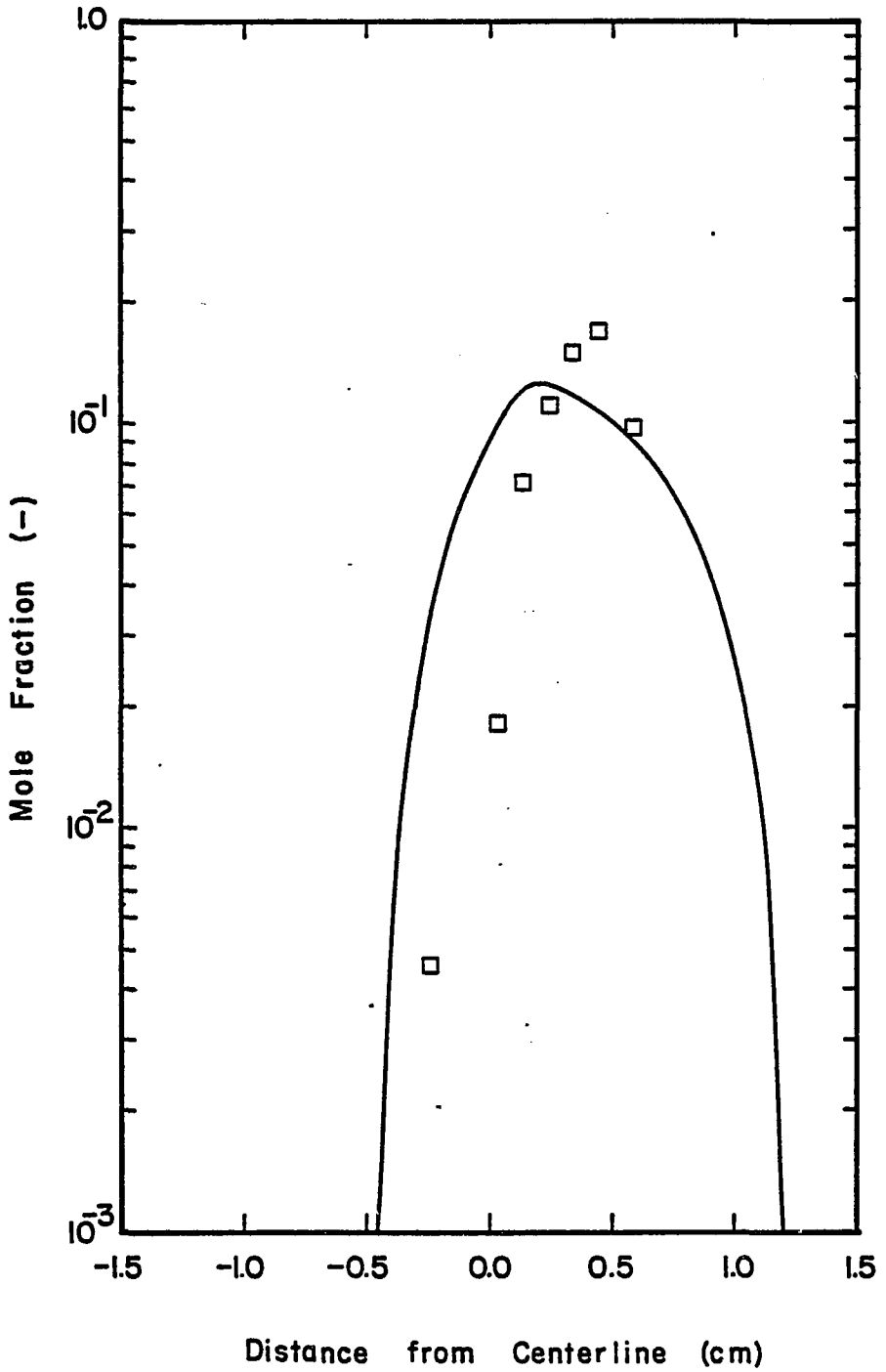

Figure 28. $CH_4/N_2/O_2$ Flame: $\varepsilon = 7.24\ sec^{-1}$, H_2O Profile (One Experiment, Experimental Values Shifted).

Figures 29 through 32 contain the profiles of CH_4, O_2, CO, CO_2, and H_2O with the experimental values plotted at the actual locations where they were measured, and are included for completeness.

Low Stretching Rate

Figure 33 shows the profiles of the reactants corresponding to case 2. In this particular case, the shifting of the profiles is not as obvious as it is in the case of high stretching rate, and the experimental data are plotted at the locations where they were measured, i.e., there are no adjustable parameters. The agreement between experimental data and the profiles predicted from theory is very good.

Comparison between theoretical values and experimental data for CO and CO_2 can be found on Figure 34. As in the high stretching case, the peak heights are in excellent agreement and the width of the profile is predicted to be wider than the measured values indicate.

The theoretical model predicts that as stretching rate decreases, the profiles of CO and CO_2 show no effect in peak height and increase in width. From Figures 25, 26, and 34, it can be observed that the experimental data are in excellent agreement with this prediction.

On Figure 35, the theoretical and experimental temperature profiles are presented. The measurements were performed with a 0.003 in. thermocouple and were corrected for radiative heat loss using equation [74], giving a good agreement between theory and experiment.

From the above-presented evidence, the following can be concluded:

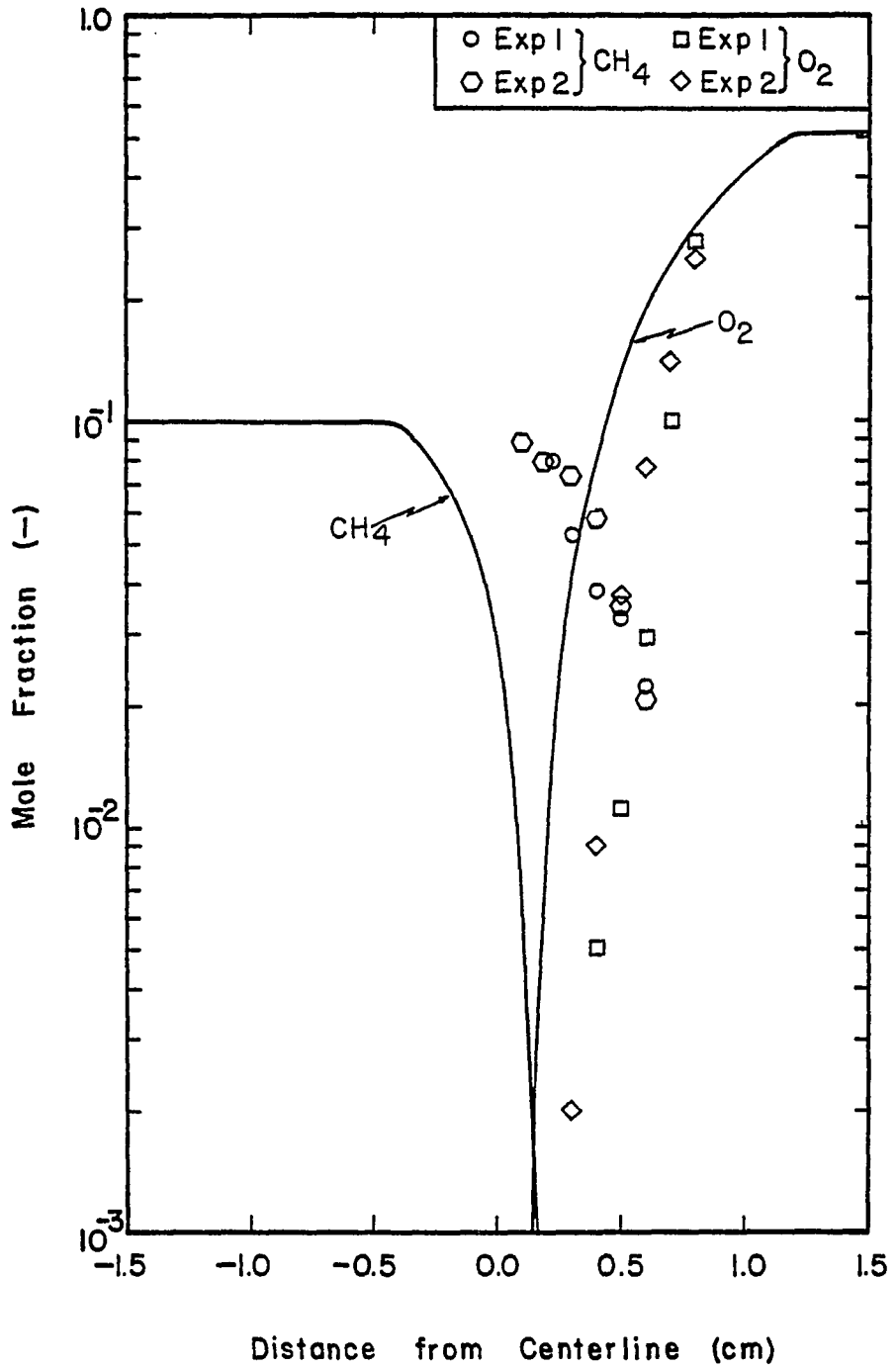

Figure 29. $CH_4/N_2/O_2$ Flame: $\varepsilon = 7.24\ sec^{-1}$, CH_4 and O_2 Profiles (Two Experiments, Experimental Values Not Shifted).

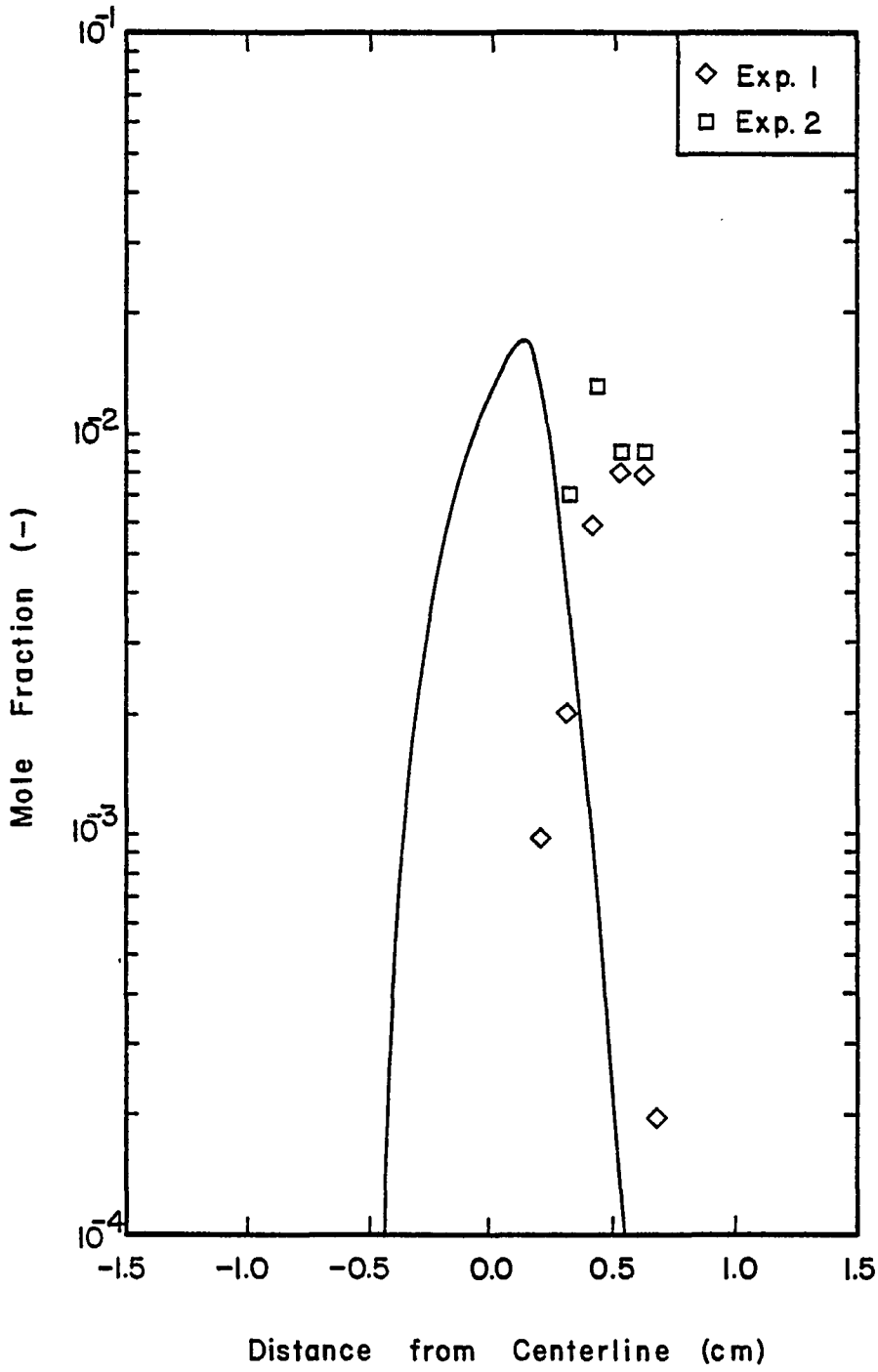

Figure 30. $CH_4/N_2/O_2$ Flame: $\varepsilon = 7.24\ sec^{-1}$, CO Profile (Two Experiments, Experimental Values Not Shifted).

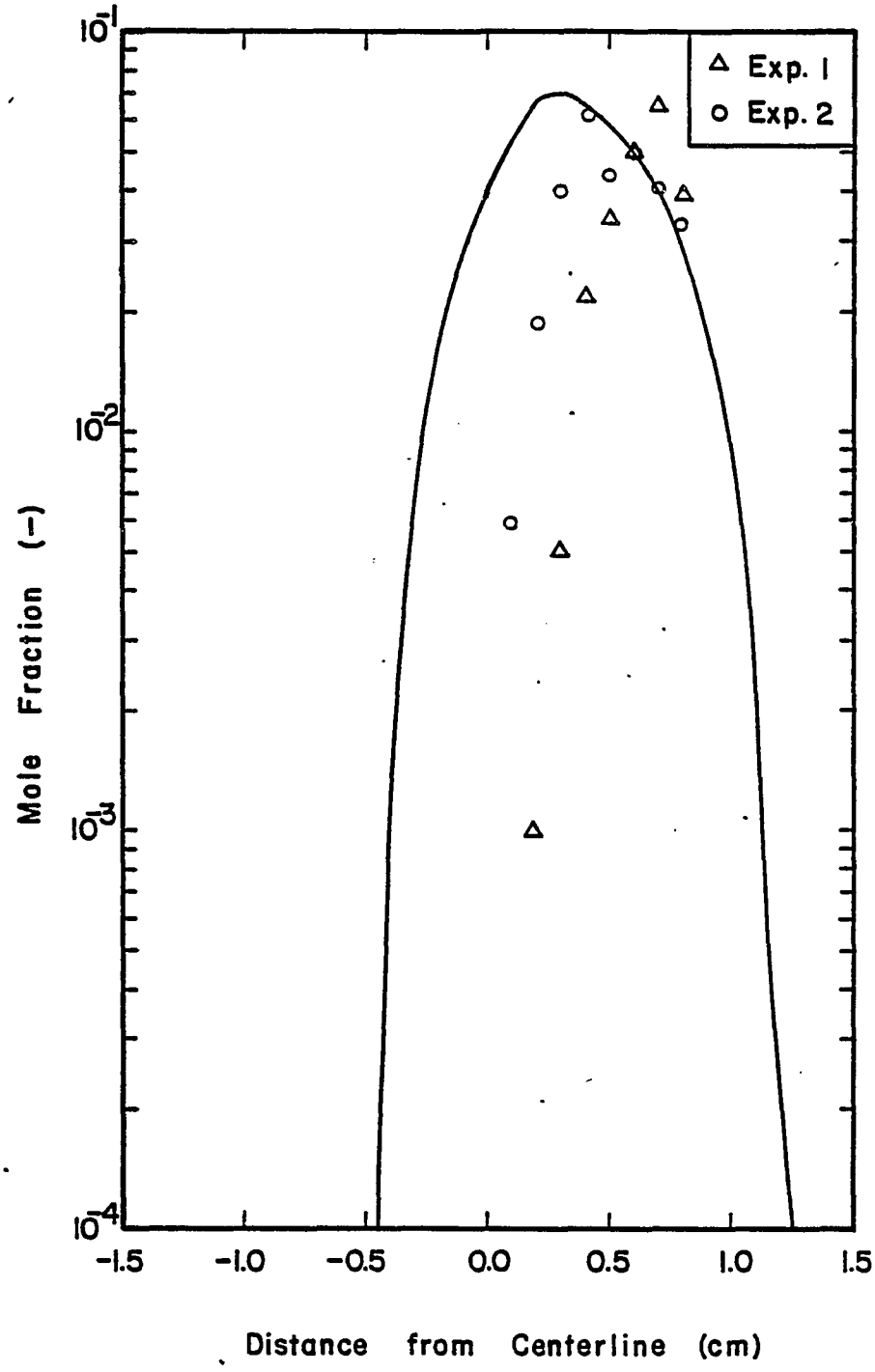

Figure 31. $CH_4/N_2/O_2$ Flame: $\varepsilon = 7.24\ sec^{-1}$, CO_2 Profile (Two Experiments, Experimental Values Not Shifted).

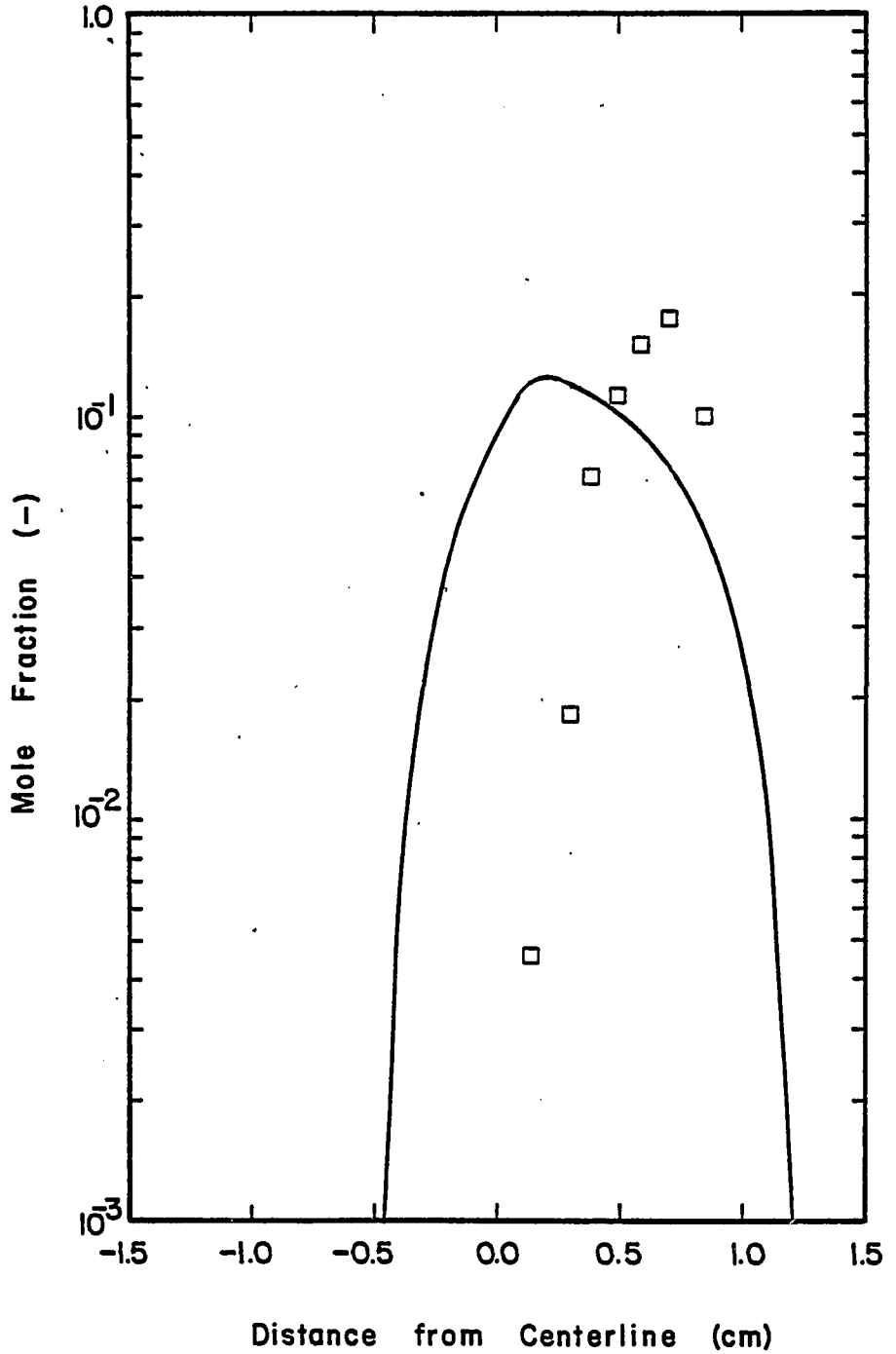

Figure 32. $CH_4/N_2/O_2$ Flame: $\varepsilon = 7.24\ sec^{-1}$, H_2O Profile (One Experiment, Experimental Values Not Shifted).

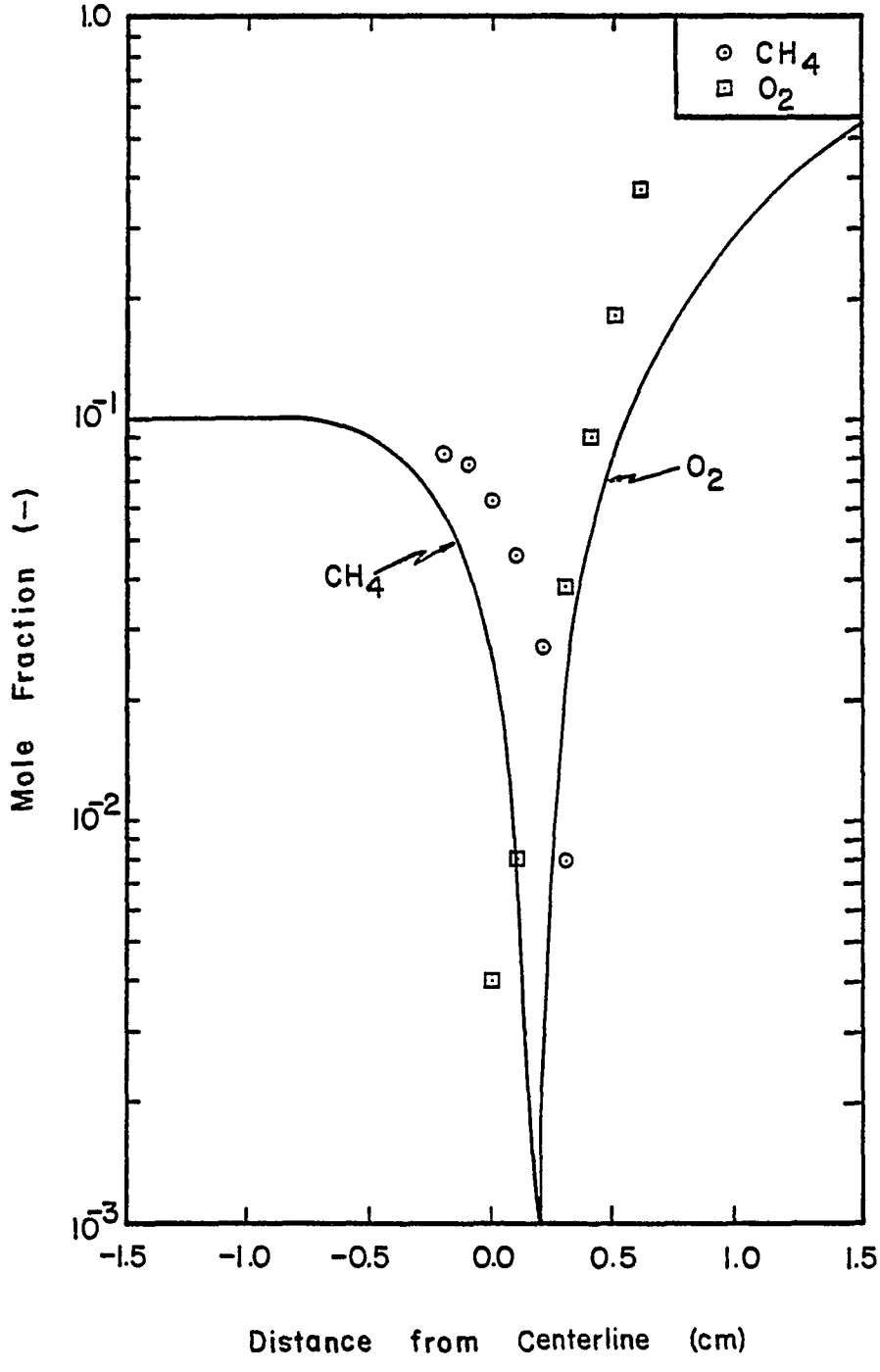

Figure 33. $CH_4/N_2/O_2$ Flame: $\varepsilon = 3.76\ sec^{-1}$, CH_4 and O_2 Profiles (One Experiment, Experimental Values Not Shifted).

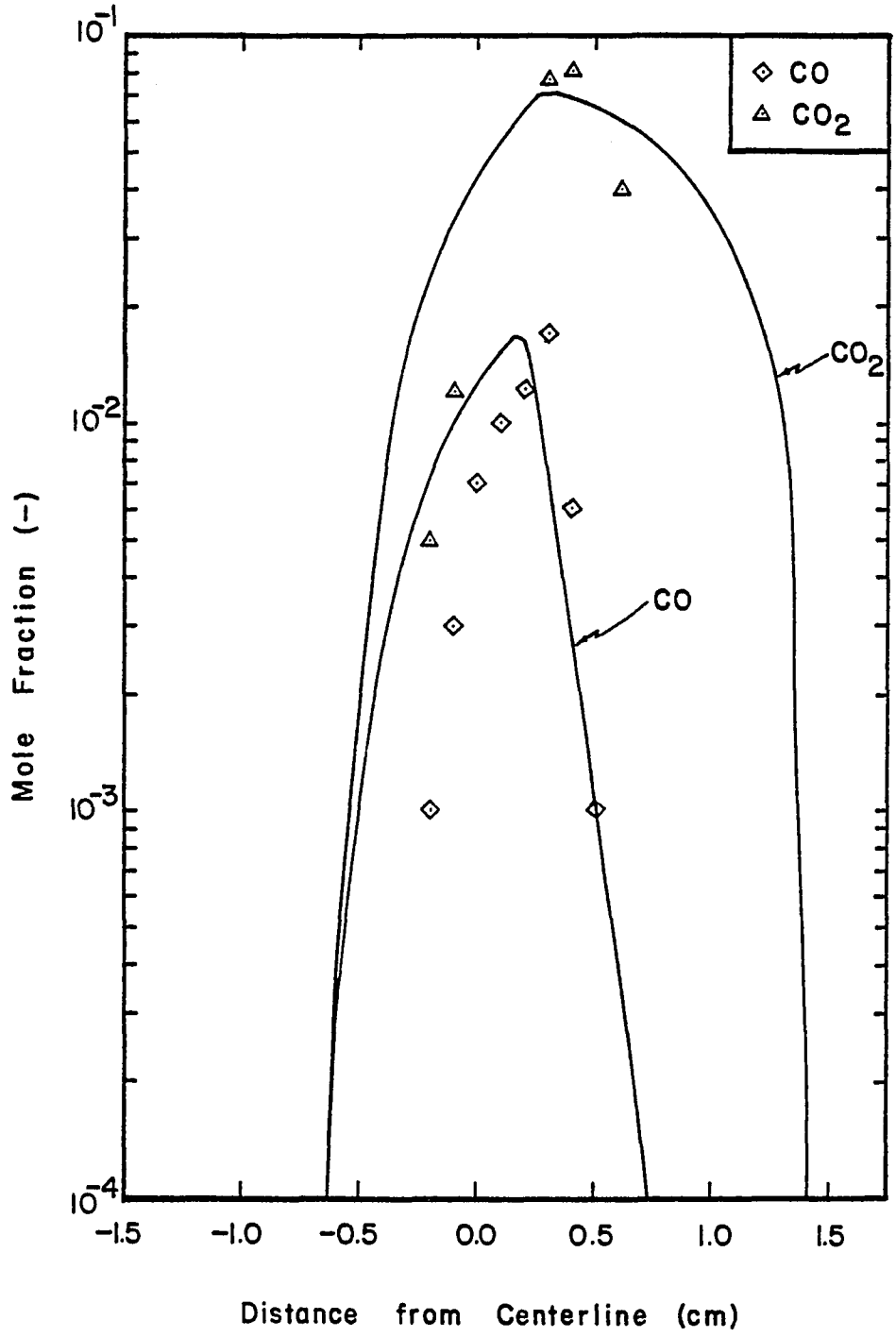

Figure 34. $CH_4/N_2/O_2$ Flame: $\varepsilon = 3.76\ sec^{-1}$, CO and CO_2 Profiles (One Experiment, Experimental Values Not Shifted).

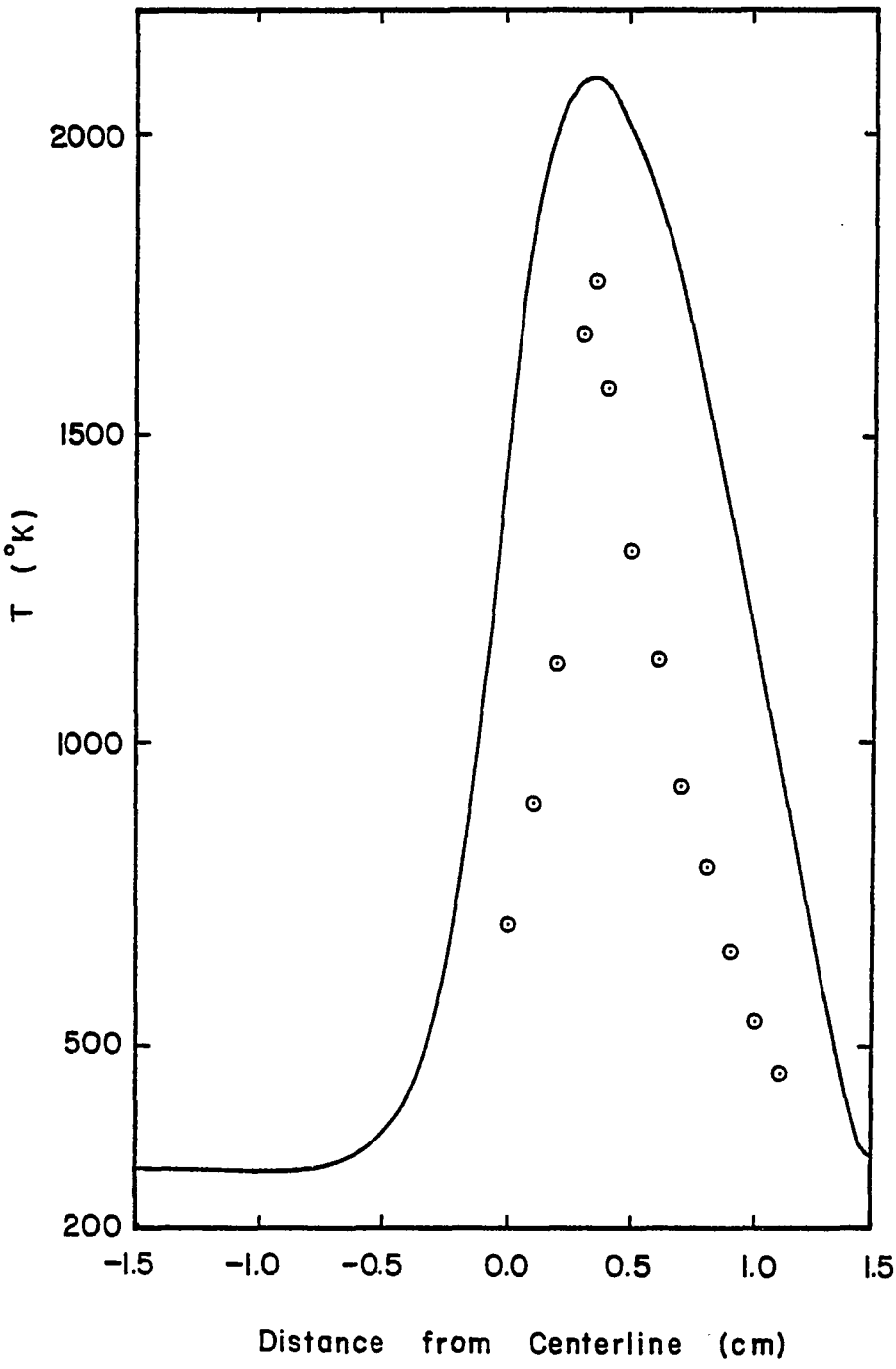

Figure 35. $CH_4/N_2/O_2$ Flame: $\varepsilon = 3.76\ sec^{-1}$, Temperature Profile (One Experiment, Experimental Values Not Shifted).

1. The experimental data are reproducible.
2. In the neighborhood of the axis of symmetry, the Laminar Opposed Jet Diffusion Flame is one-dimensional.
3. The thickness of the reaction zone is very well modeled.
4. The predicted effect of the rate of stretching on the CO and CO_2 profiles agrees very well with experimental evidence.
5. The temperature profile is well predicted.
6. Effect of stretching rate on the reaction zone thickness is well predicted.

Nitric Oxide Formation

High Stretching Rate

The predicted and measured profiles of NO in the case when a mole fraction of 10^{-3} of ammonia is injected with the fuel are presented on Figure 36. The experimental values are plotted 2.5 mm to the left of the location where they were measured and correspond to the same experiments 1 and 2 discussed in the previous section. Excellent agreement can be observed between the theoretical predictions and the experimental data. This indicates that the pyrolysis reactions of NH_3 which dominate in the presence of CH_4 are much better understood than those that dominate in the presence of CO. It would appear that the displacement of the flame by 2.5 mm did not greatly affect this profile.

Figure 37 shows the profiles of NO when a mole fraction of 2.2×10^{-3} of NH_3 is injected into the flame with the oxidizer stream. The experimental values have been shifted 2.5 mm to the left. The

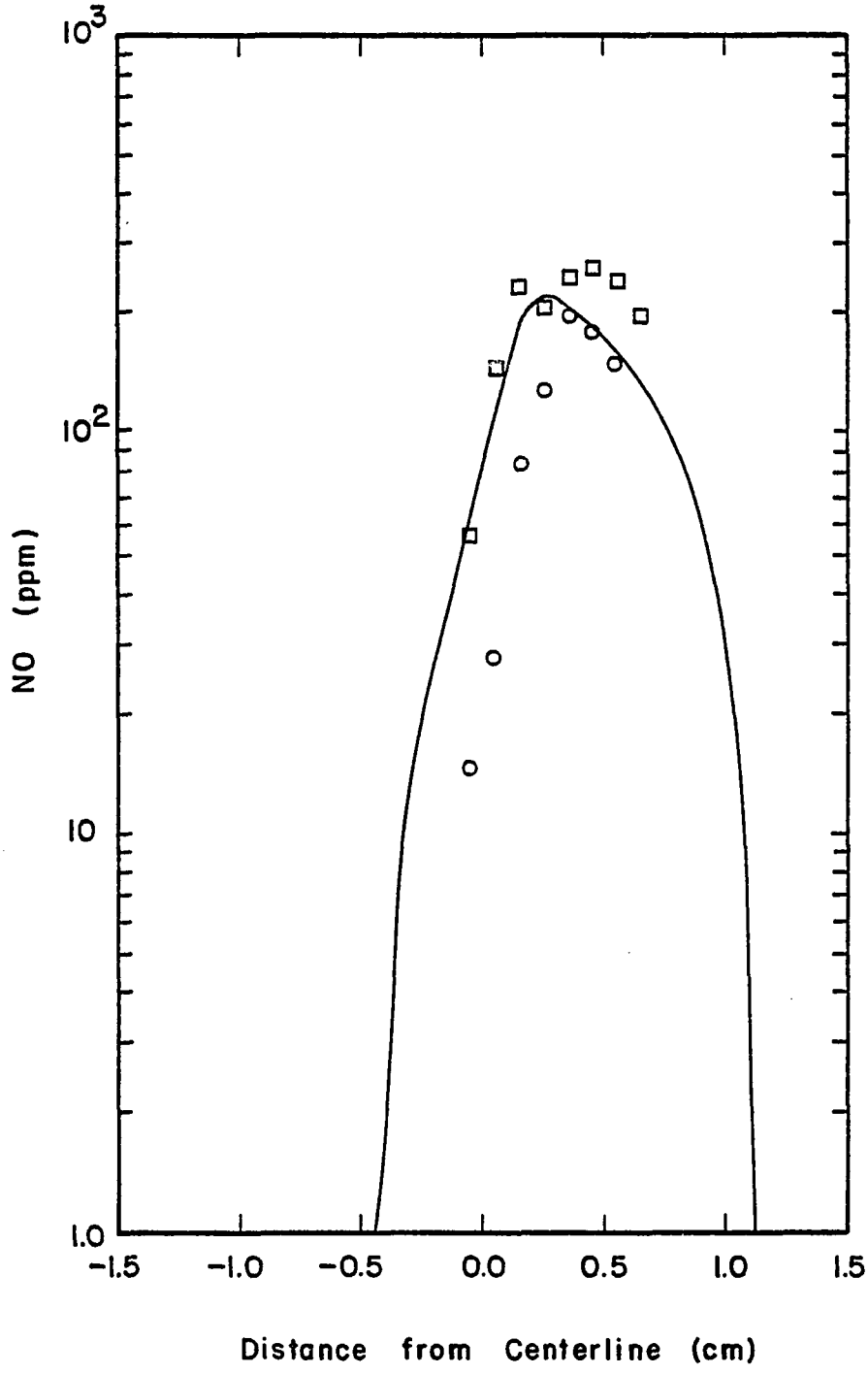

Figure 36. $CH_4/N_2/O_2$ Flame: $\varepsilon = 7.24\ sec^{-1}$, NO Profile (Two Experiments, Experimental Values Shifted, NH_3 Injected with Fuel).

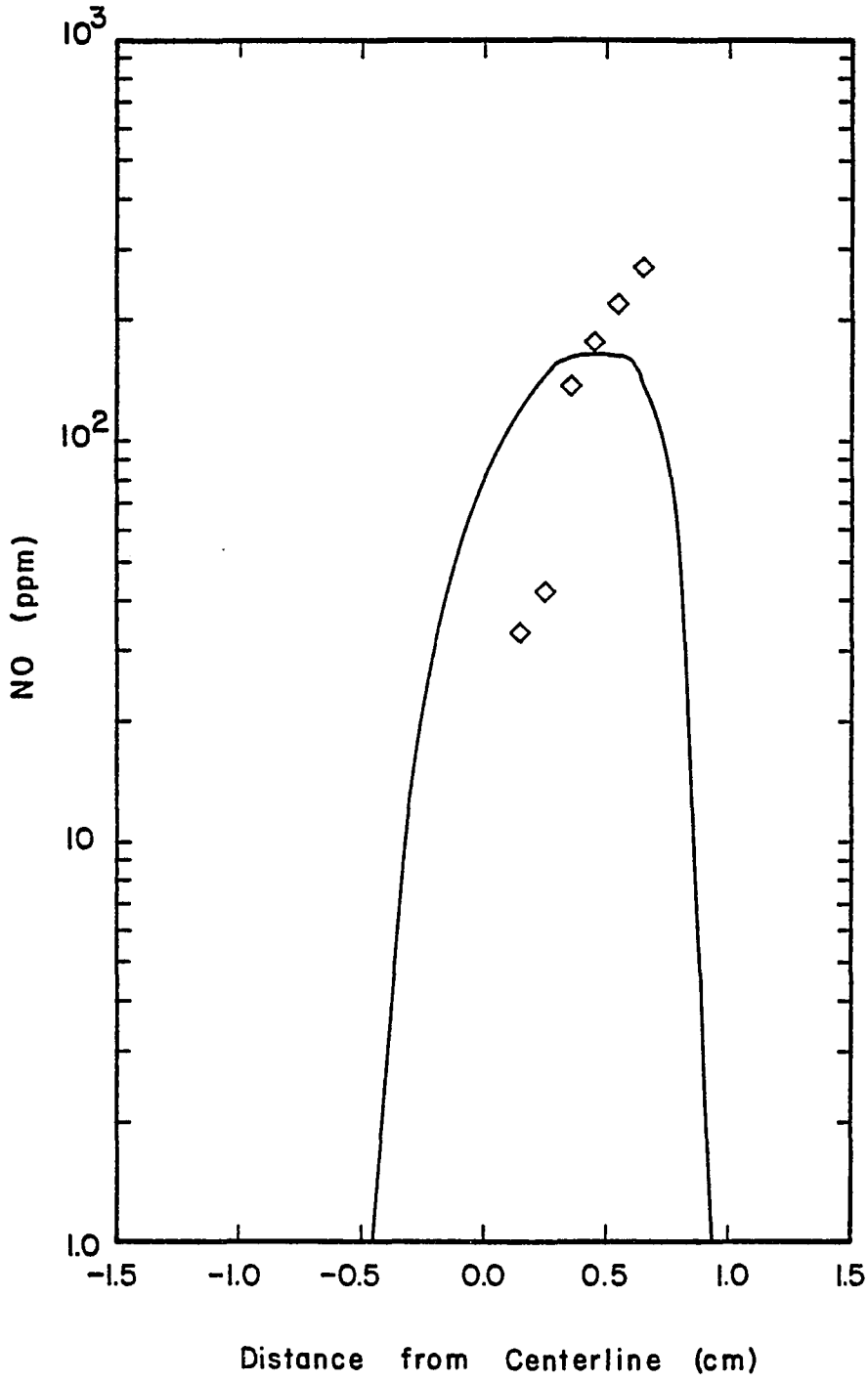

Figure 37. $CH_4/N_2/O_2$ Flame: $\varepsilon = 7.24\ sec^{-1}$, NO Profile (One Experiment, Experimental Values Shifted, NH_3 Injected with Oxidizer).

disagreement between theory and experiment may be attributed to an error in predicting the location of the flame zone.

In the present work, the peak of the NO profile lies very near the stagnation point and diffusion dominates over convection. If the flame zone is shifted towards the fuel-lean side of the flame and the velocity profile is not affected much by this shift, the peak in the predicted NO profile would be in a region where the velocity is significant in value and negative, i.e., directed towards the fuel-rich side of the flame. The fluxes due to diffusion and convection on the fuel-lean side of the NO profile would be different in sign, and a much steeper gradient would occur. Such a steep gradient would be in much better agreement with the experimental data. On the fuel-rich side of the profile, the fluxes would have the same sign and a much slower decay, as indicated by experimental evidence, would occur.

Figures 38 and 39 show the same information as Figures 36 and 37, but the experimental values are not shifted, i.e., they are drawn in the exact positions where they were measured.

Effect of Stretching Rate

On Figure 40, the profiles of NO are presented for the case when a mole fraction of NH_3 of 10^{-3} is injected into the fuel stream of a flame which has a stretching rate of 7.24 sec^{-1} and a flame with a smaller stretching rate, namely 3.76 sec^{-1}. The experimental values corresponding to the flame with the high stretching rate have been shifted 2.5 mm to the left and those corresponding to the low stretching rate flame have been drawn as measured.

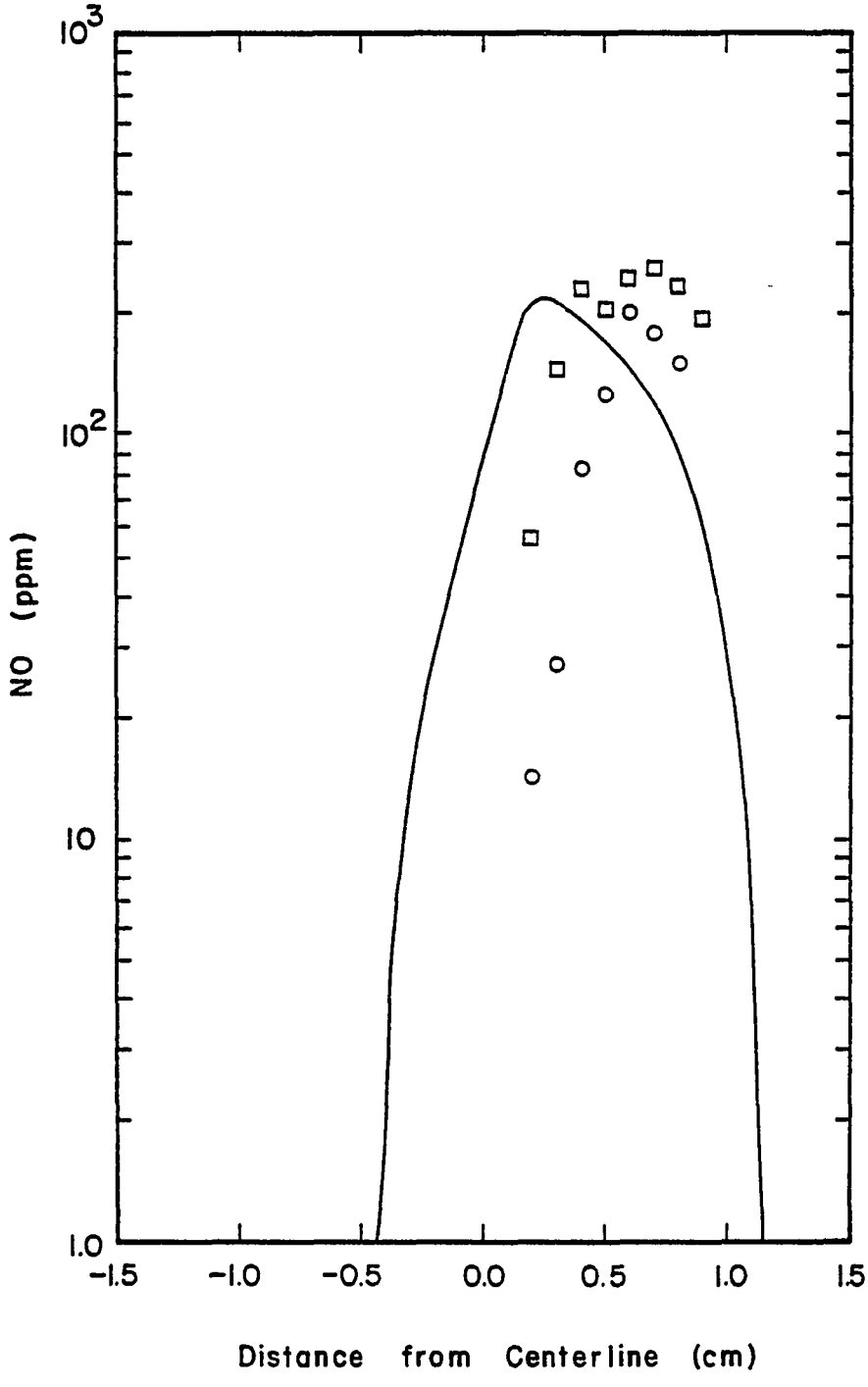

Figure 38. $CH_4/N_2/O_2$ Flame: $\varepsilon = 7.24\ sec^{-1}$, NO Profile (Two Experiments, Experimental Values Not Shifted, NH_3 Injected with Fuel).

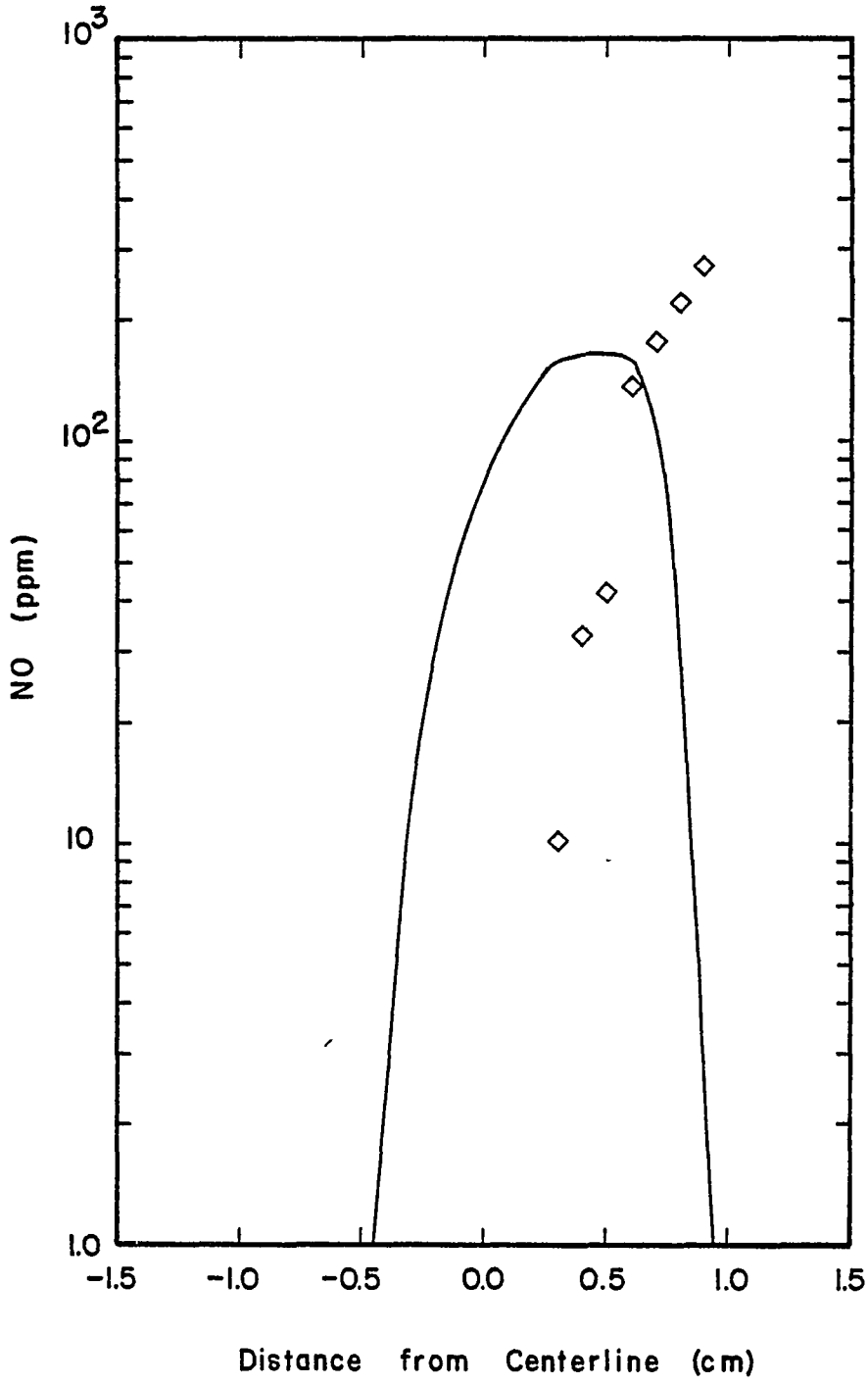

Figure 39. $CH_4/N_2/O_2$ Flame: $\varepsilon = 7.24\ sec^{-1}$, NO Profile (One Experiment, Experimental Values Not Shifted, NH_3 Injected with Oxidizer).

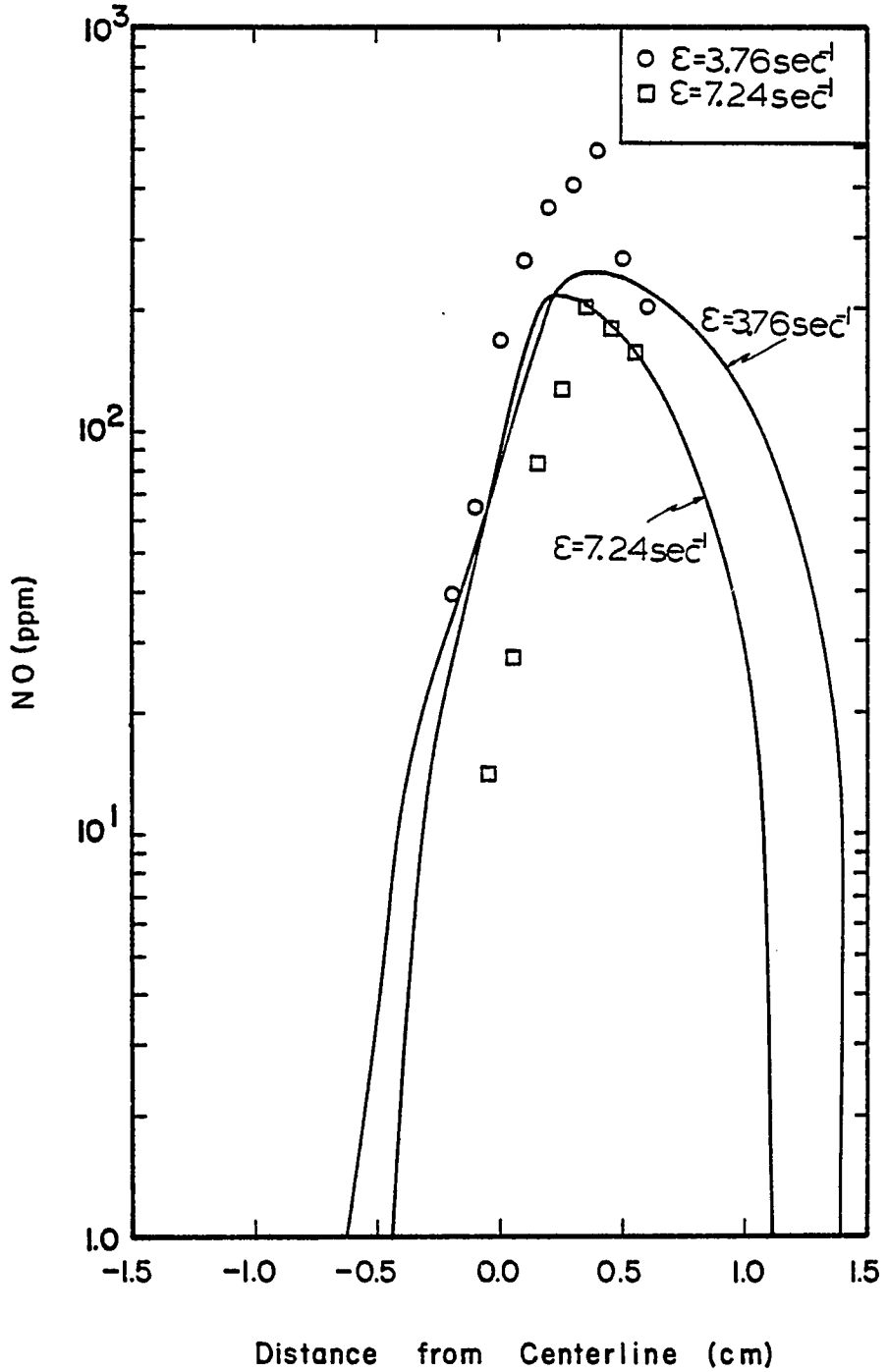

Figure 40. $CH_4/N_2/O_2$ Flame: ε = 7.24 and 3.76 sec^{-1}, Effect of Stretching Rate on NO Profile (NH_3 Injected with Fuel).

Theory predicts that the low stretching rate flame has an NO profile which is wider than the profile of the high stretching rate flame and that the peak of the profile increases as the stretching rate decreases. The experimental data verify both predictions very well, indicating that the effect of stretching rate on the formation of NO in the Laminar Opposed Jet Diffusion Flame is well modeled.

The following is concluded from the results presented in this section:

1. Theory and experiment are in close agreement when the NH_3 is injected with the fuel.
2. Theory does not predict the correct profile when NH_3 is injected with the oxidizer.
3. The effect of the stretching rate on the NO profile is well modeled in the case when the NH_3 is injected into the fuel.

Additional Predictions

Dilute Fuel

Figure 41 shows the predicted profiles of CH_3, CH_2, CH_2O, and NH_3. The peak heights of the carbon containing species are 2000 ppm, 70 ppm, and 56 ppm for CH_3, CH_2O, and CH_2, respectively. The profiles of these species are narrow and located in the fuel-rich side of the flame as was expected. The decay of the NH_3 concentration is much less pronounced in this flame than it was in the CO flame.

The concentrations of H_2 and of OH, O, and H are presented on Figure 42. The peak values of OH and O are 4000 and 960 ppm,

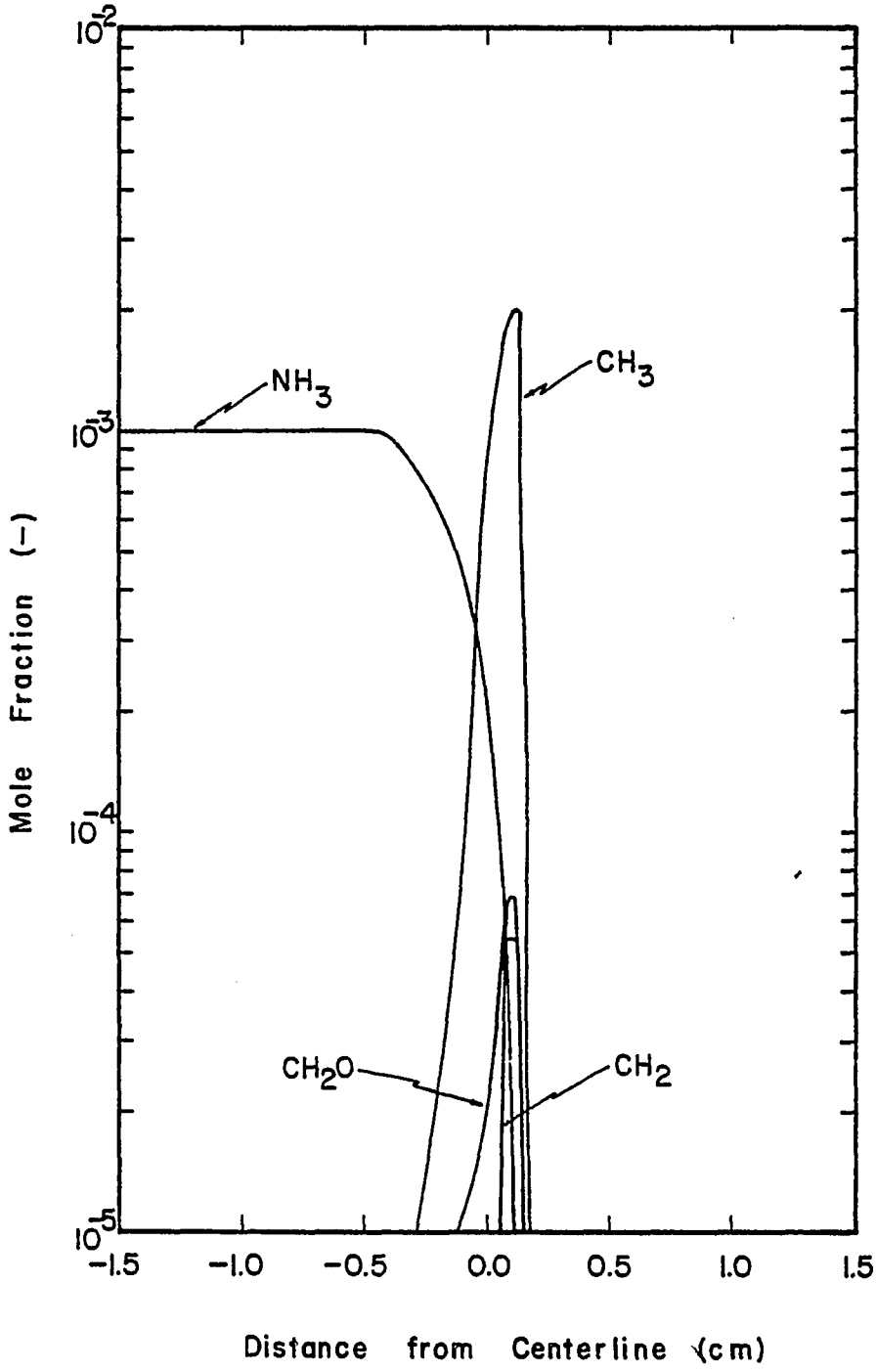

Figure 41. $CH_4/N_2/O_2$ Flame: $\varepsilon = 7.24\ sec^{-1}$; CH_3, CH_2, CH_2O, and NH_3 Profiles (NH_3 Injected with Fuel).

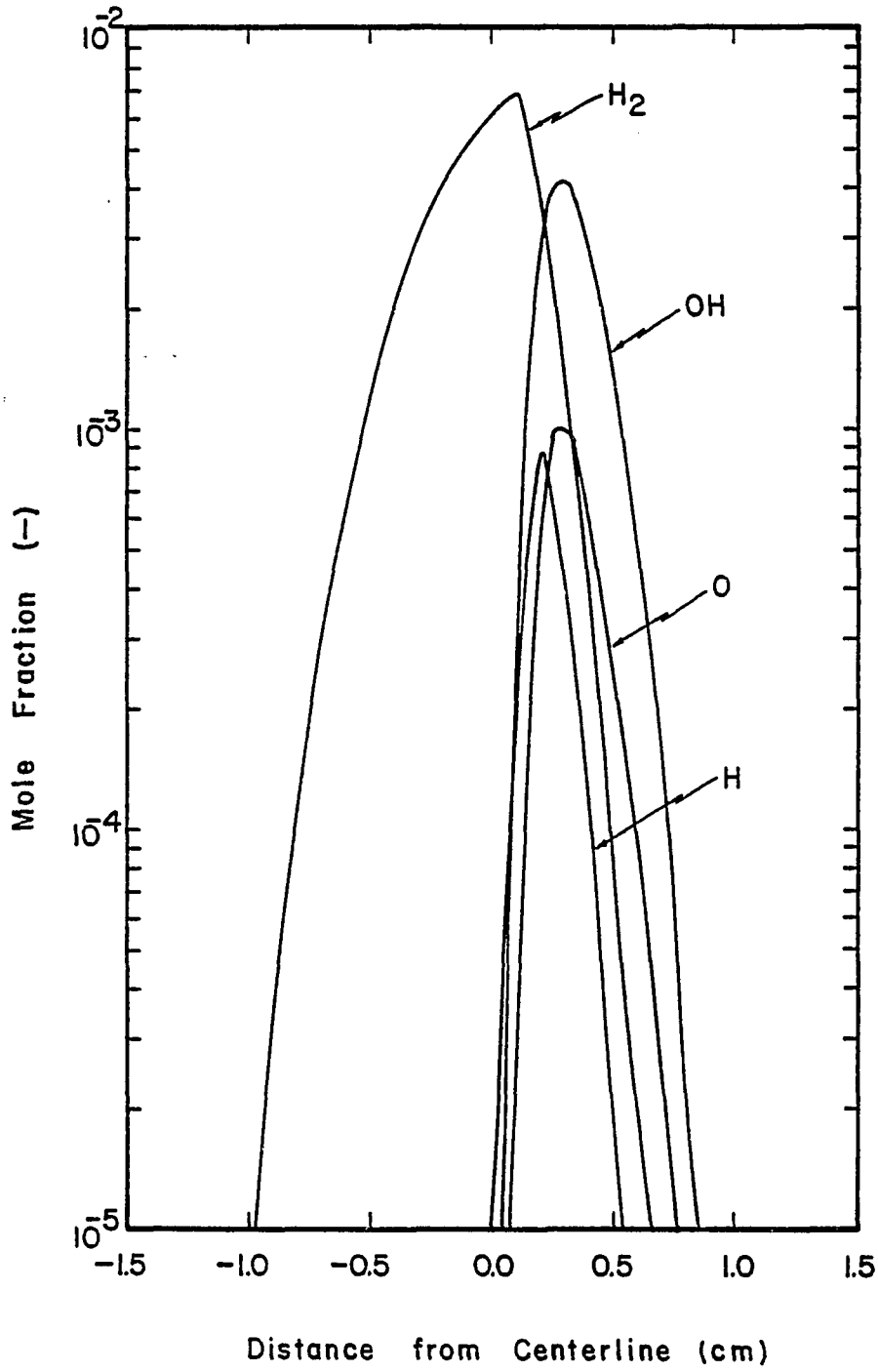

Figure 42. $CH_4/N_2/O_2$ Flame: $\varepsilon = 7.24\ sec^{-1}$; H_2, OH, O, and H Profiles.

respectively. The profiles of these two species lie in the fuel-lean zone which was intuitively expected. H_2 presents a very broad profile, which can be explained through its very large diffusion coefficient, while the profile of H atoms is much narrower due to its high reactivity. Peak values are 7000 ppm for H_2 and 1000 ppm for H.

Figure 43 represents the predicted profiles of CH, CHO, and HO_2. These species are free radicals and have very short lives. The profiles of CH and CHO have maximum values of 5.6 and 0.08 ppm, respectively, and are very narrow. Furthermore, those two profiles are located on the fuel-rich side of the flame zone. The HO_2 profile, which has a maximum value of 1.5 ppm, is very broad. This can be explained through the very large diffusion coefficients of H_2 and H.

On Figures 44 through 46, the profiles of the nitrogen containing species are shown. It can be seen that those not containing oxygen, i.e., the products of pyrolysis reactions, have their highest value on the fuel-rich side of the flame, while those containing oxygen peak on the fuel-lean side of the flame. The predicted peak value of 20 ppm for HCN is surprisingly low, but is corroborated by experiment in that not more than 20 ppm of HCN was detected with the hot wire detector of the gas chromatograph. In the present case, the peak value of N and NH are much lower, at 60 and 350 ppb, than the peak of the N profile which reaches 5.8 ppm, indicating that the pyrolysis reactions in the presence of CH_4 give good predictions.

The predicted axial velocity profile is drawn on Figure 47. It can be seen that, as in the CO flames, the velocity field far away from

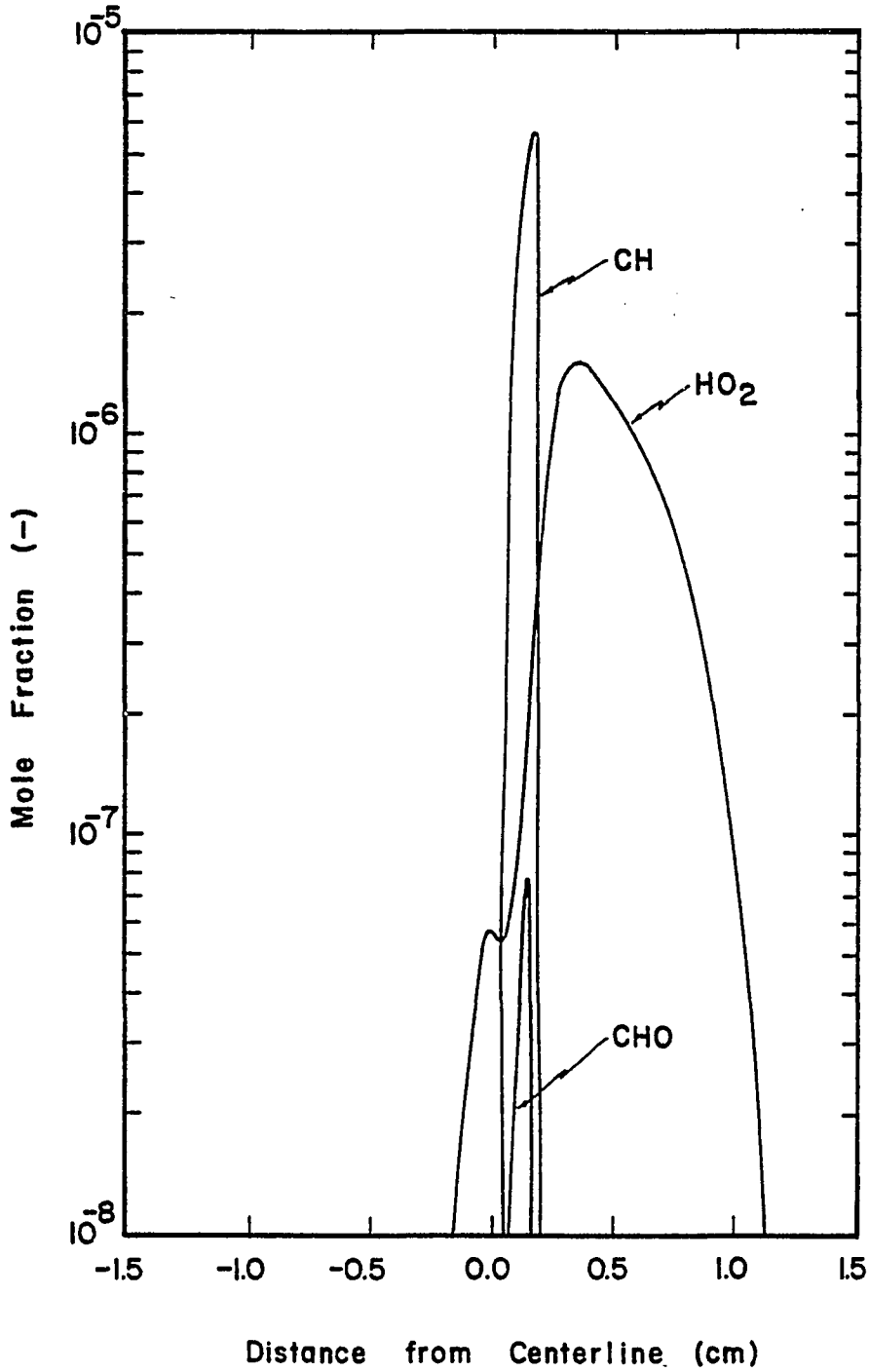

Figure 43. $CH_4/N_2/O_2$ Flame: ε = 7.24 sec^{-1}; CH, HO_2, and CHO Profiles.

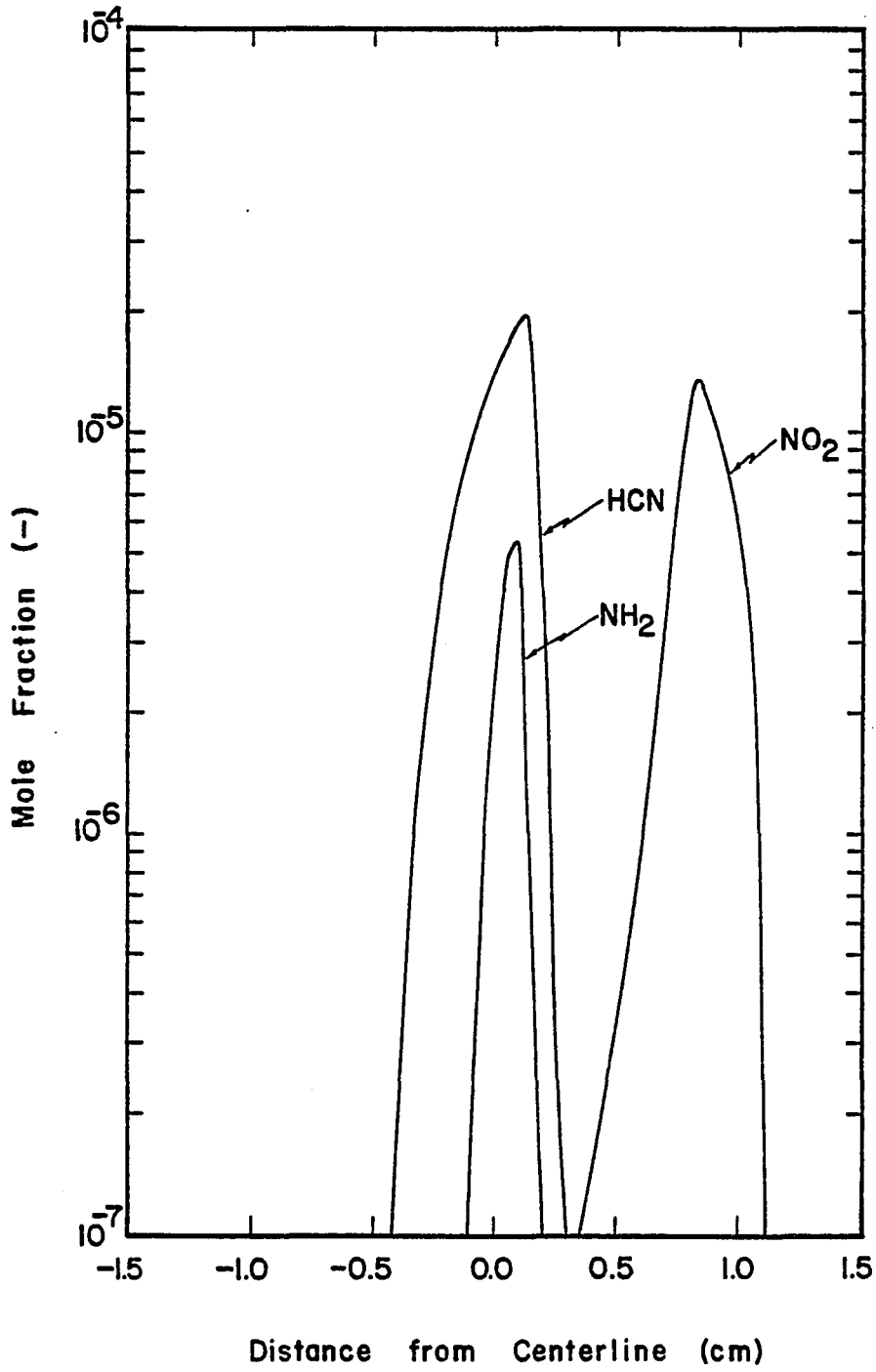

Figure 44. $CH_4/N_2/O_2$ Flame: $\varepsilon = 7.24\ sec^{-1}$; HCN, NH_3, and NO_2 Profiles (NH_3 Injected with Fuel).

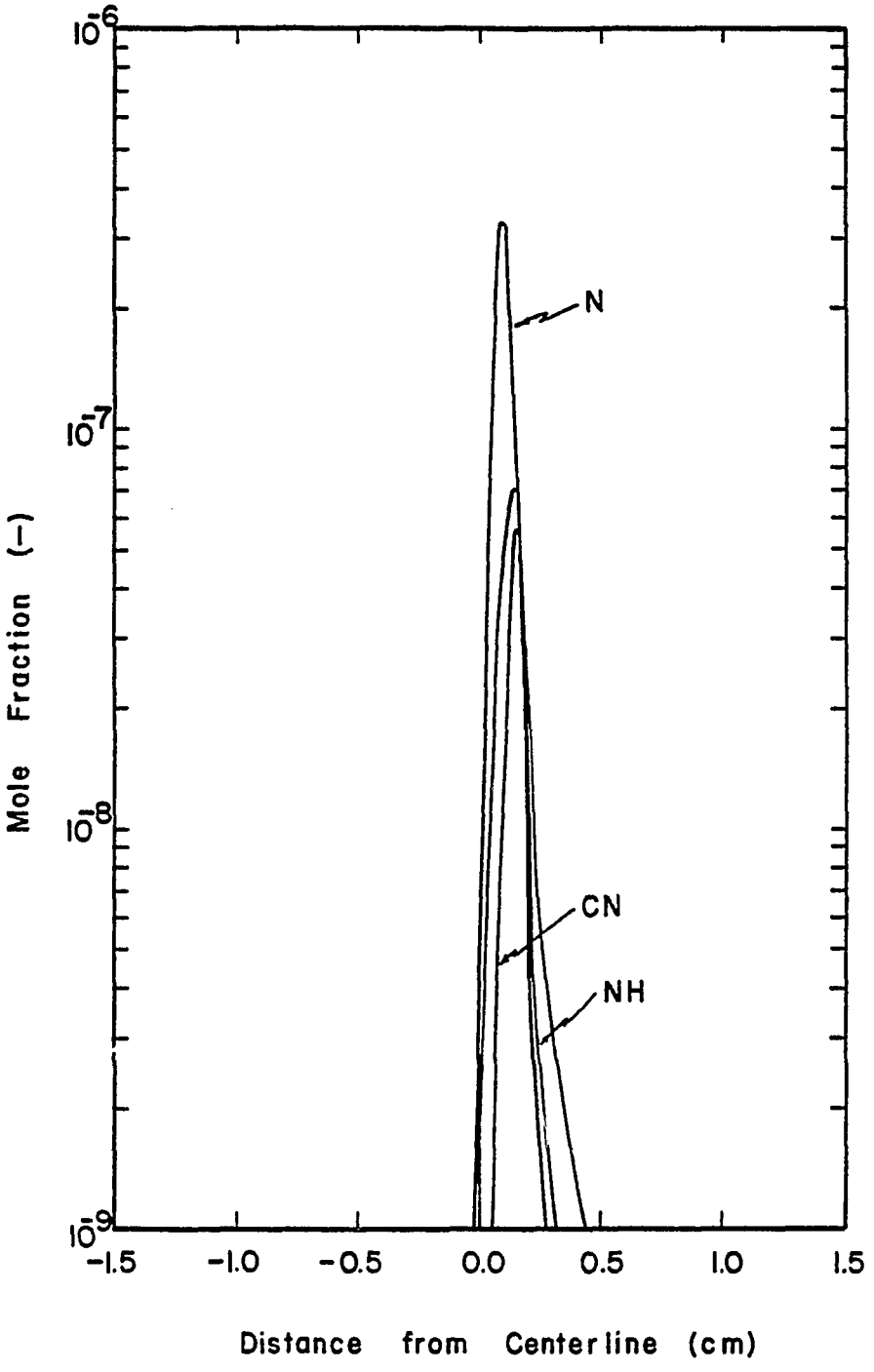

Figure 45. $CH_4/N_2/O_2$ Flame: ε = 7.24 sec^{-1}; N, CN, NH Profiles (NH_3 Injected with Fuel).

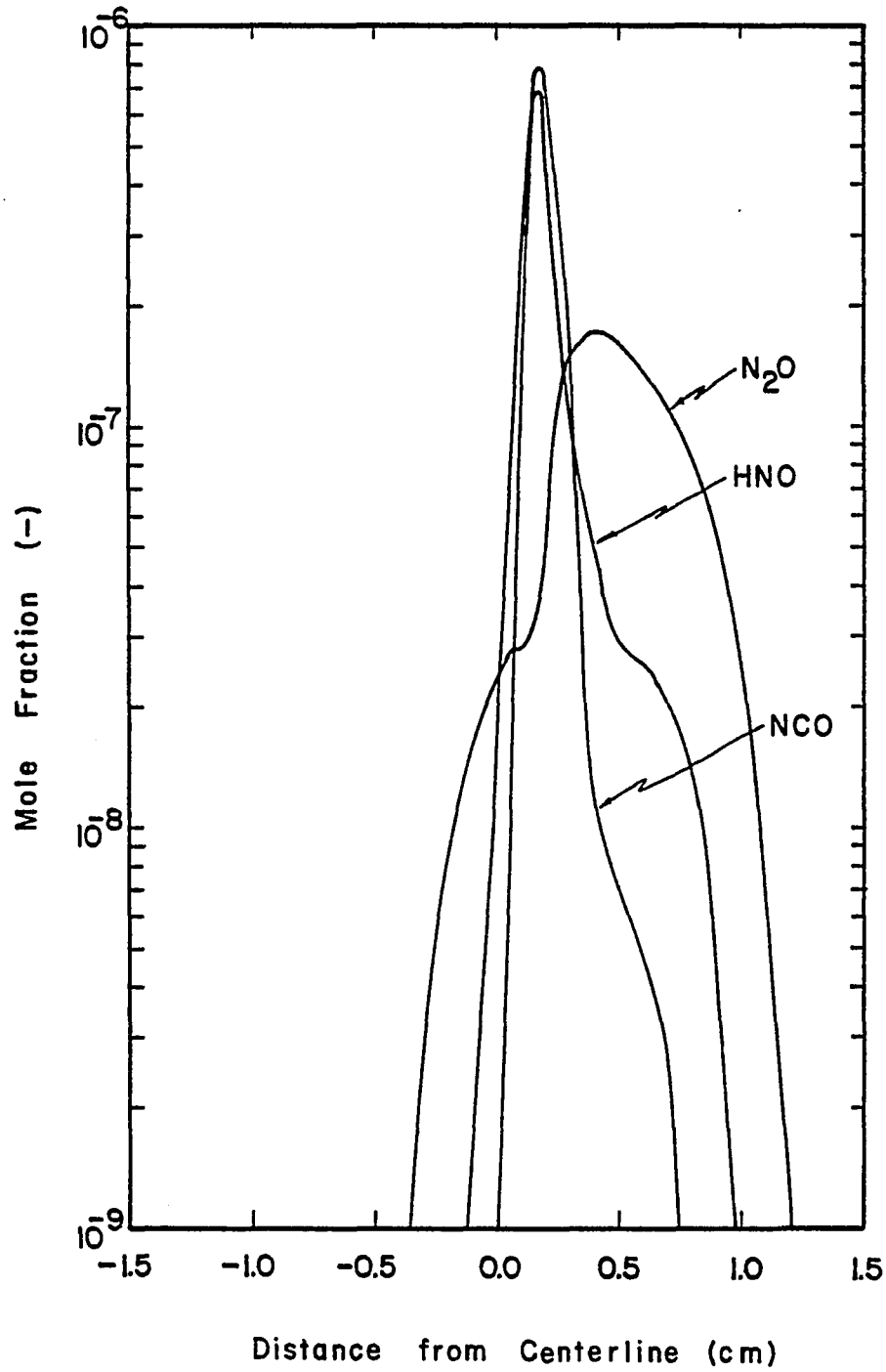

Figure 46. $CH_4/N_2/O_2$ Flame: $\varepsilon = 7.24\ sec^{-1}$; N_2O, HNO, and NCO Profiles (NH_3 Injected with Fuel).

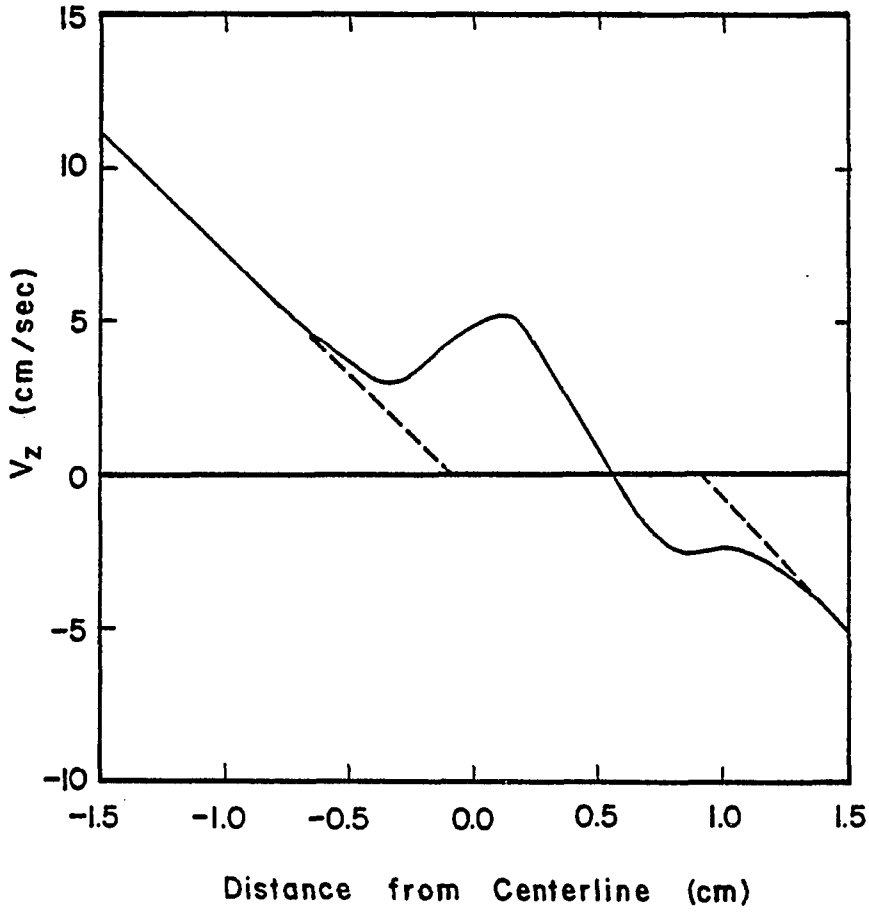

Figure 47. $CH_4/N_2/O_2$ Flame: $\varepsilon = 7.24\ sec^{-1}$, Axial Velocity Profile.

the flame zone is linear and that this linearity does not hold inside the flame zone. It is also interesting to note that due to the effect the temperature has on the velocity profiles the two jets "see" different stagnation points. If the line corresponding to the fuel jet is extrapolated, the stagnation point would be located at -0.1 cm, if the velocity profile of the oxidizer jet is extrapolated, the virtual stagnation point is 0.9 cm. The actual stagnation point is between these two virtual stagnation points, well into the fuel-lean side of the flame, namely at z = 0.55 cm.

All the profiles presented in Figures 41 through 47 correspond to a flame which has a rate of stretching of 7.24 sec^{-1}.

The effect of the stretching rate on the heat release profile is presented on Figure 48. It can be observed that with increased stretching rate the heat release profile decreases in width, while increasing in height. This suggests that the effect of the rate of stretching is that it decreases the reaction zone and within this decreased reaction zone the reactions become more intense. Therefore, the rate of stretching can be associated with the local combustion intensity in a turbulent diffusion flame.

Figure 49 shows the dependence of the rate of formation of NO on the stretching imposed on the Laminar Opposed Jet Diffusion Flame. It can be seen that when doubling the rate of stretching the rate of formation of NO increases by one order of magnitude. Nevertheless, since both reactions forming NO and reactions destroying it are of equal importance, when this profile is integrated over the z-axis, the effect

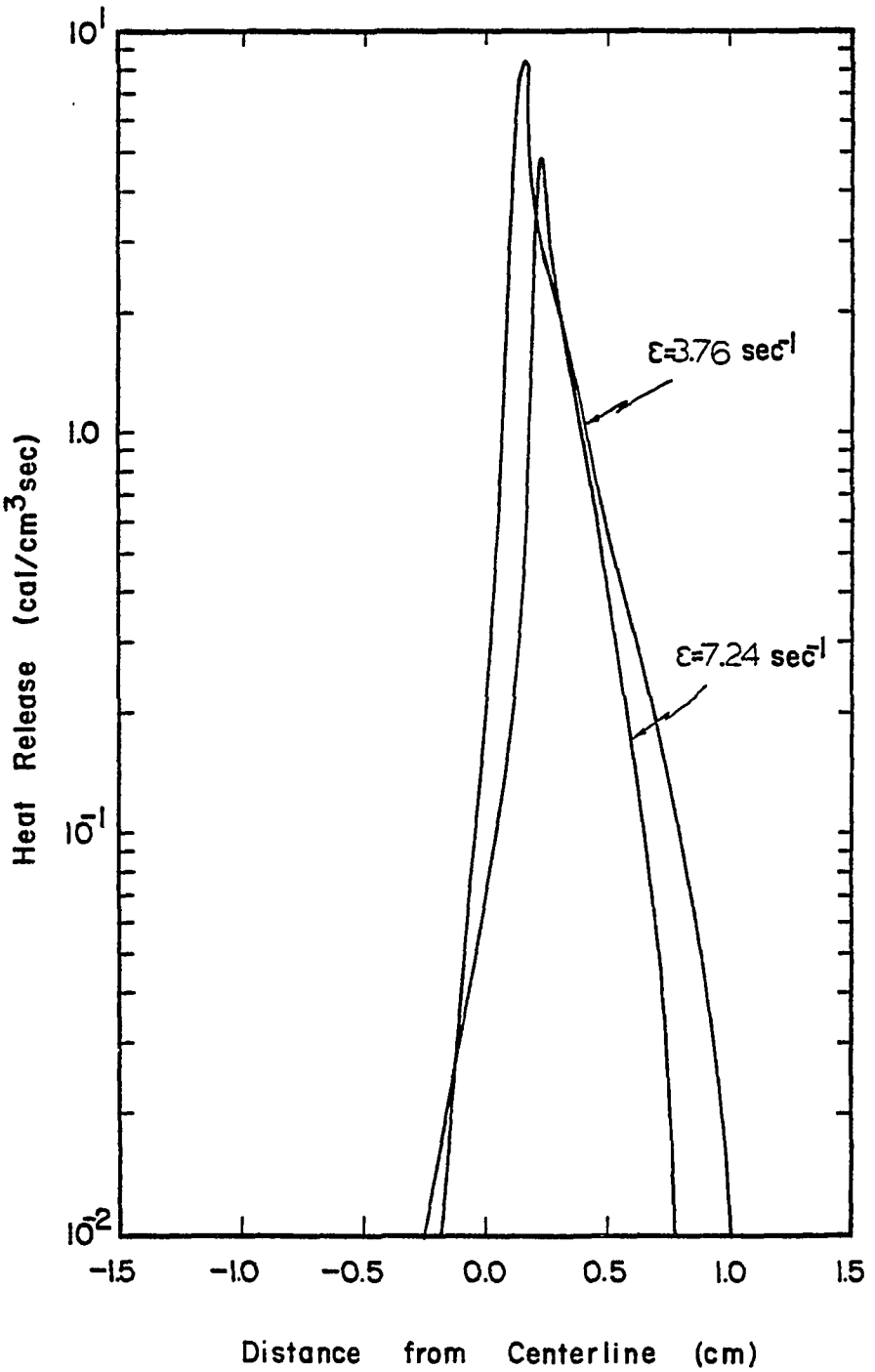

Figure 48. $CH_4/N_2/O_2$ Flame: $\varepsilon = 7.24\ sec^{-1}$, Effect of Stretching Rate on Heat Release Profile.

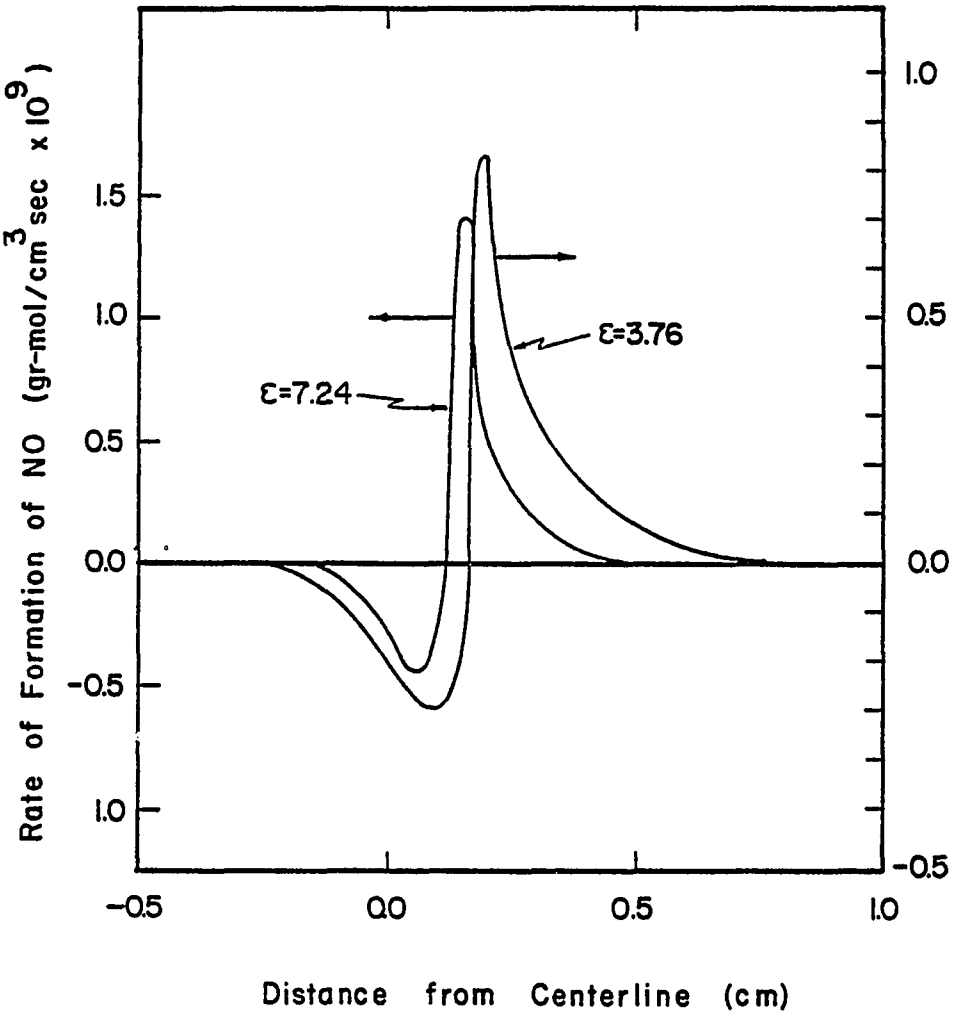

Figure 49. $CH_4/N_2/O_2$ Flame: ε = 7.24 and 3.76 sec^{-1}, Effect of Stretching Rate on Rate of Formation of NO (NH_3 Injected with Fuel).

is much smaller and it is estimated that the net rate of formation increases by a factor of two.

Pure Fuel

The model was solved for the case where the fuel stream is 98% CH_4 and 2% N_2 and the oxidizer is air. A very high stretching rate was necessary, since the steep gradients of product concentrations arising in this particular case cause the products to diffuse rapidly towards the burners. When the net flux of any species is directed towards a burner, the concentration boundary condition cannot be satisfied and the solution scheme diverges. This difficulty can be solved two ways:

1. The rate of stretching can be increased, thus increasing the convective flux away from the burners, of all species.
2. The physical spacing of the burners can be increased, maintaining the rate of stretching.

Both solutions have the same effect from an experimental point of view, in that the flow rates at the burners must be increased. In the present work, the first solution is chosen and a rate of stretching of 48.9 sec^{-1} is necessary to obtain a stable solution if the burner separation is 2 cm. Figure 50 shows the velocity profile corresponding to this solution; the velocity of the fuel is 56.5 cm/sec which is identical to 1.04 l/min in our experiment. At present, available facilities were not able to provide these large flow rates and the actual experiment could not be performed. The second velocity boundary conditions, that of the air, was calculated to be 29.9 cm/sec or 55.04 lt/min.

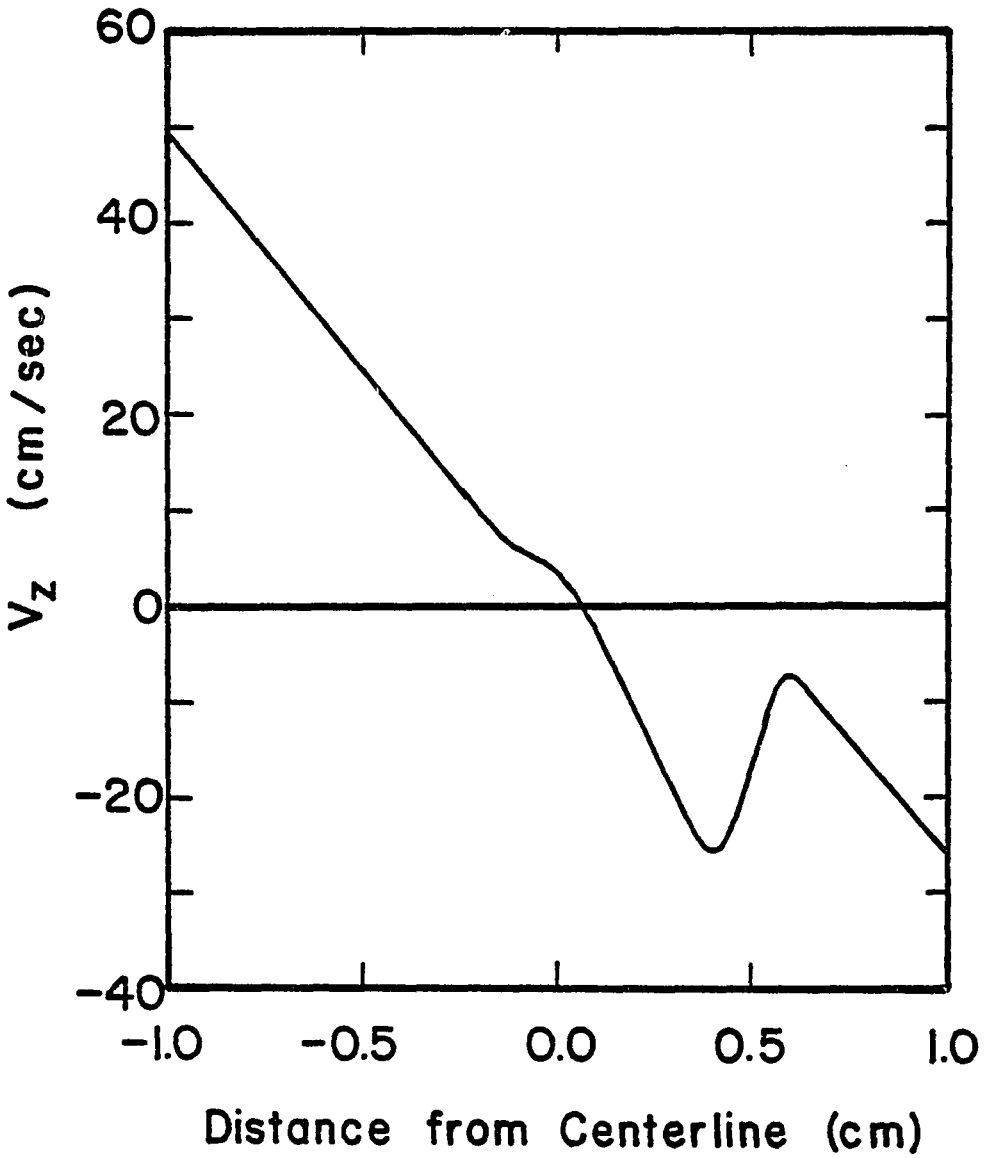

Figure 50. $CH_4/N_2/O_2$ Flame: ε = 48.9 sec^{-1}, Axial Velocity Profile (Pure CH_4, Air Flame).

Figure 51 shows the profiles of CO and CO_2. It is interesting to note how close the CO_2 profile comes to the burner from which the air is injected. If the stretching rate were less than 48.9 sec^{-1}, the concentration of CO_2 on the surface of the burner would be calculated to be different from zero, which is in contradiction with the specified boundary condition.

Figure 52 shows the profiles of the reactants and H_2O for this case and it can be observed that the region where the profiles of the reactants overlap is extremely small, which is expected intuitively for such a high stretching rate. In addition, the mesh used to solve the differential equations is shown at the bottom of this figure.

From the evidence presented above, the following conclusions can be reached:

1. NH_3 is pyrolyzed more slowly in the presence of CH_4 than it is in the presence of CO.
2. NH and N concentrations are predicted to be much lower than the NH_2 concentration.
3. An increase in the rate of stretching decreases with the width of the reaction zone.
4. The stretching rate increases the combustion intensity of reactions in the flame zone.
5. The rate of stretching increases the rate of formation of NO.
6. A very high stretching rate is necessary to obtain a Flat Laminar Opposed Jet Diffusion Flame if it is desired to burn pure fuel with air.

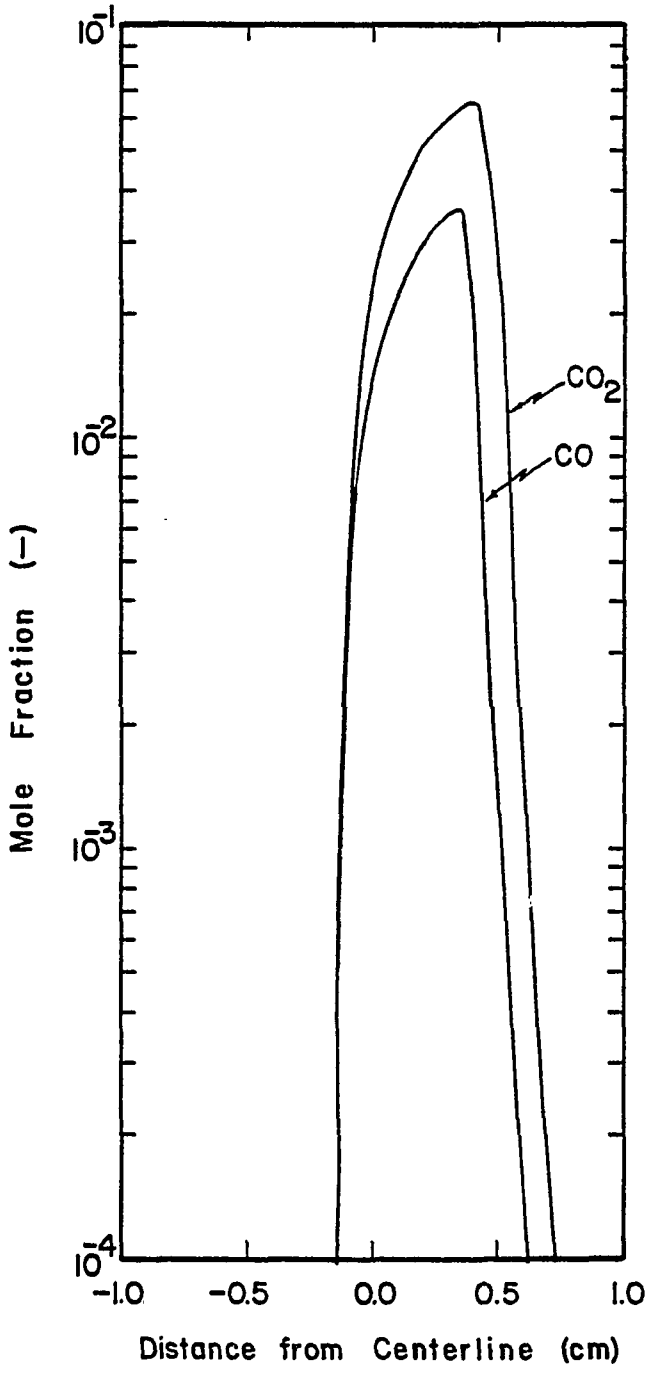

Figure 51. $CH_4/N_2/O_2$ Flame: ε = 48.9 sec^{-1}, CO and CO_2 Profiles (Pure CH_4, Air Flame).

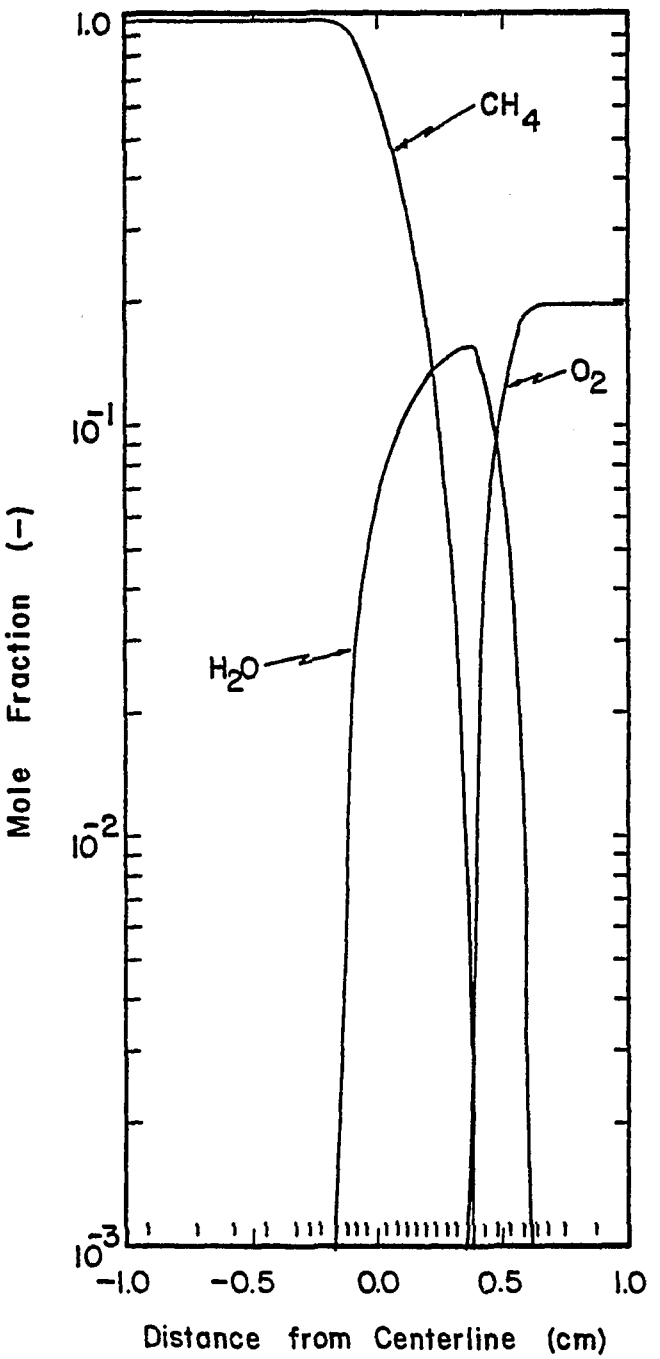

Figure 52. $CH_4/N_2/O_2$ Flame: ε = 48.9 sec^{-1}; CH_4, H_2O, and O_2 Profiles (Pure CH_4, Air Flame).

CHAPTER 7

CONCLUSIONS

The detailed reaction zone structure of the Laminar Opposed Jet Diffusion Flame can be modeled and the predictions are in good agreement with experiment.

It is shown that the strong interaction between heat release and conservation of momentum in a Laminar Opposed Jet Diffusion Flame causes the axial velocity profile to be non-linear. Because of this non-linearity, a (mathematically) Flat Flame can only be achieved if the proper velocity boundary conditions are used. If the velocity at either jet is specified, the velocity of the second jet can only be found after simultaneously solving the equations of conservation of total mass and momentum and those representing conservation of species and energy. It is further shown that if the proper velocities are used in a laboratory-scale experiment the resulting flame is one-dimensional in species concentration and in temperature. In the laboratory experiments, excellent agreement between theory and experimental results is achieved, although no adjustable parameter is used to fit the experimental results.

For given ambient conditions, i.e., concentrations and temperature at the boundaries, the problem depends on only one additional parameter, namely the rate of stretching.

The Laminar Flat Opposed Jet Diffusion Flame can be viewed as a novel tool that can be utilized as a prototype model in the simulation

of single-phase or two-phase turbulent diffusion flames. Furthermore, from a fundamental point of view, the Opposed Jet Diffusion Flame may be useful in determining the kinetics of combustion and/or formation of trace species in diffusion flames and in studying fuel pyrolysis and early combustion phenomena, such as the formation of soot.

The reaction zone structure is well-modeled and in almost all cases experimental and theoretical values are in excellent agreement, especially in the height of the profiles, which is a severe test of the model. However, the location of the flame zone appeared to be shifted approximately 2.5 mm towards the fuel-lean side of the flame in the experiments in all but one flame. It is thought that this may be caused by a combination of possible things, such as faulty kinetic information in the reaction scheme, neglected radiative heat loss, or neglected thermal diffusion.

In those studies of ammonia conversion to nitric oxide in $CO/N_2/O_2$, agreement between theory and experimental evidence is quantitative for the case where ammonia is injected with the oxidizer and only qualitative when ammonia is injected with the fuel stream. Of the complex set of reactions considered in the simulation, different reactions dominate in the fuel-lean and fuel-rich sides of the flame and the present experimental data indicate that the kinetic information for the oxidation reactions is essentially correct. The disagreement in the case when the NH_3 is injected into the fuel stream may be attributed to the shifting of the flame, which would change its velocity profile, or to uncertainties in the kinetic and thermochemical

information pertaining to ammonia pyrolysis and used in this work. Additional experiments, to be reported elsewhere, cast doubt on the ammonia pyrolysis mechanisms and rates employed in this work.

In $CH_4/O_3/N_2$ flames, theoretical and experimental profiles of NO are in good agreement when the ammonia is supplied with the fuel stream. If the NH_3 is injected with the oxidizer, the agreement is not good. This disagreement may be attributed to a combination of two error sources, one being the incorrect location of the flame zone, the other being inaccuracies in the kinetic and thermochemical information used in the present theoretical predictions.

The predicted effect of the rate of stretching, a key parameter in this model, on the flame zone thickness is in excellent agreement with experimental data obtained in this work. Furthermore, the effect on the profile of NO is also very well modeled. This indicates that the effect of stretching rate is well represented in the model and that it can be used as a prototype model in the simulation of much more complicated turbulent diffusion flames.

CHAPTER 8

RECOMMENDATIONS FOR FUTURE WORK

The results of the present investigation provide numerous suggestions for future work, both of a fundamental and a more applied nature. Some of the areas which are particularly worthy of note are:

1. Complex kinetic mechanisms: This work clearly establishes that there still is need of further investigation of the reaction mechanism used to simulate the formation of NO from fuel nitrogen. Of particular importance are those reactions which dominate the formation of NO in a very fuel-rich, carbon monoxide flame. There is also some doubt about the validty of the reactions which become important in the formation of NO in fuel-lean methane flames. Furthermore, it is of interest to determine if the shifting noted in the experimental results of the present work can be explained by changes in the kinetic information of the reactions used to simulate the combustion process of carbon monoxide and methane.

   From an experimental point of view, it is desirable to have a wider flame zone, since this would permit better spatial resolution and more accuracy of the measurements. Such a flame could be obtained under sub-atmospheric conditions.

2. Early phenomena in coal combustion: The Opposed Jet Diffusion Flame is an excellent tool to study early pyrolysis combustion

phenomena, and if used with pulverized coal as the fuel, can shed significant insight into the ignition mechanism of coal flames and/or early coal devolatilization phenomena.

3. Soot formation: A further possible application of the Opposed Jet Diffusion Flame is the study of formation of soot particles arising from cracking of fuels in very fuel-rich regions of diffusion flames.

4. Trace species formation in turbulent diffusion flames: The Opposed Jet Diffusion Flame contains both complex kinetics determining the formation of trace species and an aerodynamic stretching phenomena. This makes it a very attractive prototype model to be included in a model of turbulent diffusion flames based on the existence of coherent flamelets undergoing strain in their own plane. The final link between these two models has not been established yet and further work is needed in this area.

5. Diffusion flames around coal particles: Coal burns in a second regime with a diffusion flame surrounding the particle (Wendt, 1979). The model describing the Opposed Jet Diffusion Flame can be modified to simulate this situation and then used to predict the rate of formation of NO during this second regime of coal combustion.

NOMENCLATURE

$\underline{\underline{A}}$	Block tridiagonal matrix.
A_i	Variable coefficient in equation [45].
B_i	Variable coefficient in equation [45].
c	Molar density (gr-mol/cm^3).
C_i	General dependent variable.
C_p	Heat capacity (cal/gr-mol °K).
d	Diameter of the thermocouple bead (cm).
D_A	Pseudo binary diffusion coefficient of species A in gaseous mixture.
D_{ij}	Binary diffusion coefficient of species i in species j (cm^2/sec).
$\underline{\underline{E}}$	Strain rate tensor.
$\underline{\underline{F}}$	Vector of forcing functions (see equation [56]).
$\underline{\underline{F}}^*$	Block vector of forcing functions (see equation [63]).
$\underline{g}$	Body force vector.
$\underline{G}$	Auxiliary vector (see equation [66]).
G_{ij}	Auxiliary variables (see equation [44]).
k	Thermal conductivity of gaseous mixture (cal/cm-sec °K).
k_i	Thermal conductivity of species i (cal/cm-sec °K).
ℓ	Separation of burners (cm).
$\underline{\underline{L}}$	Lower triangular matrix.
m	Number of grid points.
M_i	Molecular weight of species i (gr/gr-mol).

n	Number of gases in mixture.
nr	Number of chemical reactions.
nsp	Number of species in reaction set.
N	nsp + 1.
$\underline{N}_A$	Flux of species A (gr-mol/cm^2-sec).
P	Pressure (atm).
$\underline{q}$	Heat flux vector (cal/cm^2-sec).
r	Radial distance (cm).
r_j	Rate of reaction j (gr-mol/cm^3-sec).
R_A	Rate of formation of species A (gr-mol/cm^3-sec).
R_i	Forcing function (see equation [45]).
$\underline{\underline{S}}_p$	Auxiliary matrix (see equation [59]).
T	Temperature (°K).
T_c	Temperature of the thermocouple (°K).
T_g	Temperature of the gas (°K).
$\underline{\underline{T}}_p$	Auxiliary matrix (see equation [58]).
$\underline{\underline{U}}$	Upper triangular matrix.
$\underline{\underline{U}}_p$	Auxiliary matrix (see equation [58]).
v	Axial velocity (cm/sec).
$\underline{v}$	Velocity vector (cm/sec).
v_r	Radial component of $\underline{v}$ (cm/sec).
v_z	Axial component of $\underline{v}$ (cm/sec).
V	Molar volume (cm^3/gr-mol).
x_A	Mole fraction of species A.
z	Dimensionless axial distance.
z'	Axial distance (cm).

Greek Symbols

$\alpha_{i,p}$ Auxiliary variable (see equation [51]).

$\beta_{i,p}$ Auxiliary variable (see equation [52]).

$\gamma_{i,p}$ Auxiliary variable (see equation [53]).

$\underline{\Delta c}^*$ Block vector of corrections.

$\underline{\Delta c}_p$ Vector of corrections.

$\Delta C_{j,p}$ Correction to variable j at point p.

Δh_j Heat of reaction j (cal/gr-mol).

Δz Increment on grid.

$\underline{\underline{\delta}}$ Unity matrix.

ε Stretching rate (sec^{-1}).

ε_i Energy of interaction of species i (erg/molecule).

θ Dimensionless temperature = $\frac{T-298}{298}$

λ Under-relaxation factor.

μ Viscosity of mixture (g/cm-sec).

μ_i Viscosity of species i (g/cm-sec).

ρ Density (g/cm^3).

σ_i Collision diameter of species i (Å).

$\underline{\underline{\tau}}$ Shear stress tensor.

ϕ_{ij} Auxiliary variable (see equation [41]).

ψ Similarity transformation (see equation [20]).

Ω_D Collision integral for diffusion.

Ω_μ Collision integral for viscosity and thermal conductivity.

Subscripts

∞	Refers to distance from flame zone.
1	Refers to distance from flame zone on fuel side.
2	Refers to distance from flame zone on oxidizer side.
i	Refers to dependent variable i.
p	Refers to grid point.

Superscripts

k	Refers to iteration number.
n	Refers to iteration number.

APPENDIX

COMPUTER PROGRAM

```
      PROGRAM READ(INPUT,OUTPUT,TAPE6=INPUT,TAPE5=OUTPUT,
     1  TAPE4)
      CALL BRUTO
      STOP
      END
      SUBROUTINE BRUTO
      COMMON /A/NSP,NR,MATRIX(86,30),ID,I(73),LS,NAMSPE,LSTSPE(30)
     1  ,AF(86),TEF(86),EF(86)
     2  ,AR(86),TER(86),ER(86)
     3  ,LISTBC(30),RBC(30),ALBC(30),NBC
     4  ,TB(86),N2(86),NTB,NN2
     5  ,CREAT(30,86),NCR(30),DESTR(30,86)
     6  ,NDS(30),SPEF(86,2),NSPEF(86),NSPER(86),SPER(86,2)
     7  ,MULT(30,2),NMULT,NNN2,NN3
      INTEGER SPERXN,CREAT,DESTR,SPEF,SPER
      INTEGER TB
      DIMENSION IFOR(3)
      DIMENSION DH(30),ACP(30),BCP(30),CCP(30),DCP(30)
      NSP=0
      NR=0
      NBC=0
      NMULT=0
      DO 100 K=1,86
      DO 100 J=1,30
100   MATRIX(K,J)=0
      WRITE(5,84)
84    FORMAT(*1ECHO CARDS:*/* **** *******)
123   READ(6,50)ID,(I(K),K=1,73)
      IF(EOF(6).NE.0)GO TO 1000
50    FORMAT(A6,1X,73A1)
C
C
C     FIND COMMA AFTER NAME OF AUTHOR
C
C
      DO 102 K=1,73
      IF(I(K).NE.1H,)GO TO 102
      L=K
      GO TO 1
102   CONTINUE
      WRITE(5,91)
91    FORMAT(*0COMMA MISSING ON CARD*)
      RETURN
C
C
C     ECHO CARD
```

```
C
C
1       WRITE(5,90)ID,(I(K),K=1,73)
90      FORMAT(*0*,A6,*,*,73A1)
C
C
C       ELIMINATE NAME OF AUTHOR
C
C
        IF(ID.EQ.6HBOUCON)GO TO 2
        LP1=L+1
        LF=73-L
        DO 101 K=LP1,73
101     I(K-L)=I(K)
C
C
C       CALL APROPRIATE SUBROUTINE TO INTERPRET CARD
C
C
        IF(ID.EQ.6HSTOICH)CALL NAME
        IF(ID.EQ.6HFRATCO)CALL FORWD
        IF(ID.EQ.6HRRATCO)CALL BACKWD
2       IF(ID.EQ.6HBOUCON)CALL BOUNDA
        GO TO 123
C
C
C       FORM INFORMATION PERTINENT TO CALCULATION OF REACTION
C       RATES
C
C
1000    CONTINUE
        WRITE(5,1999)((MATRIX(K,J),J=1,30),K=1,86)
1999    FORMAT(*0*,30I3)
        CALL NITR3B
        CALL GENINF
C
C
C       REARRANGE BOUNDARY CONDITIONS
C
C
        CALL ARRANG
C
C
C       GET THERMOCHEMICAL DATA
C
C
        CALL THERMD(NSP,LSTSPE,DH,ACP,BCP,CCP,DCP)
```

```
      WRITE(5,80)(LSTSPE(J),J=1,NSP)
80    FORMAT(*1REACTION MATRIX:*/* *,8(*=*),* *,6(*=*)/
     1  *OREACT#  *,20(2X,A3))
C
C
C     GENERATE FORMAT TO PRINT MATRIX
C
C
      LA1=NSP/10
      LA2=NSP-LA1*10
      IF1=10H(20(*0*,I6
      IF5=1H,
      ENCODE(10,180,IF2)LA1
      ENCODE(10,180,IF3)LA2
180   FORMAT(I1)
      IF4=7H(2X,I3)
      IF5=3H/))
      ENCODE(10,190,IFOR)IF1,IF5,IF2,IF3,IF4,IF6
190   FORMAT(A10/3A1,A7/A3)
      PRINT IFOR,(J,(MATRIX(J,K),K=1,NSP),J=1,NR)
81    FORMAT(*0*,10I2)
      WRITE(5,70)(TB(J),J=1,NTB)
70    FORMAT(*1REACTIONS CONTAINING A THIRD BODY*/
     1  * *,9(*=*),1X,10(*=*),1X,*=*,1X,5(*=*),1X,4(*=*)/
     2  (30I3))
      WRITE(5,71)(N2(J),J=1,NN2)
71    FORMAT(////*OREACTIONS CONTAINING N2*/* *,9(*=*),1X,
     1  10(*=*),1X,2(*=*)/(30I3))
      WRITE(5,72)(MULT(J,2),MULT(J,1),J=1,NMULT)
72    FORMAT(////*OREACTIONS WITH MULTIPLE SEPCIES*/
     1  * *,9(*=*),* =*=* *,8(*=*),1X,7(*=*)/
     2  *OREACTION SPECIES*/(*0*,T3,I3,5X,I3))
      WRITE(5,74)
74    FORMAT(*1SPECIES #*,3X,*REACTIONS FORMING IT*)
      DO 105 J=1,NSP
      NC=NCR(J)
      WRITE(5,73)J,(CREAT(J,L),L=1,NC)
73    FORMAT(*0*,3X,I3,3X,20I3)
105   CONTINUE
      WRITE(5,75)
75    FORMAT(*1SPECIES #*,3X,*REACTIONS DESTROYING IT*)
      DO 106 J=1,NSP
      ND=NDS(J)
      WRITE(5,73)J,(DESTR(J,L),L=1,ND)
106   CONTINUE
      WRITE(5,76)
76    FORMAT(*1REACTION #*,5X,*SPECIES IN FORWARD*,
```

```
     1  5X,*SPECIES IN REVERSE*/1H ,18X,*EXPRESSION*,13X,
     2  *EXPRESSION*)
        DO 107 J=1,NR
        NSF=NSPEF(J)
        NSR=NSPER(J)
        IF(NSF.EQ.1)WRITE(5,77)J,(SPEF(J,L),L=1,NSF),(SPER(J,L),L=1,
     1  NSR)
        IF(NSF.EQ.2)WRITE(5,78)J,(SPEF(J,L),L=1,NSF),(SPER(J,L),L=1,
     1  NSR)
77      FORMAT(*0*,4X,I3,12X,I3,22X,2I3)
78      FORMAT(*0*,4X,I3,12X,2I3,19X,2I3)
107     CONTINUE
        DO 103 J=1,NR
        ER(J)=ER(J)*1000.
103     EF(J)=EF(J)*1000.
        WRITE(5,82)(J,AF(J),TEF(J),EF(J),J=1,NR)
        WRITE(5,83)(J,AR(J),TER(J),ER(J),J=1,NR)
82      FORMAT(*1FORWARD RATES:*/* *,7(*=*),* *,5(*=*)/
     1  (*0R*,I2,*=*,E10.4,4H*T**,F5.2,5H*EXP(,F7.0,
     2  11H/(1.986*T))))
83      FORMAT(*1REVERSE RATES:*/* *,7(*=*),* *,5(*=*)/
     1  (*0R*,I2,*=*,E10.4,4H*T**,F5.2,5H*EXP(,F7.0,
     2  11H/(1.986*T))))
        WRITE(5,86)(LSTSPE(J),ALBC(J),RBC(J),J=1,NSP)
86      FORMAT(*1BOUNDARY CONDITIONS*/* *,8(*=*),1X,10(*=*)
     1  /*0SPECIES*,6X,*LBC*,11X,*RBC*,/(*0*,1X,A5,3X,
     2  E11.3,3X,E11.3))
        WRITE(5,87)(LSTSPE(J),DH(J),ACP(J),BCP(J),CCP(J),
     1  DCP(J),J=1,NSP)
87      FORMAT(*1THERMOCHEMICAL INFORMATION*/* *,14(*=*),1X,
     1  11(*=*)/*0SPECIES*,6X,*HO*,14X,*CP*/
     2  (1X,A5,3X,E11.3,5X
     3  ,E11.3,*+*,E11.3,9H*ALOG(T)+,E11.3,3H*T+,E11.3,5H*T**2))
        CALL OUTPUT(DH,ACP,BCP,CCP,DCP)
        RETURN
        END
        SUBROUTINE BACKWD
        COMMON /A/NSP,NR,MATRIX(86,30),ID,I(73),LS,NAMSPE,LSTSPE(30)
     1  ,AF(86),TEF(86),EF(86)
     2  ,AR(86),TER(86),ER(86)
        DIMENSION IBL(10)
        DATA IBL/10*1H /
C
C
C       THIS SUBPROGRAM FINDS REVERS REACTION RATE INFORMATION
C       ON CARDS
C
```

```
C
C
C
C       ELIMINATE BLANKS FROM STRING
C
C
        CALL NOBLAN
        LI=1
        DO 100 II=1,3
C
C
C       FIND COMMA
C
C
        DO 101 J=LI,73
        K=J
        IF(I(K).EQ.1H,)GO TO 1
101     CONTINUE
        WRITE(5,80)
80      FORMAT(*1COULD NOT FIND COMMA*)
        STOP
1       K=K-1
        LE=K-LI+1
        LF=10-LE
C
C
C       ENCODE STRING INTO VARIABLE NUM
C
C
        NUM=10H
        IF(LE.EQ.10)ENCODE(10,190,NUM)(I(J),J=LI,K)
        IF(LE.NE.10)ENCODE(10,190,NUM)(IBL(J),J=1,LF),
     1  (I(J),J=LI,K)
190     FORMAT(10A1)
C
C
C       DECODE NUM INTO ONE OF THREE VARIABLES
C       II=1 ==> NUM IS A PREEXPONENTIAL
C       II=2 ==> NUM IS A TEMPERATURE EXPONENT
C       II=3 ==> NUM IS AN ACTIVATION ENERGY
C
C
        IF(II.EQ.1)DECODE(10,191,NUM)AR(NR)
        IF(II.EQ.2)DECODE(10,191,NUM)TER(NR)
        IF(II.EQ.3)DECODE(10,191,NUM)ER(NR)
191     FORMAT(E10.0)
100     LI=K+2
```

```
      RETURN
      END
      SUBROUTINE FORWD
      COMMON /A/NSP,NR,MATRIX(86,30),ID,I(73),LS,NAMSPE,LSTSPE(30)
     1  ,AF(86),TEF(86),EF(86)
      DIMENSION IBL(10)
      DATA IBL/10*1H /
C
C
C     THIS SUBPROGRAM FINDS FORWARD REACTION RATE INFORMATION
C     ON CARD
C
C
C
C
C     ELIMINATE BLANKS FROM STRING
C
C
      CALL NOBLAN
      LI=1
      DO 100 II=1,3
C
C
C     FIND COMMA
C
C
      DO 101 J=LI,73
      K=J
      IF(I(K).EQ.1H,)GO TO 1
101   CONTINUE
      WRITE(5,80)
80    FORMAT(*1COULD NOT FIND COMMA*)
      STOP
1     K=K-1
      LE=K-LI+1
      LF=10-LE
C
C
C     ENCODE STRING INTO VARIABLE NUM
C
C
      NUM=10H
      IF(LE.EQ.10)ENCODE(10,190,NUM)(I(J),J=LI,K)
      IF(LE.NE.10)ENCODE(10,190,NUM)(IBL(J),J=1,LF),
     1  (I(J),J=LI,K)
190   FORMAT(10A1)
C
```

```
C
C       DECODE NUM INTO ONE OF THREE VARIABLES
C       II=1 ==> NUM IS A PREEXPONENTIAL
C       II=2 ==> NUM IS A TEMPERATURE EXPONENT
C       II=3 ==> NUM IS AN ACTIVATION ENERGY
C
C
        IF(II.EQ.1)DECODE(10,191,NUM)AF(NR)
        IF(II.EQ.2)DECODE(10,191,NUM)TEF(NR)
        IF(II.EQ.3)DECODE(10,191,NUM)EF(NR)
191     FORMAT(E10.0)
100     LI=K+2
        RETURN
        END
        SUBROUTINE NAME
        COMMON /A/NSP,NR,MATRIX(86,30),ID,I(73),LS,NAMSPE,LSTSPE(30)
        LOGICAL LS
C
C
C       THIS SUBPROGRAM FORMS THE SPECIES LIST AND REACTION MATRIX
C
C
C
C
C       ELIMINATE BLANKS FROM STRING
C
C
        CALL NOBLAN
        CALL PLSEQ
C
C
C       LS INDICATES SIDE OF REACTION
C       LS=.T. ==> SPECIES IS ON LEFT OF = SIGN
C       LS=.F. ==> SPECIES IS ON RIGHT OF = SIGN
C
C
        LS=.TRUE.
C
C
C       NR IS THE REACTION COUNTER
C
C
        NR=NR+1
        IF(NR.GT.86)WRITE(5,99)
99      FORMAT(*0MORE THAN 86 REACTIONS*)
C
C
```

```
C       FIND FIRST PLUS SIGN
C
C
        DO 100 J=1,73
        K=J
        IF(I(K).EQ.1H+)GO TO 1
100     CONTINUE
        WRITE(5,80)
80      FORMAT(*1PLUS SIGN MISSING ON CARD*)
        STOP
C
C
C       ENCODE STRING INTO VARIABLE NAMSPE
C
C
1       K=K-1
        ENCODE(5,190,NAMSPE)(I(J),J=1,K)
190     FORMAT(10A1)
C
C
C       ADD SPECIES TO LIST IF NOT ALREADY THERE
C
C
        CALL ADDSPE
C
C
C       UPDATE SPECIES REACTION MATRIX
C
C
        CALL FORMMT
4       K=K+2
C
C
C       IF NEXT CHARACTER IS BLANK REACTION DECIPHERING IS FINISHED
C
C
        IF(I(K).EQ.1H )RETURN
        KOLD=K
C
C
C       IS NEXT CHARACTER A PLUS,COMMA OR EQUAL SIGN?
C
C
        DO 102 J=KOLD,73
        K=J
        IF(I(K).EQ.1H+.OR.I(K).EQ.1H=.OR.I(K).EQ.1H,)GO TO 2
102     CONTINUE
```

```
      WRITE(5,80)
      STOP
2     K=K-1
C
C
C     ENCODE STRING INTO VARIABLE NAMSPE
C
C
      ENCODE(5,190,NAMSPE)(I(J),J=KOLD,K)
C
C
C     ADD SPECIES TO LIST IF NOT ALREADY THERE
C
C
      CALL ADDSPE
C
C
C     UPDATE SPECIES REACTION MATRIX
C
C
      CALL FORMMT
C
C
C     IF SEPARATOR WAS AN EQUAL SIGN SET LS=.F.,
C     INDICATING START OF RIGHT SIDE OF REACTION
C
C
      IF(I(K+1).EQ.1H=)LS=.FALSE.
      GO TO 4
      END
      SUBROUTINE ADDSPE
      COMMON /A/NSP,NR,MATRIX(86,30),ID,I(73),LS,NAMSPE,LSTSPE(30)
C
C
C     THIS SUBPROGRAM ADDS A SPECIES TO THE LIST IF IT
C     IS NOT ALREADY THERE
C
C
      IF(NSP.EQ.0)GO TO 1
      DO 100 J=1,NSP
      IF(NAMSPE.EQ.LSTSPE(J))RETURN
100   CONTINUE
1     NSP=NSP+1
      IF(NSP.GT.30)WRITE(5,90)
90    FORMAT(*0MORE THAN 30 SPECIES*)
      LSTSPE(NSP)=NAMSPE
      RETURN
```

```
      END
      SUBROUTINE NOBLAN
      COMMON /A/NSP,NR,MATRIX(86,30),ID,I(73),LS,NAMSPE,LSTSPE(30)
C
C
C     THIS SUBPROGRAM ELIMINATES ALL BLANKS FROM STRING I
C
C
      K=0
      DO 100 J=1,73
      IF(I(J).EQ.1H )GO TO 100
      K=K+1
      I(K)=I(J)
100   CONTINUE
      K=K+1
      DO 101 J=K,73
101   I(J)=1H
      RETURN
      END
      SUBROUTINE FORMMT
      COMMON /A/NSP,NR,MATRIX(86,30),ID,I(73),LS,NAMSPE,LSTSPE(30)
      LOGICAL LS
C
C
C     THIS SUBPROGRAM UPDATES THE REACTION MATRIX
C
C
      L=1
      DO 100 J=1,NSP
      IF(NAMSPE.NE.LSTSPE(J))GO TO 100
      K=J
      GO TO 1
100   CONTINUE
      WRITE(5,93)
93    FORMAT(*0COULD NOT FIND SPECIES IN LIST*)
      STOP
1     IF(NAMSPE.NE.1HM.OR..NOT.LS)GO TO 3
      L=9
      GO TO 2
3     IF(LS)L=-1
2     MATRIX(NR,K)=MATRIX(NR,K)+L
      RETURN
      END
      SUBROUTINE BOUNDA
      COMMON /A/NSP,NR,MATRIX(86,30),ID,I(73),LS,NAMSPE,LSTSPE(30)
     1  ,AF(86),TEF(86),EF(96)
     2  ,AR(86),TER(86),ER(86)
```

```
     3  ,LISTBC(30),RBC(30),ALBC(30),NBC
        DIMENSION IBL(10)
        DATA IBL/10*1H /
        NBC=NBC+1
C
C
C       ELIMINATE BLANKS FROM STRING
C
C
        CALL NOBLAN
C
C
C       FIND COMMA
C
C
        DO 100 J=1,73
        K=J
        IF(I(J).EQ.1H,)GO TO 1
100     CONTINUE
        WRITE(5,90)
90      FORMAT(*1COULD NOT FIND COMMA*)
        STOP
C
C
C       ENCODE SPECIES NAME IN BOUNDARY CONDITION LIST
C
C
1       K=K-1
        ENCODE(10,180,LISTBC(NBC))(I(J),J=1,K)
180     FORMAT(10A1)
        K=K+4
C
C
C       FIND COMMA
C
C
        DO 101 J=K,73
        L=J
        IF(I(J).EQ.1H,)GO TO 2
101     CONTINUE
        WRITE(5,90)
        STOP
C
C
C       STORE BOUNDARY CONDITION
C
C
```

```
2       LE=L-K
        LF=10-LE
        L=L-1
        NUM=10H
        IF(LE.EQ.10)ENCODE(10,180,NUM)(I(J),J=K,L)
        IF(LE.NE.10)ENCODE(10,180,NUM)(IBL(J),J=1,LF),
     1  (I(J),J=K,L)
C
C
C       DECODE
C
C
        IF(I(K-2).EQ.1HR)DECODE(10,182,NUM)RBC(NBC)
        IF(I(K-2).EQ.1HL)DECODE(10,182,NUM)ALBC(NBC)
182     FORMAT(E10.0)
        RETURN
        END
        SUBROUTINE ARRANG
        COMMON /A/NSP,NR,MATRIX(86,30),ID,I(73),LS,NAMSPE,LSTSPE(30)
     1  ,AF(86),TEF(86),EF(86)
     2  ,AR(86),TER(86),ER(86)
     3  ,LISTBC(30),RBC(30),ALBC(30),NBC
        DIMENSION RRBC(30),ALLBC(30)
        IF(NBC.EQ.0)GO TO 2
        DO 100 J=1,NSP
        RRBC(J)=RBC(J)
        ALLBC(J)=ALBC(J)
        RBC(J)=0.
100     ALBC(J)=0.
C
C
C       SCAN SPECIES LIST
C
C
        DO 101 J=1,NSP
C
C
C       DETERMINE IF BOUNDARY CONDITION IS SPECIFIED FOR
C       SPECIES J
C
C
        DO 102 L=1,NBC
        K=L
        IF(LSTSPE(J).EQ.LISTBC(L))GO TO 1
102     CONTINUE
        GO TO 101
1       RBC(J)=RRBC(K)
```

```
        ALBC(J)=ALLBC(K)
101     CONTINUE
        RETURN
2       DO 103 L=1,NSP
        RBC(L)=0.
103     ALBC(L)=0.
        RETURN
        END
      SUBROUTINE THERMO (M,REACIN,DH,ACP,BCP,CCP,DCP)
C       THIS SUBROUTINE ONLY GOOD FOR 5 CHARACTER SPECIES
C     VERSION DATED 6/1/74
C     JOLW DEPT OF CHEM ENG UNIV OF ARIZ
C       ADDITIONS BY W. A. HAHN DEPT OF CHEM ENG UNIV OF ARIZ
C       DATED 4/27/79
C     SET THERMOCHEMICAL PROPERTIES FOR SPECIES 1 TO M BY
C     REFERENCE TO LIBRARY FLIBSP
C     PREVIOUSLY ASSIGNED THERMOCHEMICAL DATA HAS PRECEDENCE
      REAL DH(M),ACP(M),BCP(M),CCP(M),DCP(M)
        INTEGER REACIN(M)
        DIMENSION FLIBSP(100,8)
        DATA BLANK/5H     /
      ILAST=100
C     NOW COME LIBRARY DATA STATEMENTS
C     USE PROGRAM RITLIB TO CONSTRUCT THESE STATEMENTS FROM FREE
C     FORMAT  ENTHAL DATA CARDS
      DATA(FLIBSP(  1,J),J=1,8)/
     15HBR    , 2.674000E+01, 7.975850E+00,-6.043090E-01, 1.610050E-03
     2,-2.931590E-07, 0.          , 0.          /
      DATA(FLIBSP(  2,J),J=1,8)/
     15HBR2   , 7.387000E+00, 5.281750E+00, 6.232620E-01,-6.919080E-04
     2, 1.245570E-07, 0.          , 0.          /
      DATA(FLIBSP(  3,J),J=1,8)/
     15HBRO   , 3.000000E+01,-3.140000E+00, 1.970000E+00,-1.950000E-03
     2, 2.840000E-07, 0.          , 0.          /
      DATA(FLIBSP(  4,J),J=1,8)/
     15HC     , 1.708860E+02, 4.705340E+00, 5.697940E-02,-1.999380E-04
     2, 6.781610E-08, 0.          , 0.          /
      DATA(FLIBSP(  5,J),J=1,8)/
     15HCCL   , 1.320000E+02,-1.004890E+00, 1.614980E+00,-1.599640E-03
     2, 2.183200E-07, 0.          , 0.          /
      DATA(FLIBSP(  6,J),J=1,8)/
     15HCCL2O ,-5.260000E+01,-2.304680E+01, 6.772340E+00,-5.966110E-03
     2, 7.382460E-07, 0.          , 0.          /
      DATA(FLIBSP(  7,J),J=1,8)/
     15HCCL4  ,-2.294000E+01,-2.894230E+01, 9.141740E+00,-1.065250E-02
     2, 1.578620E-06, 0.          , 0.          /
      DATA(FLIBSP(  8,J),J=1,8)/
```

```
15HC2N2  , 7.387000E+01,-1.107180E+01, 4.354790E+00,-5.980510E-04
2,-2.022330E-07, 0.          , 0.          /
 DATA(FLIBSP(  9,J),J=1,8)/
15HCH2   , 9.500000E+01,-2.108650E+00, 1.494330E+00, 3.705390E-03
2,-8.405950E-07, 0.          , 0.          /
 DATA(FLIBSP( 10,J),J=1,8)/
15HCH2CL , 2.680000E+01,-2.750000E+01, 6.310000E+00, 3.930000E-03
2,-1.240000E-06, 0.          , 0.          /
 DATA(FLIBSP( 11,J),J=1,8)/
15HDUMMY ,-2.283000E+01,-3.605010E+01, 8.563190E+00,-2.262270E-03
2,-1.207760E-07, 0.          , 0.          /
 DATA(FLIBSP( 12,J),J=1,8)/
15HCH3   , 3.194000E+01,-4.495370E+00, 1.950380E+00, 7.056920E-03
2,-1.600880E-06, 0.          , 0.          /
 DATA(FLIBSP( 13,J),J=1,8)/
15HCH3CL ,-2.066000E+01,-2.755100E+01, 6.314550E+00, 3.928550E-03
2,-1.238650E-06, 0.          , 0.          /
 DATA(FLIBSP( 14,J),J=1,8)/
15HCH4   ,-1.789500E+01,-8.495480E+00, 2.340330E+00, 1.192830E-02
2,-2.604930E-06, 0.          , 0.          /
 DATA(FLIBSP( 15,J),J=1,8)/
15HCH3O  , 3.500000E+00, 1.400000E+01, 0.          , 0.
2, 0.          , 0.          , 0.          /
 DATA(FLIBSP( 16,J),J=1,8)/
15HCH3O2 , 6.700000E+00, 1.600000E+01, 0.          , 0.
2, 0.          , 0.          , 0.          /
 DATA(FLIBSP( 17,J),J=1,8)/
15HDUMMY ,-3.130000E+01, 1.800000E+01, 0.          , 0.
2, 0.          , 0.          , 0.          /
 DATA(FLIBSP( 18,J),J=1,8)/
15HCN    , 1.110000E+02, 5.011570E+00, 2.678180E-01, 1.169990E-03
2,-9.017350E-08, 0.          , 0.          /
 DATA(FLIBSP( 19,J),J=1,8)/
15HCO    ,-2.641700E+01, 7.808410E+00,-2.880390E-01, 2.598410E-03
2,-5.285100E-07, 0.          , 0.          /
 DATA(FLIBSP( 20,J),J=1,8)/
15HCOCL  ,-1.500000E+01,-1.483620E+00, 2.179280E+00,-6.446450E-04
2,-4.385590E-08, 0.          , 0.          /
 DATA(FLIBSP( 21,J),J=1,8)/
15HCO2   ,-9.405400E+01,-1.479040E+01, 4.213280E+00,-1.338610E-03
2,-2.732100E-08, 0.          , 0.          /
 DATA(FLIBSP( 22,J),J=1,8)/
15HCOS   ,-3.308000E+01,-1.436950E+01, 4.395560E+00,-2.628420E-03
2, 2.474690E-07, 0.          , 0.          /
 DATA(FLIBSP( 23,J),J=1,8)/
15HC.R   , 0.          ,-2.093820E+01, 4.179050E+00,-3.106030E-03
2, 3.149130E-07, 0.          , 0.          /
```

```
 DATA(FLIBSP( 24,J),J=1,8)/
15HCS     , 5.500000E+01,-1.942680E+00, 1.621570E+00,-8.092230E-04
2, 3.793490E-08, 0.          , 0.          /
 DATA(FLIBSP( 25,J),J=1,8)/
15HCS2    , 2.798000E+01,-1.339300E+01, 4.447710E+00,-3.747600E-03
2, 4.476140E-07, 0.          , 0.          /
 DATA(FLIBSP( 26,J),J=1,8)/
15HCL     , 2.892200E+01, 6.299980E-01, 9.053570E-01,-1.879110E-03
2, 3.317850E-07, 0.          , 0.          /
 DATA(FLIBSP( 27,J),J=1,8)/
15HCL2    , 0.          , 3.031890E-01, 1.460940E+00,-1.713630E-03
2, 2.896740E-07, 0.          , 0.          /
 DATA(FLIBSP( 28,J),J=1,8)/
15HCL2O   , 2.100000E+01,-9.468450E+00, 3.912040E+00,-4.612630E-03
2, 6.882580E-07, 0.          , 0.          /
 DATA(FLIBSP( 29,J),J=1,8)/
15HCLO    , 2.419200E+01,-3.137240E+00, 1.972880E+00,-1.951250E-03
2, 2.835670E-07, 0.          , 0.          /
 DATA(FLIBSP( 30,J),J=1,8)/
15HCLO2   , 2.500000E+01,-1.673190E+01, 4.923350E+00,-4.534770E-03
2, 6.060190E-07, 0.          , 0.          /
 DATA(FLIBSP( 31,J),J=1,8)/
15HH      , 5.210000E+01, 4.963800E+00, 7.888670E-04,-1.507070E-06
2, 2.971030E-10, 0.          , 0.          /
 DATA(FLIBSP( 32,J),J=1,8)/
15HHBR    ,-8.710000E+00, 1.102570E+01,-8.874450E-01, 3.421430E-03
2,-6.152520E-07, 0.          , 0.          /
 DATA(FLIBSP( 33,J),J=1,8)/
15HHCL    ,-2.206300E+01, 1.233660E+01,-1.119600E+00, 3.550060E-03
2,-5.989300E-07, 0.          , 0.          /
 DATA(FLIBSP( 34,J),J=1,8)/
15HHCN    , 3.120000E+01,-4.314490E+00, 2.170060E+00, 1.955310E-03
2,-4.569310E-07, 0.          , 0.          /
 DATA(FLIBSP( 35,J),J=1,8)/
15HHCO    ,-2.900000E+00, 9.795120E-01, 1.091020E+00, 3.433800E-03
2,-7.908330E-07, 0.          , 0.          /
 DATA(FLIBSP( 36,J),J=1,8)/
15HHCOCL ,-4.010000E+01, 8.910000E+00, 0.          , 0.
2, 0.          , 0.          , 0.          /
 DATA(FLIBSP( 37,J),J=1,8)/
15HH2     , 0.          , 1.076520E+01,-7.662020E-01, 1.943940E-03
2,-1.639720E-07, 0.          , 0.          /
 DATA(FLIBSP( 38,J),J=1,8)/
15HH2O    ,-5.779800E+01, 1.446890E+01,-1.452530E+00, 6.445390E-03
2,-1.021790E-06, 0.          , 0.          /
 DATA(FLIBSP( 39,J),J=1,8)/
15HH2O2   ,-3.253000E+01,-2.300560E+01, 6.099370E+00,-5.256040E-03
```

```
2, 1.164080E-06, 0.          , 0.          /
 DATA(FLIBSP( 40,J),J=1,8)/
15HH2S    ,-4.880000E+00, 7.393540E+00,-1.644450E-01, 5.763500E-03
2,-1.135340E-06, 0.          , 0.          /
 DATA(FLIBSP( 41,J),J=1,8)/
15HH2SO4  ,-1.770000E+02,-6.708090E+01, 1.573760E+01,-1.127610E-02
2, 1.335460E-06, 0.          , 0.          /
 DATA(FLIBSP( 42,J),J=1,8)/
15HDUMMY  ,-1.945480E+02,-7.132130E+01, 1.974880E+01,-2.810950E-02
2, 5.152310E-06, 0.          , 0.          /
 DATA(FLIBSP( 43,J),J=1,8)/
15HHNO    , 2.380000E+01,-2.749050E+00, 1.799980E+00, 2.338060E-03
2,-6.296870E-07, 0.          , 0.          /
 DATA(FLIBSP( 44,J),J=1,8)/
15HDUMMY  ,-1.834000E+01,-2.296690E+01, 6.045180E+00,-2.343610E-03
2, 8.413850E-08, 0.          , 0.          /
 DATA(FLIBSP( 45,J),J=1,8)/
15HDUMMY  ,-1.884000E+01,-2.217750E+01, 5.945140E+00,-2.480700E-03
2, 1.352330E-07, 0.          , 0.          /
 DATA(FLIBSP( 46,J),J=1,8)/
15HHNO3   ,-3.210000E+01,-4.630880E+01, 1.068120E+01,-6.475140E-03
2, 5.948060E-07, 0.          , 0.          /
 DATA(FLIBSP( 47,J),J=1,8)/
15HHOCL   ,-2.200000E+01,-4.621960E+00, 2.379970E+00,-1.515120E-04
2,-6.465450E-08, 0.          , 0.          /
 DATA(FLIBSP( 48,J),J=1,8)/
15HHO2    , 5.000000E+00,-4.117920E+00, 2.113130E+00, 1.231010E-03
2,-3.713790E-07, 0.          , 0.          /
 DATA(FLIBSP( 49,J),J=1,8)/
15HHSO2   ,-6.870000E+01, 1.790000E+01, 0.          , 0.
2, 0.          , 0.          , 0.          /
 DATA(FLIBSP( 50,J),J=1,8)/
15HHSO3   ,-4.160000E+01,-7.130000E+01, 1.970000E+01,-2.810000E-02
2, 5.150000E-06, 0.          , 0.          /
 DATA(FLIBSP( 51,J),J=1,8)/
15HN      , 1.129650E+02, 4.897090E+00, 1.394790E-02,-3.476940E-05
2, 9.086190E-09, 0.          , 0.          /
 DATA(FLIBSP( 52,J),J=1,8)/
15HNCO    , 2.250000E+01,-1.400000E+01, 4.070000E+00,-1.740000E-03
2, 1.150000E-08, 0.          , 0.          /
 DATA(FLIBSP( 53,J),J=1,8)/
15HNH     , 8.100000E+01, 1.290910E+01,-1.215650E+00, 3.522060E-03
2,-5.563000E-07, 0.          , 0.          /
 DATA(FLIBSP( 54,J),J=1,8)/
15HNH2    , 4.007000E+01, 1.283420E+01,-1.186080E+00, 6.736980E-03
2,-1.221380E-06, 0.          , 0.          /
 DATA(FLIBSP( 55,J),J=1,8)/
```

```
15HNH3    ,-1.097000E+01, 2.076940E+00, 7.192330E-01, 7.895560E-03
2,-1.503310E-06, 0.           , 0.           /
 DATA(FLIBSP( 56,J),J=1,8)/
15HN2     , 0.           , 9.398720E+00,-5.854900E-01, 3.007380E-03
2,-5.814880E-07, 0.           , 0.           /
 DATA(FLIBSP( 57,J),J=1,8)/
15HN2H    , 6.400000E+01, 1.230000E+01, 0.           , 0.
2, 0.           , 0.           , 0.           /
 DATA(FLIBSP( 58,J),J=1,8)/
15HN2H2   , 5.090000E+01,-1.323580E+01, 3.628570E+00, 3.977690E-03
2,-1.062780E-06, 0.           , 0.           /
 DATA(FLIBSP( 59,J),J=1,8)/
15HN2H3   , 3.650000E+01, 2.150000E+01, 0.           , 0.
2, 0.           , 0.           , 0.           /
 DATA(FLIBSP( 60,J),J=1,8)/
15HN2H4   , 2.279000E+01,-3.961740E+01, 9.048390E+00, 7.655280E-04
2,-6.031690E-07, 0.           , 0.           /
 DATA(FLIBSP( 61,J),J=1,8)/
15HN2O    , 1.961000E+01,-1.429780E+01, 4.208650E+00,-1.719060E-03
2, 2.628100E-08, 0.           , 0.           /
 DATA(FLIBSP( 62,J),J=1,8)/
15HN2O2   , 4.070000E+01, 1.900000E+01, 0.           , 0.
2, 0.           , 0.           , 0.           /
 DATA(FLIBSP( 63,J),J=1,8)/
15HN2O3   , 1.980000E+01,-2.963030E+01, 8.184250E+00,-4.961160E-03
2, 3.718460E-07, 0.           , 0.           /
 DATA(FLIBSP( 64,J),J=1,8)/
15HN2O4   , 2.710000E+00,-5.392960E+01, 1.316310E+01,-9.502930E-03
2, 9.354370E-07, 0.           , 0.           /
 DATA(FLIBSP( 65,J),J=1,8)/
15HN2O5   , 2.700000E+00,-7.293340E+01, 1.777610E+01,-1.851580E-02
2, 2.515100E-06, 0.           , 0.           /
 DATA(FLIBSP( 66,J),J=1,8)/
15HNO     , 2.158000E+01, 6.659640E+00,-3.921990E-02, 2.147850E-03
2,-4.646340E-07, 0.           , 0.           /
 DATA(FLIBSP( 67,J),J=1,8)/
15HNO2    , 7.910000E+00,-1.392030E+01, 4.058530E+00,-1.714970E-03
2, 6.334160E-09, 0.           , 0.           /
 DATA(FLIBSP( 68,J),J=1,8)/
15HNO3    , 1.700000E+01,-4.865530E+01, 1.104520E+01,-1.075340E-02
2, 1.403600E-06, 0.           , 0.           /
 DATA(FLIBSP( 69,J),J=1,8)/
15HO      , 5.955900E+01, 7.543190E+00,-4.328670E-01, 5.150510E-04
2,-7.497180E-08, 0.           , 0.           /
 DATA(FLIBSP( 70,J),J=1,8)/
15HOH     , 9.432000E+00, 1.496990E+01,-1.542370E+00, 3.542890E-03
2,-5.105730E-07, 0.           , 0.           /
```

```
      DATA(FLIBSP( 71,J),J=1,8)/
     15HO2     , 0.           , 7.291320E-01, 1.082690E+00, 1.221010E-04
     2,-3.786750E-08, 0.           , 0.           /
      DATA(FLIBSP( 72,J),J=1,8)/
     15HS      , 0.           ,-1.425010E+01, 4.420860E+00,-1.397370E-02
     2, 3.169150E-06, 0.           , 0.           /
      DATA(FLIBSP( 73,J),J=1,8)/
     15HS.C    , 0.           , 2.755520E+00, 1.174050E-01, 6.636170E-03
     2, 4.469610E-08, 0.           , 0.           /
      DATA(FLIBSP( 74,J),J=1,8)/
     15HSH     , 3.460000E+01, 1.771180E+01,-1.976840E+00, 4.534240E-03
     2,-7.583210E-07, 0.           , 0.           /
      DATA(FLIBSP( 75,J),J=1,8)/
     15HSO     , 1.640000E+00,-2.975500E+00, 1.848640E+00,-1.344150E-03
     2, 1.410170E-07, 0.           , 0.           /
      DATA(FLIBSP( 76,J),J=1,8)/
     15HSO2    ,-7.094700E+01,-1.548660E+01, 4.538170E+00,-3.200460E-03
     2, 3.297430E-07, 0.           , 0.           /
      DATA(FLIBSP( 77,J),J=1,8)/
     15HSO3    ,-9.459000E+01,-3.455900E+01, 8.533070E+00,-7.053190E-03
     2, 7.992620E-07, 0.           , 0.           /
      DATA(FLIBSP( 78,J),J=1,8)/
     15HS2     , 3.084000E+01,-1.934960E+00, 1.804840E+00,-1.979840E-03
     2, 2.970560E-07, 0.           , 0.           /
      DATA(FLIBSP( 79,J),J=1,8)/
     15HS2O    ,-1.350000E+01,-1.311080E+01, 4.372590E+00,-4.361750E-03
     2, 5.817900E-07, 0.           , 0.           /
      DATA(FLIBSP( 80,J),J=1,8)/
     15HS8     , 2.420000E+01,-2.065250E+01, 1.091260E+01,-1.365620E-02
     2, 2.112040E-06, 0.           , 0.           /
C
C
C        ADDITIONS BY W.A. HAHN
C
C
      DATA(FLIBSP( 81,J),J=1,8)/
     15HCH2O   ,-2.595000E+01,-2.830000E+01, 6.160000E+00, 1.340000E-03
     2,-7.760000E-07, 0.           , 0.           /
      DATA(FLIBSP( 82,J),J=1,8)/
     15HCHO    , 9.000000E+00,-1.150000E+01, 3.330000E+00, 3.500000E-04
     2,-3.410000E-07, 0.           , 0.           /
      DATA(FLIBSP( 83,J),J=1,8)/
     15HCH     , 1.420000E+02, 2.190000E+01,-2.950000E+00, 7.560000E-03
     2,-1.300000E-06, 0.           , 0.           /
C
      DO 10 I=1,M
      IERR=0
```

```
      IF(ACP(I).NE.0.) GO TO 10
      DO 20 K=1,ILAST
      II=K
        SLIB=FLIBSP(K,1)
        ENCODE(10,1003,DLIB) REACIN(I)
 1003   FORMAT(A10)
      IF (SLIB.EQ.DLIB) GO TO 21
   20 CONTINUE
      IERR=1
      GO TO 22
   21 CONTINUE
      DH(I)=FLIBSP(II,2)*1.E3
      ACP(I)=FLIBSP(II,3)
      BCP(I)=FLIBSP(II,4)
      CCP(I)=FLIBSP(II,5)
      DCP(I)=FLIBSP(II,6)
   22 CONTINUE
      IF (IERR.NE.0)
     1WRITE(5,1001) I,REACIN(I)
 1001 FORMAT(1H1,10X,*SPECIES NUMBER*,I4,2X,A6,*NOT IN THERMOCHEMICAL
     1LIBRARY*)
   10 CONTINUE
      RETURN
      END
        SUBROUTINE NITR3B
        COMMON /A/NSP,NR,MATRIX(86,30),ID,I(73),LS,NAMSPE,LSTSPE(30)
     1  ,AF(86),TEF(86),EF(86)
     2  ,AR(86),TER(86),ER(86)
     3  ,LISTBC(30),RBC(30),ALBC(30),NBC
     4  ,TB(86),N2(86),NTB,NN2
        INTEGER TB
C
C
C       THIS SUBPROGRAM GENERATES A VECTOR CONTAINING THE
C       REACTIONS INVOLVING N2 AND A THIRD BODY
C
C
C       FIND OUT IF N2 IS A SPECIES
C
C
        DO 100 J=1,NSP
        K=J
        IF(LSTSPE(J).EQ.2HN2)GO TO 1
100     CONTINUE
        GO TO 2
C
C
```

```
C       GENERATE VECTOR CONTAINING # OF REACTIONS INVOLVING N2
C
C       ELEMENT<0 ==> N2 ON LEFT HAND SIDE
C       ELEMENT>0 ==> N2 ON RIGHT HAND SIDE
C
C
1       NN2=0
        DO 101 J=1,NR
        IF(MATRIX(J,K).EQ.0)GO TO 101
        NN2=NN2+1
        N2(NN2)=ISIGN(J,MATRIX(J,K))
101     CONTINUE
C
C
C       ELIMINATE N2 FROM REACTION MATRIX
C       AND FROM SPECIES LIST
C
C
        NSP=NSP-1
        DO 102 J=K,NSP
        LSTSPE(J)=LSTSPE(J+1)
        DO 102 L=1,NR
102     MATRIX(L,J)=MATRIX(L,J+1)
C
C
C       FIND OUT IF THIRD BODY IS A SPECIES
C
C
2       DO 200 J=1,NSP
        K=J
        IF(LSTSPE(J).EQ.1HM)GO TO 3
200     CONTINUE
        GO TO 4
C
C
C       GENERATE VECTOR CONTAINIG # OF REACTIONS INVOLVING M
C
C
3       NTB=0
        DO 201 J=1,NR
        IF(MATRIX(J,K).EQ.0)GO TO 201
        NTB=NTB+1
        TB(NTB)=J
201     CONTINUE
C
C
C       ELIMINATE THIRD BODY FROM REACTION MATRIX
```

```
C       AND FROM SPECIES LIST
C
C
4       NSP=NSP-1
        DO 202 J=K,NSP
        LSTSPE(J)=LSTSPE(J+1)
        DO 202 L=1,NR
202     MATRIX(L,J)=MATRIX(L,J+1)
        RETURN
        END
        SUBROUTINE GENINF
        COMMON /A/NSP,NR,MATRIX(86,30),ID,I(73),LS,NAMSPE,LSTSPE(30)
     1  ,AF(86),TEF(86),EF(86)
     2  ,AR(86),TER(86),ER(86)
     3  ,LISTBC(30),RBC(30),ALBC(30),NBC
     4  ,TB(86),N2(86),NTB,NN2
     5  ,CREAT(30,86),NCR(30),DESTR(30,86)
     6  ,NDS(30),SPEF(86,2),NSPEF(86),NSPER(86),SPER(86,2)
     7  ,MULT(30,2),NMULT,NNN2,NN3
        INTEGER SPERXN,CREAT,DESTR,SPEF,SPER
C
C
C       THIS SUBPROGRAM CREATES THE INFORMATION NECESARY TO
C       CALCULATE THE RATE OF FORMATION OF EACH SPECIES AND
C       THE JACOBIAN OF THIS VECTOR
C
C
        DO 100 J=1,NSP
        NCR(J)=0
        NDS(J)=0
        DO 100 K=1,NR
        IF(MATRIX(K,J).EQ.0)GO TO 100
        IF(MATRIX(K,J).LT.0)GO TO 1
        NCR(J)=NCR(J)+1
        CREAT(J,NCR(J))=K
        GO TO 100
1       NDS(J)=NDS(J)+1
        DESTR(J,NDS(J))=K
100     CONTINUE
        DO 101 J=1,NR
        NSPEF(J)=0
        NSPER(J)=0
        DO 101 K=1,NSP
        MAT=MATRIX(J,K)
6       IF(MAT)2,101,3
2       NSPEF(J)=NSPEF(J)+1
        IF(NSPEF(J).LE.2)GO TO 4
```

```
      WRITE(5,90)J
90    FORMAT(*1REACTION*,I3,*HAS MORE THAN 2 SPECIES*
     1,*FORWARD*)
      STOP
4     SPEF(J,NSPEF(J))=K
      MAT=MAT+1
      GO TO 6
3     NSPER(J)=NSPER(J)+1
      IF(NSPER(J).LE.2)GO TO 5
      WRITE(5,91)J
91    FORMAT(*1REACTION*,I3,*HAS MORE THAN 2 SPECIES*
     1,*BACKWARD*)
      STOP
5     SPER(J,NSPER(J))=K
      MAT=MAT-1
      GO TO 6
101   CONTINUE
      DO 102 J=1,NR
      IF(NSPER(J).EQ.1)GO TO 7
      IF(SPER(J,1).EQ.SPER(J,2))GO TO 8
7     IF(NSPEF(J).EQ.1)GO TO 102
      IF(SPEF(J,1).NE.SPEF(J,2))GO TO 102
      NMULT=NMULT+1
      MULT(NMULT,1)=SPEF(J,1)
      MULT(NMULT,2)=-J
      GO TO 102
8     NMULT=NMULT+1
      MULT(NMULT,1)=SPER(J,1)
      MULT(NMULT,2)=J
102   CONTINUE
      NNN2=0
      NN3=0
      DO 103 J=1,NSP
      IF(NDS(J).GT.NNN2)NNN2=NDS(J)
      IF(NCR(J).GT.NN3)NN3=NCR(J)
103   CONTINUE
      RETURN
      END
      SUBROUTINE OUTPUT(DH,ACP,BCP,CCP,DCP)
      COMMON /A/NSP,NR,MATRIX(86,30),ID,I(73),LS,NAMSPE,LSTSPE(30)
     1,AF(86),TEF(86),EF(86)
     2,AR(86),TER(86),ER(86)
     3,LISTBC(30),RBC(30),ALBC(30),NBC
     4,TB(86),N2(86),NTB,NN2
     5,CREAT(30,86),NCR(30),DESTR(30,86)
     6,NDS(30),SPEF(86,2),NSPEF(86),NSPER(86),SPER(86,2)
     7,MULT(30,2),NMULT,NNN2,NN3
```

```
      INTEGER SPERXN,CREAT,DESTR,SPEF,SPER
      DIMENSION DH(30),ACP(30),BCP(30),CCP(30),DCP(30)
      NN1=NMULT
      IF(NN1.EQ.0)NN1=1
      WRITE(4)NSP,NR,NTB,NN2,NN1,NMULT,NNN2,NN3
      WRITE(4)(TB(J),J=1,NTB)
      WRITE(4)(N2(J),J=1,NN2)
      WRITE(4)(NCR(J),J=1,NSP)
      WRITE(4)(NDS(J),J=1,NSP)
      WRITE(4)(MULT(J,1),MULT(J,2),J=1,NN1)
      DO 200 J=1,NSP
      NC=NCR(J)
      WRITE(4)(CREAT(J,L),L=1,NC)
      ND=NDS(J)
      WRITE(4)(DESTR(J,L),L=1,ND)
200   CONTINUE
      WRITE(4)(NSPEF(J),J=1,NR)
      WRITE(4)(NSPER(J),J=1,NR)
      DO 201 J=1,NR
      NSF=NSPEF(J)
      NSR=NSPER(J)
      WRITE(4)(SPEF(J,L),L=1,NSF)
      WRITE(4)(SPER(J,L),L=1,NSR)
201   CONTINUE
      WRITE(4)(AF(J),TEF(J),EF(J),J=1,NR)
      WRITE(4)(AR(J),TER(J),ER(J),J=1,NR)
      WRITE(4)(LSTSPE(J),ALBC(J),RBC(J),J=1,NSP)
      WRITE(4)(DH(J),ACP(J),BCP(J),CCP(J),DCP(J),J=1,NSP)
      RETURN
      END
      SUBROUTINE PLSEQ
      COMMON /A/NSP,NR,MATRIX(86,30),ID,I(73)
C
C
C     THIS SUBPROGRAM ELIMINATES THE SEQUENCES "+="
C     AND "+," FROM STOICH CARDS
C
C
      DO 100 J=1,72
      K=J
      IF(I(J).EQ.1H+.AND.I(J+1).EQ.1H=)GO TO 1
100   CONTINUE
      GO TO 3
1     DO 101 J=K,72
101   I(J)=I(J+1)
      I(73)=1H
3     DO 102 J=1,72
```

```
      K=J
      IF(I(J).EQ.1H+.AND.I(J+1).EQ.1H,)GO TO 2
102   CONTINUE
      RETURN
2     DO 103 J=K,72
103   I(J)=I(J+1)
      I(73)=1H
      RETURN
```

```
      PROGRAM FUELN(INPUT,OUTPUT,TAPE6=INPUT,TAPE5=OUTPUT,TAPE3,
     1  TAPE4,TAPE7,TAPE8)
      INTEGER WIDTH,TB,CREAT,DESTR,SPEF,SPER
      REAL LA,LB,LLA,NEWV
      DIMENSION TB(7),N2(1),NCR(15),
     1  NDS(15),CREAT(15,12),DESTR(15,14),NSPEF(39),
     2  NSPER(39),SPEF(39,2),SPER(39,2),AF(39),TEF(39),EF(39),AR(39),
     3  TER(39),ER(39),LSTSPE(15),LA(16),LB(16),HO(15),ACP(15),
     4  BCP(15),CCP(15),DCP(15),MULT(4,2)
      DIMENSION X(31),C(16,31),DXE(31),DXW(31),T(16,31),
     1  BETA(16,31),R(16,31),RI(16,31),S(16,16,31),H(15),
     2  HP(15),DH(39),DHP(39),RR(39),RF(39),RRP(39),RFP(39),
     3  AL(496,34),DELC(16,31),U(16,31),G(16,31),DIFFU(15,31),
     4  THK(31),CNEW(16,31),ADIF(16),HEAT(31)
      DIMENSION PRESS(31),VZ(31),AMU(31),DIFF1(31),CPAV(31)
     1  ,A1(31),A2(31),A3(31),A(31),B(31),CI(31),D(31),UBAR(31)
     2  ,DUM1(31),DUM2(31),UBARN(31),RNO(31)
      DIMENSION LAD(16),NEWV(31)
      LOGICAL LWA,LWGR,LWDEL,LWREA,LWTR,ISNPN,THIRD,AMOLN2,ISNO
      THIRD=.TRUE.
      AMOLN2=.TRUE.
      ICH=0
      M=31
      MM1=M-1
      F=1.
      ASSIGN 8 TO JUMP
      READ(7)NSP,NR,NTB,NN2,NN1,NMULT,NNN2,NN3
      IF(NTB.NE.0)GO TO 23
      NTB=1
      THIRD=.FALSE.
23    READ(7)(TB(J),J=1,NTB)
      IF(NN2.NE.0)GO TO 24
      NN2=1
      AMOLN2=.FALSE.
24    READ(7)(N2(J),J=1,NN2)
      READ(7)(NCR(J),J=1,NSP)
      READ(7)(NDS(J),J=1,NSP)
      READ(7)(MULT(I,1),MULT(I,2),I=1,NN1)
      DO 100 J=1,NSP
      NC=NCR(J)
      READ(7)(CREAT(J,L),L=1,NC)
      ND=NDS(J)
      READ(7)(DESTR(J,L),L=1,ND)
100   CONTINUE
      READ(7)(NSPEF(J),J=1,NR)
      READ(7)(NSPER(J),J=1,NR)
```

```
      DO 101 J=1,NR
      NSF=NSPEF(J)
      NSR=NSPER(J)
      READ(7)(SPEF(J,L),L=1,NSF)
      READ(7)(SPER(J,L),L=1,NSR)
101   CONTINUE
      READ(7)(AF(J),TEF(J),EF(J),J=1,NR)
      READ(7)(AR(J),TER(J),ER(J),J=1,NR)
      READ(7)(LSTSPE(J),LA(J),LB(J),J=1,NSP)
      READ(7)(HO(J),ACP(J),BCP(J),CCP(J),DCP(J),J=1,NSP)
C     AF(1)=0.
C     AR(1)=0.
      LA(8)=0.98
      LA(7)=0.0
      LA(13)=0.0
      LB(14)=0.2
      NN=NSP+1
20    READ(6,50)LA(NN),LB(NN)
50    FORMAT(2F9.6)
      DO 200 I=1,NR
      ER(I)=-ER(I)
200   EF(I)=-EF(I)
      WRITE(5,90)
90    FORMAT(*1SET OF REACTIONS*,37X,*REACTION RATES*/
     1  * === == *,9(***),37X,8(*=*),1X,5(*=*))
      DO 102 J=1,NR
      IL=LSTSPE(SPEF(J,1))
      WRITE(5,91)IL
91    FORMAT(*0*,A5)
      IF(NSPEF(J).EQ.1)GO TO 1
      IL=LSTSPE(SPEF(J,2))
      WRITE(5,92)IL
92    FORMAT(***,5X,***,A5)
1     IL=LSTSPE(SPER(J,1))
      WRITE(5,93)IL
93    FORMAT(***,17X,*=*,A5)
      IF(NSPER(J).EQ.1)GO TO 2
      IL=LSTSPE(SPER(J,2))
      WRITE(5,94)IL
94    FORMAT(***,23X,***,A5)
      IF(.NOT.AMOLN2)GO TO 4
2     DO 103 I=1,NN2
      IF(N2(I).EQ.J)GO TO 3
103   CONTINUE
      GO TO 4
3     IF(N2(I).LT.0)WRITE(5,95)
95    FORMAT(***,5X,***,5HN2    )
```

```
      IF(N2(I).GT.0)WRITE(5,96)
96    FORMAT(***,23X,***,5HN2    )
      IF(.NOT.THIRD)GO TO 9
4     DO 104 I=1,NTB
      IF(TB(I).EQ.J)GO TO 5
104   CONTINUE
      GO TO 9
5     WRITE(5,97)
97    FORMAT(***,11X,***,5HM     ,12X,***,5HM     )
9     WRITE(5,98)AF(J),TEF(J),EF(J)
98    FORMAT(***,53X,*FORWARD:  *,E10.4,4H*T**,F5.2,5H*EXP(,
     1 F8.0,11H/(1.986*T)))
      WRITE(5,99)AR(J),TER(J),ER(J)
99    FORMAT(* *,53X,*REVERSE:  *,E10.4,4H*T**,F5.2,5H*EXP(,
     1 F8.0,11H/(1.986*T)))
102   CONTINUE
      DO 201 I=1,NR
      ER(I)=-ER(I)/1.986
201   EF(I)=-EF(I)/1.986
      WRITE(5,190)(LSTSPE(J),LA(J),LB(J),HO(J),ACP(J),BCP(J),
     1 CCP(J),DCP(J),J=1,NSP)
190   FORMAT(*1BOUNDARY CONDITIONS*,20X,*THERMOCHEMICAL*
     1 ,* INFORMATION*/* *,8(**=*),1X,10(**=*),20X,14(**=*),1X
     2 ,11(**=*)/*0SPECIES*,6X,*UPPER BC*,3X,*LOWER BC*,8X
     3 ,*H0*,14X,*CP*/(*0*,1X,A5,3X,E11.3,3X,E11.3,5X,E11.3
     4 ,5X,E11.3,**,E11.3,9H*ALOG(T)+,E11.3,3H*T+,E11.3
     5 ,5H*T**2))
C     CALL TRSP1(C,THK,DIFFU,LWTR,PRESS,LSTSPE,NSP,M,NN.AMU)
      CALL TRSP1(LSTSPE,NSP,C,NN,M,PRESS,DIFFU,AMU,THK,LWTR,
     1 6HN2    )
      ISNO=.FALSE.
      DO 126 I=1,NSP
      IF(6HNO    .NE.LSTSPE(I))GO TO 126
      NNO=I
      ISNO=.TRUE.
126   CONTINUE
      WIDTH=2*NN+1
      NT=NN*M
      NA=2*(NN+1)
7     IC=0
      READ(6,53)RRR,ICMAX,W,NCH
      W=W*F
53    FORMAT(E12.4,I3,F5.2,I3)
      READ(6,51)LLA,DIST,PRESSI
51    FORMAT(5E12.4)
      TO=298.*LA(NN)+298.
      VV=LLA*DIST/(4000./(60.*3.141592*2.5**4*82.05*TO))/PRESSI
```

```
      EPS=2*LLA*82.05*TO/PRESSI
      WRITE(5,192)LLA,DIST,VV,EPS,PRESSI
192   FORMAT(*1A=*,E11.3/*OSEPARATION BETWEEN BURNERS=*,
     1 E11.3/*OFLOW RATES=*,E11.3,*LT/MIN*/
     2 *ORATE OF STRETCHING=*,E11.3/*OPRESSURE OF THE SYSTEM=*,
     3 F6.3)
      DIST=DIST/2.
      ICMAX=ICMAX-1
      READ(6,52)LWA,LWGR,LWDEL,LWREA,LWTR
52    FORMAT(10L1)
      READ(6,52)ISNPN
      IF(.NOT.ISNPN)GO TO 453
      DO 9453 I=1,NSP
      J=I
      IF(5HN    .EQ.LSTSPE(I))GO TO 454
9453  CONTINUE
      WRITE(5,9454)
9454  FORMAT(*1DID NOT FIND N AS A SPECIE,BUT RECOMBINATION*,
     1 * RXN IS SPECIFIED*)
      STOP
454   NPN=J
453   CONTINUE
C     CALL GRID(X,M,RRR,0.140)
C     READ(3)ARGH,UBAR,VZ,FINVAL
C     READ(3)C,UBAR,VZ,FINVAL
C     READ(3)X,C,VZ,FINVAL
      READ(3)C,UBAR,VZ,FINVAL,X
C     READ(3)C,UBAR,VZ
C     FINVAL=-9.36
C     READ(3)C
C     GO TO 98765
C     FINVAL=-2.*LLA*82.05*(298.*LB(NN)+298.)*DIST*1.0
C     C(10,13)=.391E-2
C     C(13,30)=.800E-14
      DO 800 I=1,M
      IF(C(16,I).EQ.0.)C(16,I)=1.E-49
800   CONTINUE
C     DO 850 I=24,39
C850  C(NN,I)=C(NN,I)/10.
C     C(NN,15)=0.7
C     C(NN,16)=2.36
C     C(NN,17)=5.71
C     C(NN,18)=7.39
C     C(NN,19)=5.71
C     C(NN,20)=2.36
C     C(NN,21)=0.7
C     C(3,18)=0.1E-3
```

```
C       C(7,18)=0.1E-3
C       C(10,18)=0.1E-2
98765   CONTINUE
        DO 600 I=1,M
600     PRESS(I)=PRESSI
C       CALL CHGE(C,UBAR,VZ,0.140,PRESSI,M,NN,X,LA,LB,DIST,LLA,
C     1 RRR,FINVAL)
C       FINVAL=-2.*LLA*DIST/(PRESSI/(82.05*(C(NN,I)*298.+298.)))
        WRITE(5,193)((C(I,J),I=1,14),J=1,M)
        WRITE(5,292)((C(I,J),I=15,NN),J=1,M)
193     FORMAT(*1*,14E9.3/(* *,14E9.3))
292     FORMAT(*1*,2E9.3/(* *,2E9.3))
        CALL SDELTA(X,DXE,DXW,M,LWDEL)
C8      CALL TRSPO(C,THK,DIFFU,LWTR,PRESS,LSTSPE,NSP,M,NN,AMU)
8       CONTINUE
        CALL TRSPO(LSTSPE,NSP,C,NN,M,PRESS,DIFFU,AMU,THK,LWTR,
     1  6HN2    )
        CALL DIFF(DXE,DXW,M,PRESS,NN,PRESSI,DIFF1,A1,A2,A3)
88      CONTINUE
        CALL NEWREA(C,RI,S,M,NSP,NN,LWREA,NR,DIST,
     1  SPEF,NSPEF,SPER,NSPER,TB,NTB,N2,NN2,AR,AF,TER,
     2  TEF,ER,EF,DESTR,CREAT,NDS,NCR,HO,ACP,BCP,CCP,DCP,
     3  H,HP,DH,DHP,RR,RF,RRP,RFP,NNN2,NN3,DIFFU,THK,
     4  MULT,NMULT,NN1,PRESS,VZ,DIFF1,CPAV,LLA,UBAR,
     5  ISNPN,NPN,THIRD,AMOLN2)
        DO 810 I=1,M
        IF(C(16,I).GT.0.1)GO TO 810
        DO 811 J=1,NN
        RI(J,I)=0.
        DO 811 L=1,NN
811     S(J,L,I)=0.
810     CONTINUE
        DO 125 I=1,M
        IF(.NOT.ISNO)GO TO 125
        RNO(I)=RI(NNO,I)
125     HEAT(I)=RI(NN,I)
C       WRITE(8,38877)(RNO(I),I=1,M)
38877   FORMAT(* *,10E11.3)
C       WRITE(8,38977)NNO
38977   FORMAT(* *,I5)
        CALL NEWGR(DXE,DXW,M,NSP,NN,LA,PRESS,VZ,DIFFU,C,A1
     1  ,A2,A3,T,BETA,R,LB,CPAV,THK,DIST,LLA,PRESSI,UBAR
     2  ,RI,S,FINVAL)
        IF(IC.EQ.0)GO TO 10
        IF(IC/NCH*NCH.EQ.IC.AND.W.LT.0.99)W=W*2.
10      DO 105 I=1,NN
        DO 106 J=1,M
```

```
106      S(I,I,J)=S(I,I,J)+BETA(I,J)
         DO 107 J=2,MM1
107      U(I,J)=-RI(I,J)-T(I,J)*C(I,J-1)-BETA(I,J)*C(I,J)-
     1   R(I,J)*C(I,J+1)
         U(I,1)=-RI(I,1)-T(I,1)*LA(I)-BETA(I,1)*C(I,1)-
     1   R(I,1)*C(I,2)
105      U(I,M)=-RI(I,M)-T(I,M)*C(I,MM1)-BETA(I,M)*C(I,M)-
     1   R(I,M)*LB(I)
         CALL SBAND(T,S,R,AL,WIDTH,M,NN,DELC,U,NT,NA,G)
         WRITE(5,802)(DELC(NN,I),I=1,M)
802      FORMAT(* *,10E11.3)
C        DO 698 I=1,M
C698     DELC(NN,I)=0.
         DO 890 J=1,NN
         DO 891 I=1,5
891      DELC(J,I)=0.
         DO 892 I=30,31
892      DELC(J,I)=0.
890      CONTINUE
         DO 108 I=1,NN
         DO 109 J=1,M
109      CNEW(I,J)=C(I,J)+DELC(I,J)*W
         AM=0.
         DO 110 J=1,M
         IF(CNEW(I,J).GT.AM)AM=CNEW(I,J)
110      CONTINUE
         IF(AM.GT.1.E-6)GO TO 25
         ADIF(I)=0.
         GO TO 108
25       L=6
         MM2=M-6
         K=MM2
         AM=AM*1.E-2
         DO 111 J=6,MM2
         IF(CNEW(I,J).LT.AM)GO TO 111
         L=J
         GO TO 11
111      CONTINUE
11       DO 112 J=6,MM2
         IF(CNEW(I,M+1-J).LT.AM)GO TO 112
         K=M+1-J
         GO TO 12
112      CONTINUE
12       AA=0.
         DO 113 J=L,K
         IF(C(I,J).EQ.0.)GO TO 113
         AAA=ABS(DELC(I,J)/C(I,J))
```

```
      IF(AAA.GT.AA)LAD(I)=J
      IF(AAA.GT.AA)AA=AAA
113   CONTINUE
      ADIF(I)=AA
108   CONTINUE
C     WN=0.10/ADIF(NN)
C     IF(WN.LE.1.5*W)W=WN
C     IF(WN.GT.1.5*W)W=1.5*W
      IF(W.GT.1.0)W=1.0
      DO 198 I=1,NN
      DO 198 J=1,M
198   CNEW(I,J)=C(I,J)+DELC(I,J)*W
C     WRITE(5,299)((CNEW(I,J),I=1,NN),J=1,M)
      DO 114 J=1,M
      IF(C(NN,J).GT.10.)STOP
114   CONTINUE
      DO 115 I=1,NN
      DO 115 J=1,M
      IF(CNEW(I,J).LE.0.)GO TO 14
      C(I,J)=CNEW(I,J)
      GO TO 115
14    K=J+1
      IF(K.LT.M)GO TO 15
      C(I,J)=1.E-50
      GO TO 115
15    DO 116 L=K,M
      IF(CNEW(I,L).GT.0.)GO TO 16
116   CONTINUE
      L=M
16    L=L-1
      IF(J.NE.1)GO TO 17
      CNEW(I,J)=1.E-50
      C(I,1)=1.E-50
      K=K+1
      IF(CNEW(I,2).GT.0.)GO TO 115
17    IF(L.NE.M-1)GO TO 18
      CNEW(I,M)=1.E-50
      C(I,M)=1.E-50
18    K=K-1
      IF(L.EQ.M)L=L-1
      DO 117 L1=K,L
      C(I,L1)=(CNEW(I,L+1)-CNEW(I,K-1))/(X(L+1)-X(K-1))*
     1(X(L1)-X(K-1))+CNEW(I,K-1)
117   CNEW(I,L1)=C(I,L1)
115   CONTINUE
      WRITE(5,299)((C(I,J),I=1,14),J=1,M)
      WRITE(5,293)((C(I,J),I=15,NN),J=1,M)
```

```
299     FORMAT(*0*,14E9.3/(* *,14E9.3))
293     FORMAT(*0*,2E9.3/(* *,2E9.3))
        WRITE(5,199)(ADIF(I),I=1,NN)
        WRITE(5,294)(LAD(I),I=1,16)
294     FORMAT(*0*,14I9/(* *,14I9))
        WRITE(8,199)(ADIF(I),I=1,NN)
C       WRITE(5,99778)(LA(I),I=1,NN),(LB(I),I=1,NN)
99778   FORMAT(* *,11E11.3)
199     FORMAT(*0*,14E9.3/(* *,14E9.3))
        IC=IC+1
        WRITE(5,194)IC,W
        WRITE(8,194)IC,W
194     FORMAT(*0ITERATION#*,I4/*0RELAXATION FACTOR=*,E11.3)
        W1=W
        DO 87 I=1,NN
        IF(ADIF(I).GT.0.1)GO TO 89
87      CONTINUE
        ASSIGN 88 TO JUMP
89      CONTINUE
        W1=1.
        CALL FLUIDS(PRESSI,LA,LB,LLA,M,NSP,NN,AMU,C,VZ,UBAR,
     1  A1,A2,A3,DXE,DXW,A,B,CI,D,PRESS,DUM1,DUM2,DIST,UBARN,
     2  FINVAL,W1,NEWV)
        IF(IC.GT.ICMAX)GO TO 19
        DO 124 I=1,M
C       IF(C(NN,I).GT.0.1)GO TO 21
        GO TO 21
124     CONTINUE
        GO TO 22
21      DO 118 I=1,NN
        IF(ADIF(I).GT.0.005)GO TO JUMP,(8,88)
118     CONTINUE
22      WRITE(5,195)
195     FORMAT(*1YOU WILL NOT BELIEVE IT BUT THIS FANTASTIC*,
     1  * PROGRAM CONVERGED*)
19      CONTINUE
        WRITE(4)C,UBAR,VZ,FINVAL,X
        DO 119 J=1,M
119     C(NN,J)=C(NN,J)*298.+298.
        WRITE(5,299)((C(I,J),I=1,14),J=1,M)
        WRITE(5,293)((C(I,J),I=15,NN),J=1,M)
        DO 121 J=1,M
        IF(.NOT.ISNO)GO TO 121
        RNO(J)=RNO(J)/(DIST*DIST)*PRESS(J)/(82.05*(C(NN,J)*298.+298.))
     1  *DIFFU(NNO,J)
121     HEAT(J)=HEAT(J)*298.*THK(J)/(DIST*DIST)
        WRITE(5,196)(HEAT(J),J=1,M)
```

```
196      FORMAT(*0HEAT RELEASE*/* ====*,1X,7(*=*)/(* *,10E11.3))
         IF(ISNO)WRITE(5,290)(RNO(I),I=1,M)
290      FORMAT(*0RATE OF FORMATION OF NO*/*==== == *,9(*=*),
     1   * == ==*/(* *,10E11.3))
         IF(ISNO)CALL INTNO(RNO,M,DXE,DXW,A1,A2,A3,FE)
         DO 122 I=1,M
122      X(I)=X(I)*DIST
         WRITE(5,291)FE
291      FORMAT(*0THE INTEGRATED RATE OF FORMATION OF NO IS=*,
     1   E11.3,*GR.-MOL/CM**2/SEC*)
         WRITE(5,197)(X(I),I=1,M)
197      FORMAT(*1THE GRID IS AS FOLLOWS*/(* *,E11.3))
         STOP
13       DO 123 J=1,4
C        STOP
123      BACKSPACE 6
         REWIND 3
         F=F/2.
         NCH=NCH*2
         ICH=ICH+1
         IF(ICH.LE.2)GO TO 20
         WRITE(5,5598)
5598     FORMAT(*1I DO NOT SEE MUCH FUTURE FOR YOU MY DEAR BOY*)
         STOP
         END
         SUBROUTINE CHGE(C,UBAR,VZ,NEWPK,PRESSI,M,NN,X,LA,LB,DIST,
     1   LLA,RRR,FINVAL)
         REAL NEWX,LA,LB,LLA,NEWPK
         DIMENSION NEWX(31),C(NN,M),UBAR(M),VZ(M),X(M),LA(NN),LB(NN),
     1   UBARN(31),VZN(31),CN(16,31)
         CALL GRID(NEWX,31,1.10,NEWPK)
         WRITE(5,94)(X(I),NEWX(I),I=1,70)
94       FORMAT(* *,2E11.3)
         DO 99 I=1,M
         IF(NEWX(I).GE.X(1))GO TO 1
         DO 100 J=1,NN
100      CN(J,I)=(C(J,1)-LA(J))*(NEWX(I)+1.)/(X(1)+1.)+LA(J)
         UBARN(I)=(UBAR(1)-82.05*(LA(NN)*298.+298.)/PRESSI)*
     1   (NEWX(I)+1.)/(X(1)+1.)+82.05*(LA(NN)*298.+298.)
         VZN(I)=(VZ(1)-2*LLA*82.05*(LA(NN)*298.+298.)*DIST)*(NEWX(I)+
     1   1.)/(X(1)+1.)+2.*LLA*82.05*(LA(NN)*298.+298.)*DIST
99       CONTINUE
1        MM1=M-1
         DO 101 I=1,M
         DO 102 J=1,MM1
         IF(NEWX(I).LT.X(J))GO TO 102
         IF(NEWX(I).GT.X(J+1))GO TO 102
```

```
      VZN(I)=(VZ(J+1)-VZ(J))/(X(J+1)-X(J))*(NEWX(I)-X(J))+VZ(J)
      UBARN(I)=(UBAR(J+1)-UBAR(J))/(X(J+1)-X(J))*(NEWX(I)-X(J))+
     1 UBAR(J)
      DO 103 K=1,NN
103   CN(K,I)=(C(K,J+1)-C(K,J))/(X(J+1)-X(J))*(NEWX(I)-X(J))+C(K,J)
      GO TO 101
102   CONTINUE
101   CONTINUE
      DO 106 I=1,M
      IF(NEWX(I).LT.X(M))GO TO 106
      UBARN(I)=(82.05*(LB(NN)*298.+298.)/PRESSI-UBAR(M))*(NEWX(I)-X(M)
     1 )/(1.0-X(M))+UBAR(M)
      VZN(I)=(FINVAL-VZ(M))*(NEWX(I)-X(M))/(1.0-X(M))+VZ(M)
      WRITE(5,95)FINVAL,VZ(M),NEWX(M),X(M)
95    FORMAT(*0FINVAL=*,E11.3,* VZ*,E11.3,* NX*,E11.3
     1 ,* X*,E11.3)
      DO 104 K=1,NN
104   CN(K,I)=(LB(K)-C(K,M))*(NEWX(I)-X(M))/(1.0-X(M))+C(K,M)
106   CONTINUE
      DO 105 I=1,M
      UBAR(I)=UBARN(I)
      VZ(I)=VZN(I)
      X(I)=NEWX(I)
      DO 105 J=1,NN
105   C(J,I)=CN(J,I)
      WRITE(5,90)(UBAR(I),I=1,70)
90    FORMAT(*1FROM CHGE WITH LOVE*/(* *,10E11.3))
      WRITE(5,91)(VZ(I),I=1,70)
91    FORMAT(///(* *,10E11.3))
      WRITE(5,92)((C(I,J),I=1,14),J=1,70)
      WRITE(5,93)((C(I,J),I=15,16),J=1,70)
93    FORMAT(* *,2E9.3)
92    FORMAT(* *,14E9.3)
      RETURN
      END
      SUBROUTINE FLUIDS(PRESSI,LA,LB,LLA,M,N,NN,AMU,C,VZ,UBAR,
     1 A1,A2,A3,DXE,DXW,A,B,CI,D,PRESS,DUM1,DUM2,DIST,UBARN,
     2 FINVAL,W1,NEWV)
      DIMENSION LA(NN),LB(NN),AMU(M),C(NN,M),VZ(M),UBAR(M),
     1 A1(M),A2(M),A3(M),DXE(M),DXW(M),A(M),B(M),CI(M),D(M)
     2 ,PRESS(M),DUM1(M),DUM2(M),UBARN(M)
      DIMENSION NEWV(M)
      DIMENSION WT(15),FRAC(31)
      REAL LLA,LA,LB,NEWV,NEWFIN
      DATA WT/30.,28.,2.,29.,1.,44.,16.,16.,14.,15.,17.,18.,
     1 13.,32.,33./
      DO 200 I=1,M
```

```
      FRAC(I)=0.
      DO 201 J=1,N
201   FRAC(I)=FRAC(I)+WT(J)*C(J,I)
      FRACN=1.
      DO 202 J=1,N
202   FRACN=FRACN-C(J,I)
      IF(FRACN.LE.0.)GO TO 200
      FRAC(I)=FRAC(I)+28.*FRACN
200   CONTINUE
      WRITE(5,999)(FRAC(I),I=1,M)
999   FORMAT(* *,10E12.3)
      K=0
C     WRITE(5,93)
      DO 104 I=1,M
104   UBARN(I)=UBAR(I)
1     CONTINUE
93    FORMAT(*0START FLUIDS*)
      RHOIN=FRAC(1)/82.05*PRESSI/(298.*LA(NN)+298.)*LLA*DIST*DIST
      UBINSQ=(82.05*(LA(NN)*298.+298.)/PRESSI)**2.
      RHOIN=RHOIN*UBINSQ
      MM1=M-1
      TP=LA(NN)*298.+298.
      PP=PRESSI
      RHOP=FRAC(1)/82.05*PP/TP
      AMUP=AMU(1)
      VP=2.*LLA*DIST*82.05*(LA(NN)*298.+298.)/PRESSI
      UP=82.05*TP/PP
      TE=C(NN,1)*298.+298.
      PE=PRESS(1)
      RHOE=FRAC(1)/82.05*PE/TE
      AMUE=AMU(1)
      VE=VZ(1)
      UE=UBARN(1)
      DO 100 I=1,MM1
      TW=TP
      PW=PP
      RHOW=RHOP
      AMUW=AMUP
      VW=VP
      UW=UP
      TP=TE
      PP=PE
      RHOP=RHOE
      AMUP=AMUE
      VP=VE
      UP=UE
      TE=298.*C(NN,I+1)+298.
```

```
      PE=PRESS(I+1)
      RHOE=FRAC(I+1)/82.05*PE/TE
      AMUE=AMU(I+1)
      VE=VZ(I+1)
      UE=UBARN(I+1)
      AP=DXW(I)*A2(I)*AMUE/AMUP-A3(I)-DXE(I)*A1(I)*AMUW/AMUP
     1 -RHOP*VP/AMUP*DIST
      BP=-RHOP*LLA*UP/AMUP*DIST*DIST
      A(I)=A1(I)*(2.-DXE(I)*AP)
      B(I)=-(2.*(A1(I)+A2(I))+A3(I)*AP-BP)
      CI(I)=A2(I)*(2.+DXW(I)*AP)
100   D(I)=-RHOIN/AMUP
      TW=TP
      PW=PP
      RHOW=RHOP
      AMUW=AMUP
      VW=VP
      UW=UP
      TP=TE
      PP=PE
      RHOP=RHOE
      AMUP=AMUE
      VP=VE
      UP=UE
      TE=298.*LB(NN)+298.
      PE=PRESSI
      RHOE=FRAC(M)/82.05*PE/TE
      AMUE=AMU(M)
      VE=FINVAL
      UE=82.05*TE/PE
      AP=DXW(M)*A2(M)*AMUE/AMUP-A3(M)-DXE(M)*A1(M)*AMUW/AMUP
     1 -RHOP*VP/AMUP*DIST
      BP=-RHOP*LLA*UP/AMUP*DIST*DIST
      A(M)=A1(M)*(2.-DXE(M)*AP)
      B(M)=-(2.*(A1(M)+A2(M))+A3(M)*AP-BP)
      CI(M)=A2(M)*(2.+DXW(M)*AP)
      D(M)=-RHOIN/AMUP
      D(1)=D(1)-A(1)*(82.05*(LA(NN)*298.+298.))/PRESSI
      D(M)=D(M)-CI(M)*(82.05*(LB(NN)*298.+298.))/PRESSI
      CALL TRIDAG(1,M,A,B,CI,D,UBARN,DUM1,DUM2,M)
C     WRITE(5,90)(UBARN(I),I=1,M)
      K=K+1
      IF(K.LT.20)GO TO 1
      DO 102 I=1,M
102   UBAR(I)=UBAR(I)*(1.-W1)+UBARN(I)*W1
      WRITE(5,90)(UBAR(I),I=1,M)
      RHOIN=FRAC(1)/82.05*PRESSI/(LA(NN)*298.+298.)
```

```
      VO=2.*LLA*DIST*82.05*(LA(NN)*298.+298.)/PRESSI
      RHOVO=RHOIN*VO
      RHOV1=RHOVO-2.*LLA*RHOIN*DXW(1)*UBAR(1)*DIST
      RHO1=FRAC(1)/82.05*PRESS(1)/(C(NN,1)*298.+298.)
      NEWV(1)=RHOV1/RHO1
      DO 101 I=1,MM1
      RHOV2=(DXE(I)*A1(I)*RHOVO+A3(I)*RHOV1-2.*LLA*RHO1*
     1  UBAR(I)*DIST)/(DXW(I)*A2(I))
      RHO2=FRAC(I+1)/82.05*PRESS(I+1)/(C(NN,I+1)*298.+298)
      NEWV(I+1)=RHOV2/RHO2
      RHOVO=RHOV1
      RHOV1=RHOV2
      RHO1=FRAC(I+1)/82.05*PRESS(I+1)/(C(NN,I+1)*298.+298.)
101   CONTINUE
      NEWFIN=(DXE(M)*A1(M)*RHOVO+A3(M)*RHOV1-2.*LLA*RHO1*UBAR(M)
     1  *DIST)/(DXW(M)*A2(M))
      RHO2=FRAC(M)/82.05*PRESSI/(LB(NN)*298.+298.)
      NEWFIN=NEWFIN/RHO2
C     WRITE(5,91)(NEWV(I),I=1,M),NEWFIN
90    FORMAT(*0UBAR*/(* *,10E11.3))
91    FORMAT(*0VZ*/(* *,10E11.3))
      DO 103 I=1,M
103   VZ(I)=VZ(I)*(1.-W1)+NEWV(I)*W1
      FINVAL=FINVAL*(1.-W1)+NEWFIN*W1
      WRITE(5,91)(VZ(I),I=1,M),FINVAL
C     WRITE(5,92)(A(I),B(I),CI(I),D(I),I=1,M)
92    FORMAT(*1*,4E11.3/(* *,4E11.3))
C     WRITE(5,94)
94    FORMAT(*0FINISHED FLUIDS*)
      RETURN
      END
      SUBROUTINE NEWREA(C,RI,DRDC,M,N,NN,LW,NR,DIST,
     1  SPEF,NSPEF,SPER,NSPER,TB,NTB,N2,NN2,AR,AF,TER,TEF,
     2  ER,EF,DESTR,CREAT,NDS,NCR,HO,ACP,BCP,CCP,DCP,H,HP,DH,
     3  DHP,RR,RF,RRP,RFP,NNN2,NN3,DIFFU,THK,MULT,NMULT,NN1,
     4  PRESS,VZ,DIFF1,CPAV,LLA,UBAR,ISNPN,NPN,THIRD,AMOLN2)
      DIMENSION C(NN,M),RI(NN,M),DRDC(NN,NN,M),
     1  SPEF(NR,2),SPER(NR,2),NSPEF(NR),PRESS(M),VZ(M),DIFF1(M),
     2  NSPER(NR),TB(NTB),N2(NN2),AR(NR),AF(NR),TER(NR),TEF(NR),
     3  ER(NR),EF(NR),DESTR(N,NNN2),CREAT(N,NN3),NDS(N),NCR(N),
     4  HO(N),ACP(N),BCP(N),CCP(N),DCP(N),H(N),DH(NR),HP(N),DHP(NR),
     5  RF(NR),RR(NR),RRP(NR),RFP(NR),DIFFU(N,M),THK(M),MULT(NN1,2)
     6  ,CPAV(M),UBAR(M)
      REAL LLA
      INTEGER SPEF,SPER,DESTR,CREAT,TB
      LOGICAL LW,ISNPN,THIRD,AMOLN2
      NPN=9
```

```
      AUX1=298.*(ALOG(298.)-1.)
      AUX2=298.*298.
      AUX3=AUX2*298.
      ACPN2=9.39872
      BCPN2=-0.585490
      CCPN2=0.300738E-2
      DCPN2=-0.581488E-6
      DO 101 I=1,M
      DO 118 J=1,NN
118   RI(J,I)=0.
      T=298.*C(NN,I)+298.
      AMOLC=PRESS(I)/(82.05*T)
      CN2=1.
      DO 106 J=1,N
106   CN2=CN2-C(J,I)
      DO 102 J=1,NR
      RF(J)=AF(J)*T**TEF(J)*EXP(-EF(J)/T)
      RR(J)=AR(J)*T**TER(J)*EXP(-ER(J)/T)
      ND=NSPEF(J)
      RF(J)=RF(J)*AMOLC**(NSPEF(J)-1)
      DO 103 K=1,ND
103   RF(J)=RF(J)*C(SPEF(J,K),I)
      ND=NSPER(J)
      RR(J)=RR(J)*AMOLC**(NSPER(J)-1)
      DO 104 K=1,ND
104   RR(J)=RR(J)*C(SPER(J,K),I)
102   CONTINUE
      IF(.NOT.THIRD)GO TO 3
      DO 105 J=1,NTB
      RF(TB(J))=RF(TB(J))*AMOLC
105   RR(TB(J))=RR(TB(J))*AMOLC
3     IF(.NOT.AMOLN2)GO TO 4
      DO 107 J=1,NN2
      IF(N2(J))14,107,15
14    NA=-N2(J)
      RF(NA)=RF(NA)*CN2*AMOLC
      GO TO 107
15    RR(N2(J))=RR(N2(J))*CN2*AMOLC
107   CONTINUE
4     DO 108 J=1,N
      A=0.
      ND=NDS(J)
      IF(ND.EQ.0)GO TO 11
      DO 109 K=1,ND
109   A=A-(RF(DESTR(J,K))-RR(DESTR(J,K)))
11    ND=NCR(J)
      IF(ND.EQ.0)GO TO 108
```

```
      DO 117 K=1,ND
117   A=A+(RF(CREAT(J,K))-RR(CREAT(J,K)))
108   RI(J,I)=A
      IF(NMULT.EQ.0)GO TO 20
      DO 400 J=1,NMULT
      IF(MULT(J,2))21,400,22
21    NNM=-MULT(J,2)
      RI(MULT(J,1),I)=RI(MULT(J,1),I)-(RF(NNM)-RR(NNM))
      GO TO 400
22    NNM=MULT(J,2)
      RI(MULT(J,1),I)=RI(MULT(J,1),I)+(RF(NNM)-RR(NNM))
400   CONTINUE
20    DO 110 J=1,NN
      DO 110 K=1,NN
110   DRDC(J,K,I)=0.
      DO 111 J=1,N
      IF(NDS(J).EQ.0)GO TO 111
      ND=NDS(J)
      DO 112 K=1,ND
      ND1=NSPEF(DESTR(J,K))
      DO 113 L=1,ND1
      CC=C(SPEF(DESTR(J,K),L),I)
      DRDC(J,SPEF(DESTR(J,K),L),I)=DRDC(J,SPEF(DESTR(J,K),L),I)
     1 -RF(DESTR(J,K))/CC
113   CONTINUE
      ND1=NSPER(DESTR(J,K))
      DO 119 L=1,ND1
      CC=C(SPER(DESTR(J,K),L),I)
      DRDC(J,SPER(DESTR(J,K),L),I)=DRDC(J,SPER(DESTR(J,K),L),I)
     1 +RR(DESTR(J,K))/CC
119   CONTINUE
112   CONTINUE
111   CONTINUE
      DO 114 J=1,N
      IF(NCR(J).EQ.0)GO TO 114
      ND=NCR(J)
      DO 115 K=1,ND
      NTT=CREAT(J,K)
      ND1=NSPER(CREAT(J,K))
      DO 116 L=1,ND1
      CC=C(SPER(CREAT(J,K),L),I)
      DRDC(J,SPER(CREAT(J,K),L),I)=DRDC(J,SPER(CREAT(J,K),L),I)-
     1 RR(CREAT(J,K))/CC
116   CONTINUE
      ND1=NSPEF(CREAT(J,K))
      DO 120 L=1,ND1
      CC=C(SPEF(CREAT(J,K),L),I)
```

```
      DRDC(J,SPEF(CREAT(J,K),L),I)=DRDC(J,SPEF(CREAT(J,K),L),I)+
     1  RF(CREAT(J,K))/CC
120   CONTINUE
115   CONTINUE
114   CONTINUE
      IF(NMULT.EQ.0)GO TO 26
      DO 402 J=1,NMULT
      IF(MULT(J,2))27,402,28
27    NNM=-MULT(J,2)
      ND=NSPEF(NNM)
      DO 403 L=1,ND
403   DRDC(MULT(J,1),SPEF(NNM,L),I)=DRDC(MULT(J,1),SPEF(NNM,L),I)
     1  -RF(NNM)/C(SPEF(NNM,L),I)
      ND=NSPER(NNM)
      DO 404 L=1,ND
404   DRDC(MULT(J,1),SPER(NNM,L),I)=DRDC(MULT(J,1),SPER(NNM,L),I)
     1  +RR(NNM)/C(SPER(NNM,L),I)
      GO TO 402
28    NNM=MULT(J,2)
      ND=NSPEF(NNM)
      DO 405 L=1,ND
405   DRDC(MULT(J,1),SPEF(NNM,L),I)=DRDC(MULT(J,1),SPEF(NNM,L),I)
     1  +RF(NNM)/C(SPEF(NNM,L),I)
      ND=NSPER(NNM)
      DO 406 L=1,ND
406   DRDC(MULT(J,1),SPER(NNM,L),I)=DRDC(MULT(J,1),SPER(NNM,L),I)
     1  -RR(NNM)/C(SPER(NNM,L),I)
402   CONTINUE
      S=0.
      S1=1.
26    DO 200 J=1,N
      H(J)=H0(J)+ACP(J)*(T-298.)+BCP(J)*(T*(ALOG(T)-1.)-AUX1)+
     1  0.5*CCP(J)*(T*T-AUX2)+DCP(J)/3.*(T**3-AUX3)
      HP(J)=(ACP(J)+BCP(J)*ALOG(T)+CCP(J)*T+DCP(J)*T*T)*298.
      S1=S1-C(J,I)
200   S=S+HP(J)*C(J,I)
      DO 201 J=1,NR
      DH(J)=0.
      DHP(J)=0.
      ND=NSPER(J)
      DO 202 K=1,ND
      DH(J)=DH(J)+H(SPER(J,K))
202   DHP(J)=DHP(J)+HP(SPER(J,K))
      ND=NSPEF(J)
      DO 203 K=1,ND
      DH(J)=DH(J)-H(SPEF(J,K))
203   DHP(J)=DHP(J)-HP(SPEF(J,K))
```

```
201      CONTINUE
         HN2=ACPN2*(T-298.)+BCPN2*(T*(ALOG(T)-1.)-AUX1)
     1   +0.5*CCPN2*(T*T-AUX2)+DCPN2*(T**3-AUX3)/3.
         HPN2=(ACPN2+BCPN2*ALOG(T)+CCPN2*T+DCPN2*T*T)*298.
         CPAV(I)=(S+S1*HPN2)/298.
         DO 215 J=1,NN2
         IF(N2(J))1,215,2
1        DH(-N2(J))=DH(-N2(J))-HN2
         DHP(-N2(J))=DHP(-N2(J))-HPN2
         GO TO 215
2        DH(N2(J))=DH(N2(J))+HN2
         DHP(N2(J))=DHP(N2(J))+HPN2
215      CONTINUE
         AMOLCP=-AMOLC/T
         DO 204 J=1,NR
         RFP(J)=RF(J)*(TEF(J)/T+EF(J)/(T*T)+(NSPEF(J)-1)/AMOLC
     1   *AMOLCP)*298.
204      RRP(J)=RR(J)*(TER(J)/T+ER(J)/(T*T)+(NSPER(J)-1)/AMOLC
     1   *AMOLCP)*298.
         DO 219 J=1,NTB
         RFP(TB(J))=RFP(TB(J))+AMOLCP/AMOLC*298.*RF(TB(J))
219      RRP(TB(J))=RRP(TB(J))+AMOLCP/AMOLC*298.*RR(TB(J))
         DO 220 J=1,NN2
         IF(N2(J))16,220,17
16       NA=-N2(J)
         RFP(NA)=RFP(NA)+AMOLCP/AMOLC*298.*RF(NA)
         GO TO 220
17       RRP(N2(J))=RRP(N2(J))+AMOLCP/AMOLC*298.*RR(N2(J))
220      CONTINUE
         DO 205 J=1,NR
205      RI(NN,I)=RI(NN,I)-(RF(J)-RR(J))*DH(J)
         RI(NN,I)=RI(NN,I)*AMOLC
308      DO 306 J=1,NR
         ND=NSPER(J)
         DO 307 K=1,ND
307      DRDC(NN,SPER(J,K),I)=DRDC(NN,SPER(J,K),I)+RR(J)/
     1   C(SPER(J,K),I)*DH(J)
         ND=NSPEF(J)
         DO 309 K=1,ND
309      DRDC(NN,SPEF(J,K),I)=DRDC(NN,SPEF(J,K),I)-RF(J)/
     1   C(SPEF(J,K),I)*DH(J)
306      CONTINUE
         DO 310 J=1,N
310      DRDC(NN,J,I)=DRDC(NN,J,I)*AMOLC
         DO 212 J=1,N
         A=0.
         ND=NDS(J)
```

```
      IF(ND.EQ.0)GO TO 9
      DO 213 K=1,ND
213   A=A-(RFP(DESTR(J,K))-RRP(DESTR(J,K)))
9     ND=NCR(J)
      IF(ND.EQ.0)GO TO 212
      DO 216 K=1,ND
216   A=A+(RFP(CREAT(J,K))-RRP(CREAT(J,K)))
212   DRDC(J,NN,I)=A
      IF(NMULT.EQ.0)GO TO 23
      DO 401 J=1,NMULT
      IF(MULT(J,2))24,401,25
24    NNM=-MULT(J,2)
      DRDC(MULT(J,1),NN,I)=DRDC(MULT(J,1),NN,I)
     1-(RFP(NNM)-RRP(NNM))
      GO TO 401
25    NNM=MULT(J,2)
      DRDC(MULT(J,1),NN,I)=DRDC(MULT(J,1),NN,I)
     1+(RFP(NNM)-RRP(NNM))
401   CONTINUE
23    DO 214 J=1,NR
214   DRDC(NN,NN,I)=DRDC(NN,NN,I)-(RFP(J)-RRP(J))*DH(J)-
     1(RF(J)-RR(J))*DHP(J)
      DRDC(NN,NN,I)=DRDC(NN,NN,I)*AMOLC+RI(NN,I)*AMOLCP*298.
     1/AMOLC
      IF(.NOT.ISNPN)GO TO 101
      RFNPN=1.E18/T*AMOLC*AMOLC*C(NPN,I)*C(NPN,I)
      RRNPN=4.83E24/T*EXP(-114388.97/T)*AMOLC*CN2
      RI(NPN,I)=RI(NPN,I)-2.*(RFNPN-RRNPN)
      DRDC(NPN,NPN,I)=DRDC(NPN,NPN,I)-4.*RFNPN/C(NPN,I)
      WRITE(5,876)RFNPN,RRNPN,RI(NPN,I),DRDC(NPN,NPN,I)
876   FORMAT(* *,4E11.3)
101   CONTINUE
      DO 300 J=1,M
      DO 300 I=1,N
      RI(I,J)=RI(I,J)/DIFFU(I,J)*DIST*DIST
      DO 300 L=1,NN
300   DRDC(I,L,J)=DRDC(I,L,J)/DIFFU(I,J)*DIST*DIST
      DO 301 J=1,M
      RI(NN,J)=RI(NN,J)/(THK(J)*298.)*DIST*DIST
      DO 301 I=1,NN
301   DRDC(NN,I,J)=DRDC(NN,I,J)/(THK(J)*298.)*DIST*DIST
      IF(LW)WRITE(5,90)((RI(I,J),I=1,NN),J=1,M)
90    FORMAT(*1*,11E11.3/(* *,11E11.3))
      IF(LW)WRITE(5,91)(((DRDC(I,J,L),J=1,NN),I=1,NN),L=1,M)
91    FORMAT(*1*,11E11.3/10(* *,11E11.3/)////48(11(* *,
     1 11E11.3/)////))
      RETURN
```

```
      END
      FUNCTION YLIN(T,K)
      COMMON/YLINV/F
      DIMENSION F(81,3),A(81),B(81),C(81)
      EQUIVALENCE (F(1,1),A(1)),(F(1,2),B(1)),(F(1,3),C(1))
      IF (T.GT.A(81)) GO TO 40
      IF(K.EQ.3)GO TO 30
      DO 20 I=2,81
      IF (A(I).LT.T) GO TO 20
      YLIN=B(I-1)+(T-A(I-1))*(B(I)-B(I-1))/(A(I)-A(I-1))
      RETURN
   20 CONTINUE
30    DO 50 I=2,81
      IF (A(I).LT.T) GO TO 50
      YLIN=C(I-1)+(T-A(I-1))*(C(I)-C(I-1))/(A(I)-A(I-1))
      RETURN
   50 CONTINUE
   40 WRITE(5,90)
90    FORMAT(*0SHIT*)
      RETURN
      END
      SUBROUTINE TRSP1(LSTSPE,N,C,NN,M,PRESS,DIFFU,AMU,THK,LW,
     1 DIL)
      LOGICAL LW
      DIMENSION TRSPIN(28,4),INDEX(28),AMUI(28),AKI(28)
      DIMENSION LSTSPE(N),C(NN,M),PRESS(M),DIFFU(N,M),
     1 AMU(M),THK(M)
      DATA(TRSPIN( 1,K),K=1,4)/6HCH4    ,16.043,148.600,   3.8/
      DATA(TRSPIN( 2,K),K=1,4)/6HO2     ,32.000,106.700,   3.5/
      DATA(TRSPIN( 3,K),K=1,4)/6HN2     ,28.016, 71.400,   3.8/
      DATA(TRSPIN( 4,K),K=1,4)/6HCO     ,28.011, 91.700,   3.7/
      DATA(TRSPIN( 5,K),K=1,4)/6HH2     , 2.016, 59.700,   2.8/
      DATA(TRSPIN( 6,K),K=1,4)/6HNH3    ,17.032,558.300,   2.9/
      DATA(TRSPIN( 7,K),K=1,4)/6HHCN    ,27.027,569.100,   3.6/
      DATA(TRSPIN( 8,K),K=1,4)/6HNO     ,30.008,116.700,   3.5/
      DATA(TRSPIN( 9,K),K=1,4)/6HCO2    ,44.011,195.200,   3.9/
      DATA(TRSPIN(10,K),K=1,4)/6HCH     ,13.019,148.000,   3.8/
      DATA(TRSPIN(11,K),K=1,4)/6HCH2    ,14.027,148.000,   3.8/
      DATA(TRSPIN(12,K),K=1,4)/6HCH3    ,15.035,148.600,   3.8/
      DATA(TRSPIN(13,K),K=1,4)/6HCHO    ,29.019, 91.700,   3.7/
      DATA(TRSPIN(14,K),K=1,4)/6HCH2O   ,30.027, 91.700,   3.7/
      DATA(TRSPIN(15,K),K=1,4)/6HCH3O   ,31.035, 91.700,   3.7/
      DATA(TRSPIN(16,K),K=1,4)/6HCN     ,26.019,106.700,   3.5/
      DATA(TRSPIN(17,K),K=1,4)/6HH2O    ,18.016,506.000,   2.7/
      DATA(TRSPIN(18,K),K=1,4)/6HH      , 1.008, 18.350,   3.0/
      DATA(TRSPIN(19,K),K=1,4)/6HOH     ,17.008,506.000,   2.7/
      DATA(TRSPIN(20,K),K=1,4)/6HO      ,16.000,218.900,   2.5/
```

```
      DATA(TRSPIN(21,K),K=1,4)/6HHO2   ,33.008,106.700,   3.5/
      DATA(TRSPIN(22,K),K=1,4)/6HN     ,14.008,218.900,   2.5/
      DATA(TRSPIN(23,K),K=1,4)/6HHNO   ,31.016,106.700,   3.5/
      DATA(TRSPIN(24,K),K=1,4)/6HNH    ,15.016,106.700,   3.5/
      DATA(TRSPIN(25,K),K=1,4)/6HNH2   ,16.024,106.700,   3.5/
      DATA(TRSPIN(26,K),K=1,4)/6HN2O   ,44.016,232.400,   3.8/
      DATA(TRSPIN(27,K),K=1,4)/6HNO2   ,46.008,232.400,   3.8/
      DATA(TRSPIN(28,K),K=1,4)/6HNCO   ,42.019,106.700,   3.5/
      FKTR=2.*SQRT(2.)
      DO 100 I=1,N
      DO 101 J=1,28
      K=J
      ENCODE(10,190,NANA)TRSPIN(J,1)
190   FORMAT(A6)
      IF(LSTSPE(I).EQ.NANA)GO TO 1
101   CONTINUE
      WRITE(5,90)LSTSPE(I)
90    FORMAT(*1SPECIES *,A6,*NOT IN TRANSPORT LIBRARY*)
      STOP
1     INDEX(I)=K
100   CONTINUE
      DO 104 J=1,28
      K=J
      ENCODE(10,190,NANA)TRSPIN(J,1)
      ENCODE(10,190,NANB)DIL
      IF(NANB.EQ.NANA)GO TO 2
104   CONTINUE
      WRITE(5,91)DIL
91    FORMAT(*1SPECIES *,A6,*,THE DILUENT IS NOT IN THE*,
     1  * TRANSPORT LIBRARY*)
      STOP
2     IDIL=K
C     WRITE(5,96)(INDEX(I),I=1,N),IDIL
96    FORMAT(* *,20I5)
      RETURN
      ENTRY TRSPO
      DO 103 L=1,M
      T=C(NN,L)*298.+298.
      T1=SQRT(T)
      T2=T*T1
      FRA=1.
      DO 102 J=1,N
102   FRA=FRA-C(J,L)
      PREF=0.001858*T2/PRESS(L)
C     WRITE(5,290)FRA,PREF
290   FORMAT(*0*,10E11.3)
      DO 105 I=1,N
```

```
      ID=INDEX(I)
      S=0.
      DO 106 J=1,N
      IF(I.EQ.J)GO TO 106
      JD=INDEX(J)
      SIGIJ=0.5*(TRSPIN(ID,4)+TRSPIN(JD,4))
      AKOEIJ=T/(SQRT(TRSPIN(ID,3)*TRSPIN(JD,3)))
C     WRITE(5,95)AKOEIJ,T,TRSPIN(ID,3),TRSPIN(JD,3)
95    FORMAT(*0*,4E11.3/(* *,4E11.3))
      OMEGAD=1.06036/AKOEIJ**0.15610
      IF(AKOEIJ.LT.24.)OMEGAD=OMEGAD+0.193/EXP(0.47635*AKOEIJ)+
     1 1.03587/EXP(1.52996*AKOEIJ)+1.76474/EXP(3.89411*AKOEIJ)
      DIJ=PREF*SQRT(1./TRSPIN(ID,2)+1./TRSPIN(JD,2))/
     1 (SIGIJ*SIGIJ*OMEGAD)
      S=S+C(J,L)/DIJ
C     WRITE(5,291)ID,JD,SIGIJ,AKOEIJ,OMEGAD,DIJ,S,C(J,L)
291   FORMAT(*0*,2I5,9E11.3)
106   CONTINUE
      SIGIJ=0.5*(TRSPIN(ID,4)+TRSPIN(IDIL,4))
      AKOEIJ=T/(SQRT(TRSPIN(ID,3)*TRSPIN(IDIL,3)))
C     WRITE(5,95)AKOEIJ,T,TRSPIN(ID,3),TRSPIN(IDIL,3)
      OMEGAD=1.06036/AKOEIJ**0.15610
      IF(AKOEIJ.LT.24.)OMEGAD=OMEGAD+0.193/EXP(0.47635*AKOEIJ)+
     1 1.03587/EXP(1.52996*AKOEIJ)+1.76474/EXP(3.89411*AKOEIJ)
      DIJ=PREF*SQRT(1./TRSPIN(ID,2)+1./TRSPIN(IDIL,2))/
     1 (SIGIJ*SIGIJ*OMEGAD)
      S=S+FRA/DIJ
C     WRITE(5,291)ID,JD,SIGIJ,AKOEIJ,OMEGAD,DIJ,S,FRA
105   DIFFU(I,L)=(1.-C(I,L))/S
      DO 107 I=1,N
      ID=INDEX(I)
      SIGSQ=TRSPIN(ID,4)**2
      AKOEI=T/TRSPIN(ID,3)
C     WRITE(5,94)AKOEI,T,TRSPIN(ID,3)
94    FORMAT(*0*,3E11.3/(* *,3E11.3))
      OMEGAM=1.16145/AKOEI**0.14874
      IF(AKOEI.LT.15.)OMEGAM=OMEGAM+0.52487/EXP(0.7732*AKOEI)+
     1 2.16178/EXP(2.43787*AKOEI)
      AMUI(I)=2.6693E-5*SQRT(TRSPIN(ID,2)*T)/(SIGSQ*OMEGAM)
      AKI(I)=1.9891E-4*SQRT(T/TRSPIN(ID,2))/(SIGSQ*OMEGAM)
C     WRITE(5,292)ID,SIGSQ,AKOEI,OMEGAM,AMUI(I),AKI(I)
292   FORMAT(*0*,I5,10E11.3)
107   CONTINUE
      SIGSQ=TRSPIN(IDIL,4)**2
      AKOEI=T/TRSPIN(IDIL,3)
      OMEGAM=1.16145/AKOEI**0.14874
      IF(AKOEI.LT.15.)OMEGAM=OMEGAM+0.52487/EXP(0.7732*AKOEI)+
```

```
     1  2.16178/EXP(2.43787*AKDEI)
        AMUDIL=2.6693E-5*SQRT(TRSPIN(IDIL,2)*T)/(SIGSQ*OMEGAM)
        AKDIL=1.9891E-4*SQRT(T/TRSPIN(IDIL,2))/(SIGSQ*OMEGAM)
C       WRITE(5,292)IDIL,SIGSQ,AKDEI,OMEGAM,AMUDIL,AKDIL
        IF(LW)WRITE(5,93)(AMUI(I),I=1,N),AMUDIL
        IF(LW)WRITE(5,93)(AKI(I),I=1,N),AKDIL
        S1=0.
        S2=0.
        DO 108 I=1,N
        ID=INDEX(I)
        AMI=TRSPIN(ID,2)
        SS1=0.
        SS2=0.
        DO 109 J=1,N
        IF(I.EQ.J)GO TO 109
        JD=INDEX(J)
        AMJ=TRSPIN(JD,2)
        F1=(AMJ/AMI)**0.25
        F2=1./F1
        F3=SQRT(1.+AMI/AMJ)
        FIIJ=(1.+SQRT(AMUI(I)/AMUI(J))*F1)**2/(FKTR*F3)
        GIJ=1.065*(1.+SQRT(AKI(I)/AKI(J))*F2)**2/(FKTR*F3)
        SS1=SS1+C(J,L)/C(I,L)*FIIJ
        SS2=SS2+C(J,L)/C(I,L)*GIJ
C       WRITE(5,293)F1,F2,F3,FIIJ,GIJ,SS1,SS2
293     FORMAT(*0*,10E11.3)
109     CONTINUE
        AMJ=TRSPIN(IDIL,2)
        F1=(AMJ/AMI)**0.25
        F2=1./F1
        F3=SQRT(1.+AMI/AMJ)
        FIIJ=(1.+SQRT(AMUI(I)/AMUDIL)*F1)**2/(FKTR*F3)
        GIJ=1.065*(1.+SQRT(AKI(I)/AKDIL)*F2)**2/(FKTR*F3)
        SS1=SS1+FRA/C(I,L)*FIIJ
        SS2=SS2+FRA/C(I,L)*GIJ
        S1=S1+AMUI(I)/(1.+SS1)
        S2=S2+AKI(I)/(1.+SS2)
C       WRITE(5,293)F1,F2,F3,FIIJ,GIJ,SS1,SS2,S1,S2
108     CONTINUE
        AMI=TRSPIN(IDIL,2)
        SS1=0.
        SS2=0.
        DO 209 J=1,N
        JD=INDEX(J)
        AMJ=TRSPIN(JD,2)
        F1=(AMJ/AMI)**0.25
        F2=1./F1
```

```
      F3=SQRT(1.+AMI/AMJ)
      FIIJ=(1.+SQRT(AMUDIL/AMUI(J))*F1)**2/(FKTR*F3)
      GIJ=1.065*(1.+SQRT(AKDIL/AKI(J))*F2)**2/(FKTR*F3)
      SS1=SS1+C(J,L)/FRA*FIIJ
      SS2=SS2+C(J,L)/FRA*GIJ
C     WRITE(5,293)F1,F2,F3,FIIJ,GIJ,SS1,SS2
209   CONTINUE
      S1=S1+AMUDIL/(1.+SS1)
      S2=S2+AKDIL/(1.+SS2)
      AMU(L)=S1
      THK(L)=S2
C     WRITE(5,293)S1,S2,AMU(L),THK(L)
103   CONTINUE
      IF(LW)WRITE(5,92)((DIFFU(I,J),I=1,N),J=1,M)
92    FORMAT(* *,13E9.3)
      IF(LW)WRITE(5,93)(AMU(I),I=1,M)
93    FORMAT(*0*,10E11.3/(* *,10E11.3))
      IF(LW)WRITE(5,93)(THK(I),I=1,M)
      RETURN
      END
      SUBROUTINE DIFF(DXE,DXW,M,PRESS,NN,PRESSI,DIFF1,A1,A2,A3)
      DIMENSION DXE(M),DXW(M),PRESS(M),A1(M),A2(M),A3(M),
     1 DIFF1(M)
      MM1=M-1
      PP=PRESSI
      PE=PRESS(1)
      DO 100 I=1,MM1
      PW=PP
      PP=PE
      PE=PRESS(I+1)
      A1(I)=1./(DXW(I)*(DXE(I)+DXW(I)))
      A2(I)=1./(DXE(I)*(DXE(I)+DXW(I)))
      A3(I)=(DXW(I)-DXE(I))/(DXE(I)*DXW(I))
100   DIFF1(I)=DXW(I)*A2(I)*PE-A3(I)*PP-DXE(I)*A1(I)*PW
      PW=PP
      PP=PE
      PE=PRESSI
      A1(M)=1./(DXW(M)*(DXE(M)+DXW(M)))
      A2(M)=1./(DXE(M)*(DXE(M)+DXW(M)))
      A3(M)=(DXW(M)-DXE(M))/(DXE(M)*DXW(M))
      DIFF1(M)=DXW(M)*A2(M)*PE-A3(M)*PP-DXE(M)*A1(M)*PW
      DO 101 I=1,M
      IF(DIFF1(I).LT.1.E-12)DIFF1(I)=0.
101   CONTINUE
C     WRITE(5,90)(DIFF1(I),I=1,M)
90    FORMAT(*0DERIVATIVE1*/(* *,10E11.3))
      RETURN
```

```
      END
      SUBROUTINE NEWGR(DXE,DXW,M,N,NN,LA,PRESS,VZ,DIFFU,C,A1,A2,A3
     1  ,ALFA,BETA,GAMA,LB,CPAV,THK,DIST,LLA,PRESSI,UBAR,RI,DRDC,
     2  FINVAL)
      DIMENSION DXE(M),DXW(M),LA(NN),LB(NN),PRESS(M),VZ(M),
     1  DIFFU(N,M),C(NN,M),A1(M),A2(M),A3(M),ALFA(NN,M),
     2  BETA(NN,M),GAMA(NN,M),CPAV(M),THK(M),UBAR(M),
     3  RI(NN,M),DRDC(NN,NN,M)
      REAL LLA,LA,LB
      LOGICAL LW
C     WRITE(5,91)M
      MM1=M-1
91    FORMAT(*0IN NEWGR*,I3)
C     WRITE(5,92)(A1(I),A2(I),A3(I),I=1,M)
92    FORMAT(*0*,3E11.3/(* *,3E11.3))
      DO 100 J=1,N
      TP=LA(NN)*298.+298.
      PP=PRESSI
      CP=PP/(82.05*TP)
      TE=298.*C(NN,1)+298.
      PE=PRESS(1)
      CE=PE/(82.05*TE)
      VP=2.*LLA*DIST*82.05*(LA(NN)*298.+298)/PRESSI
      VE=VZ(1)
      DP=DIFFU(J,1)
      DE=DIFFU(J,1)
      DO 100 I=1,MM1
      TW=TP
      PW=PP
      CW=CP
      VW=VP
      DW=DP
      TP=TE
      PP=PE
      CP=CE
      VP=VE
      DP=DE
      TE=298.*C(NN,I+1)+298.
      PE=PRESS(I+1)
      CE=PE/(82.05*TE)
      VE=VZ(I+1)
      DE=DIFFU(J,I+1)
C     WRITE(5,96)DXW(I),CE,CP,DE,DP,DXE(I),CW,CP,DW,DP,DIST,
C    1 VE,VP,VW
96    FORMAT(* *,14E9.3)
      AP=DXW(I)*A2(I)*CE/CP*DE/DP-A3(I)-DXE(I)*A1(I)*CW/CP*DW/DP
     1  -DIST*VP/DP
```

```
C       WRITE(5,96)AP
        BP=DXW(I)*A2(I)*(-DIST*CE/CP*VE/DP)-A3(I)*(-DIST*VP/DP)
     1  -DXE(I)*A1(I)*(-DIST*CW/CP*VW/DP)
     2  -2.*LLA*DIST*DIST*UBAR(I)/DP
C       WRITE(5,96)BP
        ALFA(J,I)=A1(I)*(2.-AP*DXE(I))
        BETA(J,I)=-(2.*(A1(I)+A2(I))+AP*A3(I)-BP)
100     GAMA(J,I)=A2(I)*(2.+AP*DXW(I))
C       WRITE(5,93)
93      FORMAT(*0FINISHED 100*)
        TW=TP
        PW=PP
        CW=CP
        VW=VP
        TP=TE
        PP=PE
        CP=CE
        VP=VE
        TE=LB(NN)*298.+298.
        PE=PRESSI
        CE=PE/(82.05*TE)
        VE=FINVAL
        DO 101 J=1,N
        DW=DIFFU(J,MM1)
        DP=DIFFU(J,M)
        DE=DP
C       WRITE(5,96)DXW(M),CE,CP,DE,DP,DXE(M),CW,CP,DW,DP,DIST,
C     1 VE,VP,VW
        AP=DXW(M)*A2(M)*CE/CP*DE/DP-A3(M)-DXE(M)*A1(M)*CW/CP*DW/DP
     1  -DIST*VP/DP
C       WRITE(5,96)AP
        BP=DXW(M)*A2(M)*(-DIST*CE/CP*VE/DP)-A3(M)*(-DIST*VP/DP)
     1  -DXE(M)*A1(M)*(-DIST*CW/CP*VW/DP)
     2  -2.*LLA*DIST*DIST*UBAR(M)/DP
C       WRITE(5,96)BP
        ALFA(J,M)=A1(M)*(2.-AP*DXE(M))
        BETA(J,M)=-(2.*(A1(M)+A2(M))+AP*A3(M)-BP)
101     GAMA(J,M)=A2(M)*(2.+AP*DXW(M))
C       WRITE(5,94)
94      FORMAT(*0FINISHED 101*)
        TP=LA(NN)*298.+298.
        PP=PRESSI
        CONCP=1./82.05*PP/TP
        CPAVP=CPAV(1)
        VP=2.*LLA*DIST*82.05*(LA(NN)*298.+298.)/PRESSI
        AKP=THK(1)
        TE=298.*C(NN,1)+298.
```

```
      PE=PRESS(1)
      CONCE=1./82.05*PE/TE
      CPAVE=CPAV(1)
      VE=VZ(1)
      AKE=THK(1)
      DO 102 I=1,MM1
      TW=TP
      PW=PP
      CONCW=CONCP
      CPAVW=CPAVP
      VW=VP
      AKW=AKP
      TP=TE
      PP=PE
      CONCP=CONCE
      CPAVP=CPAVE
      VP=VE
      AKP=AKE
      TE=298.*C(NN,I+1)+298.
      PE=PRESS(I+1)
      CONCE=1./82.05*PE/TE
      CPAVE=CPAV(I+1)
      VE=VZ(I+1)
      AKE=THK(I+1)
C     WRITE(5,96)DXW(I),AKE,AKP,DXE(I),AKW,AKP,DIST,CONCP,CPAVP,
C    1 VP,UBAR(I)
      AP=DXW(I)*A2(I)*AKE/AKP-A3(I)-DXE(I)*A1(I)*AKW/AKP
     1 -DIST*CONCP*CPAVP*VP/AKP
C     WRITE(5,96)AP
      BP=DXW(I)*A2(I)*(-DIST*CONCE*CPAVE*VE/AKP)
     1 -A3(I)*(-DIST*CONCP*CPAVP*VP/AKP)
     2 -DXE(I)*A1(I)*(-DIST*CONCW*CPAVW*VW/AKP)
     3 -DIST*DIST*LLA*2.*CONCP*CPAVP*UBAR(I)/AKP
      DBDT=298.*DIST/AKP*(DXW(I)*A2(I)*(CONCE*CPAVE*VE/TE)
     1 -A3(I)*(CONCP*CPAVP*VP/TP)-DXE(I)*A1(I)*(CONCW*CPAVW
     2 *VW/TW)+2.*LLA*DIST*CPAVP*UBAR(I)*CONCP/TP)
      RI(NN,I)=RI(NN,I)-BP
      DRDC(NN,NN,I)=DRDC(NN,NN,I)-DBDT
C     WRITE(5,96)BP,DBDT
      ALFA(NN,I)=A1(I)*(2.-DXE(I)*AP)
      BETA(NN,I)=-(2.*(A1(I)+A2(I))+AP*A3(I)-BP)
102   GAMA(NN,I)=A2(I)*(2.+AP*DXW(I))
      TW=TP
      PW=PP
      CONCW=CONCP
      CPAVW=CPAVP
      VW=VP
```

```
      AKW=AKP
      TP=TE
      PP=PE
      CONCP=CONCE
      CPAVP=CPAVE
      VP=VE
      AKP=AKE
      TE=298*LB(NN)+298.
      PE=PRESSI
      CONCE=1./82.05*PE/TE
      CPAVE=CPAV(M)
      VE=FINVAL
      AKE=THK(M)
C     WRITE(5,96)DXW(M),AKE,AKP,DXE(M),AKW,AKP,DIST,CONCP,CPAVP,
C    1 VP,UBAR(M)
      AP=DXW(M)*A2(M)*AKE/AKP-A3(M)-DXE(M)*A1(M)*AKW/AKP
     1 -DIST*CONCP*CPAVP*VP/AKP
C     WRITE(5,96)AP
      BP=DXW(M)*A2(M)*(-DIST*CONCE*CPAVE*VE/AKP)
     1 -A3(M)*(-DIST*CONCP*CPAVP*VP/AKP)
     2 -DXE(M)*A1(M)*(-DIST*CONCW*CPAVW*VW/AKP)
     3 -DIST*DIST*LLA*2.*CONCP*CPAVP*UBAR(M)/AKP
      DBDT=298.*DIST/AKP*(DXW(M)*A2(M)*(CONCE*CPAVE*VE/TE)
     1 -A3(M)*(CONCP*CPAVP*VP/TP)-DXE(M)*A1(M)*(CONCW*CPAVW
     2 *VW/TW)+2.*LLA*DIST*CPAVP*UBAR(M)*CONCP/TP)
      RI(NN,M)=RI(NN,M)-BP
      DRDC(NN,NN,M)=DRDC(NN,NN,M)-DBDT
C     WRITE(5,96)BP,DBDT
      ALFA(NN,M)=A1(M)*(2.-AP*DXE(M))
      BETA(NN,M)=-(2.*(A1(M)+A2(M))+AP*A3(M)-BP)
      GAMA(NN,M)=A2(M)*(2.+AP*DXW(M))
C     WRITE(5,90)((ALFA(J,I),J=1,NN),I=1,M)
C     WRITE(5,90)((BETA(J,I),J=1,NN),I=1,M)
C     WRITE(5,90)((GAMA(J,I),J=1,NN),I=1,M)
90    FORMAT(*1*11E11.3/(* *,11E11.3))
C     WRITE(5,95)
95    FORMAT(*0FINISHED ALL*)
C     WRITE(5,190)((RI(I,J),I=1,NN),J=1,M)
190   FORMAT(*1*,11E11.3/(* *,11E11.3))
C     WRITE(5,191)(((DRDC(I,J,L),J=1,NN),I=1,NN),L=1,M)
191   FORMAT(*1*,11E11.3/10(* *,11E11.3/)////48(11(* *,
     1 11E11.3/)////))
      RETURN
      END
      SUBROUTINE SBAND(T,SS,RR,AL,W,NP,NSP,P,Q,NT,N2,G)
      INTEGER W,WP,R,S,WPP1,SM1,RP1,WPP2,RM1
      DIMENSION T(NSP,NP),SS(NSP,NSP,NP),RR(NSP,NP),AL(NT,N2),P(NT)
```

```
     1  ,Q(NT),G(NT)
        WP=(W-1)/2
        WPP1=WP+1
        WPP2=WP+2
        N=NP*NSP
        DO 100 IP=1,NP
        DO 100 ISP=1,NSP
        R=(IP-1)*NSP+ISP
        IS=R-WPP1
        IF(R.LT.WPP1)IS=0
        JS=WPP1+1-R
        IF(R.GT.N-WP)JS=JS+ISP
        L1=MAXO(1,R-WP)
        L2=MINO(N,R+WP)
        AL(R,R+JS)=1.
        DO 101 S=L1,R
        IF(S.NE.1)GO TO 1
        IF(IP.EQ.1)GO TO 2
        AL(R,S-IS)=T(ISP,IP)
        GO TO 101
2       AL(R,S-IS)=SS(ISP,1,IP)
        GO TO 101
1       IF(L1.GT.S-1)GO TO 12
        A=0.
        SM1=S-1
        DO 102 K=L1,SM1
        KS=WPP1+1-K
        IF(K.GT.N-WP)KS=KS+K-K/NSP*NSP
102     A=A+AL(R,K-IS)*AL(K,S+KS)
        IF(S.LE.(IP-1)*NSP)GO TO 6
        IF(S.LT.IP*NSP+1)GO TO 7
        IF(S.LT.R+WP)GO TO 6
        B=RR(ISP,IP)
        GO TO 8
6       B=0.
        GO TO 8
7       B=SS(ISP,S-(IP-1)*NSP,IP)
8       AL(R,S-IS)=B-A
        GO TO 101
12      AL(R,S-IS)=T(ISP,IP)
101     CONTINUE
        RP1=R+1
        IF(RP1.GT.N)GO TO 100
        DO 103 S=RP1,L2
        L3=MAXO(1,S-WP)
        IF(R.NE.1)GO TO 3
        IF(S.EQ.L2)GO TO 5
```

```
      AL(R,S+JS)=SS(1,S,1)/AL(R,R-IS)
      GO TO 103
5     AL(R,S+JS)=RR(1,1)/AL(R,R-IS)
      GO TO 103
3     IF(L3.GT.R-1)GO TO 4
      A=0.
      RM1=R-1
      DO 104 K=L3,RM1
      KS=WPP1+1-K
      IF(K.GT.N-WP)KS=KS+K-K/NSP*NSP
104   A=A+AL(R,K-IS)*AL(K,S+KS)
      IF(S.LE.(IP-1)*NSP)GO TO 9
      IF(S.LT.IP*NSP+1)GO TO 10
      IF(S.LT.R+WP)GO TO 9
      B=RR(ISP,IP)
      GO TO 11
9     B=0.
      GO TO 11
10    B=SS(ISP,S-(IP-1)*NSP,IP)
11    AL(R,S+JS)=(B-A)/AL(R,R-IS)
      GO TO 103
4     AL(R,S+JS)=RR(ISP,IP)/AL(R,R-IS)
103   CONTINUE
100   CONTINUE
92    FORMAT(*1*,9E11.3/(* *,9E11.3))
      G(1)=Q(1)/AL(1,1)
      DO 1000 I=2,WPP1
      A=0.
      IM1=I-1
      DO 1001 J=1,IM1
1001  A=A+AL(I,J)*G(J)
1000  G(I)=(Q(I)-A)/AL(I,I)
      DO 1002 I=WPP2,N
      A=0.
      DO 1003 J=1,WP
1003  A=A+AL(I,J)*G(J+I-WPP1)
1002  G(I)=(Q(I)-A)/AL(I,WPP1)
90    FORMAT(*1*,8E11.3/(* *,8E11.3))
      LAST=2*WPP1
      K=N
      P(N)=G(N)/AL(N,LAST)
      DO 1004 I=2,WPP1
      K=K-1
      A=0.
      IK=N+1
      IM1=I-1
      DO 1005 J=1,IM1
```

```
      IK=IK-1
C     WRITE(5,91)K,LAST,J,IK
91    FORMAT(* *,6I4)
1005  A=A+AL(K,LAST-J+1)*P(IK)
1004  P(K)=(G(K)-A)/AL(K,LAST-I+1)
      DO 1006 I=WPP2,N
      K=K-1
      A=0.
      IK=K+WPP1
      DO 1007 J=1,WP
      IK=IK-1
C     WRITE(5,91)K,LAST,J,IK
1007  A=A+AL(K,LAST-J+1)*P(IK)
1006  P(K)=(G(K)-A)/AL(K,WPP1+1)
      RETURN
      END
      SUBROUTINE GRID(X,M,R,PMID)
      DIMENSION X(M)
      MM1=M-1
      DIFF=1.E20
      DO 99 J=2,MM1
      MP=J
      A=0.
      DX=1.
      DO 100 I=1,MP
      A=A+DX
100   DX=DX/R
      DX=(PMID+1.)/A
      X(1)=-1.+DX
      DX=DX/R
      DO 101 I=2,MP
      X(I)=X(I-1)+DX
101   DX=DX/R
      MPP1=MP+1
      A=0.
      DX=1.
      MPL1=M+1
      DO 102 I=MPP1,MPL1
      A=A+DX
102   DX=DX*R
      DX=(1.-PMID)/A
      DO 103 I=MPP1,M
      X(I)=X(I-1)+DX
103   DX=DX*R
C     WRITE(5,90)(X(I),I=1,M)
90    FORMAT(* *,14E9.3)
      IF(ABS(2.*X(MP)-X(MP-1)-X(MP+1)).GT.DIFF)GO TO 99
```

```
      DIFF=ABS(2.*X(MP)-X(MP-1)-X(MP+1))
      L=J
99    CONTINUE
      MP=L
      A=0.
      DX=1.
      DO 1100 I=1,MP
      A=A+DX
1100  DX=DX/R
      DX=(PMID+1.)/A
      X(1)=-1.+DX
      DX=DX/R
      DO 1101 I=2,MP
      X(I)=X(I-1)+DX
1101  DX=DX/R
      MPP1=MP+1
      A=0.
      DX=1.
      DO 1102 I=MPP1,MPL1
      A=A+DX
1102  DX=DX*R
      DX=(1.-PMID)/A
      DO 1103 I=MPP1,M
      X(I)=X(I-1)+DX
1103  DX=DX*R
      RETURN
      END
      SUBROUTINE SDELTA(X,DXE,DXW,M,LW)
      DIMENSION DXE(M),DXW(M),X(M)
      LOGICAL LW
      MMM=M-1
      DO 100 I=2,MMM
      DXE(I)=X(I+1)-X(I)
100   DXW(I)=X(I)-X(I-1)
      DXE(1)=X(2)-X(1)
      DXW(1)=X(1)+1.
      DXE(M)=1.-X(M)
      DXW(M)=X(M)-X(M-1)
      IF(LW)WRITE(5,90)
90    FORMAT(*1X,DXE,DXW*)
      IF(LW)WRITE(5,91)(X(I),DXE(I),DXW(I),I=1,M)
91    FORMAT(* *,3E11.3)
      RETURN
      END
      SUBROUTINE TRIDAG(IF,L,A,B,C,D,V,BETA,GAMMA,M)
      DIMENSION A(M),B(M),C(M),V(M),BETA(M),GAMMA(M),D(M)
      BETA(IF)=B(IF)
```

```
      GAMMA(IF)=D(IF)/BETA(IF)
      IFP1=IF+1
      DO 1 I=IFP1,L
      BETA(I)=B(I)-A(I)*C(I-1)/BETA(I-1)
1     GAMMA(I)=(D(I)-A(I)*GAMMA(I-1))/BETA(I)
      V(L)=GAMMA(L)
      LAST=L-IF
      DO 2 K=1,LAST
      I=L-K
2     V(I)=GAMMA(I)-C(I)*V(I+1)/BETA(I)
      RETURN
      END
      SUBROUTINE INTNO(RNO,M,DXE,DXW,A1,A2,A3,FE)
      DIMENSION RNO(M),DXE(M),DXW(M),A1(M),A2(M),A3(M)
      FW=0.
      FP=RNO(1)*DXW(1)
      DO 100 I=2,M
      FE=(RNO(I-1)+A3(I-1)*FP+DXE(I-1)*A1(I-1)*FW)/(A2(I-1)*DXW(I-1))
      FW=FP
      FP=FE
100   CONTINUE
      RETURN
      END
```

REFERENCES

Anagnostou, E., and A. E. Potter, "Flame Strength of Propane-Oxygen Flames at Low Pressures in Turbulent Flow," Ninth Symposium (International) on Combustion, p. 1, The Combustion Institute, Pittsburgh, Pennsylvania (1962).

Andrews, G. E., D. Bradley, and S. B. Lwakabamba, "Turbulence and Turbulent Flame Propagation -- A Critical Appraisal," Comb. and Flame, 24, p. 285 (1975).

Bird, R. B., W. E. Stewart, and E. N. Lightfoot, Transport Phenomena, John Wiley & Sons, Inc., New York (1960).

Bracco, F. V., "Nitric Oxide Formation in Droplet Diffusion Flames," Fourteenth Symposium (International) on Combustion, p. 831, The Combustion Institute, Pittsburgh, Pennsylvania (1973).

Burke, S. P., and T. E. W. Schuman, "Diffusion Flames," First Symposium on Combustion, p. 2, The Combustion Institute, Pittsburgh, Pennsylvania (1928).

Carnahan, B., H. A. Luther, and J. O. Wilkes, Applied Numerical Methods, John Wiley & Sons, Inc., New York (1969).

Chan, Y. N. I., I. Birnbaum, and L. Lapidus, "Solution of Stiff Differential Equations and the Use of Imbedding Techniques," Ind. Eng. Fundam., 17, p. 133 (1978).

Corley, T. L., Senior Research Engineer, Energy and Environmental Research Corp., Irvine, California, personal communication (1979).

Dayal, S. K., and T. P. Pandya, "Structure of Counterflow Diffusion Flame in Transverse Electric Fields," Comb. and Flame, 35, p. 277 (1979).

Energy and Environmental Research Corp. Staff, Irvine California, personal communications (1979).

Fairbanks, D. F., and C. R. Wilke, "Diffusion Coefficients in Multicomponent Gas Mixtures," Ind. Eng. Chem., 42, p. 471 (1950).

Fendell, F. E., "Ignition and Extinction in Combustion of Initially Unmixed Reactants," J. Fluid Mech., 21, p. 281 (1965).

Fenimore, C. P., "Formation of Nitric Oxide in Premixed Hydrocarbon Flames," Thirteenth Symposium (International) on Combustion, p. 373, The Combustion Institute, Pittsburgh, Pennsylvania (1971).

Field, M. A., D. W. Gill, B. B. Morgan, and P. G. W. Hawksley, Combustion of Pulverized Coal, BCURA Leatherhead, Cherey and Sons, Ltd., Bamburg, England (1967).

Fristrom, R. M., and A. A. Westenberg, Flame Structure, McGraw-Hill Book Company, Inc., New York (1965).

Gibson, C. H., and P. A. Libby, "On Turbulent Flows with Fast Chemical Reactions. Part II. The Distribution of Reactants and Products Near a Reacting Surface," Comb. Sci. and Tech., 6, p. 29 (1972).

Hawthorne, W. R., Selected Combustion Problems, Fundamental and Aeronautical Applications, Butterworth, London (1954).

Jones, F. L., P. M. Becker, and R. J. Meinsohn, "A Mathematical Model of the Opposed Jet Diffusion Flame: Effect of an Electric Field on Concentration and Temperature Profiles," Comb. and Flame, 19, p. 351 (1972).

Kau, C. J., Senior Research Engineer, Energy and Environmental Research Corp., Irvine, California, personal communication (1979).

Levy, J. M., J. L. Longwell, A. F. Sarofim, T. L. Corley, M. Heap, and T. J. Tyson, "NO_x Abatement in Fossil Fuel Combustion: Chemical Kinetic Considerations," Proc. of the Third Stationary Source Combustion Symposium, Vol. 4. Fundamental Combustion Research and Environmental Assessment, Interagency Energy/Environment Research and Development Program Report No. EPA-600/7-79-050d, February (1979).

Marble, F. E., and J. E. Broadwell, "The Coherent Flame Model for Turbulent Chemical Reactions," Project SQUID, 29314-6001-RU-00 (1977).

Mason, H. B., and L. R. Waterland, "Environmental Assessment of Stationary Source NO_x Combustion Modification Technologies," Proc. of the Second Stationary Source Combustion Symposium, EPA-600/7-77-073a, p. 38, July (1977).

Milne, L. M., and C. B. E. Thomson, Theoretical Hydrodynamics, The Macmillan Company, New York (1961).

Mitchell, R. E., and A. F. Sarofim, "Nitrogen Oxide Formation in Laminar Methane-Air Diffusion Flames," The Combustion Institute, Fall Meeting, Stanford Research Institute, Palo Alto, California (1975).

Otsuka, Y., and T. Niioka, "On the Deviation of the Flame from the Stagnation Point in Opposed Jet Diffusion Flames," Comb. and Flame, 19, p. 171 (1972).

Otsuka, Y., and T. Niioka, "The One Dimensional Diffusion Flame in a Two Dimensional Counter Flow Burner," Comb. and Flame, 21, p. 163 (1973).

Pandya, T. P., and F. J. Weinberg, "The Study of the Structure of Laminar Diffusion Flames by Optical Methods," Ninth Symposium (International) on Combustion, p. 587, The Combustion Institute, Pittsburgh, Pennsylvania (1962).

Pandya, T. P., and F. J. Weinberg, "The Structure of Flat Counter-Flow Diffusion Flames," Proc. Roy. Soc. (London), Ser. A, 279, p. 544 (1964).

Peaceman, D. W., Fundamentals of Numerical Reservoir Simulation, Elsevier Scientific Publishing Company, New York (1977).

Pershing, D. W., and J. O. L. Wendt, "Pulverized Coal and Combustion: The Influence of Flame Temperature and Coal Composition on Thermal and Fuel NO_x," Sixteenth Symposium (International) on Combustion, p. 389, The Combustion Institute, Pittsburgh, Pennsylvania (1976).

Potter, A. E., and J. N. Butler, "A Novel Combustion Measurement Based on the Extinguishment of Diffusion Flames," ARS Journal, 29, p. 54 (1959).

Potter, A. E., S. Heimel, and J. N. Butler, "Apparent Flame Strength: A Measure of Maximum Reaction Rate in Diffusion Flames," Eighth Symposium (International) on Combustion, p. 1027, The Combustion Institute, Pittsburgh, Pennsylvania (1960).

Reid, R. C., and T. K. Sherwood, The Properties of Gases and Liquids, McGraw-Hill Book Company, Inc., New York (1958).

Schlichting, H., Boundary Layer Theory, 4th Edition, McGraw-Hill Book Company, Inc., New York (1962).

Snyder, W. T., "Preliminary Observations of a One-Dimensional Turbulent Propane-Air Flame," Eighth Symposium (International) on Combustion, p. 573, The Combustion Institute, Pittsburgh, Pennsylvania (1962).

Spalding, D. B., "Theory of Mixing and Chemical Reaction in the Opposed Jet Diffusion Flame," ARS Journal, 31, p. 763 (1961).

Sternling, L. V., and J. O. L. Wendt, "On the Oxidation of Fuel Nitrogen in a Diffusion Flame," AIChE J., 20, p. 81 (1974).

Styles, A. C., and N. A. Chigier, "Combustion of Air Blast Atomized Spray Flames," Sixteenth Symposium (International) on Combustion, p. 619, The Combustion Institute, Pittsburgh, Pennsylvania (1976).

Tyson, T. J., "An Implicit Integration Method for Chemical Kinetics," Paper 9840-6002-R000, TRW Space Tech. Lab., Redondo Beach, California (1964).

von Kàrmàn, T., "Combustion in Turbulent Flames," Fourth Symposium (International) on Combustion, p. 924, The Combustion Institute, Pittsburgh, Pennsylvania (1952).

Wendt, J. O. L., "Fundamental Coal Combustion Mechanisms and Pollutant Formation in Furnaces," accepted for publication in Progress in Energy and Comb. Science (1979).

Wendt, J. O. L., C. H. Martinez, D. G. Lilley, and T. L. Corley, "Numerical Solution of Stiff Boundary Valued Problems in Kinetics and Diffusion," Chem. Eng. Sci., 34, p. 527 (1979).

Wendt, J. O. L., and O. E. Schulze, "On the Fate of Fuel Nitrogen during Coal Char Combustion," AIChE J., 22, p. 102 (1976).

Williams, F. A., Combustion Theory, Addison-Wesley, New York (1968).

Williams, F. A., "An Approach to Turbulent Flame Theory," J. Fluid Mech., 40, p. 401 (1970).

Williams, F. A., "Turbulent Mixing in Non-Reactive and Reactive Flows," Purdue University, S. N. B. Murthy, ed., p. 189 (1974).

Wootan, E. C., "Fate of Fuel Nitrogen in Laminar Premixed Flat Flames," M.S. Thesis, University of Arizona, Tucson (In Prep.).

Zeldovich, J., "The Oxidation of Nitrogen in Combustion and Explosions," Acta Physicochim., U.R.S.S., 21, p. 577 (1946).